

Inaugural dissertation
for
obtaining the doctoral degree
of the
Combined Faculty of Mathematics, Engineering and Natural Sciences
of the
Ruprecht - Karls - University
Heidelberg

Presented by
M.Sc. Franjo Banovic
born in: Zagreb, Croatia
Oral examination: 15.06.2022

Signal transduction during CNS invasion
by *Listeria monocytogenes*
and the role of CD44 in the invasion

Referees: Prof. Dr. rer. nat. Michael Lanzer
Prof. Dr. med. Horst Schrotten

For my girls

**Eidesstattliche Versicherung gemäß § 8 der Promotionsordnung für die
Naturwissenschaftlich-Mathematische Gesamtfakultät der Universität Heidelberg**

1. Bei der eingereichten Dissertation zu dem Thema

Signal transduction during CNS invasion by *Listeria monocytogenes* and the role of CD44
in the invasion

handelt es sich um meine eigenständig erbrachte Leistung.

2. Ich habe nur die angegebenen Quellen und Hilfsmittel benutzt und mich keiner unzulässigen Hilfe Dritter bedient. Insbesondere habe ich wörtlich oder sinngemäß aus anderen Werken übernommene Inhalte als solche kenntlich gemacht.
3. Die Arbeit oder Teile davon habe ich ~~wie folgt~~/bislang nicht¹⁾ an einer Hochschule des In- oder Auslands als Bestandteil einer Prüfungs- oder Qualifikationsleistung vorgelegt.
4. Die Richtigkeit der vorstehenden Erklärungen bestätige ich.
5. Die Bedeutung der eidesstattlichen Versicherung und die strafrechtlichen Folgen einer unrichtigen oder unvollständigen eidesstattlichen Versicherung sind mir bekannt.

Ich versichere an Eides statt, dass ich nach bestem Wissen die reine Wahrheit erklärt und nichts verschwiegen habe.

.....

Ort und Datum

.....

Unterschrift

¹⁾ Nicht Zutreffendes streichen. Bei Bejahung sind anzugeben: der Titel der andernorts vorgelegten Arbeit, die Hochschule, das Jahr der Vorlage und die Art der Prüfungs- oder Qualifikationsleistung.

SUMMARY

Listeria monocytogenes (*Lm*) is an opportunistic, facultatively intracellular pathogen that enters the host via contaminated food, causing listeriosis. Given opportunity, *Lm* can enter the bloodstream by penetrating the gut barrier, reach the liver and the spleen and persist in them. Rarely, it can also invade the fetus in pregnant women or the central nervous system (CNS), namely brain, causing a serious condition characterized by a very high mortality rate and lasting neurological problems in survivors.

Direct penetration into cells in general is mediated by binding of listerial surface virulence factors (VFs) – primarily those belonging to internalin family – to specific cellular receptors, leading to uptake by zipper-type endocytosis, even in non-phagocytic cells. The best-known receptors exploited by *Lm* in this manner are adherens junction protein E-cadherin (Ecad) and receptor tyrosine kinase (RTK) Met – Ecad is bound by internalin (InIA) and Met is bound by internalin B (InIB). There are two barriers through which *Lm* can pass to enter the brain: blood-brain barrier (BBB) and blood-cerebrospinal fluid barrier (BCSFB). The exact mechanisms of entry into the brain remain elusive, with research mostly focusing on interactions between listerial VFs and their binding partners, e.g. InIA and Ecad, InIB and Met (and its co-receptor CD44v6) or internalin F (InIF) and vimentin.

The investigation of host cell response during infection by *Lm* was done in *in vitro* models of the BBB and the BCSFB, chiefly in human brain microvascular endothelial cells (HBMEC) for the BBB and human choroid plexus papilloma (HIBCPP) cells for the BCSFB. Part of the *in vitro* experiments aimed to reproduce the findings from other cell lines in HBMEC and/or HIBCPP cells (e.g. effects of MAPK, dynamin and vimentin inhibition as well as deletion of InIA, InIB and/or InIF on bacterial invasion rates). The other part of *in vitro* experiments consisted of an analysis of the effects of CD44v6-blocking peptides on bacterial invasion rates, as well as the investigation into involvement of various RTKs other than Met in listerial invasion. Finally, a series of infection experiments with mice was performed, with an aim to deduce the dependence of the successful development of systemic, orally acquired listeriosis on immunosuppression and CD44v6-Met-InIB interactions.

The results presented within this study outline a) the potentially InIF-independent role of vimentin and b) possible involvement of multiple previously unreported RTKs in listerial invasion, as well as c) importance of immunosuppression for efficient chronic infection of mice. No effect of CD44v6-blocking peptides on either the bacterial invasion into different cell lines or the development of systemic infection in mice was observed during the experiments, and more investigative effort is necessary to elucidate the question further.

ZUSAMMENFASSUNG

Listeria monocytogenes ist ein opportunistisch fakultativ intrazellulärer Erreger, der den menschlichen Wirt durch kontaminierte Nahrungsmittel infizieren und dadurch Listeriose hervorrufen kann. Listerien können unter bestimmten Umständen die gastrointestinale Barriere überqueren, wodurch sie in den Blutkreislauf gelangen und verschiedene Organe wie beispielsweise Leber und Milz infizieren können. In seltenen Fällen kann *Lm* während der Schwangerschaft den Fötus infizieren; oder bei Invasion des zentralen Nervensystems (ZNS) können mitunter schwere Erkrankungen des Gehirns ausgelöst werden, die mit einer hohen Mortalitätsrate verbunden sind und in bleibenden neurologischen Problemen bei Überlebenden resultieren kann.

Direkte Invasion in Wirtszellen wird im Allgemeinen durch das Binden bakterieller Oberflächenproteine -primär Mitglieder aus der Proteinfamilie der Internaline- an spezifische zelluläre Rezeptoren bewerkstelligt wodurch *Lm* durch Endozytose nach dem Zipper-Mechanismus, auch in nicht-phagozytierende Zellen, invadieren kann. Die bekanntesten Rezeptoren, die während der Invasion von *Lm* verwendet werden, sind das Zelladhäsionsprotein E-Cadherin und die Rezeptortyrosinkinase Met. E-Cadherin bindet an Internalin (InIA) und Met an Internalin B (InIB). *Lm* kann im Wesentlichen über zwei physiologische Barrieren in das Gehirn gelangen: die Blut-Hirn-Schranke und die Blut-Liquor Schranke. Der exakte Mechanismus für den Eintritt ins Gehirn bleibt schwer aufzuklären. Aktuelle Forschung fokussiert sich auf die Interaktion zwischen den Virulenzfaktoren von *Lm* und deren Bindungspartner, wie beispielsweise InIA und E-Cadherin, InIB und Met (und dessen Korezeptor CD44v6), sowie Internalin F (InIF) und Vimentin.

Die Untersuchung der Wirtszellantwort während der Infektion mit *Lm* erfolgte mithilfe *in vitro* Zellmodellen der Blut-Hirn- und Blut-Liquor-Schranke. Als *in vitro* Modell der Blut-Hirn-Schranke kamen humane mikrovaskuläre Hirnendothelzellen (HBMEC) und für die Blut-Liquor-Schranke eine Papillomzelllinie vom Epithel des Plexus choroideus (HIBCPC) zum Einsatz. Der erste Teil der Experimente beschäftigte sich damit die Erkenntnisse von anderen Zelllinien mit HBMEC und/oder HIBCPC Zellen zu reproduzieren (z.B. Einfluss von MAPK-, Dynamin- und Vimentin-Inhibition sowie Deletion von InIA, InIB und InIF auf bakterielle Invasionsraten). In zweiten Teil wurde der Einfluss eines CD44v6-Blockingpeptids auf die bakteriellen Invasionsraten. Auch wurde untersucht ob andere Rezeptortyrosinkinasen als Met an der Invasion von Listerien beteiligt sind. Weiterhin wurden Infektionsexperimente mit Mäusen durchgeführt mit dem Ziel die Abhängigkeit der erfolgreichen Entwicklung einer systemischen, oral erworbenen Listeriose von der Immunsuppression und einer CD44v6-Met-InIB-Interaktion abzuleiten.

Die Ergebnisse der vorliegenden Arbeit beschreiben a) eine potenziell InIF-abhängige Rolle von Vimentin, b) die mögliche Beteiligung von verschiedenen Rezeptortyrosinkinasen, die zuvor noch nicht charakterisiert wurden und c) die Bedeutung der Immunsuppression für eine effiziente chronische Infektion von Mäusen. Es wurde kein Effekt des verwendeten CD44v6-Blockingpeptids auf sowohl bakterielle Invasion in den verwendeten Zelllinien, als auch in der Entwicklung einer systemischen Infektion von Mäusen beobachtet. Um diese Fragestellung zu klären, erfordert es weiterführende Untersuchungen.

TABLE OF CONTENTS

| | |
|---|----|
| SUMMARY | 1 |
| ZUSAMMENFASSUNG | 2 |
| TABLE OF CONTENTS | 4 |
| 1. INTRODUCTION | 9 |
| 1.1. <i>Listeria monocytogenes</i> | 9 |
| 1.1.1. Classification | 9 |
| 1.1.2. Pathology of listeriosis | 10 |
| 1.2. CNS barriers..... | 10 |
| 1.2.1. Intercellular junctions | 12 |
| 1.2.1.1. Tight junctions | 12 |
| 1.2.1.2. Adherens junctions | 13 |
| 1.2.2. CNS barrier composition | 15 |
| 1.2.2.1. BBB | 15 |
| 1.2.2.2. BCSFB..... | 17 |
| 1.2.3. Models of CNS barriers..... | 18 |
| 1.2.3.1. BBB <i>in vitro</i> models | 19 |
| 1.2.3.2. BCSFB <i>in vitro</i> models..... | 22 |
| 1.3. Listerial CNS invasion routes | 23 |
| 1.3.1. Hematogenous route | 24 |
| 1.3.2. Neurogenous route..... | 25 |
| 1.4. Virulence factors of <i>Listeria monocytogenes</i> | 26 |
| 1.4.1. Internalins..... | 27 |
| 1.4.1.1. InlA | 28 |
| 1.4.1.2. InlB | 29 |
| 1.4.1.3. InlF..... | 31 |
| 1.4.1.4. Other CNS-invasion related internalins..... | 32 |
| 1.4.2. Listeriolysin O | 34 |
| 1.4.3. Other CNS-invasion related virulence factors | 35 |
| 1.5. Transmembrane proteins relevant to listerial invasion..... | 37 |
| 1.5.1. Receptor tyrosine kinases | 37 |
| 1.5.2. CD44..... | 38 |
| 1.5.2.1. CD44v6 | 38 |
| 2. MATERIALS AND METHODS | 40 |

| | | |
|------------|---|----|
| 2.1. | Materials | 40 |
| 2.1.1. | <i>Listeria monocytogenes</i> | 40 |
| 2.1.1.1. | <i>Listeria monocytogenes</i> strains..... | 40 |
| 2.1.1.2. | Media and plates used for <i>Listeria monocytogenes</i> | 40 |
| 2.1.2. | Cellular models | 40 |
| 2.1.2.1. | Cell lines..... | 40 |
| 2.1.2.1.1. | HIBCPP (human CP epithelium-derived, papilloma) | 40 |
| 2.1.2.1.2. | HBMEC (human brain microvascular endothelium-derived, immortalized) .. | 41 |
| 2.1.2.1.3. | HeLa cells | 41 |
| 2.1.2.1.4. | bEnd.3 (mouse cerebral endothelium-derived, immortalized) | 41 |
| 2.1.2.2. | Cell media | 41 |
| 2.1.3. | Animal models | 42 |
| 2.1.3.1. | Mouse strains | 42 |
| 2.1.4. | Peptides..... | 42 |
| 2.1.5. | Antibodies..... | 42 |
| 2.1.5.1. | Primary antibodies | 42 |
| 2.1.5.2. | Secondary antibodies | 44 |
| 2.1.6. | Media | 44 |
| 2.1.7. | Buffers, chemicals and solutions | 46 |
| 2.1.8. | Primers for PCR..... | 48 |
| 2.1.9. | Size standards | 50 |
| 2.1.10. | Kits..... | 50 |
| 2.1.11. | Laboratory equipment | 50 |
| 2.1.12. | Software | 52 |
| 2.1.13. | Consumables | 53 |
| 2.2. | Methods..... | 54 |
| 2.2.1. | <i>Listeria monocytogenes</i> | 54 |
| 2.2.1.1. | Generation and long-term storage of <i>Lm</i> working aliquots | 54 |
| 2.2.1.2. | Bacterial cultivation and preparation of inoculums for <i>in vitro</i> experiments | 55 |
| 2.2.1.3. | Preparation of inocula for <i>in vivo</i> experiments and generation of <i>Lm</i> calibration curve | 56 |
| 2.2.1.4. | Strain verification via PCR..... | 56 |
| 2.2.2. | <i>In vitro</i> experiments | 58 |
| 2.2.2.1. | Cell cultivation | 58 |

| | | |
|------------|---|----|
| 2.2.2.1.1. | Cell culture initiation, maintenance and passage | 58 |
| 2.2.2.1.2. | Culture slide, cell culture plate and cell culture insert cell cultivation..... | 59 |
| 2.2.2.2. | Barrier integrity assessment..... | 61 |
| 2.2.2.3. | Cellular infection experiment setup..... | 63 |
| 2.2.2.3.1. | Setup in cell culture plates and culture slides | 63 |
| 2.2.2.3.2. | Setup in culture inserts..... | 63 |
| 2.2.2.4. | Cell viability assessment..... | 64 |
| 2.2.3. | <i>In vivo</i> experiments..... | 67 |
| 2.2.3.1. | Animal ethics statement..... | 67 |
| 2.2.3.2. | Preparation of contaminated bread | 67 |
| 2.2.3.3. | Infection of mice | 68 |
| 2.2.3.4. | Administration of immunosuppressants and CD44v6-blocking peptides | 68 |
| 2.2.3.5. | Sacrificing of mice and organ extraction | 69 |
| 2.2.3.6. | Homogenization and plating of organs | 70 |
| 2.2.4. | Molecular techniques..... | 71 |
| 2.2.4.1. | IF microscopy | 71 |
| 2.2.4.1.1. | Sample preparation and staining | 71 |
| 2.2.4.1.2. | IF microscopy and image generation | 73 |
| 2.2.4.1.3. | Bacterial quantification | 73 |
| 2.2.4.2. | PCR..... | 74 |
| 2.2.4.2.1. | RNA isolation..... | 74 |
| 2.2.4.2.2. | cDNA synthesis..... | 74 |
| 2.2.4.2.3. | Semi-quantitative PCR..... | 75 |
| 2.2.4.3. | Western blotting..... | 76 |
| 2.2.4.3.1. | Protein extract generation and extract concentration measurement..... | 76 |
| 2.2.4.3.2. | Sample preparation..... | 77 |
| 2.2.4.3.3. | Gel electrophoresis | 77 |
| 2.2.4.3.4. | Wet Western blot..... | 78 |
| 2.2.4.3.5. | Detection and result analysis..... | 78 |
| 2.2.4.4. | RTK phosphorylation array | 79 |
| 2.2.4.4.1. | Protein extract generation and extract concentration measurement..... | 79 |
| 2.2.4.4.2. | RTK phosphorylation array protocol and result analysis..... | 79 |
| 2.2.5. | Statistics | 81 |
| 3. | RESULTS..... | 82 |

| | | |
|----------|---|-----|
| 3.1. | Listerial invasion <i>in vitro</i> | 82 |
| 3.1.1. | HBMEC and HIBCPP cells express proteins relevant for <i>Lm</i> invasion | 82 |
| 3.1.2. | Confirmation of differential side-specific invasion of HBMEC and HIBCPP cells by <i>Lm</i> 87 | |
| 3.1.3. | Different internalins are required for invasion of <i>Lm</i> into HBMEC and HIBCPP cells | 89 |
| 3.1.4. | Modulation of surface vimentin reduces the invasion of <i>Lm</i> into HBMEC cells..... | 90 |
| 3.1.5. | Incubation with CD44v6-blocking peptides has no effect on listerial invasion rates | 93 |
| 3.2. | Downstream cellular signaling affected by listerial invasion | 95 |
| 3.2.1. | <i>Lm</i> invasion upregulates inflammation-related genes but does not affect the transcription of interaction partners of listerial VFs in HBMEC and HIBCPP cells | 95 |
| 3.2.2. | Infection with <i>Lm</i> activates components of the MAPK pathways in HBMEC..... | 97 |
| 3.2.3. | Inhibition of MAPK signaling reduces listerial invasion into HBMEC | 98 |
| 3.2.4. | Inhibition of the dynamin assembly machinery reduces listerial invasion into HBMEC 100 | |
| 3.2.5. | <i>Lm</i> invasion activates multiple RTKs in both HBMEC and HIBCPP cells | 101 |
| 3.3. | Listerial invasion <i>in vivo</i> | 105 |
| 3.3.1. | <i>Lm</i> is able to infect mice of both tested strains (BALB/cByJRj and C57BL/6JRj) and spreads systemically to various organs of immunosuppressed mice | 105 |
| 3.3.2. | Treatment with CD44v6-blocking peptides results in no observable difference in the bacterial load in organs of immunosuppressed C57BL/6JRj mice | 107 |
| 4. | DISCUSSION | 109 |
| 4.1. | Listerial infection in <i>in vitro</i> BBB/BCSFB cellular models | 109 |
| 4.1.1. | Role of Ecad and Met in cellular attachment and invasion by <i>Lm</i> | 110 |
| 4.1.1.1. | Role of CD44 in cellular attachment and invasion by <i>Lm</i> | 112 |
| 4.1.2. | Role of vimentin in cellular attachment and invasion by <i>Lm</i> | 113 |
| 4.2. | Cellular signaling in the CNS during listerial invasion | 113 |
| 4.2.1. | Effects of cellular attachment and invasion by <i>Lm</i> on gene transcription levels | 113 |
| 4.2.2. | Effects of cellular attachment and invasion by <i>Lm</i> on MAPK signaling pathways... | 114 |
| 4.2.3. | Role of dynamin in cellular attachment and invasion by <i>Lm</i> | 115 |
| 4.2.4. | RTKs in cellular attachment and invasion by <i>Lm</i> | 115 |
| 4.3. | Listerial infection in <i>in vivo</i> mouse models | 120 |
| 4.3.1. | Effect of immunosuppression on efficiency of oral infection by <i>Lm</i> in mice | 120 |
| 4.3.2. | Effect of CD44v6-blocking peptides on efficiency of oral infection by <i>Lm</i> in mice.. | 122 |
| 5. | CONCLUSION AND OUTLOOK | 123 |
| | REFERENCE LIST | 124 |

| | |
|------------------------|-----|
| ABBREVIATIONS..... | 153 |
| LIST OF FIGURES | 155 |
| LIST OF TABLES | 157 |
| ACKNOWLEDGEMENTS | 158 |

1. INTRODUCTION

1.1. *Listeria monocytogenes*

Listeria monocytogenes (*Lm*) is a ubiquitous gram-positive, facultative anaerobe with a high tolerance for various environmental hazards (low temperature, low pH and high salinity) primarily recognized as a food contaminant (Radoshevich and Cossart 2018). It is also an opportunistic pathogen able to easily enter (or exit) and survive within various phagocytic and non-phagocytic cells and a causative agent of listeriosis in humans and livestock (Radoshevich and Cossart 2018). Although the overall yearly number of globally reported cases of infection with *Lm* is relatively small, it is medically relevant due to high incidence of blood-borne systemic spread of the bacterium in infected people, particularly those who are immunocompromised (Radoshevich and Cossart 2018; Banović, Schroten, and Schwerk 2020).

1.1.1. Classification

Two main (and mutually compatible) systems of classification within the species are the traditional classification and the clonal complex (CC) classification. The traditional classification divides various listerial isolates and strains into lineages, serogroups and serotypes, while the CC classification distributes them into distinct CCs (Maiden et al. 1998; Maury et al. 2016). Four lineages of *Lm* have been universally recognized so far, as well as 4 PCR serogroups and 13 serotypes (Piffaretti et al. 1989; Wiedmann et al. 1997; Doumith et al. 2004; Orsi, den Bakker, and Wiedmann 2011; Maury et al. 2016). Lineages I and II contain most of the clinically relevant strains, and most of the strains used as models for listerial research (10403S, EGD and EGDe) belong to a single serovar of lineage II, 1/2a (Maury et al. 2016). Distribution of different listerial isolates into CC is based on the closeness of allelic profiles of seven predetermined housekeeping genes established through multilocus sequence typing (MLST) (Maury et al. 2016). In short, isolates and strains with at least six matching sequences were grouped together into a single CC. The older observation that there is a distinct difference between listerial isolates found in food and those found in infected people was confirmed by this study, which found that isolates belonging to each of the newly identified CCs were commonly found either in food (e.g. CC121, CC9), clinical samples (e.g. CC1, CC2, CC4 and CC6) or neither, but not in both (Maiden et al. 1998; Ragon et al. 2008; Maury et al. 2016). Curiously, the previously mentioned reference strains of *Lm* belong to CCs that are rarely found in clinical isolates: strains EGD and 10403S belong to CC7 – a relatively obscure CC in terms of occurrence – while the strain EGDe belongs to CC9, one of the more common CCs isolated from food (Maury et al. 2016).

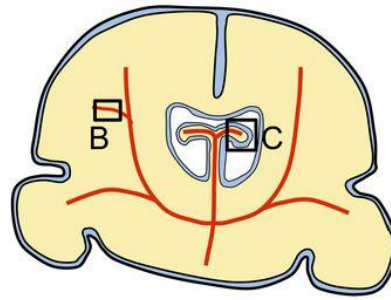
1.1.2. Pathology of listeriosis

Food primarily becomes contaminated by *Lm* when it comes into contact with human or animal feces containing the bacteria, as the gastrointestinal tract is both its most common habitat within human and animal hosts as well and the main point of entry. In the majority of immunocompetent people, *Lm* never spreads beyond the gut after entering the body, and will either colonize it asymptotically or induce a short-term gastroenteritis and be subsequently cleared from the organism (Schlech et al. 1983; Drevets and Bronze 2008; Bierne, Milohanic, and Kortebi 2018; Radoshevich and Cossart 2018). The pathogen is much more dangerous in immunocompromised people – especially those whose cell-mediated immune response is affected – since it is able to penetrate the gut barrier, invade and survive within circulating phagocytes and traverse the vascular system to disseminate into various organs of the body, with the ones preferred initially being liver and spleen (Drevets 1998; Drevets and Bronze 2008; Radoshevich and Cossart 2018; Banović, Schrotten, and Schwerk 2020). Due to inability of the immune system to fully clear the bacteria from the body within a reasonable amount of time, they might spread further into the central nervous system (CNS) and fetus (in pregnant women), which often results in long-term damage or even death (Drevets and Bronze 2008; Radoshevich and Cossart 2018; Banović, Schrotten, and Schwerk 2020).

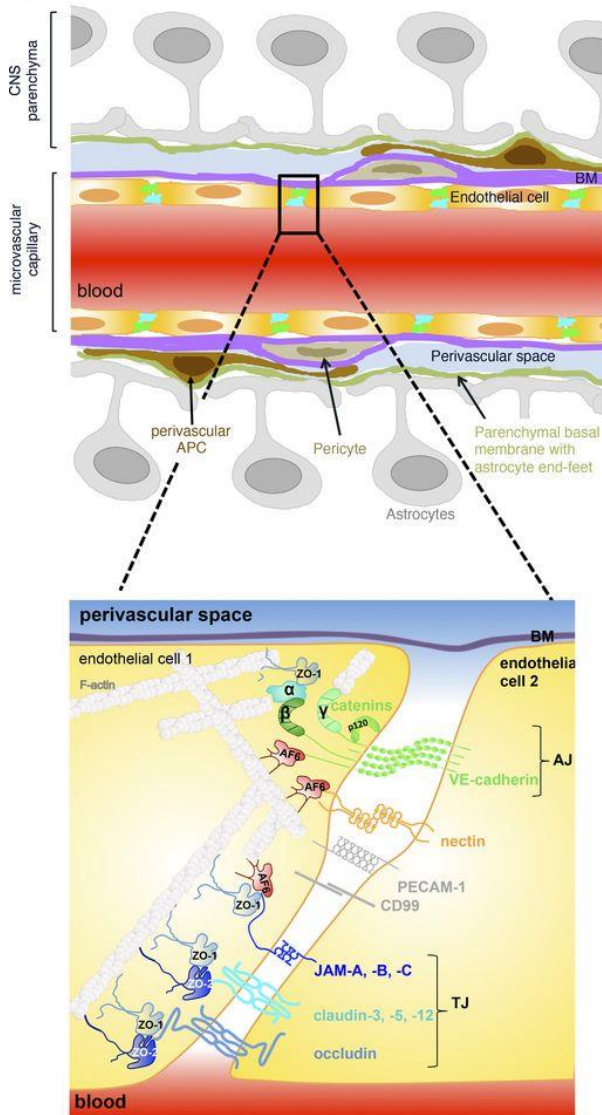
1.2. CNS barriers

The access to the CNS is tightly regulated and maintained by the barriers surrounding it. Two vascular barriers – the blood-brain barrier (BBB) and the blood-cerebrospinal fluid barrier (BCSFB) – and three tiers of non-vascular meningeal barriers – dura mater, arachnoid mater and pia mater – limit the traffic of molecules into and out of the brain and the spinal cord area, as well as normally prevent pathogens from entering them (Engelhardt, Vajkoczy, and Weller 2017; Castro Dias, Mapunda, et al. 2019) (refer to Figure 1 for depiction of vascular CNS barriers).

A



B



C

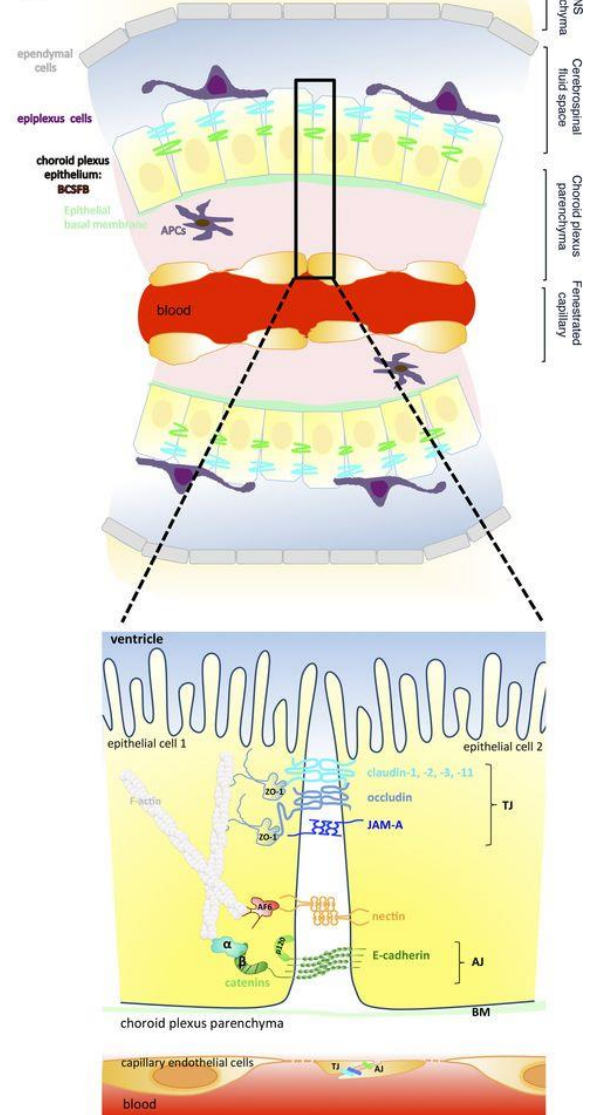


Figure 1. The architecture of vascular barriers of the brain – the BBB and the BCSFB. Depictions of both the BBB and the BCSFB contain more detailed representation of the build of their AJs and TJs. More details concerning the structures and molecules depicted in the figure can be found in their specific entries in the thesis. (A) Schematic depiction of the brain and the relative location of the BBB (marked with B) and the BCSFB (marked with C). (B) The build of the BBB: endothelial cells connected by adherens and tight junctions, supported by astrocytes, pericytes and basal membranes. (C) The build of the BCSFB: epithelial cells connected by adherens and tight junctions, supported by the basal membrane (figure taken from Tietz and Engelhardt 2015).

1.2.1. Intercellular junctions

The key characteristic shared by all CNS barriers is the presence of intercellular junctions – tight junctions (TJs) and adherens junctions (AJs) – which enable them to establish and maintain regulated traffic across the cellular layers conjoined by these junctions (Figure 1). Each barrier's full functionality also depends on the support of surrounding structures, both cellular and acellular (Engelhardt, Vajkoczy, and Weller 2017; Castro Dias, Mapunda, et al. 2019).

1.2.1.1. Tight junctions

The TJs create a tight bond between the cells, preventing paracellular trafficking of ions, molecules and freely moving cells (either own cells or pathogenic monocellular organisms), but also divide the plasma membrane of the cell into two separate parts, ensuring uneven distribution of surface components within it and resulting in the presence of two distinct cell sides – the apical and the basal/basolateral side (van Meer, Gumbiner, and Simons 1986; Huber, Egleton, and Davis 2001; Castro Dias, Mapunda, et al. 2019). The building and maintenance of the TJs is complex, requiring regulated interaction between the cytoskeleton, transmembrane proteins and the extracellular space, mediated by scaffolding proteins such as the membrane-associated guanylate kinase (MAGUK) proteins (especially zona occludens (ZO) proteins) as well as cell signaling (Bauer et al. 2014; Castro Dias, Mapunda, et al. 2019). The transmembrane proteins of the TJs are the axis around which the entire TJ is built, which is reflected in them being the TJ components with the largest representation in the literature. The three distinct groups of TJ-related transmembrane proteins are the claudins, the junctional adhesion molecules (JAM) and the TJ-associated MARVEL proteins (TAMP) (Castro Dias, Mapunda, et al. 2019).

Claudins are the largest of the three groups, with at least 27 proteins found in different tissue-specific combinations in various mammals (Anderson and Van Itallie 2009; Mineta et al. 2011). The protein chain of claudins begins with a relatively short intracellular N-terminus, continues with three loops (two extracellular ones with a short intracellular one between them) and ends with a longer intracellular C-terminus. The two extracellular loops (called ECL1 and ECL2) are involved in cell-to-cell interactions, especially interactions with the extracellular domains of claudins of neighboring cells, while the PDZ-binding motif on the C-terminus is responsible for interactions with the scaffolding proteins (Stiffler et al. 2007; Krause et al. 2009; Günzel and Yu 2013; Castro Dias, Mapunda, et al. 2019). Different claudins have subtly different functions reflected in their specific expression in different cellular barriers of the body, although they can be roughly divided into those involved in sealing the TJs and those involved in ion pore formation - unsurprisingly, the claudins found exclusively in the CNS barriers belong to the former (Amasheh et al. 2002; Anderson and Van Itallie 2009; Castro Dias, Mapunda, et al. 2019).

The JAM protein family consists of JAM-A, JAM-B and JAM-C, three immunoglobulin-like proteins with two extracellular Ig domains and a PDZ-binding motif located intracellularly on their C-terminus which binds them to the scaffolding proteins, similarly to what is found in claudins (Martín-Padura et al. 1998; Garrido-Urbani, Bradfield, and Imhof 2014). They are primarily known for their role in maintenance of the cellular polarity in endothelial and epithelial cells, although there are specific roles attributed to each of them in the TJs of different barriers (Ebnet et al. 2001; Castro Dias, Mapunda, et al. 2019).

There are three TAMP proteins found in the TJs: occludin (the first discovered TJ-specific transmembrane protein), MARVELD3 and tricellulin (Furuse et al. 1993; Hirase et al. 1997; Ikenouchi et al. 2005; Steed et al. 2009; Iwamoto, Higashi, and Furuse 2014). Although occludin was initially thought to be important for TJ formation, current understanding of its role ties it to the maintenance of the barrier function and its stability (Furuse et al. 1993; Hirase et al. 1997; Saitou et al. 2000; Iwamoto, Higashi, and Furuse 2014). The current exact place of the remaining two TAMPs in the operation of TJs remains vague, with them assumed to function as either backups or complementary to the occludin (Raleigh et al. 2010).

1.2.1.2. Adherens junctions

The role of the AJs is less clearly defined than the role of the TJs, but it can be described as supportive in regard to the TJs. Before the TJs can be formed, cells have to establish contact via the AJs, and the later complementary interplay of AJs and TJs is vital for the maintenance of the function of the cellular barriers (Tietz and Engelhardt 2015). The transmembrane protein component of the AJs – mirroring the claudins, the JAM and the TAMP proteins of the TJs – consists of the proteins belonging to the cadherin and IgSF CAM (cell adhesion molecule) superfamilies, more specifically to the classical cadherin family (belonging to the former) and the nectin family (belonging to the latter) (Indra et al. 2013; Tietz and Engelhardt 2015). The intracellular scaffolding component of the AJs that links the cadherins to both the MAGUK protein ZO-1 and the actin cytoskeleton is made up of the proteins of the catenin family (Gumbiner and McCrea 1993; Tietz and Engelhardt 2015).

Like most CAMs, classical cadherins possess a single transmembrane domain, with a relatively small part of the protein (and its C-terminus) being located intracellularly and most of its length (and N-terminus) being located extracellularly. The intracellular PDZ-binding domain tethers the cadherin to the catenins, while the extracellular domain and its constituent subdomains establish bonds with other cadherins (Meng and Takeichi 2009; Indra et al. 2013). The name cadherin is a portmanteau of “calcium-dependent adhesion”, which accurately describes the designated role of classical cadherins. Their extracellular cadherin domain contains five calcium-binding subdomains whose conformation changes on binding Ca^{2+} ions, allowing the interaction with both the cadherins on the surface of the

same cell (cis-binding) and those on the surface of the neighboring cells (trans-binding) in the presence of extracellular calcium, i.e. standard physiological conditions (Pokutta et al. 1994; Overduin et al. 1995; Meng and Takeichi 2009). This basic build is present in all 20+ members of the family, but the differences in the remainder of the extracellular domain structure lead to different binding preferences, with most classical cadherins favoring same-type (i.e. homophilic) interactions (Overduin et al. 1995; Meng and Takeichi 2009). Most of them show a tissue-specific expression (E-cadherin (Ecad) in epithelial cells, N-cadherin in neurons, VE-cadherin in the vascular endothelium, etc.), which – coupled with preferred homophilic binding – reinforces the assumed role of classical cadherins in the maintenance of tissue integrity (Takeichi 1988; Meng and Takeichi 2009; Indra et al. 2013)).

Following the CAM structure model, nectins sport a short cytoplasmic tail, a single transmembrane domain and an extracellular domain. In a manner similar to that of most junction transmembrane proteins, the intracellular part of a nectin protein contains a PDZ-binding motif which enables the interaction with the PDZ domain of the scaffolding proteins, while the extracellular part of the protein contains subdomains – specifically three immunoglobulin-like loops – aimed at intercellular interaction (Takai et al. 2008; Rikitake, Mandai, and Takai 2012). The nectin family counts only four members, although each has several splice variants with differing roles, tissue-specific expression patterns and structure which can deviate from the standard nectin build (Takai et al. 2008; Rikitake, Mandai, and Takai 2012). There are several scaffolding proteins that different variants of the four nectin family members can interact with. The one that is bound by all nectins (except for nectin-1 γ , which is a secreted protein) is afadin, an F-actin-binding protein that was also shown to interact with α -catenins, closing the AJ component interaction loop (Tachibana et al. 2000; Takai et al. 2008; Meng and Takeichi 2009; Rikitake, Mandai, and Takai 2012). Unlike the calcium-dependent cadherins, the nectins do not require calcium ions to function, belonging to the calcium-independent IgSF CAM superfamily (Rikitake, Mandai, and Takai 2012). The most striking difference between cadherins and nectins, however, is the one in interaction partner affinities: while the cadherins strongly favor homophilic transcellular interactions, the nectins prefer cell-to-cell interactions with different-type nectins (i.e. heterophilic interactions) (Yasumi et al. 2003; Meng and Takeichi 2009; Rikitake, Mandai, and Takai 2012). Interestingly, the trans-interactions between nectins of neighboring cells are much weaker than those of cadherins, indicating that they might be intended for more transient and modular contact (Koch et al. 1997; Ikeda et al. 2003). The role of the cadherins in the AJs appears to be directed towards the maintenance of homogenous tissue integrity, as evidenced by segregation of cells expressing different cadherins. Cells expressing different types of nectins are, on the other hand, able to establish more varied formations in mixed cell-type tissues, from the temporary junctions between Sertoli cells and spermatids in the testis to the precise mosaic pattern assemblies of hair cells and supporting cells

in the auditory sensory epithelium (Ozaki-Kuroda et al. 2002; Kelley 2006; Rikitake, Mandai, and Takai 2012). In contrast to classical cadherins which are used as entry points mainly by various microbial pathogens, nectins are primarily exploited by viruses: nectin-1 and nectin-2 are receptors for multiple herpesviruses – including HSV-1 and HSV-2 – while nectin-4 is a receptor for several morbilliviruses, most notably measles virus (Geraghty et al. 1998; Mühlebach et al. 2011).

1.2.2. CNS barrier composition

1.2.2.1. BBB

The BBB is the most investigated of the CNS barriers and mostly coterminous with the brain microvasculature, since its basic components are the monolayers of microvascular endothelial cells. They lack fenestrations and are tightly conjoined by TJs, with the exception of areas like the choroid plexus (CP) (Huber, Egleton, and Davis 2001; Wolburg and Paulus 2010; Engelhardt, Vajkoczy, and Weller 2017; Castro Dias, Mapunda, et al. 2019). As previously mentioned in context of CNS barriers in general, the functionality of the barrier is dependent on the communication and interaction of all cellular and acellular components of the barrier. In the case of the BBB, these would be the microvascular endothelial cells as the main player and the astrocytes, pericytes and the basal lamina as the supporting players, coming together to form the neurovascular unit (NVU) (Muioio, Persson, and Sendeski 2014) (Figure 1).

As the barrier-forming component of the BBB, the endothelial cells of the brain blood vessels have been studied extensively (Ge, Song, and Pachter 2005; Abbott, Rönnebeck, and Hansson 2006; Castro Dias, Mapunda, et al. 2019). Due to the specific conditions required by the brain for normal function – such as absence of pathogens, toxic compounds and metabolic products as well as unmitigated access to nutrients, especially glucose – the BBB endothelial cells sport many transmembrane proteins (mostly transporters or efflux pumps) which allow these requirements to be met, such as the main glucose transporter GLUT-1, whose strong expression in the BBB endothelium mirrors the high glucose consumption rate of the brain (Cornford, Hyman, and Swartz 1994; Daneman 2012). Some of these proteins are unique to the microvascular endothelium, such as Mfsd2a – the key enforcer of the low transcytosis rate in the BBB – or Pgp – the efflux pump that eliminates many complex compounds with potentially harmful effects from the brain, moving them to the blood (Daneman 2012; Ben-Zvi et al. 2014; Andreone et al. 2017). Another important feature of the BBB endothelium is the presence of a cobweb composed of glycoproteins and proteoglycans on its apical side known as the glycocalyx. It serves as an additional filter for the passage of large molecules, and its loss is believed to contribute to the pathological vascular changes such as atherogenesis (Nieuwdorp et al. 2005; Kutuzov, Flyvbjerg, and Lauritzen 2018).

The molecular composition of TJs varies across the range of different tissues in the body. When it comes to the TJ-related transmembrane proteins in the endothelial cells of the BBB, most of the diversity in terms of expression patterns comes from the claudins (Daneman et al. 2010) (Figure 1). The members of this family reported to be expressed in the microvascular endothelium are claudin-1, claudin-3, claudin-5, claudin-11, claudin-12, claudin-25 and claudin-27, although only claudin-5 was definitively proven to be crucial for the development of the TJs at the BBB (but not for its maintenance) (Nitta et al. 2003; Daneman et al. 2010; Vanlandewijck et al. 2018; Berndt et al. 2019; Sladojevic et al. 2019; Uchida et al. 2019). The roles and importance for the barrier function of the BBB of other listed claudins are still debated (although usually marked as support- or maintenance-oriented), and for some of them it is suspected (claudin-1 and claudin-12) or even outright confirmed (claudin-3) that they are not present in the endothelium of the BBB at all, mainly due to assumed cross-reactivity of antibodies commonly used for their detection (Wolburg et al. 2003; Zhang et al. 2014; Vanlandewijck et al. 2018; Castro Dias, Mapunda, et al. 2019; Castro Dias, Coisne, Lazarevic, et al. 2019; Castro Dias, Coisne, Baden, et al. 2019). All three members of the JAM family can be found in the microvasculature of the brain, but only JAM-A was confirmed to be important for the BBB, having a role in maintenance of the stability of the TJs (Padden et al. 2007; Wyss et al. 2012; Tietz et al. 2018). Finally, two of the three members of the TAMP family, occludin and tricellulin, round up the transmembrane section of the BBB TJs (Hirase et al. 1997; Iwamoto, Higashi, and Furuse 2014). The research data collected so far presents occludin as a regulatory player involved in calcium trafficking and stability maintenance rather than modeling of the TJs (Hirase et al. 1997; Saitou et al. 1998; Kuwabara et al. 2001; Murakami, Felinski, and Antonetti 2009; Iwamoto, Higashi, and Furuse 2014). Tricellulin is expressed exclusively at the tricellular junctions in the BBB (Iwamoto, Higashi, and Furuse 2014).

Proper function of the BBB is dependent on the support of the AJs as much as it relies on the closing of intracellular gaps by the TJs. While the composition of nectins in the AJs of the BBB can differ depending on the neighboring cells and tissues, their cadherin component is always VE-cadherin, due to them being formed between the cells of the microvascular endothelium (Carmeliet et al. 1999; Indra et al. 2013; Tietz and Engelhardt 2015; Castro Dias, Mapunda, et al. 2019) (Figure 1). As was previously mentioned, the formation of the AJs precedes and is required for the formation of the TJs (evidenced by the enhancing effect VE-cadherin has on the expression of claudin-5), as well as their maintenance (nectin-mediated cytoskeletal anchoring) (Takai et al. 2003; Taddei et al. 2008; Indra et al. 2013; Tietz and Engelhardt 2015).

1.2.2.2. BCSFB

The four CPs of the brain – located in lateral ventricles of the brain as well as the third and the fourth ventricle – are structures specialized for production of CNS-encircling cerebrospinal fluid (CSF), required for both the development and the maintenance of the CNS integrity and function (Wolburg and Paulus 2010; Damkier, Brown, and Praetorius 2013; Lehtinen et al. 2013; Engelhardt, Vajkoczy, and Weller 2017; Castro Dias, Mapunda, et al. 2019). Except for their role in production of the CSF, they also serve as a point of contact between the CNS and the blood. The microvascular endothelium of CPs is fenestrated, and thus not the main contributor to the barrier function of the BCSFB. Instead, the epithelium of the CP forms a TJ-conjoined monolayer acting as a BBB-like functional barrier between the blood and the CSF – the BCSFB, which also serves as one of the entry spots for immune cells traversing into the CNS (Wolburg and Paulus 2010; Damkier, Brown, and Praetorius 2013; Lun, Monuki, and Lehtinen 2015). When compared to the BBB, the main components of the BCSFB are located in the outer CP layer, specifically the cuboidal epithelial cells and the basal membrane underneath it, while the inner layer composed of fenestrated capillaries and connective tissue plays a much smaller role in the barrier function (Damkier, Brown, and Praetorius 2013; Lun, Monuki, and Lehtinen 2015) (Figure 1).

Due to its central role in the maintenance of the BCSFB and the production of CSF, the CP epithelium is the best characterized part of the CP (Wolburg and Paulus 2010; Damkier, Brown, and Praetorius 2013; Engelhardt, Vajkoczy, and Weller 2017; Castro Dias, Mapunda, et al. 2019). The existence of TJs and AJs ensures the polarity of the cellular layer, which is demonstrated by different molecular composition and appearance of the plasma membrane on the two sides of the cell. The apical surface of the CP epithelial monolayer sports microvilli and different types of cilia, which greatly increase the surface of the cells and serve as sensors and regulators of CSF flow (Banizs et al. 2005; Narita et al. 2010; Damkier, Brown, and Praetorius 2013). Each type of epithelial cells shows at least somewhat different, tissue-specific repertoire of transmembrane proteins, but there exists a general setup for how they are oriented, with same proteins always having either apical (towards the lumen) or basolateral (towards the blood) orientation across the cells (Mellman and Nelson 2008; Damkier, Brown, and Praetorius 2013). A unique feature of the CP epithelium is the inversion of this typical orientation of epithelial transmembrane proteins (despite the lack of obvious differences in polarity in comparison to other epithelial cells), which is assumingly related to its CSF-producing function (Damkier, Brown, and Praetorius 2013).

The TJs in the BCSFB formed between the CP epithelial cells are located close to the apical surface of the cells (Liddelow et al. 2012; Castro Dias, Mapunda, et al. 2019). Their build is similar to the TJs of

the BBB, with several differences in molecular composition (Figure 1). The claudins found in the BCSFB TJs are claudin-1, claudin-3, claudin-11 and, interestingly, claudin-2 – one of the claudins involved in ion pore formation (Wolburg et al. 2001; Steinemann et al. 2016; Castro Dias, Mapunda, et al. 2019). Unfortunately, there is little direct evidence for their role and involvement in the function of the BCSFB, with theories about them mostly being formed on the basis of the role these claudins have in other tissues (e.g. role of claudin-2 in Na⁺ transport in the kidney) (Gow et al. 1999; Furuse et al. 2002; Muto et al. 2010; Wolburg and Paulus 2010; Kooij et al. 2014; Castro Dias, Mapunda, et al. 2019; Castro Dias, Coisne, Lazarevic, et al. 2019). Furthermore, it is possible that even the presence of these claudins in CP epithelium cannot be assumed without doubt, due to the issues with cross-reactivity of anti-claudin antibodies (Castro Dias, Coisne, Lazarevic, et al. 2019). The only members of the JAM and TAMP families confirmed to be found at the BCSFB are JAM-A and occludin – their specific roles were not investigated in more detail, though, and it is assumed that they are similar to the ones they perform in the BBB TJs (Kratzer et al. 2012; Wyss et al. 2012; Tietz and Engelhardt 2015; Tietz et al. 2018; Castro Dias, Mapunda, et al. 2019).

The orientation of the AJs and the TJs with regard to the bloodstream differs between the microvascular endothelial and the CP epithelial cells. While in both cases the TJs are found on the apical side and the AJs basally/basolaterally to them, it is the side from which the bloodborne molecules and ions (and also pathogens) reach them that is different (i.e. from the apical side for the endothelial cells and from the basolateral side for the epithelial cells) (Figure 1). Thus, Ecad present in the CP epithelium is the first line of contact between the bloodborne substances and the junctional complexes of the BCSFB (Tietz and Engelhardt 2015; Vestweber 2015; Castro Dias, Mapunda, et al. 2019). When it comes to the nectins, two of them – nectin-1 and nectin-4 – have been noted as present in the epithelial cells of the CP, although it is possible that the others can be found in specific subpopulations of cells (Shukla et al. 2006; Indra et al. 2013; Pratakpiriya et al. 2017).

1.2.3. Models of CNS barriers

The investigation of the traits and disorders of the brain barriers requires a precise and reliable experimental model. In addition to the animal models (primarily mice, but also guinea pigs, rabbits and other animals) used especially in research of various pathological conditions, many groups tried to address this challenge over the years by creating *in vitro* models of varying complexity and properties (Redzic 2013; Ruck, Bittner, and Meuth 2015; Stone, England, and O'Sullivan 2019; Petersen et al. 2020).

1.2.3.1. BBB *in vitro* models

The first model presented for the investigation of the BBB were the *ex vivo*-derived brain microvessels, isolated through a multistep purification process (Joó 1985). While it is still a viable option, it largely fell out of favor with the rise of many cell-based *in vitro* setups, which are on average cheaper, easier to handle and more malleable (Ruck, Bittner, and Meuth 2015; Stone, England, and O'Sullivan 2019) (Figure 2). The cells used in these models are obtained from the autopsies performed on animals (e.g. mouse, rat) or humans, or from cell lines – immortalized, transformed or stem cell lines derived from the extracted cells (Lippmann et al. 2014). Each of these sources presents specific challenges which have to be considered and evaluated when setting up a cell-based model. Animal primary cells are more readily available than the ones obtained from humans, but there are enough differences between them in regard to both the sequence similarity of transmembrane proteins and their expression level that they cannot be considered a genuine substitute for human cells. Additionally, all *ex vivo* samples are short-lived post extraction and rarely last longer than a few passages, which presents a logistical problem due to decreased supply options. Transformed cell line-derived cells, on the other hand, are comparatively both long-lived and abundant, but usually do not maintain the full set of characteristics typical of the cells they originate from, and tend to lose more of them as they move into later passages (Warren et al. 2009; Ruck, Bittner, and Meuth 2015; Zhang et al. 2016; Stone, England, and O'Sullivan 2019).

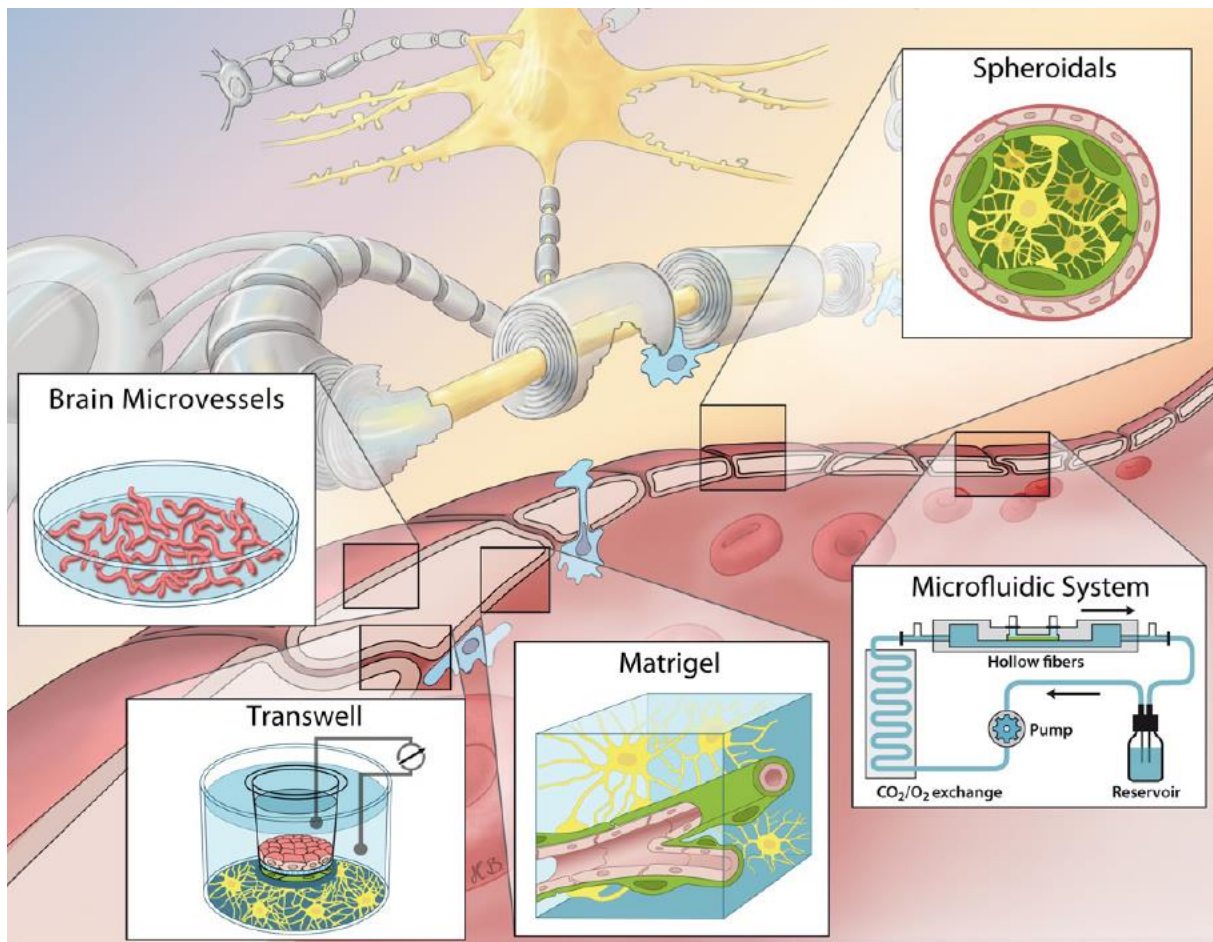


Figure 2. Overview of the types of models of the BBB (and partially the BCSFB), brain microvessel-based and the more commonly used cell-based models: 2D (transwell filter-based) and 3D (matrigel-, microfluidic system- or spheroid-based) (figure taken from Ruck, Bittner and Meuth 2015).

The cellular models designed for research of the BBB can be broadly split into 2D (transwell filter-based) and 3D (extracellular matrix- (ECM), spheroid- and microfluidic system-based) models (Ruck, Bittner, and Meuth 2015; Stone, England, and O'Sullivan 2019) (Figure 2). The most basic, cheapest and easiest to both set up and deal with is the monoculture transwell filter-based model, which utilizes microvascular endothelial cells (from any of the previously mentioned source) to form a monolayer on the surface of the filter (Borges et al. 1994; Hartz, Miller, and Bauer 2010; Bittner et al. 2013; Ruck, Bittner, and Meuth 2015; Stone, England, and O'Sullivan 2019). It allows the inspection of the cell barrier integrity (e.g. via TEER measurement), cell polarity and the passage across (or through) the barrier, and is one of the most commonly used models in research of transmigration of immune cells and pathogens across the BBB (Ruck, Bittner, and Meuth 2015; Srinivasan et al. 2015; Stone, England, and O'Sullivan 2019). The primary limitation of the model is the lack of other cell types found in the NVU and the resulting decreased accuracy of the BBB depiction (also reflected in relatively low barrier integrity) (Naik and Cucullo 2012). Introduction of one or more other BBB-relevant cell types – at first

astrocytes, but also pericytes and later neurons – was one of the attempted solutions to address this issue, with generally promising results (Gaillard et al. 2001; Nakagawa et al. 2009; Lippmann et al. 2014; Thomsen, Burkhart, and Moos 2015; Wang et al. 2015; Appelt-Menzel et al. 2017; Stone, England, and O'Sullivan 2019).

Even with this addition, the fact that the transwell filter-based models cannot simulate the entire 3D structure of the NVU and therefore gradually lose BBB-specific properties remained, which prompted the development of more complex models, collectively referred to as 3D models (Lyck et al. 2009; Urich et al. 2012; Urich et al. 2013). The primary representatives of the 3D-oriented models are the ECM- and spheroid-based models, where the cells (microvascular endothelial cells, astrocytes and pericytes) self-assemble into 3D structures, with the primary difference being the presence of ECM-simulating matrix in the former and the lack of it in the latter (Davis, Koh, and Stratman 2007; Urich et al. 2013; Ruck, Bittner, and Meuth 2015; Cho et al. 2017; Nzou et al. 2018). While the ECM-based models sport both the vessel-like structures formed by the cells in the matrix and the option to investigate the interaction between the cells and the ECM-simulating substance in which they are embedded, they are relatively expensive and difficult to establish. Additionally, the matrix used to simulate the ECM is still only an approximation of the real ECM, with many interactions impossible to observe within the scope of this model (Davis, Koh, and Stratman 2007; Ruck, Bittner, and Meuth 2015). The spheroid-based models, on the other hand, present cells self-assembled into spheroid structures with a functional barrier, with astrocytes and pericytes located inside of the spheroids and surrounded by endothelial cells. Although both the price and the complexity of setup is lower in comparison to ECM-based models, they are still relatively hard to manipulate and unable to simulate the shear stress exerted on the walls of the blood vessels by the blood, similar to the ECM-based models (Urich et al. 2013; Ruck, Bittner, and Meuth 2015; Cho et al. 2017; Nzou et al. 2018). Lastly, the microfluidic system-based models are the most complex currently available type of cell-based models for the study of the BBB, trying to incorporate the benefits of other 3D models with the added feature of blood flow simulation (Ruck, Bittner, and Meuth 2015; van der Helm et al. 2016; Oddo et al. 2019; Stone, England, and O'Sullivan 2019). In the initial approach, the cells were seeded by perfusion on the insides of the microfluidic ECM-protein coated glass or plastic channels, where they could establish a functional 3D simulacrum of the BBB. The flow of the medium – generated by the computer-controlled pump – emulated the flow of blood and the shear stress it induces in the cells (Toh et al. 2007; Ruck, Bittner, and Meuth 2015). The newer variants of the model aim to realize the “organ-on-a-chip” concept for the BBB and/or the NVU, where the cells are seeded and grown on cell culture inserts which are then incorporated into the assembly of the microfluidic system (van der Helm et al. 2016; Wang, Abaci, and Shuler 2017; Oddo et al. 2019; Stone, England, and O'Sullivan 2019; Campisi et al.

2021). Although they appear to be the most promising type of 3D model in terms of faithful replication, all microfluidic system-based models are still hindered by being costly, delicate and requiring experienced users for proper handling (Ruck, Bittner, and Meuth 2015; Stone, England, and O'Sullivan 2019).

1.2.3.2. BCSFB *in vitro* models

The majority of the currently available *in vitro* models for the BCSFB are cell-based, with the exceptions mainly focusing on extraction and cultivation of whole CPs from animal brains (Redzic 2013; Inoue et al. 2015; Petersen et al. 2020) (Figure 2). Naturally, all issues that apply to the selection of the material source (cells vs. whole organs, animal vs. human cells/tissue and primary vs. transformed cells/tissue) in the setup of the BBB models also apply to the selection of the cell source in the setup of the BCSFB models (Redzic 2013; Petersen et al. 2020).

The cell-based models are either cell culture plate-based or transwell filter-based (Redzic 2013; Petersen et al. 2020). The transwell filter-based models have a stronger representation in the more recent literature due to being much more relevant for the investigation of the transport across the BCSFB. Researchers have proposed cells from different sources as the basis for their variant of the model over the years, including primary cells from animal (pig, rat, sheep) CP epithelium and cells from cell lines from CP-origin derived transformed tissue – primary human CP epithelial cells are notably rare as a source due to the scarcity of the cellular material as well as the variation between the samples obtained from different individuals (Baehr, Reichel, and Fricker 2006; Redzic et al. 2006; Schwerk et al. 2012; Monnot and Zheng 2013; Redzic 2013; Lazarevic and Engelhardt 2016; Lauer et al. 2019).

As was the case with the BBB models, the limitations of the 2D models prompted the development of more complex simulations to investigate the BCSFB, with the models developed so far being either CP explant- or organoid-based (Lancaster and Knoblich 2014; Watanabe et al. 2017; Petersen et al. 2020). In the case of the former, the model is based on the pieces of the adult mouse CP epithelium which are able to self-organize in the medium into 3D spheroid structures possessing a lumen and a functional barrier activity, similar to the spheroid-based models described for the BBB (Petersen et al. 2020). The latter model is derived from the induced pluripotent stem cells (PSC) from human skin, which were – through careful application of required growth factors and maintenance of required growth conditions in an ECM-like matrix – guided to differentiate into neural tissue able to self-organize into brain-resembling organoids (Lancaster and Knoblich 2014; Watanabe et al. 2017). The primary advantages and limitations of these two models are reminiscent of those described for the ECM-based and spheroid-based BBB models. The explant-based model is cheaper, simpler to establish, handle and maintain and almost exclusively compiled of epithelial CP cells, but is limited in the size of

formed structures and does not provide the possibility to assess the interaction of the CP epithelium with the other cell types found in its physiological surroundings. The organoid-based model, on the other hand, provides a simplified (although still very complex) approximation of the entire brain (enabling the investigation of its development and growth as well as pathological changes), but is expensive and time-consuming to grow, often resembles fetal rather than adult tissue and lacks properly formed vasculature (Petersen et al. 2020).

1.3. Listerial CNS invasion routes

A lot of investigative effort has been directed at the ability of *Lm* to infiltrate various organs of the body of both humans and various livestock species since its discovery, but the proper understanding of the entry into the brain remains elusive (Schlech et al. 1983; Drevets and Bronze 2008; Dando et al. 2014; Radoshevich and Cossart 2018; Banović, Schrotten, and Schwerk 2020). Research conducted so far as well as comparison with other brain-invading bacterial pathogens proposes two possible (and not mutually exclusive) routes of entry – the blood-borne (hematogenous), following the penetration of the gut and establishment of bacterial reservoirs in the liver and the spleen; and the nerve-borne (neurogenous), using the cranial nerves for brain access (Figure 3) (Berche 1995; Greiffenberg et al. 1998; Drevets, Jelinek, and Freitag 2001; Drevets, Leenen, and Greenfield 2004; Drevets and Bronze 2008; Kim 2008; Karlsson et al. 2017; Pägelow et al. 2018; Herold, Schrotten, and Schwerk 2019; Schlech 2019; Precht et al. 2020; Wei, Bao, and Fan 2020). The former usually results in meningitis (sometimes difficult to distinguish from meningoencephalitis) and the latter in rhombencephalitis. Interestingly, this has led to speculation that different routes of CNS entry might be preferred in humans in comparison to domesticated ruminants, since the most common manifestation of neurolisterosis in humans is meningitis in contrast to brain abscesses and rhombencephalitis, which are the default form the disease takes in cattle, goats and sheep (Oevermann, Zurbriggen, and Vandeveldel 2010; Disson and Lecuit 2012).

1.3.1. Hematogenous route

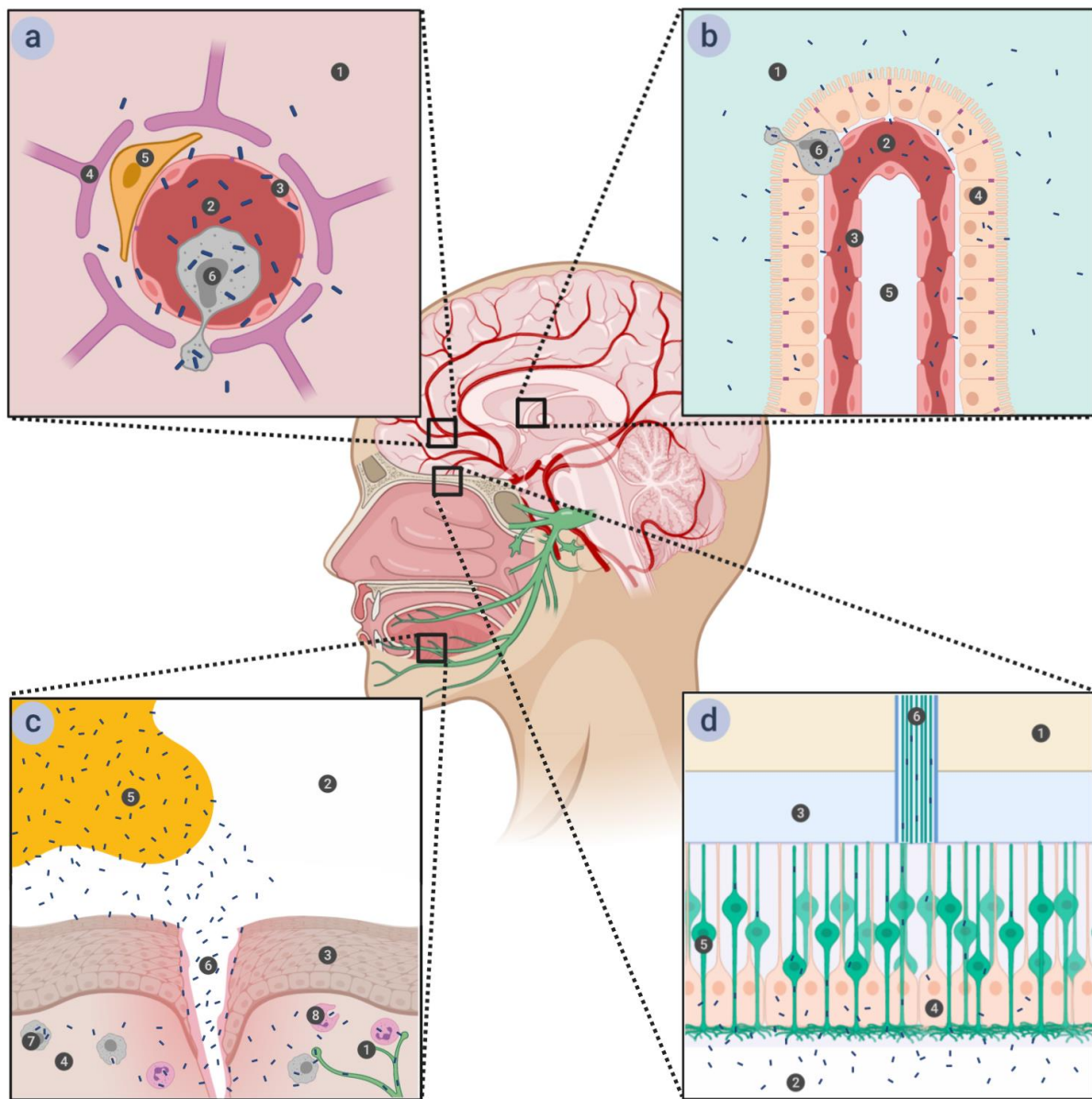


Figure 3. Different possible entry points for listerial CNS invasion. (a) Invasion across the BBB. (b) Invasion across the BCSFB. (c) Invasion through the cranial nerves. (d). Invasion through the olfactory epithelium (figure taken from Banovic, Schrotten and Schwerek 2020).

As previously mentioned, the hematogenous route of entry into the CNS requires listerial presence in the blood, assured by previous colonization of and persistence within the liver and the spleen. Due to the envelopment of the CNS components by the brain barriers, the only possible way for *Lm* to enter the brain from the blood is by crossing those barrier that border the bloodstream – the BBB and the BCSFB – either by direct action on the behalf of the bacteria or concealed within the infected phagocytes (“Trojan horse” entry) (Berche 1995; Drevets et al. 1995; Drevets and Bronze 2008; Disson

and Lecuit 2012; Gründler et al. 2013; Dando et al. 2014). It is highly likely that *Lm* does indeed utilize the hematogenous route of invasion, as many researchers were able to demonstrate that it can efficiently invade and pass through the monolayers of microvascular endothelium- (e.g. human brain microvascular endothelial cells (HBMEC)) and CP epithelium-derived cells (e.g. human choroid plexus papilloma (HIBCPP) cells) (Greiffenberg et al. 1998; Bergmann et al. 2002; Gründler et al. 2013; Dinner et al. 2017; Ghosh et al. 2018). Interestingly, it was also reported that the antibodies present in the adult human serum inhibit the entry of *Lm* into the HBMEC cell line, reflecting the clinical data that depicts neurolisteriosis as being encountered primarily in unborn or newborn children or immunocompromised adults (Hertzog et al. 2003). Since mice are the most commonly utilized animal infection model for listerial invasion, the majority of *in vivo* studies aimed at CNS penetration were performed in them, with results indicating the entry into the brain in both direct and “Trojan horse” variants (Prats et al. 1992; Drevets 1999; Ghosh et al. 2018).

1.3.2. Neurogenous route

The neurogenous route of entry into the brain – assumed to be more common in animals than in humans – relies on the bypassing of the brain barriers by penetration into and retrograde axonal transport through the nerves that connect directly to the brain. Curiously, in contrast to the hematogenous route of entry, the neurogenous route of entry does not seem to require compromised immunocompetence of the host (Drevets and Bronze 2008; Disson and Lecuit 2012; Dando et al. 2014; Banović, Schroten, and Schwerk 2020). The primary point of bacterial entry are the small lacerations in oral cavity generated through eating, where the bacteria come into contact with the host’s phagocytes (either resident or recruited), infect them and use them to reach the endings of the cranial nerves (often the trigeminal nerve) and eventually reach the brain stem (Disson and Lecuit 2012; Dando et al. 2014; Karlsson et al. 2017). The concept of neurogenous route was demonstrated in many publications that reported the ability of *Lm* to infect and spread through and via the primary neuronal cell cultures and the neuron-derived cell lines, as well as other neuron-containing *in vitro* models (e.g. brain-slice cultures) (Dons et al. 1999; Jin et al. 2001; Parra, Baquero, and Perez-Diaz 2007; Guldemann et al. 2012; Rupp et al. 2017). Since listerial rhombencephalitis is naturally occurring in ruminants and presents a higher health risk for them than for humans, most of the studies related to neurogenous route of CNS invasion were performed in them, succeeding to confirm the trigeminal nerve-based interpretation (Oevermann, Zurbriggen, and Vandeveld 2010; Karlsson et al. 2017). Experiments performed in mice infection models confirmed the findings of ruminant-focused studies, in one case reporting a direct connection between the side of the face where the facial muscles or trigeminal nerve endings were inoculated with the bacteria and the side of the brain stem first showing the symptoms of rhombencephalitis (Antal et al. 2001; Jin et al. 2001). A special case of neurogenous route entry via

the olfactory epithelium was described by Pägelow and colleagues in a study performed on newborn mice, where the mice inoculated by *Lm* nasally developed neurolisteriosis manifesting as meningitis. The authors consequently suggested that the inhalation of the *Lm*-contaminated fluid in the mother's vaginal tract might be an important – if not the main – cause of listerial meningitis in newborns (Pägelow et al. 2018).

1.4. Virulence factors of *Listeria monocytogenes*

Lm has a large number of virulence factors (VF) ranging from cell type-specific adhesins to the functionally unusual cytolysin, listeriolysin O (LLO) (Bierne et al. 2007; Camejo et al. 2011; Radoshevich and Cossart 2018; Banović, Schroten, and Schwerk 2020). The VFs presented in the introduction of this thesis are those known (or suspected) to participate in the invasion of CNS, with special focus being on the ones which were investigated within the scope of this project (Figure 4).

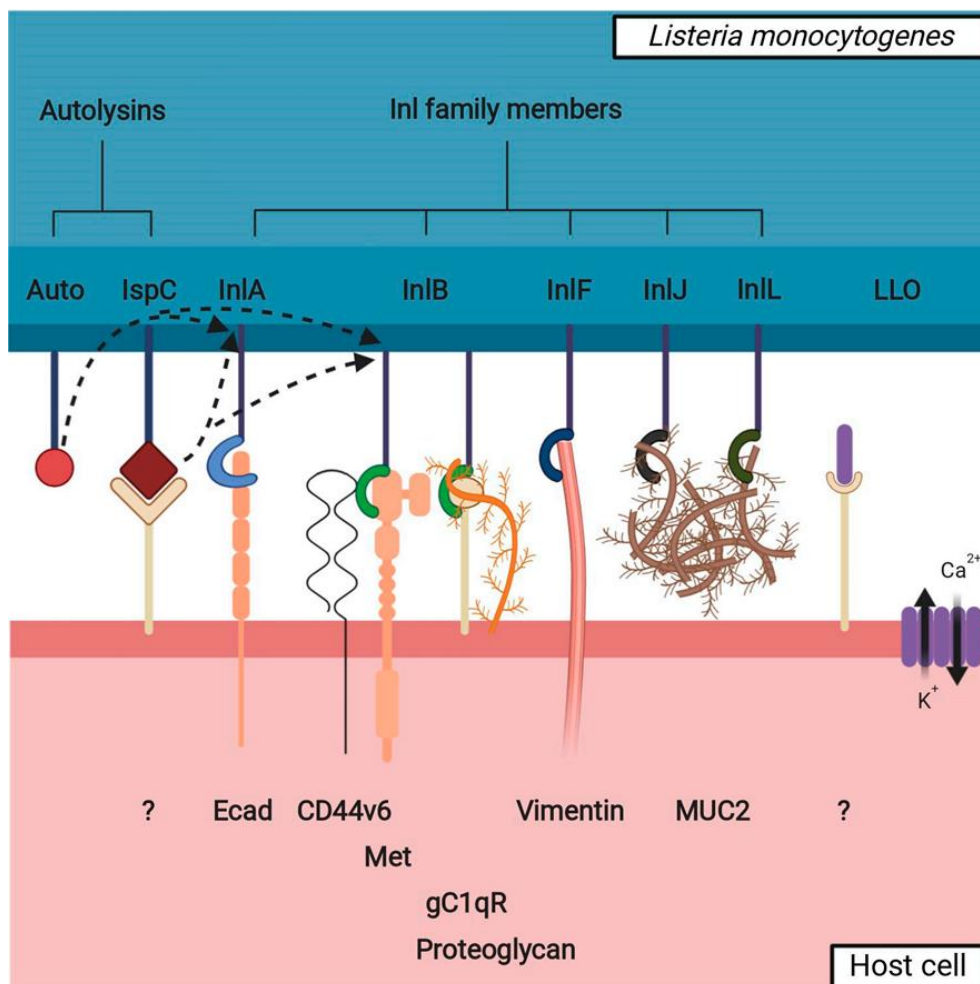


Figure 4. A graphical representation of interactions between *Lm* (in blue) and the CNS-localized, non-phagocytic host cell (in pink), mediated by listerial VF. All VF known or hypothesized to be involved in invasion are shown and named on the figure, as well as their interaction partners on the cell, if they have any. Autolytic interactions are labeled with dotted arrows and unknown interaction partners with a question mark (figure taken from Banovic, Schroten and Schwerk 2020).

1.4.1. Internalins

Internalins (InI) are a protein family of listerial VF characterized by the presence of leucine-rich repeat (LRR) domains and Sec-dependent N-terminal signal peptides (Bierne et al. 2007; Radoshevich and Cossart 2018). It is hard to establish the exact number of InIs and InI-like proteins within the entire species since they can vary widely between various isolates and strains (of which many are still poorly described), but the number usually listed in the literature is 25+, that being the number of currently known InI family members in *Lm* strain EGDe (Tsai et al. 2006; Bierne et al. 2007; Camejo et al. 2011; Radoshevich and Cossart 2018; Harter et al. 2019).

The comparable basic structure of all InIs is consistent with their purported role as adhesins and invasins – multiple copies of LRR binding motifs (normally found in eukaryotes) carried by each InI enable them to bind to host cell proteins while the possession of the signaling peptide confirms that these proteins are destined for extracellular space (Kobe and Kajava 2001; Bierne et al. 2007). The number of copies of LRR between different InI family members varies, ranging from three repeats in Lmo2445 to 28 repeats in InIL (Kobe and Kajava 2001; Bierne et al. 2007). There is also diversity in bonds linking the InIs to the bacterial surface, with three main observed variants. The first – and the most common – is the covalent bond with peptidoglycan (e.g. InIA) that InIs possessing an LPXTG motif on their C-terminus are subjected to, establishing these InIs as bacterial surface proteins. The second, present in a much smaller number of InIs, is a loose, non-covalent connection with a bacterial wall component (e.g. lipoteichoic acid (LTA)) through one of several specific C-terminal domains (e.g. GW repeat domain in InIB) that can be broken under certain conditions, leading to these InIs being present both in the bound form and in the free form. The last variation is a lack of any bond at all (e.g. InIC) due to the InI in question not containing any cell wall-anchoring domains, with these InIs being secreted into the space surrounding the bacterial cell (Bierne et al. 2007).

Despite the fact that the sequence of many InIs and InI-like proteins is known, their function and exact roles are still not very well characterized, with the exception of InIA and InIB. The genes encoding for these two proteins are located on the *inIAB* operon, which can be transcribed either fully (resulting in translation of the entire product and post-translational separation into InIA and InIB) or partially (resulting in translation of only InIA) (Gaillard et al. 1991). Although their known mechanisms and exact functions differ, both are essential for successful invasion of *Lm* into different types of non-phagocytic cells through induction of zipper-type endocytosis (Lingnau et al. 1995; Greiffenberg et al. 1998; Parida et al. 1998). Several other InIs have been at least partially characterized, where the function and the role were either deduced through identification of host cell interaction partners (InIC, InIF, InIK and InIP) or hinted at based on the available information and experimental data (InIH, InIJ, InIL) (Bergmann

et al. 2002; Bierne et al. 2007; Lindén et al. 2008; Rajabian et al. 2009; Dortet et al. 2011; Faralla et al. 2018; Ghosh et al. 2018). To complicate the matters further, many InI family members interact in ways that are not yet fully understood. It was demonstrated that single deletions or deletions of several InI family-coding genes resulted in *Lm* mutant strains that behaved differently in *in vitro* and *in vivo* models not only in regard to the wild type bacteria but also compared to each other. Most deletions and combinations of deletions resulted in various levels of inhibited pathogenicity, but some even resulted in hyperinvasiveness and increased virulence (Bergmann et al. 2002).

1.4.1.1. InIA

Commonly referred to simply as internalin and a namesake of the whole InI protein family, InIA is a surface-exposed protein rooted in the listerial cell wall by a covalent bond with the peptidoglycan layer. Ecad, a transmembrane protein normally found as a part of AJs in barrier-forming epithelial cells, was identified as its only binding partner on the surface of human cells (Gaillard et al. 1991; Mengaud et al. 1996; Drevets and Bronze 2008; Radoshevich and Cossart 2018). Importantly, InIA was markedly unable to bind N-cadherin (expressed by neuronal cells) and VE-cadherin (expressed by endothelial cells) (Mengaud et al. 1996; Tsai et al. 2006; Bonazzi, Lecuit, and Cossart 2009).

Ecad possesses an intracellular domain that enables it to – following activation – recruit the cellular actin-rearranging machinery, so that it can be internalized and shuffled between the apical and the basolateral sides of the cell – *Lm* can hijack this process to initiate a zipper-type endocytosis and infiltrate the cell (Pizarro-Cerdá, Kühbacher, and Cossart 2012; Kim et al. 2021). The binding of InIA to Ecad triggers the activation of Src – a tyrosine kinase – which then proceeds to phosphorylate Ecad and clathrin heavy chain, and phosphorylated Ecad in turn recruits Hakai – an ubiquitin ligase – which leads to ubiquitination of Ecad (Sousa et al. 2007; Bonazzi et al. 2008; Bonazzi et al. 2011; Pizarro-Cerdá, Kühbacher, and Cossart 2012). Phosphorylation of both Ecad and clathrin heavy chains as well as ubiquitination of Ecad is a prerequisite for recruitment of proteins involved in the clathrin-mediated endocytosis, including clathrin and dynamin, and leads to aggregation of Ecad at the site of bacterial contact (Veiga et al. 2007; Bonazzi et al. 2011; Pizarro-Cerdá, Kühbacher, and Cossart 2012). All of this is ultimately followed by Arp2/3-initiated actin polymerization in two waves, with the first wave being mediated by cortactin, dynamin and Src kinase, and the second wave by interactions between Ecad, α and β catenins and the Arp2/3 complex itself (Lecuit et al. 2000; Seveau et al. 2004; Sousa et al. 2007; Bonazzi et al. 2011; Pizarro-Cerdá, Kühbacher, and Cossart 2012).

Understandably, InIA has a demonstrable role in cellular adhesion and invasion models only in those cell lines that express Ecad (derived mainly from epithelial cells), where the *Lm* Δ *inIA* deletion mutant shows strong decrease in adherence to and invasion into the cells (Gaillard et al. 1991; Dramsi et al.

1993; Lingnau et al. 1995; Mengaud et al. 1996; Lecuit et al. 2004; Gründler et al. 2013; Phelps et al. 2018). Although InIA has a dominant role in anchoring of the bacteria to the cell's surface, it is not sufficient on its own for efficient invasion, and is instead dependent on various other listerial VF, from other InI family members – such as InIB, InIC and members of the InIGHE cluster – to LLO, depending on the cell line in question (Bergmann et al. 2002; Gründler et al. 2013; Phelps et al. 2018).

When observing the traversal across the epithelial barriers of the human body, InIA was shown to be indispensable for the crossing of the gut barrier, with the argument being strengthened by the fact that there are barely any clinical isolates without a complete *inIA* part of the *inIAB* operon (Lingnau et al. 1995; Lecuit et al. 2001; Jacquet et al. 2004). Interestingly, a *Lm ΔinIA* deletion mutant was strongly attenuated only in orally infected mice but not in those infected intravenously, indicating that InIA is less relevant once the bacteria enter the bloodstream (Lecuit et al. 2001). An interdependent mode of entry – where both InIA and InIB are required for the fully efficient invasion but either of them can contribute to a partially efficient one alone – was described for the fetoplacental barrier and assumed (but not yet confirmed *in vivo*) for the BCSFB (Prats et al. 1992; Disson et al. 2008; Gründler et al. 2013; Schwerk et al. 2015; Dinner et al. 2017). InIA likely plays only a minor (if any) role in the traversal across the BBB, probably due to the lack of Ecad expression in the brain microvascular endothelium which comprises it (Greiffenberg et al. 1998). Curiously, altered structure of Ecad between different species resulted in species specificity of InIA-Ecad interaction – while InIA binds strongly to human Ecad (and Ecad of species with the same composition of the InIA binding place on Ecad, e.g. guinea pig Ecad), it can barely bind to Ecad of mice or rats (Lecuit et al. 1999). The resistance of mice and rats to InIA-mediated (mainly oral) infection by *Lm* is interesting from an evolutionary point of view, but should also be considered when utilizing mouse- or rat-derived cellular or *in vivo* infection models.

1.4.1.2. InIB

InIB is the second of two InI proteins coded by the *inIAB* operon. As mentioned earlier, its attachment to the bacterial surface is non-covalent and reversible, mediated by interaction of GW modules located in the C-terminus of the protein with LTA in the bacterial cell wall – this results in approximately half of the total InIB expressed on the bacterial surface being released as free-form InIB (Dramsai et al. 1995; Jonquières et al. 1999; Marino et al. 2002; Bierne et al. 2007; Pizarro-Cerdá, Kühbacher, and Cossart 2012). Unlike InIA – which can bind to only a single receptor via its LRR domain – InIB has several known (and possibly more as-of-yet unknown) targets within the human body that can be bound by both its LRR domain and GW modules, resulting in a much broader range of cell types and tissues it can be crucial for invading into (Jonquières, Pizarro-Cerdá, and Cossart 2001; Marino et al. 2002; Pizarro-Cerdá, Kühbacher, and Cossart 2012). The N-terminal side of the protein – where the LRR domain is

located – was shown to interact with the widely expressed receptor for hepatocyte growth factor (HGF), receptor tyrosine kinase (RTK) Met (also known as hepatocyte growth factor receptor (HGFR)), as well as with secreted intestinal mucin, MUC2 (Shen et al. 2000; Jonquière, Pizarro-Cerdá, and Cossart 2001; Marino et al. 2002; Lindén et al. 2008; Pizarro-Cerdá, Kühbacher, and Cossart 2012). The C-terminal side of the protein (the side attached to LTA by the GW modules), can – following the dissociation from LTA – interact with cell surface glycosaminoglycans (GAG) (such as heparin) and the complement component 1q-binding proteins (gC1qR) (Braun, Ghebrehwet, and Cossart 2000; Jonquière, Pizarro-Cerdá, and Cossart 2001; Marino et al. 2002; Pizarro-Cerdá, Kühbacher, and Cossart 2012).

The only interaction partner of InIB implicated as an active participant in listerial invasion events so far is Met (Braun et al. 1999; Shen et al. 2000; Pizarro-Cerdá, Kühbacher, and Cossart 2012). Although the underlying roles of Ecad (the receptor for InIA) and Met differ, they are similar in their possession of domains capable of conveying a downstream signal (leading to their internalization by the cell), and also similar in the way in which *Lm* subjugates them to enter the cell (Mengaud et al. 1996; Shen et al. 2000; Pizarro-Cerdá, Kühbacher, and Cossart 2012). The binding of InIB to Met initiates dimerization and then autophosphorylation of Met – similar to what happens following the binding of its intended interaction partner, HGF (Shen et al. 2000; Ferraris et al. 2010; Pizarro-Cerdá, Kühbacher, and Cossart 2012). Phosphorylated Met subsequently recruits ubiquitin ligase Cbl and becomes ubiquitinated, priming itself for further steps in internalization of the receptor: attraction of the clathrin endocytosis-related proteins and the first wave of actin polymerization via the Arp2/3 complex (Veiga and Cossart 2005; Pizarro-Cerdá, Kühbacher, and Cossart 2012). The second wave of actin polymerization downstream of Met is more complicated, with phosphoinositide 3-kinase (PI3K) being the key player interacting with multiple different Rho GTP-ases (e.g. Cdc42) and actin rearrangement-associated proteins (e.g. N-WASP) in a combined effort which leads to Arp2/3 complex activation (Ireton et al. 1996; Bierne et al. 2001; Seveau et al. 2004; Bierne et al. 2005; Bosse et al. 2007; Jiwani et al. 2012; Pizarro-Cerdá, Kühbacher, and Cossart 2012). Curiously, a downstream signal initiated by binding of its ligand, HGF, cannot be conveyed by Met unless it is also in direct contact with its co-receptor, CD44v6 (Orian-Rousseau et al. 2002; Jung et al. 2009). Whether the same is true for the signal initiation by binding of InIB – which functionally mimics HGF but has a different binding spot – remains to be inspected, since the reported results of experiments conducted so far are controversial (Braun et al. 1999; Marino et al. 1999; Jung et al. 2009; Dortet et al. 2010).

When taking into account that it has multiple binding partners (with Met being the most established one) which are expressed by a broad range of cells in the body, it is unsurprising that InIB was identified

as an important factor for listerial invasion into many cell lines of various origin (such as endothelium-, epithelium-, fibroblast- and hepatocyte-derived cell lines), including those cell lines that express Ecad (Dramsi et al. 1995; Lingnau et al. 1995; Braun, Ohayon, and Cossart 1998; Greiffenberg et al. 1998; Braun et al. 1999; Pizarro-Cerdá, Kühbacher, and Cossart 2012). Unlike InIA, however, InIB seems to be an invasion-related VF rather than an adhesion-related one, and *Lm* likely depends on other VFs for adhesion (Jonquière et al. 1999; Pizarro-Cerdá, Kühbacher, and Cossart 2012).

InIB presumably plays a role in penetration of all cellular barriers found in the human body. This role can be supportive rather than active, as is the case in the penetration of the gut barrier – although InIA serves a dominant role in bacterial internalization at the tips of intestinal villi, InIB enhances it by speeding up the uptake of the junction proteins (Pentecost et al. 2006). The results of *in vitro* experiments indicate that the listerial invasion of BCSFB and fetoplacental barriers depends on at least a concerted effort of InIA and InIB, and more likely involves several other VFs as well, such as InIP in case of the latter (Prats et al. 1992; Disson et al. 2008; Gründler et al. 2013; Schwerk et al. 2015; Faralla et al. 2016; Dinner et al. 2017). The *in vitro* test done on the brain microvascular endothelium cell line HBMEC – which does not express Ecad but does express Met – where *Lm* Δ *inIB* deletion mutant had a major decrease in invasion rate in comparison to the wild-type bacteria demonstrated the importance of InIB for crossing of the microvascular endothelium which comprises the BBB (Greiffenberg et al. 1998). The answer to the puzzle of BBB invasion might not be so simple – there are publications that dispute the preeminence of InIB for BBB penetration, such as the one by Ghosh and colleagues, which points at InIF as the key factor instead (Ghosh et al. 2018). Species specificity in receptor binding similar to the one shown for InIA was also observed for InIB, with similar implications for infection model generation and epidemiology. InIB-Met interactions function normally for human Met (and Met with the same composition of the binding spot for InIB as human Met, e.g. mouse Met), but the binding works poorly in case of guinea pig or rabbit Met (Khelef et al. 2006).

1.4.1.3. InIF

None of the currently known InIs is as comparable to InIA in both length and structure as InIF (Dramsi et al. 1997; Bierne et al. 2007). Although it was expected to play a similar – and possibly similarly important – role in listerial invasion, deletion of InIF surprisingly had neither any observable effect on the invasion rate in cellular infection experiments nor any effect on the effectiveness of bacterial dissemination into liver or spleen in mice (Dramsi et al. 1997; Bierne et al. 2007; Kirchner and Higgins 2008).

The curious discovery of a connection between the inhibition of Rho-associated protein kinases (ROCKs) – involved in actin cytoskeleton rearrangements – and increased adhesion and invasion

potential of *Lm* demonstrated both *in vitro* and *in vivo* brought InIF into the spotlight again, since it was seemingly involved in the observed hyperinvasiveness (Riento and Ridley 2003; Noma, Oyama, and Liao 2006; Kirchner and Higgins 2008). The enhancement effect following chemical inhibition of ROCKs was observed in several murine fibroblast and hepatocyte cell lines as well as in human epithelial cell lines HeLa and HEp-2 (although it was limited to higher adhesion to the cells in the case of human cell lines), and it also resulted in higher bacterial load in livers and spleens of infected mice (Kirchner and Higgins 2008). Infection of ROCK inhibitor-treated cells with *Lm* Δ *inIF* prevented the increased virulence in tested murine fibroblast (L2) and hepatocyte (TIB 75) cell lines and mice, but not in tested human fibroblast (WI38) and epithelial (HeLa) cell lines (Kirchner and Higgins 2008). The only currently known interaction partner of InIF is vimentin, a Type 3 intermediate filament protein found in mesenchymal cells, although the mechanism of this interaction is still unknown (Ghosh et al. 2018).

The data on barrier-crossing properties of InIF is relatively scarce. The previously mentioned study by Ghosh and colleagues marks it as vital for the breaching of the BBB (Ghosh et al. 2018). The results of experiments conducted both with the human brain microvascular endothelial cell line hCMEC/D3 and in mice indicate that the interplay of InIF and vimentin is necessary for efficient invasion of the brain, since the absence of either – or the obstruction of the contact between them – ended in severely hampered invasion into the cells (or the brains of infected animals) (Ghosh et al. 2018). The data obtained by Bastounis and colleagues in HMEC-1 cells confirms the importance of interaction between bacteria and vimentin for invasion of microvascular endothelium, although nothing pointing to the role of InIF in this interaction was observed (Bastounis, Yeh, and Theriot 2018).

1.4.1.4. Other CNS-invasion related internalins

The exact mechanisms utilized by *Lm* to cross the BBB and BCSFB are still not fully clear, and the VFs involved in the barrier traversal remain unconfirmed (if suspected) *in vivo* (Radoshevich and Cossart 2018; Banović, Schroten, and Schwerk 2020). Members of the InI family present a large pool of potential candidates, but only a few of them – with the exception of InIA, InIB and InIF – have been so far connected in any direct way with the invasion of the CNS (Radoshevich and Cossart 2018; Banović, Schroten, and Schwerk 2020).

Members of the InIGHE cluster – InIG, InIH and InIE – were implicated as interconnected invasion-related VFs for entry into non-phagocytic cells (gut epithelium-derived cell line Caco-2, HBMEC and human hepatocyte-derived cell line HepG2), since the deletion of any or all members of the cluster resulted in increased invasion rates into the tested cell lines (Bergmann et al. 2002). Interestingly, introduction of additional mutations resulted in quite different outcomes in different cell lines. In Caco-2 (which express both Ecad and Met), additional deletion of InIA, InIB, InIC or any combination thereof

actually resulted in a decreased invasion rate in comparison not only to the *Lm* Δ *inIGHE* deletion mutant but also to the wild-type bacteria, signifying that *Lm* is dependent on the interaction between all of these InIs for efficient entry into the Caco-2 cells – it is still unknown if this would be applicable to the CP epithelium which comprises the BSCFB (Bergmann et al. 2002). In HBMEC (which express only Met), on the other hand, the increased invasion rate was also observed if both InIA and InIC were deleted in addition to InIGHE, but not if only one of them was removed (in which case the invasion rates dropped to the level of the wild-type bacteria – for *Lm* Δ *inICGHE* – or slightly higher than it – for *Lm* Δ *inIAGHE*), hinting at a more complex modulatory role (Bergmann et al. 2002).

InIJ is an InI expressed only within the host's body, characterized by its unique cysteine-containing LRRs and the presence of a mucin-binding protein (MucBP) domain in its structure (Sabet et al. 2005; Bierne et al. 2007; Bublitz et al. 2008; Sabet et al. 2008). Its deletion decreases the pathogenicity of both orally and intravenously administered *Lm* in mice, and it was also reported as commonly found in bacteria isolated from ruminants suffering from *Lm*-induced rhombencephalitis (Sabet et al. 2008; Balandyté et al. 2011). The role of InIJ in listerial virulence was associated with its capability to bind to secreted mucins (such as MUC2) – the exact mechanism of this binding remains elusive, since InIJ is able to bind to them without the assistance of its MucBP domain (Lindén et al. 2008). The non-pathogenic relative of *Lm*, *Listeria innocua*, was able to adhere to placental epithelium-derived JEG-3 cells after being transfected with a vector carrying InIJ, demonstrating a potential role of InIJ as an adhesin (Sabet et al. 2008). It is unknown if InIJ plays the same role in regard to other epithelial cells (such as gut- or CP-derived cell lines).

Another MucBP-possessing InI potentially involved in CNS invasion is InIL (also known as ORF626 and Lmo2026), which was identified by screening of mutants of the *Lm* EGDe strain (*Lm* EGDe) generated by signature-tagged mutagenesis for anomalies or defects in brain invasion in mice (Autret et al. 2001; Bierne et al. 2007; Popowska et al. 2017). A *Lm* EGDe Δ *inIL* deletion mutant showed decreased virulence in mouse infection experiments, with the animals infected by it remaining alive for the duration of the experiment (in contrast to the animals infected by wild-type bacteria, which all died) (Autret et al. 2001). Since the mutant bacteria were not found in the brains of the infected animals but were found in their livers and spleens, it was hypothesized that InIL might be specifically involved in spreading to the brain. In *in vitro* experiments, the *Lm* EGDe Δ *inIL* deletion mutant behaved similarly to the wild-type bacteria in terms of invasiveness in epithelium-derived (Caco-2, HeLa and Vero) and macrophage-derived (J774) cell lines, but not in hepatocyte-derived HepG2 cells, where the invasion rate was strongly attenuated (Autret et al. 2001). Mechanism of action of InIL is as of yet not revealed, although it was proposed that it might be related to the binding of host mucins – with or without

involvement of the MucBP domain, similarly to InIJ (Autret et al. 2001; Bierne et al. 2007; Popowska et al. 2017). It is also unsure how relevant InIL is for the virulence of *Lm* in a broader, species-wide sense, since it was so far detected only in the *Lm* EGDe (Bierne et al. 2007).

1.4.2. Listeriolysin O

LLO, the cholesterol-dependent cytolysin (CDC) encoded by the *hly* gene, is arguably the most investigated non-InI listerial VF and the only real toxin (in the strictest sense of the word) produced by *Lm* (Camejo et al. 2011; Hamon et al. 2012; Osborne and Brumell 2017). The mode of action of all CDCs is similar: monomers of the toxin bind to the cell-surface cholesterol, insert themselves into the plasma membrane and oligomerize to form pores, leading to unregulated exchange and mixing of extracellular and intracellular content and the eventual death of the cell (Hamon et al. 2012; Osborne and Brumell 2017; Christie et al. 2018).

LLO is an unusual member of the CDC family due to its apparent adaptation to function within as well as outside the cell, signified by the possession of the N-terminal PEST sequence which promotes its internalization and limits the plasma membrane damage it might otherwise cause (Hamon et al. 2012; Osborne and Brumell 2017; Chen et al. 2018). Containment by the phagosome is not a deterrent to LLO at all, since its activity is actually enhanced by the acidification of the phagosomal interior and reaches its peak at pH = 5.5. This leads to the disruption of phagosomal function and its eventual degradation, which does not protect only the integrity of LLO itself but also of endocytosed *Lm*, and enables both to reach the cytoplasmic space (Schuerch, Wilson-Kubalek, and Tweten 2005; Hamon et al. 2012; Osborne and Brumell 2017). After it is released into the cytoplasm, it can still insert itself into the plasma membrane, but also into the membranes of endoplasmic reticulum (ER) and mitochondria. The broader range of targets for insertion, relatively low-key activity (outside of the phagosomes) in comparison to the rest of CDC family and a number of published findings highlight LLO as a versatile, subtle player involved in modulation of many parts of cellular biochemistry (Ca_{2+} , mitogen-activated protein kinase (MAPK) and NF κ B signaling; ER and mitochondrial disruption; etc.), but also as an active participant in cellular invasion (Schuerch, Wilson-Kubalek, and Tweten 2005; Gekara et al. 2007; Stavru et al. 2011; Vadia et al. 2011; Hamon et al. 2012; Vadia and Seveau 2014; Zhang, Bae, and Wang 2015; Osborne and Brumell 2017; Christie et al. 2018; Lam et al. 2018). Unsurprisingly, *Lm* isolates lacking a functional *hly* gene (as well as *Lm* Δ *hly* deletion mutants) are functionally avirulent both *in vitro* and *in vivo* (Gaillard, Berche, and Sansonetti 1986; Cossart et al. 1989; Hamon et al. 2012; Osborne and Brumell 2017).

When it comes to relevance of LLO for CNS invasion, it was implicated as involved in both the hematogenous and the neurogenous invasion pathways (Vadia et al. 2011; Dando et al. 2014; Vadia and Seveau 2014; Pägelow et al. 2018). In the case of hematogenous invasion, it was suggested that LLO either initiates paracellular transport across the BBB by temporary disruptions of the barrier through its pore-forming activity (demonstrated in the HBMEC cell line), promotes bacterial internalization (either independently or assisting the InI family members) through its involvement in cellular signaling (demonstrated in hepatocyte-derived HepG2, Hep3B, PLC5, and Huh7 cell lines but not in BBB- or BCSFB-relevant cell lines), or both (Vadia et al. 2011; Vadia and Seveau 2014; Zhang, Bae, and Wang 2015; Lam et al. 2018; Phelps et al. 2018; Radoshevich and Cossart 2018). Regarding the neurogenous invasion, a study using newborn mice as an *in vivo* infection model demonstrated that the expression of LLO is mandatory for the bacteria to reach the brain via the olfactory epithelium and adjoined nerves following an intranasal inoculation in a manner independent of the presence of the products of *inlAB* operon, although no detailed account of this mechanism has been presented so far (Pägelow et al. 2018).

1.4.3. Other CNS-invasion related virulence factors

As mentioned earlier, *Lm* has a plethora of different VFs which assist it in its traversal of the host. Although InI family members are the most commonly mentioned in regard of CNS invasion, there are also other proteins suspected to participate in this process (Banović, Schroten, and Schwerk 2020).

Autolysins are a group of bacterial hydrolases which have a role in alteration of bacterial cell's surface through cleavage of the covalent bonds in the peptidoglycan layer (Shockman and Höltje 1994). They have often been linked to the pathogenic activity of various bacterial species that contain them by enabling them to shuffle through the arsenal of peptidoglycan-linked VFs, and *Lm* is no exception: autolysins Ami, Auto, IspC, MurA, P45 and p60 have all been implicated in listerial virulence (Milohanic et al. 2001; Lenz et al. 2003; Pilgrim et al. 2003; Cabanes et al. 2004; Popowska 2004; Wang and Lin 2007, 2008). Two of these autolysins, Auto and IspC, are notable for being investigated more thoroughly, which led to the designation of roles for them in the infection process. Both are surface proteins attached to the bacterial cell wall via GW motifs – sharing this trait with InIB – and both exhibit N-acetylglucosaminidase activity, required for rearrangement of the listerial peptidoglycan layer (Cabanes et al. 2004; Popowska 2004; Wang and Lin 2007; Vollmer et al. 2008; Wang and Lin 2008; Bublitz et al. 2009; Camejo et al. 2011; Ronholm et al. 2012). *In vitro* experiments demonstrated that they are important for entry into various cell lines (Both – Caco-2, Vero; Auto – guinea pig epithelium-derived GPc16, HEp2, L2; IspC – HepG2, human fibroblast-derived L132, sheep CP epithelium-derived SCP), but only IspC was also found to be required for adhesion to the cells (demonstrated in Caco-2,

HepG2, SCP and Vero cell lines) (Cabanes et al. 2004; Wang and Lin 2008). In the animal infection experiments (in guinea pigs and mice for Auto and only in mice for IspC), the deletion mutants of both Auto and IspC yielded a significantly lower load of bacteria in the tested organs in comparison to the wild-type bacteria (all organs for *Lm Δaut*, all organs but spleen for *Lm ΔispC*) and also resulted in comparatively lower mortality (Cabanes et al. 2004; Wang and Lin 2008). Concerning the role in the penetration of the CNS, there is no real data on Auto beside the point that its deletion also resulted in decreased invasion into the brain of the infected animals (Cabanes et al. 2004). In case of IspC, however, there are signs that it might hold a role in the penetration of the BCSFB but not the BBB. While the brain was one of the organs in which mutant bacteria lacking IspC invaded at a lower rate in mouse infection experiments, the same *in vitro* study that reported *Lm ΔispC* as having a strong defect in adhesion to and invasion into SCP cells (representing the BCSFB) also reported no real difference in either adhesion or invasion rates between the mutant and wild-type bacteria in regards to HBMEC (representing the BBB) (Wang and Lin 2008). From what has been understood so far, it can be assumed that Auto has a supportive role in the virulence tied to its activity as an autolysin, while IspC was also implied as an adhesin (with a currently unknown binding partner on the host cell surface) in addition to the peptidoglycan rearrangement role (Wang and Lin 2008; Camejo et al. 2011).

The fact that the common laboratory strains of *Lm* are not fully representative of the listerial clinical landscape has recently brought the investigative focus on the listerial isolates from the groupings of *Lm* identified as being clinically relevant (Maury et al. 2016). The experiments that compared the behavior of the bacteria belonging to the reference strain EGDe and those belonging to CC1, CC4 and CC6 in animal infection models (humanized mice) found the latter to be much more harmful, leading to both more common and more rapid development of serious cases of listeriosis (i.e. systemic spread to various organs). The epidemiological data mirrored these results, connecting the strains belonging to these CCs with fetoinvasive and neuroinvasive listeriosis as well as disease emergence in immunocompetent people. This understandably led to additional effort towards the identification of novel VFs which might contribute to their enhanced virulence (Maury et al. 2016). An interesting example related to CNS invasiveness is a set of six genes involved in cellobiose metabolism found in isolates from CC4, known as cellobiose-family phosphotransferase system (PTS) and later dubbed the *Listeria* pathogenicity island 4 (LIPI-4) (Eisenreich et al. 2010; Maury et al. 2016). It was demonstrated to be necessary for substantial brain and placental invasion in both orally and intravenously infected humanized mice - the deletion mutant of CC4-refferent strain, *Lm* LM09-00558 ΔPTS, was present in both the blood and the organs in the same numbers as the wild-type strain, with only the bacterial loads in the brain (and fetus and placenta of pregnant mice) being strongly reduced in comparison (Maury et al. 2016). LIPI-4 ostensibly provides CC4 *Lm* isolates with an additional source of sugar –

cellobiose – to exploit, and this might be vital for the bacterial survival and growth in the parts of the body where the usually readily available and utilizable sugars are not present. Still, the exact role this might play in the invasion process remains unclear (Eisenreich et al. 2010; Maury et al. 2016).

1.5. Transmembrane proteins relevant to listerial invasion

1.5.1. Receptor tyrosine kinases

RTKs are a large group of transmembrane proteins dedicated to initiation of downstream intracellular signaling when triggered by ligands specific to each receptor, which they bind with high affinity (e.g. HGF for Met). Being the receptors for various cytokines, growth factors and hormones, they have a regulatory role in multiple cellular processes including cellular growth and proliferation, migration and survival (Lemmon and Schlessinger 2010; Haqshenas and Doerig 2019). Understandably, many tumors exhibit abnormalities in RTK expression or signaling, making RTKs important targets for research in both cancer biology and cancer treatment development (Lemmon and Schlessinger 2010; Haqshenas and Doerig 2019).

The basic build of all RTKs is relatively similar: they possess an extracellular N-terminal domain with a ligand-binding site, a single transmembrane region and an intracellular C-terminal domain with tyrosine kinase activity (Lemmon and Schlessinger 2010; Haqshenas and Doerig 2019). Upon binding of their designated ligand, RTKs dimerize and undergo autophosphorylation, where the intracellular kinase component of each of the two monomers in the dimer pair phosphorylates specific tyrosine residues on its opposite in specific order. This enables binding of cytoplasmic signaling proteins – primarily those containing Src homology 2 and phosphotyrosine binding domains – and their subsequent phosphorylation, conveying the signal delivered by the ligand further downstream. Insulin receptor is an exception to this model, since it is normally found in dimerized form and separates into monomers upon ligand binding and activation (Lemmon and Schlessinger 2010; Haqshenas and Doerig 2019). The binding of the ligand also causes the recruitment of the endocytosis machinery and results in internalization (shortly described on the example of Met and its ligand HGF in 1.4.1.2.). This brings the kinase site of the activated RTKs in contact with many previously inaccessible intracellular signaling proteins – such as protein kinase B (PKB, also Akt) and extracellular signal-regulated kinases 1 and 2 (ERK1/2) – and allows their phosphorylation (Miaczynska 2013; Haqshenas and Doerig 2019). Several factors – including ligand concentration and abundance of the RTK on the cellular surface – determine whether the RTKs carried by any given endosome will be returned to the cellular surface or degraded (Miaczynska 2013; Haqshenas and Doerig 2019).

1.5.2. CD44

CD44 proteins are a family of transmembrane glycoproteins involved in a wide range of cellular functions, including (but not limited to) cellular differentiation, growth and mobility. Although various members of the family have different characteristics and roles, they are all able to interact with components of the ECM – particularly GAGs such as hyaluronan – serving as communication points between the cell and its immediate surroundings (Ponta, Sherman, and Herrlich 2003).

All CD44 proteins are encoded by a single gene – different forms of CD44 are generated by posttranslational modifications and/or alternative splicing (Screaton et al. 1992; Ponta, Sherman, and Herrlich 2003). CD44 pre-mRNA contains 20 exons, of which the first 5 and the last 5 (“standard” exons) are always included in the final product, while the 10 in the middle (“variant” exons) are optional. Translation of the CD44 mRNA that contains only the standard exons results in the most common form of CD44 – known as CD44s – which is present in most cells of the human body. On the other hand, variant versions of CD44 with specialized roles – known as CD44v – have a much more limited distribution, with different cell types and tissues having preferred combinations of variant exons spliced into the final mRNA product (Screaton et al. 1992; Ponta, Sherman, and Herrlich 2003). Both CD44s and CD44v share a common design, with a short cytoplasmic C-terminal side of the protein (designated for signal transduction), a single transmembrane region and a long extracellular portion which can be further divided into the stem and amino-terminal loop regions. The main difference in the build between the two is present in the stem region, since the inclusion of additional variant exons results in elongation of this part of the protein, bringing the amino-terminal loop and its GAG-binding motifs further away from the plasma membrane as well as potentially adding new binding motifs not present in CD44s (Screaton et al. 1992; Ponta, Sherman, and Herrlich 2003).

Defects in the expression and/or structure of CD44 proteins have been connected with cellular malfunctions, particularly those related to immune cell activity (e.g. reaction to pathogens, tumorigenesis, etc.) (Ponta, Sherman, and Herrlich 2003). Curiously, it was observed that the lack of CD44 (e.g. in CD44 null mice or CD44 $-/-$ cell lines) is tolerated much better than the later disruption or removal of CD44 (i.e. by induced knockout). This appears to be the result of the ability of the cell to compensate for the initial absence of CD44 and work around it, which becomes impossible once CD44 is integrated into its signaling and communication network (Ponta, Sherman, and Herrlich 2003).

1.5.2.1. CD44v6

Publications on involvement of CD44 in cellular signaling or pathological conditions often do not make it clear whether the findings were specific to CD44s, one or more of the CD44v isoforms, or could be

attributed to all CD44 proteins (Ponta, Sherman, and Herrlich 2003; Montanari et al. 2018). One of the more notable exceptions, however, is found in the research done on CD44v isoforms containing variant exon 6 – collectively referred to as CD44v6 – which were identified as co-receptors of Met as well as relevant factors in metastatic spread of several types of tumors (Naor et al. 2002; Orian-Rousseau et al. 2002; Orian-Rousseau et al. 2007; Jung et al. 2009). In its role as a co-receptor for HGF binding to Met, both the extracellular and the intracellular parts of the protein are required for proper signal transduction following the binding of the growth factor (Orian-Rousseau et al. 2002; Orian-Rousseau et al. 2007). A tripeptide sequence encoded by the v6 exon in the stem region of CD44v6 is necessary for contact with Met, and mutations of amino-acids in this sequence as well as blocking by site-specific antibodies and peptides prevent the activation of Met *in vitro*. Interestingly, the effect of blocking antibodies and peptides is species-specific, due to the sequence variation across observed species (RWH in humans, GWQ in mice and EWQ in rats) (Matzke et al. 2005). The C-terminal cytoplasmic tail, on the other hand, provides a link to the actin cytoskeleton through binding of ERM proteins. The end result is a complex formed by the ligand (HGF), receptors (Met and CD44v6) and cytoskeletal components (ERM proteins and actin), which brings all the players involved in further signal transduction into close proximity (Orian-Rousseau et al. 2007).

2. MATERIALS AND METHODS

2.1. Materials

2.1.1. *Listeria monocytogenes*

2.1.1.1. *Listeria monocytogenes* strains

Lm used in this study belonged to the strain EGDe (serotype 1/2a) (Kaufmann et al., 1984). Wild-type bacteria of this strain as well as isogenic deletion mutants EGDe $\Delta inIA$ (Lingnau et al. 1995), EGDe $\Delta inIB$ (Lingnau et al. 1995), EGDe $\Delta inIAB$ (Parida et al. 1998) and EGDe $\Delta inIF$ were all provided by Prof. Trinad Chakraborty (Institute for Medical Microbiology, University of Gießen, Gießen, Germany).

2.1.1.2. Media and plates used for *Listeria monocytogenes*

Lm was incubated in brain heart infusion (BHI) medium (BD, Franklin Lakes, NJ, USA) when grown overnight in preparation for replenishing of bacterial stocks or performing of infection experiments. The medium used for long-term storage at -80 °C was a 7:3 mixture of BHI medium and glycerol (Carl Roth, Karlsruhe, Germany). During the infection experiments, bacteria were co-incubated with the cells in either 1% HIBCPP medium or 1% HBMEC medium, depending on the cell line used in any given experiment (refer to 2.1.2.2.). An overview of the used media can be found in 2.1.5.

Columbia sheep blood agar plates (Oxoid, Wesel, Germany) were used for bacterial colony growth and determining the number of colony-forming units (CFU) following the *in vitro* experiments. Oxford (*Listeria*-selective formulation) agar plates (Oxoid, Wesel, Germany) were used for bacterial colony growth and determining the number of CFU following the experiments with mice.

2.1.2. Cellular models

2.1.2.1. Cell lines

2.1.2.1.1. HIBCPP (human CP epithelium-derived, papilloma)

HIBCPP was the human cell line used to mimic the BCSFB *in vitro* in this study. The cell line was initially characterized and described by Ishiwata and colleagues (Ishiwata et al. 2005). Further work by Schwerk and colleagues presented it as an efficient *in vitro* model for the BCSFB due to the presence of TJs between the cells and the confirmed cellular polarity (Schwerk et al. 2012). A stable cellular barrier function achieved through TJ formation – confirmed by low permeability for complex sugars and high transepithelial electric resistance (TEER) – is essential for limiting traffic through the cell layer, and polarity of the cells enables the setup of a model in which the cellular response can be observed from either the apical or the basolateral side of the cell layer, with the former corresponding to the CSF-oriented side and the latter to the blood-oriented side of the BCSFB (Schwerk et al. 2012). The HIBCPP-based *in vitro* BCSFB model has been successfully used over the years and enabled insight into

interactions between bacteria and BCSFB (Schwerk et al. 2012; Gründler et al. 2013; Steinmann et al. 2013; Borkowski et al. 2014; Dinner et al. 2017). HIBCPP cells were originally provided by Prof. Hiroshi Ishikawa (Department of NDU Life Sciences, Nippon Dental University, Niigata, Japan).

2.1.2.1.2. HBMEC (human brain microvascular endothelium-derived, immortalized)

The cells used in this study as the main *in vitro* model of the BBB belong to the HBMEC line characterized and described by Stins and colleagues (Stins, Badger, and Kim 2001). Since its introduction more than two decades ago, the HBMEC cell line has been established as a suitable and often-used model for bacteria-BBB interactions (Greiffenberg et al. 1998; Greiffenberg et al. 2000; Bergmann et al. 2002; Hertzog et al. 2003; Sokolova et al. 2004; Tenenbaum et al. 2007; Wang and Lin 2008; Zhang, Bae, and Wang 2015). The cells used in this thesis were originally provided by Prof. Kwang Sik Kim (Division of Pediatric Infectious Diseases, The Johns Hopkins University School of Medicine, Baltimore, MD, USA).

2.1.2.1.3. HeLa cells

HeLa cells were used in a study by Jung and colleagues to test the effect of CD44v6-blocking antibodies and peptides on listerial invasion of cellular barriers (Jung et al. 2009). They were used in this study as a control in the experiment meant to replicate the results obtained by Jung and colleagues (Jung et al. 2009).

2.1.2.1.4. bEnd.3 (mouse cerebral endothelium-derived, immortalized)

bEnd.3 cells have been widely used in mouse-based vascular research. They originate from BALB/c mouse strain and were originally described by Montesano and colleagues, as well as confirmed to be endothelial in nature due to the presence of von Willebrand factor and their capacity for uptake of labeled low density lipoprotein (Montesano et al. 1990). Since they have been used as a basis for mouse BBB models as well and since the effect of CD44v6-blocking peptides was reported to be species-specific, bEnd.3 cells were included in the study to provide an additional, mouse-based control in the experiment conducted to confirm the results obtained by Jung and colleagues (Omidi et al. 2003; Jung et al. 2009). The bEnd.3 cells were provided by Dr. Mario Vitacolonna (Institute of Molecular and Cell Biology, Faculty of Biotechnology, Mannheim University of Applied Sciences, Mannheim, Germany).

2.1.2.2. Cell media

Cell medium used for the growth of HIBCPP cells was 10% HIBCPP medium, while the medium used for infection experiments was 1% HIBCPP medium. For HBMEC, bEnd.3 and HeLa cells, there was a separate set of media: 10% HBMEC medium was used for the growth of the cells, while 1% HBMEC

medium was used in infection experiments. An overview of the composition of all used media can be found in 2.1.5.

2.1.3. Animal models

2.1.3.1. Mouse strains

Mouse strains used in the experiments were BALB/cByJRj (Janvier Labs, Le Genest-Saint-Isle, France) and C57BL/6JRj (Janvier Labs, Le Genest-Saint-Isle, France). All the mice were female and 6 weeks old on delivery, since younger, female mice are known to be more susceptible to listerial infection (Pasche et al. 2005). After the delivery of each batch of mice, one week was given for acclimatization before the beginning of the experiment. The mice were kept in individually ventilated cages (IVC) with no more than 4 mice per cage.

2.1.4. Peptides

Following peptides were used in *in vitro* and *in vivo* experiments to hinder the invasion by *Lm*. They were obtained as lyophilized powder from the laboratory of Prof. Veronique Orian-Rousseau (Institute of Biological and Chemical Systems – Functional Molecular Systems, Karlsruhe Institute of Technology, Karlsruhe, Germany).

| Peptide | Sequence | Stock concentration |
|---|---------------------------------------|---------------------|
| Human-specific CD44v6-blocking peptide (KR14) | NH ₂ - KEQWFGNRWHEGYR-COOH | 1 mg/ml in PBS |
| Mouse-specific CD44v6-blocking peptide (QP14) | NH ₂ - QETWFQNGWQGKNP-COOH | 1 mg/ml in PBS |

2.1.5. Antibodies

2.1.5.1. Primary antibodies

Following primary antibodies were used for immunofluorescence (IF) staining following *in vitro* infection experiments with *Lm*.

| Antibody | Manufacturer |
|------------------------|---|
| Chicken anti-vimentin | BioLegend, San Diego, CA, USA |
| Goat anti-c-Met | Abcam, Cambridge, UK |
| Mouse anti-Ecad | BD, Franklin Lakes, NJ, USA |
| Rabbit anti- <i>Lm</i> | Meridian Life Science, Memphis, TN, USA |
| Rabbit anti-ZO-1 | Invitrogen, Carlsbad, CA, USA |

Following primary antibodies were used for Western blotting of protein extracts obtained from *in vitro* infection experiments with *Lm*. Mouse anti-CD44 (Hermes3) and Mouse anti-CD44v6 (BIWA) antibodies were obtained from Prof. Veronique Orian-Rousseau (Institute of Biological and Chemical Systems – Functional Molecular Systems, Karlsruhe Institute of Technology, Karlsruhe, Germany) and were marked with asterisks below.

| Antibody | Manufacturer |
|---|---|
| Chicken anti-vimentin | BioLegend, San Diego, CA, USA |
| Goat anti-c-Met | Abcam, Cambridge, UK |
| Mouse anti-CD44 (Hermes3) | * |
| Mouse anti-CD44v6 (BIWA) | * |
| Mouse anti-Ecad | BD, Franklin Lakes, NJ, USA |
| Mouse anti-tubulin | Santa Cruz Biotechnology, Dallas, TX, USA |
| Mouse anti- β -actin | Sigma-Aldrich, St. Louis, MO, USA |
| Rabbit anti-BLK | Affinity Biosciences, Cincinnati, OH, USA |
| Rabbit anti-Erk1/2 | Cell Signaling, Denver, MA, USA |
| Rabbit anti-ETK | Affinity Biosciences, Cincinnati, OH, USA |
| Rabbit anti-JAK2 | Affinity Biosciences, Cincinnati, OH, USA |
| Rabbit anti-JAK2/3 | Affinity Biosciences, Cincinnati, OH, USA |
| Rabbit anti-JNK | Cell Signaling, Denver, MA, USA |
| Rabbit anti-LTK | Affinity Biosciences, Cincinnati, OH, USA |
| Rabbit anti-p38 | Cell Signaling, Denver, MA, USA |
| Rabbit anti-phospho BLK (Tyr389) | Affinity Biosciences, Cincinnati, OH, USA |
| Rabbit anti-phospho Erk1/2 | Cell Signaling, Denver, MA, USA |
| Rabbit anti-phospho ETK (Tyr566) | Affinity Biosciences, Cincinnati, OH, USA |
| Rabbit anti-phospho JAK2 (Tyr570) | Affinity Biosciences, Cincinnati, OH, USA |
| Rabbit anti-phospho JAK3 (Tyr981) | Affinity Biosciences, Cincinnati, OH, USA |
| Rabbit anti-phospho JNK | Cell Signaling, Denver, MA, USA |
| Rabbit anti-phospho LTK/ALK (Tyr672/Tyr1278) | Affinity Biosciences, Cincinnati, OH, USA |
| Rabbit anti-phospho MER/TYRO3 (Tyr753/Tyr685) | Affinity Biosciences, Cincinnati, OH, USA |
| Rabbit anti-phospho p38 | Cell Signaling, Denver, MA, USA |
| Rabbit anti-phospho ZAP70 (Tyr493) | Affinity Biosciences, Cincinnati, OH, USA |

| | |
|-------------------|---|
| Rabbit anti-TYRO3 | Affinity Biosciences, Cincinnati, OH, USA |
| Rabbit anti-ZAP70 | Affinity Biosciences, Cincinnati, OH, USA |
| Rabbit anti-ZO-1 | Invitrogen, Carlsbad, CA, USA |

2.1.5.2. Secondary antibodies

Following secondary antibodies were used for IF staining following *in vitro* infection experiments with *Lm*.

| Antibody | Manufacturer |
|--------------------------------------|-------------------------------|
| Chicken anti-rabbit Alexa Fluor® 488 | Invitrogen, Carlsbad, CA, USA |
| Chicken anti-rabbit Alexa Fluor® 594 | Invitrogen, Carlsbad, CA, USA |
| Donkey anti-goat Alexa Fluor® 594 | Invitrogen, Carlsbad, CA, USA |
| Donkey anti-rabbit Alexa Fluor® 488 | Invitrogen, Carlsbad, CA, USA |
| Goat anti-chicken Alexa Fluor® 488 | Invitrogen, Carlsbad, CA, USA |
| Goat anti-chicken Alexa Fluor® | Invitrogen, Carlsbad, CA, USA |
| Goat anti-mouse Alexa Fluor® 594 | Invitrogen, Carlsbad, CA, USA |

Following secondary antibodies were used for Western blotting of protein extracts obtained from *in vitro* infection experiments with *Lm*.

| Antibody | Manufacturer |
|---------------------|--|
| Donkey anti-chicken | Millipore, Burlington, MA, USA |
| Donkey anti-goat | Millipore, Burlington, MA, USA |
| Donkey anti-rabbit | Millipore, Burlington, MA, USA |
| Goat anti-mouse | Thermo Fisher Scientific, Waltham, MA, USA |

2.1.6. Media

Following media were used for growth and storage of cells and bacteria as well as for experimental procedures.

| Medium | Components | Manufacturer |
|-----------------------------------|--|-----------------------------|
| Brain heart infusion medium (BHI) | BHI powder dissolved in distilled water and autoclaved | BD, Franklin Lakes, NJ, USA |

| | | |
|---|---|--------------------------------------|
| HBMEC medium – 1% serum (1% HBMEC) | DMEM/F-12 (1x) medium with L-glutamine, 15 mM HEPES and no phenol red | Life Technologies, Carlsbad, CA, USA |
| | Fetal calf serum (FCS) – 1% v/v | Life Technologies, Carlsbad, CA, USA |
| HBMEC medium – 10% serum (10% HBMEC) | DMEM/F-12 (1x) medium with L-glutamine, 15 mM HEPES and phenol red | Life Technologies, Carlsbad, CA, USA |
| | FCS – 10% v/v | Life Technologies, Carlsbad, CA, USA |
| HIBCPP medium – 1% serum (1% HIBCPP) | DMEM/F-12 (1x) medium with L-glutamine, 15 mM HEPES and no phenol red | Life Technologies, Carlsbad, CA, USA |
| | FCS – 1% v/v | Life Technologies, Carlsbad, CA, USA |
| | Human recombinant insulin solution (10 mg/ml) – 0.05% v/v | Sigma-Aldrich, St. Louis, MO, USA |
| HIBCPP medium – 10% serum (10% HIBCPP) | DMEM/F-12 (1x) medium with L-glutamine, 15 mM HEPES and phenol red | Life Technologies, Carlsbad, CA, USA |
| | FCS – 10% v/v | Life Technologies, Carlsbad, CA, USA |
| | Human recombinant insulin solution (10 mg/ml) – 0.05% v/v | Sigma-Aldrich, St. Louis, MO, USA |
| Listeria -80 °C storage medium | BHI medium | BD, Franklin Lakes, NJ, USA |
| | Glycerol – 30% v/v | Carl Roth, Karlsruhe, Germany |
| Serum-free medium (SFM) | DMEM/F-12 (1x) medium with L-glutamine, 15 mM HEPES and no phenol red | Life Technologies, Carlsbad, CA, USA |
| BSA-complemented serum-free medium (SFM/1% BSA) | DMEM/F-12 (1x) medium with L-glutamine, 15 mM HEPES and no phenol red | Life Technologies, Carlsbad, CA, USA |

| | |
|--|---------------------------|
| Bovine serum albumin (BSA) – 1% m/v | Merck, Darmstadt, Germany |
|--|---------------------------|

2.1.7. Buffers, chemicals and solutions

Following buffers, chemicals and solutions were used in this study. Water from the MilliQ® ultrapure water filtering system (Millipore, Billerica, MA, USA) was used for preparation of agarose gels, buffer and chemical dilutions, or in any other instance where usage of purified (but not sterile) water is mentioned in this study.

| Product | Components | Manufacturer |
|---|--|--|
| Alexa Fluor™ 660 Phalloidin | | Invitrogen, Carlsbad, CA, USA |
| Cyclosporine A | Powdered compound suspended in dH ₂ O (stock 10 mg/ml) | Biosynth/Carbosynth, Staad, Switzerland |
| 4',6-diamidino-2-phenylindole (DAPI) | | Merck, Darmstadt, Germany |
| Dimethyl sulfoxide (DMSO) | | Sigma-Aldrich, St. Louis, MO, USA |
| Dithiothreitol (DTT) – 1 M | | Sigma-Aldrich, St. Louis, MO, USA |
| Ethylenediaminetetraacetic acid (EDTA) | | Sigma-Aldrich, St. Louis, MO, USA |
| Ethanol (80%) | | S.A.R. Plus, Bexbach, Germany |
| Ethanol (absolute, 99.9%) | | J.T. Baker, Radnor, PA, USA |
| Ethidium bromide | | AppliChem, Darmstadt, Germany |
| Fluorescein isothiocyanate (FITC)-Inulin (100 µg/ml) | | Sigma-Aldrich, St. Louis, MO, USA |
| Formaldehyde (37%) | | NeoLab, Heidelberg, Germany |
| Sterile distilled water (dH ₂ O) | | Life Technologies, Carlsbad, CA, USA |
| Hydrocortisone sodium succinate | Powdered compound dissolved in 0,9% NaCl solution (stock 50 mg/ml) | Sigma-Aldrich, St. Louis, MO, USA |
| HyPro Medical 3% spray foam | 3% hydrogen peroxide | Analisis, Namur, Belgium |
| Isoflurane | | CP-Pharma, Burgdorf, Germany |
| Ketamine (10%) | | WDT, Garbsen, Germany |

| | | |
|--|--|--------------------------------------|
| NuPAGE™ LDS Sample Buffer (4X) | | Invitrogen, Carlsbad, CA, USA |
| NuPAGE™ MOPS SDS Running Buffer (20X) | | Invitrogen, Carlsbad, CA, USA |
| NuPAGE™ Transfer Buffer (20X) | | Invitrogen, Carlsbad, CA, USA |
| Dulbecco's phosphate buffered solution with Ca ²⁺ and Mg ²⁺ (PBS+) | | Life Technologies, Carlsbad, CA, USA |
| Dulbecco's phosphate buffered solution without Ca ²⁺ and Mg ²⁺ (PBS) | | Life Technologies, Carlsbad, CA, USA |
| PBS complemented with BSA (1% BSA/PBS) | Dulbecco's phosphate buffered solution without Ca ²⁺ and Mg ²⁺ (PBS) | Life Technologies, Carlsbad, CA, USA |
| | BSA – 1% m/v | Merck, Darmstadt, Germany |
| PBS complemented with BSA and Triton X-100 (1% BSA/0.5% Triton/PBS) | Dulbecco's phosphate buffered solution without Ca ²⁺ and Mg ²⁺ (PBS) | Life Technologies, Carlsbad, CA, USA |
| | BSA – 1% m/v | Merck, Darmstadt, Germany |
| | Triton X-100 | Sigma-Aldrich, St. Louis, MO, USA |
| ProLong™ Gold Antifade | | Invitrogen, Carlsbad, CA, USA |
| RLT Lysis Buffer | RLT Lysis Buffer | Qiagen, Hilden, Germany |
| | 10 mM β-mercaptoethanol | Sigma-Aldrich, St. Louis, MO, USA |
| Skim milk powder | | Obtained in the supermarket |
| Softasept N | | |
| TAE Buffer (1X) | 40 mM Tris | Carl Roth, Karlsruhe, Germany |
| | 20 mM acetic acid | Merck, Darmstadt, Germany |
| | 1 mM EDTA (pH = 0.3) | Carl Roth, Karlsruhe, Germany |
| TBS buffer (titrated to pH 7.6 with 25% HCl) (10X) | 0.1 mM Tris | Carl Roth, Karlsruhe, Germany |
| | 1.5 mM NaCl | Carl Roth, Karlsruhe, Germany |
| TBS-T buffer | 100 ml TBS buffer (10X) | B. Braun, Melsungen, Germany |
| | 890 ml dH ₂ O | |

| | | |
|--------------------------------------|---|--------------------------------------|
| | 10 ml Tween20 – 10% (v/v) | AppliChem, Darmstadt, Germany |
| Trypan Blue solution (0.4%) | | Sigma-Aldrich, St. Louis, MO, USA |
| Trypsin-EDTA (0.25%) with phenol red | | Life Technologies, Carlsbad, CA, USA |
| Withaferin A | Powdered compound dissolved in DMSO (stock 1 mg/ml) | Merck, Darmstadt, Germany |
| Xylazine (2%) | | WDT, Garbsen, Germany |

2.1.8. Primers for PCR

All the primers listed as originating in this study were generated using Primer-BLAST online tool (<https://www.ncbi.nlm.nih.gov/tools/primer-blast/>). All listed primers were manufactured by Sigma-Aldrich (Steinheim, Germany) and delivered as lyophilized powder, which was then reconstituted with sterile distilled water (see 2.1.6.). The concentration of the primer stocks thus generated was 100 pmol/ μ l.

Following oligonucleotide primers were used for PCRs performed on *Lm* samples in this study.

| Target (<i>gene name</i>) | Primer | Sequence (5' → 3') | Reference |
|-----------------------------|--------------|-----------------------------|-----------------|
| InIA (<i>inIA</i>) | A2 (forward) | TGCTCAGGCAGCTACAATTACAC | (Gründler 2014) |
| | A2 (reverse) | TAAGAGCCATTGCAGTTCCTACTG | (Gründler 2014) |
| | A3 (forward) | CGGCTAGAACTATCCAGTAACACG | (Gründler 2014) |
| | A3 (reverse) | TGGCTGCGTCACGGTTC | (Gründler 2014) |
| InIB (<i>inIB</i>) | B2 (forward) | AGCACGTGCTAGTAAATAGAAGTAGTG | (Gründler 2014) |
| | B2 (reverse) | TTAAGCAGCGCAAAGGTGATTC | (Gründler 2014) |
| | B3 (forward) | TCATTTACCACAGCTGGAAAGTTTG | (Gründler 2014) |
| | B3 (reverse) | GGGTTTTGTCCAAACCGAATTT | (Gründler 2014) |

Following oligonucleotide primers were used for PCRs performed on human cell samples in this study.

| Target (<i>gene name</i>) | Primer | Sequence (5' → 3') | Reference |
|-----------------------------|--------------------|----------------------|------------|
| Vimentin (<i>VIM</i>) | Vimentin (forward) | AGAGAGAGGAAGCCGAAAAC | This study |

| | | | |
|--|------------------------|-------------------------|---|
| | Vimentin (reverse) | TGGATTTCTCTTCGTGGAGTT | This study |
| E-cadherin (<i>CDH1</i>) | E-cad (forward) | CCTGCCAATCCCGATGA | Group of Prof. Horst Schroten (unpublished) |
| | E-cad (reverse) | TGCCCCATTTCGTTCAAGTA | Group of Prof. Horst Schroten (unpublished) |
| c-Met (<i>MET</i>) | c-Met (forward) | ATCTTGGGACATCAGAGGGT | This study |
| | c-Met (reverse) | TCGTGATCTTCTCCAGTGA | This study |
| ZO-1 (<i>TJP1</i>) | ZO-1 (forward) | GCCAAGCAATGGCAGTCTC | Group of Prof. Horst Schroten (unpublished) |
| | ZO-1 (reverse) | CTGGGCCGAAGAAATCCCATC | Group of Prof. Horst Schroten (unpublished) |
| IL-6 (<i>IL6</i>) | IL-6 (forward) | AACCTGAACCTTCCAAGATGG | (Borkowski et al. 2014) |
| | IL-6 (reverse) | TCTGGCTTGTTCTCACTACT | (Borkowski et al. 2014) |
| IL-8 (<i>CXCL8</i>) | IL-8 (forward) | CAAGAGCCAGGAAGAAACCA | (Schneider et al. 2012) |
| | IL-8 (reverse) | GTCCACTCTCAATCACTCTCAG | (Schneider et al. 2012) |
| TNF α (<i>TNF</i>) | TNF α (forward) | GAGCACTGAAAGCATGATCC | (Borkowski et al. 2014) |
| | TNF α (reverse) | CGAGAAGATGATCTGACTGCC | (Borkowski et al. 2014) |
| CD44/CD44c5 (<i>CD44</i>) – constant exon, present in all isoforms of CD44 | CD44 (forward) | AGGAGCAGCACTTCAGGAGGT | Group of Prof. Veronique Orian-Rousseau (unpublished) |
| | CD44 (reverse) | TGCTGTCCGTGATCCAGGGAC | Group of Prof. Veronique Orian-Rousseau (unpublished) |
| CD44v6 (<i>CD44</i>) | CD44v6 (forward) | ACGGAAGAAACAGCTACCCAG A | Group of Prof. Veronique Orian-Rousseau (unpublished) |
| | CD44v6 (reverse) | GCTGTCCCTGTTGTCGAATGG | Group of Prof. Veronique Orian-Rousseau (unpublished) |
| GAPDH (<i>GAPDH</i>) | GAPDH (forward) | TGTTGCCATCAATGACCCCTT | (Borkowski et al. 2014) |
| | GAPDH (reverse) | CTCCACGACGTACTIONCAGCG | (Borkowski et al. 2014) |

2.1.9. Size standards

The size standard used to determine the size of DNA fragments in agarose gel electrophoreses performed during the course of this study was Gene Ruler 100 bp DNA Ladder (Thermo Fisher Scientific, Waltham, MA, USA).

The size standard used to compare the molecular weight of proteins in the Western blots performed during the course of this study was Novex Sharp Protein Standard (Life Technologies, Carlsbad, CA, USA).

2.1.10. Kits

Following kits were used for generation of data presented in this study.

| Product | Manufacturer |
|--|---|
| AffinityScript QPCR cDNA Synthesis Kit | Agilent, Santa Clara, CA, USA |
| DC Protein Assay | Bio-Rad Laboratories, Hercules, CA, USA |
| Human RTK Phosphorylation Array C1 | RayBiotech, Norcross, GA, USA |
| LIVE/DEAD Viability/Cytotoxicity Kit for mammalian cells | Invitrogen, Carlsbad, CA, USA |
| Immobilon Western Chemiluminescent HRP | Millipore, Billerica, MA, USA |
| RNeasy Micro Kit | Qiagen, Hilden, Germany |
| RNeasy Mini Kit | Qiagen, Hilden, Germany |
| RNAse free DNase Set | Qiagen, Hilden, Germany |
| Taq DNA Polymerase Kit (1000U) | Qiagen, Hilden, Germany |

2.1.11. Laboratory equipment

Following devices were used to perform the work presented in this study.

| Model | Product | Manufacturer |
|---------------------|------------------------|--|
| Analog Vortex Mixer | Analog Vortex Mixer | VWR, Radnor, PA, USA |
| Apotome® | Apotome | Zeiss, Oberkochen, Germany |
| Vaporiser Tec3 | Anaesthetic machine | Provet, Lyssach, Switzerland |
| Vacunsafe Comfort | Aspiration system | INTEGRA Biosciences, Zizers, Switzerland |
| Pipetboy Comfort | Automatic pipette pump | INTEGRA Biosciences, Zizers, Switzerland |
| Herasafe™ | Biosafety cabinet | Thermo Fisher Scientific, Waltham, MA, USA |

| | | |
|--|--|--|
| Heracell 240 | Cell culture/CO ₂ incubator | Thermo Fisher Scientific, Waltham, MA, USA |
| MIKRO 200R (with 242A Rotor) | Centrifuge | Andreas Hettich, Tuttlingen, Germany |
| ROTANTA 460R (with 5624 Rotor) | Centrifuge | Andreas Hettich, Tuttlingen, Germany |
| Chemi Smart 5100 | Chemiluminescence detector | Vilber Lourmat, Eberhardzell, Germany |
| WPA CO8000 | Densitometer | Biochrom, Cambridge, UK |
| Sub-Cell GT | Electrophoresis cell | Bio-Rad Laboratories, Hercules, CA, USA |
| XCell SureLock Mini-Cell | Electrophoresis cell | Invitrogen, Carlsbad, CA, USA |
| Biovision-3026WL/26MX | Gel documentation system | Vilber Lourmat, Eberhardzell, Germany |
| Hemocytometer (Neubauer chamber); 0.1 mm depth; 0.0025 mm ² | Hemocytometer | NeoLab, Heidelberg, Germany |
| Fisherbrand™ 850 | Homogenizer | Thermo Fisher Scientific, Waltham, MA, USA |
| 18000-45 | Hot bead sterilizer | FST, Heidelberg, Germany |
| 766 | Laboratory pH meter | Knick, Berlin, Germany |
| Axiovert 40C | Light microscope | Zeiss, Oberkochen, Germany |
| Observer Z1 | Light microscope | Zeiss, Oberkochen, Germany |
| Macrolon box (3 l) | Macrolon box | Heidelberg University, Heidelberg, Germany |
| VMS-C4-2 | Magnetic hotplate stirrer | VWR, Radnor, PA, USA |
| PicoFuge® II | Microcentrifuge | Stratagene, San Diego, CA, USA |
| GM500 (for mice) | Microisolator cage | Tecniplast, Buguggiate, Italy |
| GM500 (for mice) and DGM rack | Microisolator cage rack | Tecniplast, Buguggiate, Italy |
| MWG758 | Microwave oven | Clatronic, Kempen, Germany |
| Infinite M200 | Multiwell plate reader | Tecan, Männedorf, Switzerland |
| Reference (2.5 / 10 µl) | Pipette | Eppendorf, Hamburg, Germany |
| Research (20 / 100 / 200 / 1000 µl) | Pipette | Eppendorf, Hamburg, Germany |
| Duomax 1030 | Platform shaker | Heidolph Instruments, Schwabach, Germany |
| Titramax 1000 | Platform shaker | Heidolph Instruments, Schwabach, Germany |
| Power Pac™ Basic | Power supply | Bio-Rad Laboratories, Hercules, CA, USA |
| CPA 623 S Toploading Balance | Precision scale | Sartorius, Göttingen, Germany |
| ED224S Extend Analytical Balance | Precision scale | Sartorius, Göttingen, Germany |

| | | |
|---|---------------------------------|--|
| Refrigerated/Heating Circulator | Refrigerated/Heating Circulator | Julabo Labortechnik, Seelbach, Germany |
| DuraPorter™ | Safety box | Carl Roth, Karlsruhe, Germany |
| NanoDrop® ND1000 | Spectrophotometer | Peqlab, Erlangen, Germany |
| Micro-Adson Tissue Forceps – Angled, 1x2 teeth | Surgical forceps | Hugo Sachs Elektronik – Harvard Apparatus, March-Hugstetten, Germany |
| Special Cut Eye Scissors – Straight, Sharp/Sharp / Ultra-Edge Operating Scissors - Straight, Sharp/Blunt / Vannas Spring Scissors with Round Handles – Straight, Sharp/Sharp / Vannas Tübingen Spring Scissors – Straight, Sharp/Sharp | Surgical scissors | Hugo Sachs Elektronik – Harvard Apparatus, March-Hugstetten, Germany |
| Thermocycler 2720 | Thermocycler | Applied Biosystems, Foster City, CA, USA |
| Thermomixer Compact | Thermomixer | Eppendorf, Hamburg, Germany |
| TE22 Mighty Small Transfer Tank | Transfer tank | Hoefer, Inc., Holliston, MA, USA |
| 5075 ELV | Vertical autoclave | Systec, Linden, Germany |
| Millicell®-ERS | Voltohmeter | Millipore, Billerica, MA, USA |
| STX 01 | Voltohmeter chopstick electrode | Millipore, Billerica, MA, USA |
| SW22 | Water bath | Julabo Labortechnik, Seelbach, Germany |
| Milli-Q® | Water purification system | Millipore, Billerica, MA, USA |

2.1.12. Software

Following software programs were used in obtaining and adapting data presented in this study.

| Software | Manufacturer |
|----------------------------|---------------------------------------|
| Chemi-Capt | Vilber Lourmat, Eberhardzell, Germany |
| i-control | Tecan, Männedorf, Switzerland |
| ImageJ 1.47v | Wayne Rasband (retired from NIH) |
| Vision-Capt | Vilber Lourmat, Eberhardzell, Germany |
| Zeiss ZEN Imaging Software | Zeiss, Oberkochen, Germany |

2.1.13. Consumables

Following single-use components were used for performance of experiments in this study.

| Product | Manufacturer |
|--|---|
| Discardit™ II syringes (5 ml) | BD, Franklin Lakes, NJ, USA |
| Microlance 3 hypodermic needles (20G x 1 1/2" / 23G x 1" / 25G x 5/8" / 27G x 1/2" / 30G x 1/2") | BD, Franklin Lakes, NJ, USA |
| Plastipak™ syringes (1 ml) | BD, Franklin Lakes, NJ, USA |
| Serological pipettes (5 / 10 / 25 ml) | BD, Franklin Lakes, NJ, USA |
| Nitrocellulose membrane (pore size: 0.45 µm) | Bio-Rad Laboratories, Hercules, CA, USA |
| Safe-lock Centrifuge Tubes (0.5 / 1.5 / 2 / 5 ml) | Eppendorf, Hamburg, Germany |
| Falcon® 8-well Culture Slide | Falcon (Corning), Corning, NY, USA |
| Falcon® Cell Strainer (40 µm) | Falcon (Corning), Corning, NY, USA |
| Disposable surgical blades No. 11 | Feather Safety Razor, Osaka, Japan |
| Cryo.s™ 1 ml cryogenic vials | Greiner Bio-One, Kremsmünster, Austria |
| Centrifuge tubes (15 / 50 ml) | Greiner Bio-One, Kremsmünster, Austria |
| Semi-micro cuvettes | Greiner Bio-One, Kremsmünster, Austria |
| ThinCert™ cell culture inserts for 24-well plates (pore diameter: 3 µm) | Greiner Bio-One, Kremsmünster, Austria |
| ThinCert™ cell culture inserts for 12-well plates (pore diameter: 3 µm) | Greiner Bio-One, Kremsmünster, Austria |
| Cell culture flasks, filter-capped (50 ml – 25 cm ² / 250 ml – 75 cm ²) | Greiner Bio-One, Kremsmünster, Austria |
| NuPAGE™ Novex™ 4-12 % Bis-Tris gels (1.5 mm, 15 wells) | Life Technologies, Carlsbad, CA, USA |
| Cover glasses | Marienfeld, Lauda-Königshofen, Germany |
| Microscope slides | Marienfeld, Lauda-Königshofen, Germany |
| Polypropylene plastix boxes with lids (2 l) | Neupack Verpackungen, Hamburg, Germany |
| MicroWell™ 96-well plates (black, uncoated) | Nunc, Roskilde, Denmark |
| MicroWell™ 96-well plates (transparent, uncoated) | Nunc, Roskilde, Denmark |
| S-Monovette® (1.2 ml, lithium-heparin) | Sarstedt, Nümbrecht, Germany |
| CytoOne® cell culture plates (6 / 12 / 24 well) | STARLAB, Hamburg, Germany |

| | |
|--|---------------------------------|
| TipOne® graduated sterile filter tips (100 / 200 / 1000 µl) | STARLAB, Hamburg, Germany |
| TipOne® graduated sterile filter tips (10 µl – maximum volume 20 µl) | STARLAB, Hamburg, Germany |
| TipOne® RPT graduated sterile filter tips (100 / 200 / 1000 µl) | STARLAB, Hamburg, Germany |
| TipOne® RPT graduated sterile filter tips (10 µl – maximum volume 20 µl) | STARLAB, Hamburg, Germany |
| Chromatography paper (thickness: 3 mm) | Whatman (Cytiva), Maidstone, UK |

2.2. Methods

2.2.1. *Listeria monocytogenes*

2.2.1.1. Generation and long-term storage of *Lm* working aliquots

To enable performance of experiments with *Lm* over a longer time period while still using bacteria from the same batch, working aliquots were generated for all listerial strains used in the study (*Lm* EGDe wt, *Lm* EGDe $\Delta inIA$, *Lm* EGDe $\Delta inIB$, *Lm* EGDe $\Delta inIAB$, *Lm* EGDe $\Delta inIF$) and then stored in deep freeze.

To generate the working aliquots, bacteria were first grown overnight on Columbia sheep agar blood plates. On the following day, a single colony from each of the grown strains was picked off the plates, transferred to 10 ml of BHI medium in centrifuge tubes and grown overnight in the water bath (37 °C for 6 h). In the morning, overnight bacterial cultures were centrifuged (10 min, 3500 rpm), after which the supernatant was discarded and the bacterial pellets resuspended in 1 ml of sterile PBS. The optical density (OD₆₀₀) of the bacterial suspensions was measured so that their final concentration in aliquot stocks (BHI:glycerol = 7:3) can be adjusted: it was set to either 1 x 10⁹ bacteria/ml (in samples prepared for *in vitro* experiments) or 6 x 10⁹ bacteria/ml (in samples prepared for *in vivo* experiments). The final volume of working aliquots pipetted into microcentrifuge tubes was 100 µl, resulting in either 1 x 10⁸ bacteria/aliquot (in samples prepared for *in vitro* experiments) or 6 x 10⁸ bacteria/aliquot (in samples prepared for *in vivo* experiments). Aliquots were subsequently flash-frozen in liquid N₂ and stored at -80 °C.

2.2.1.2. Bacterial cultivation and preparation of inoculums for *in vitro* experiments

The bacteria used for the experiments were grown and prepared as previously described by Dinner and colleagues, except that different readings of OD₆₀₀ (as measured on spectrophotometer) were determined for concentration of 1x10⁸ CFU/ml for each bacterial strain used to prepare inoculums for *in vitro* experiments (Table 1) (Dinner et al. 2017).

Table 1. OD₆₀₀ readings corresponding with the concentration of 1 x 10⁸ CFU/ml used for preparation of inoculum for *in vitro* experiments

| Bacterial strain | OD ₆₀₀ |
|--------------------------------------|-------------------|
| <i>Lm</i> EGDe wt | 0.2 |
| <i>Lm</i> EGDe Δ <i>inIA</i> | 0.4 |
| <i>Lm</i> EGDe Δ <i>inIB</i> | 0.1 |
| <i>Lm</i> EGDe Δ <i>inIAB</i> | 0.6 |
| <i>Lm</i> EGDe Δ <i>inIF</i> | 0.2 |

Before each experiment, a listerial aliquot (generation of aliquots described in 2.2.1.1.) was taken out of the deep freeze, thawed, added to 10 ml of BHI medium in a centrifuge tube and incubated for 6 h in the water bath (37 °C) with moderate agitation. After the end of the incubation period, all traces of BHI medium had to be removed so that the bacteria can be resuspended in SFM and have their OD₆₀₀ measured. The washing steps consisted of two centrifugations (10 min, 3500 rpm) followed by removal of the supernatant and resuspension in SFM (in 10 ml after the 1st centrifugation step and in 1 ml after the 2nd centrifugation step). The bacteria resuspended in SFM were measured with a spectrophotometer and adjusted to OD₆₀₀ values corresponding to the concentration of 1 x 10⁸ CFU/ml (Table 1) so that they could be used as inoculum for the experiment. Since it is not possible to distinguish between living, metabolically active and dividing bacteria on one side and the dead or metabolically inactive on the other through spectrophotometric measurement, it has to be taken into account that any given measured OD₆₀₀ value corresponds to a concentration of all bacteria in the sample, living or dead. The actual number of the living bacteria present in the prepared inoculum was determined precisely by subjecting a known volume of it to serial dilution (10-fold steps), plating 10 μ l of three highest dilutions in duplicates on Columbia sheep agar blood plates followed by overnight incubation (5% CO₂, 37 °C) and subsequent quantification of the grown bacteria on the following day. Separate bacterial controls were set up for each time-point (always at least the beginning and the end of the experiment) and each of the experimental conditions and ran in parallel with the main experiment. The number of living bacteria was determined as described for the inoculum. By this procedure, a growth curve for the bacteria in all of the experimental conditions was generated.

2.2.1.3. Preparation of inocula for *in vivo* experiments and generation of *Lm* calibration curve

The concentration of inocula used for *in vivo* experiments was 1×10^8 CFU/2-6 μ l \rightarrow $1.7-5 \times 10^{10}$ CFU/ml, and was therefore too high to precisely correlate to any OD₆₀₀ value – it had to be set each time by extrapolation from a reference calibration growth curve instead (Figure 5). The reference calibration curve was generated by setting up an overnight culture of *Lm* which was measured next day and diluted in a range of samples from OD₆₀₀ = 0.015-0.99 (Dinner et al. 2017). Each of the dilutions was plated on Columbia sheep blood agar plates (Oxoid, Wesel, Germany) and the colonies were counted on the following day (Dinner et al. 2017). Afterwards, each OD₆₀₀ value could be correlated to a specific bacterial concentration due to the bacteria being plated in a known volume of medium and with a known dilution factor, and the linear curve could be generated using these values.

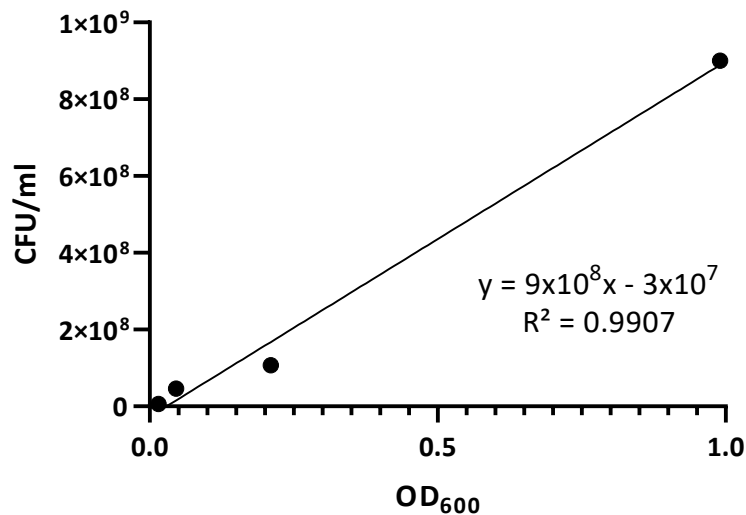


Figure 5. Calibration curve for *Lm* EGDe wt used for calculation of bacterial concentration of inoculums used for *in vivo* experiments

2.2.1.4. Strain verification via PCR

The bacteria mentioned in 2.1.1.1. were either wild type bacteria or specific isogenic deletion mutants of *Lm* EGDe. While strain verification for strain EGDe Δ *inlF* was performed in the group of Prof. Trinad Chakraborty (Institute for Medical Microbiology, University of Gießen, Gießen, Germany) before it was delivered, the identity of the other strains was verified during the course of this study. Namely, PCR was performed to amplify the genes in which the strains differ among themselves – *inlA* and *inlB*, as was previously done in the group of Prof. Horst Schrotten (Gründler et al. 2013; Dinner et al. 2017).

To obtain the bacterial DNA, all four tested strains (*Lm* EGDe wt, EGDe Δ *inlA*, EGDe Δ *inlB* and EGDe Δ *inlAB*) were diluted, plated separately on Columbia sheep blood agar plates and grown overnight in a Heracell 240 incubator (37 °C, 5% CO₂). On the following day, a single colony was picked from each

of the plates, dissolved in 50 µl of distilled water and boiled (99 °C, 15 min) on Thermomixer Compact to lyse the cells and release the DNA. The method description for the PCR reaction as well as subsequent gel agarose electrophoresis can be found under 2.2.4.2.3. The reaction mixtures for PCR as well as the PCR program used for strain verification are shown in Tables 2 and 3, respectively.

Table 2. PCR reaction mixture for *Lm* strain verification (for a single sample)

| Component | Volume (µl) |
|--|-------------|
| 10x PCR Buffer | 2 |
| dNTP mixture (10 mM each) | 0.8 |
| Fw + rev primer pair mix (1:10 of each primer stock) | 0.8 |
| Taq polymerase | 0.2 |
| DNA sample | 2 |
| RNA-free dH ₂ O | 14.2 |
| Total | 20 |

Table 3. PCR program for *Lm* strain verification

| Step | Time (min) | Temperature (°C) |
|----------------------|------------|------------------|
| Initial denaturation | 5 | 94 |
| Denaturation | 1 | 94 |
| Primer annealing | 1 | 60 |
| Extension | 2 | 72 |
| Final extension | 7 | 72 |
| Rest | ∞ | 4 |

} 35x

Primers used for the verification PCR are listed under 2.1.7., and the combinations used for testing with expected product size for each of the samples are shown in Table 4. The products of primer pairs A1 (fw + rev) and B1 (fw + rev) should not be observed in any of the samples since they serve as the negative control. The products of primer pairs A2 (fw + rev) and B2 (fw + rev) should be observed only in the samples from specific deletion mutants (EGDe $\Delta inIA$ for A2 and EGDe $\Delta inIB$ for B2): since the components of primer pair A2 (fw + rev) as well as primer pair B2 (fw + rev) bind to parts of the genome upstream and downstream of the *inIA* (in case of primer pair A2) or *inIB* (in case of primer pair B2) genes, the amplified result can be either the entire gene (if not deleted) or a truncated form of the gene (if deletion is present). Due to the extension time used in the PCR program (Table 3) being too short for the amplification of the entire gene, only the truncated form products could be observed.

The products of primer pairs A3 (fw + rev) and B3 (fw + rev) should be observed only in the samples which do not have deletions of the specific genes (*inIA* for A3 and *inIB* for B3): since the components of primer pair A3 (fw + rev) as well as primer pair B2 (fw + rev) bind to parts of the genome within the *inIA* (in case of primer pair A3) or *inIB* (in case of primer pair B3) genes, the amplified product is present only if the entire gene is present in the strain from which the sample originates. The product of the final primer pair, mixed pair A2 (fw) + B2 (rev), should be observed only in the double deletion mutant strain, EGDe $\Delta inIAB$: since the primer A2 (fw) binds to the part of the genome slightly upstream of the *inIA* gene and the primer B2 (rev) bind to part of the genome slightly downstream of the *inIB* gene, the amplified result can be either the entire *inIAB* operon (if not deleted) or its truncated form (if deletion of the entire operon is present). Due to the extension time used in the PCR program (Table 3) being too short for the amplification of the entire operon, only the truncated form product could be observed. Analysis of the *Lm* strains as described above resulted in the expected PCR amplification products (data not shown).

Table 4. Combinations of primers used for *Lm* strain verification PCR and the expected product size for each of the combinations by strain

The products with sizes indicated in brackets are expected with longer elongation times of the PCR, but were not observed as the products in this study.

| Primer pair | Product size (bp) | | | |
|--------------------|-------------------|------------------------------|------------------------------|-------------------------------|
| | <i>Lm</i> EGDe wt | <i>Lm</i> EGDe $\Delta inIA$ | <i>Lm</i> EGDe $\Delta inIB$ | <i>Lm</i> EGDe $\Delta inIAB$ |
| A2 (fw) + A2 (rev) | (2281) | 235 | (2281) | / |
| A3 (fw) + A3 (rev) | 988 | / | 988 | / |
| B2 (fw) + B2 (rev) | (2181) | (2181) | 399 | / |
| B3 (fw) + B3 (rev) | 1000 | 1000 | / | / |
| A2 (fw) + B2 (rev) | (4502) | (2456) | (2720) | 315 |

2.2.2. *In vitro* experiments

2.2.2.1. Cell cultivation

2.2.2.1.1. Cell culture initiation, maintenance and passage

All the cell lines used in the experiments – HBMEC, HIBCPP, HeLa and bEnd.3 cells – were grown in 75 cm² cell culture flasks in the time between the experiments. They were kept in the incubator (5% CO₂, 37 °C), the cell medium was changed every second day, and the cells were split and passaged once a week to avoid overgrowth of the cells in the flask.

Since all the used cell lines are immortalized or cancer lines, there is a set number of passages after which they cannot be considered genetically and physiologically close to the original culture anymore. Therefore, a new aliquot of the culture had to be taken into culture periodically. After careful thawing, the aliquot was added and slowly mixed with 15 ml of pre-warmed medium (10% HIBCPP or 10% HBMEC, where the former was used for HIBCPP cells and the latter for HBMEC, bEnd.3 and HeLa cells) in a 50 ml centrifuge tube, transferred to 75 cm² cell culture flask and left in the incubator (5% CO₂, 37 °C). The medium was changed on the next day and every second day afterwards, and the cells were not passaged until they reached confluency (confirmed by light microscopy). The time to reach confluency varied between different cell lines: for HIBCPP cells it was 3-4 weeks and for the remaining cell lines 1-2 weeks.

Before passaging the cells, they had to be detached from the flask surface through trypsin digestion. The old medium was discarded and they were washed twice with pre-warmed PBS to remove components of the medium as well as products of cellular metabolism that could interfere with the activity of trypsin. Following that, they were covered with 3 ml of 0.25% Trypsin-EDTA and left in the incubator to detach – the time for incubation varied depending on the cell density in the flask as well as the cell line in question, but it was in the range of 5-20 min. After this period, the activity of trypsin was halted by addition of 10 ml of pre-warmed 10% HIBCPP or 10% HBMEC medium (depending on the cell line). The resulting cellular suspension was transferred to a 50 ml centrifuge tube, mixed briefly using the Analog Vortex Mixer and centrifuged (10 min, 800 rpm). To estimate the number of living cells in the suspension, 10 µl of it was taken before the centrifugation began, mixed 1:1 with 0.4% Trypan Blue solution (which stains dead but not living cells) and assessed on the hemocytometer. After the end of the centrifugation, the supernatant was discarded and fresh, pre-warmed medium was added: its volume was calculated to set the concentration of cells in the suspension to 1 x 10⁶ cells/ml.

The cellular suspension obtained in this manner was used to either passage the cells to a new flask or seed them for the incoming experiments. If it was used for passaging, a set volume (reflecting a set calculated number of cells – 1-2 x 10⁶ cells for HIBCPP cells, 2-4 x 10⁵ cells for HBMEC, bEnd.3 or HeLa cells) was added to 10-15 ml of pre-warmed 10% HIBCPP or 10% HBMEC medium in a 75 cm² cell culture flask and placed in the incubator (5% CO₂, 37 °C).

2.2.2.1.2. Culture slide, cell culture plate and cell culture insert cell cultivation

To set up the cells for the infection experiments, they were seeded either on ThinCert™ cell culture inserts (HIBCPP cells), in Falcon® 8-well culture slides (the remaining cell lines, in experiments intended for analysis by DIF microscopy) or in CytoOne® cell culture plates (the remaining cell lines, in experiments intended for analysis by other methods). Cells in all of these setups were always grown

until they were confluent (confirmed by barrier integrity assessment described in 2.2.2.2 for HIBCPP cells on cell culture inserts or by light microscopy for all the cell lines grown in culture slides or culture plates) before the experiments, which required between 2-7 days, depending on the cell line and the initial number of seeded cells. The expected number of cells for each of the used cell lines when confluent in various models can be found in Table 5.

Table 5. Expected number of cells per compartment for all of the used cell lines (when confluent).

The number of cells for the inserts for 12-well plates is listed in brackets since it was extrapolated from the number of cells for the inserts for 24-well plates.

| Cell line | Cultivation model compartments | | | | |
|-----------|--|--|--------------------------------|----------------------------------|-----------------------------------|
| | Outer filter side (cell culture insert for 24-well plates) | Outer filter side (cell culture insert for 12-well plates) | Chamber (8-well culture slide) | Well (6-well cell culture plate) | Well (24-well cell culture plate) |
| HIBCPP | 4 x 10 ⁵ cells | (1.3 x 10 ⁶ cells) | 2.5 x 10 ⁵ cells | 3.2 x 10 ⁶ cells | 6.5 x 10 ⁵ cells |
| HBMEC | / | / | 2.4 x 10 ⁵ cells | 2.4 x 10 ⁶ cells | 5.8 x 10 ⁵ cells |
| HeLa | / | / | * | * | * |
| bEnd.3 | / | / | * | * | * |

*Assumed to be similar to numbers for HBMEC based on light microscopy observation

Throughout this study, HIBCPP cells were primarily utilized in an inverted cell insert model, as described by Schwerk and colleagues (Schwerk et al. 2012). In detail, the inserts were placed upside down in wells of one size larger cell culture plates (inserts for 24-well plates in 12-well plates and inserts for 12-well plates in 6-well plates), after which the wells were filled with pre-warmed 10% HIBCPP medium in such a manner that the inside of the insert basket was filled as well and the medium reached the inner side of the filter membrane. A single droplet of medium was pipetted on the top (outer side of the filter membrane) of each culture insert as well to ensure that the membrane was properly soaked with medium. The volume of cell suspension (preparation described in 2.2.2.1.1.) corresponding to the desired number of cells was pipetted on the top of each of the inserts, and the plate with the cell-seeded culture inserts was placed in the incubator (5% CO₂, 37 °C) overnight. On the following day, the cell-seeded culture inserts were transferred together with the medium to the cell culture plates of their own size (inserts for 24-well plates in 24-well plates and inserts for 12-well plates in 12-well plates) in standard, hanging orientation and placed back in the incubator (5% CO₂, 37

°C). The name used in this study for the inside of the insert basket is “filter compartment”, while the name for the well in which the insert is hanging will be referred to as “well compartment”.

When seeding the cells in the wells of culture slides or cell culture plates, the volume of cell suspension (preparation described in 2.2.2.1.1.) corresponding to the desired number of cells was pipetted inside each well which contained pre-warmed 10% HBMEC medium, and the culture slides or cell culture plates were placed in the incubator (5% CO₂, 37 °C).

2.2.2.2. Barrier integrity assessment

All the cell lines used in this study are established models for BBB or BCSFB investigation and able to form cellular barriers through cell-to-cell binding via TJs (visual representation example for HBMEC and HIBCPP cells can be found in Figure 6). While this fact makes it acceptable to assume that the cells form a functional barrier if the cell layer is found to be confluent when working in culture slides and cell culture plates, cultivation of the cells in cell culture inserts allows more specific barrier integrity assessment tests to be performed, namely the measurement of the TEER and the layer permeability for complex sugars.

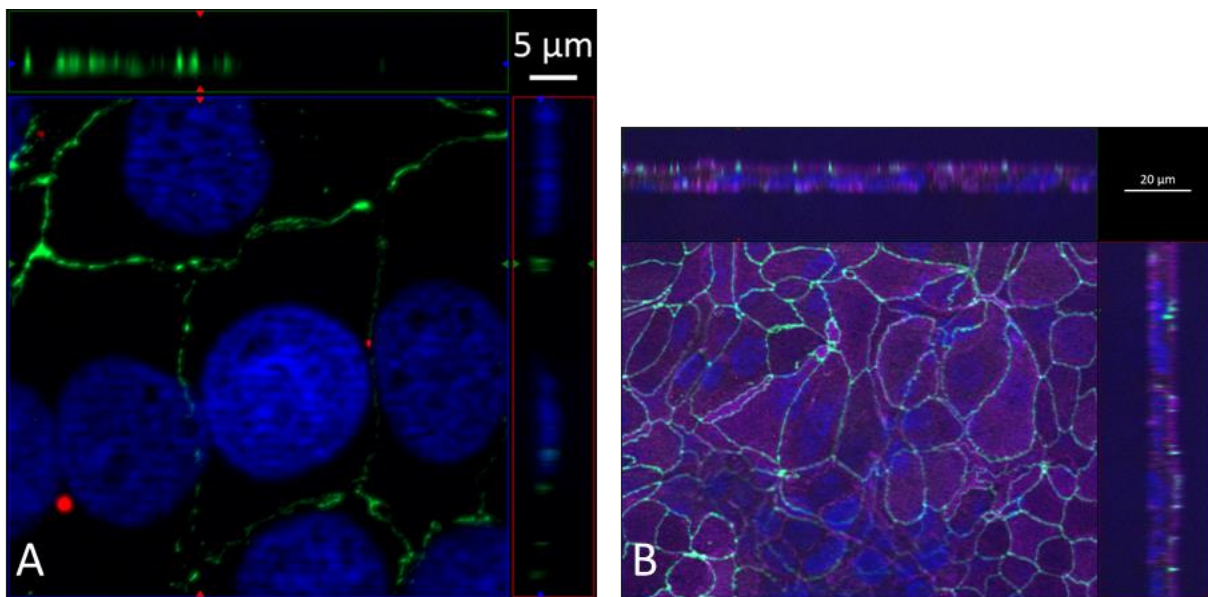


Figure 6. ZO-1 staining in HBMEC (A) and HIBCPP cells (B) outlines the presence of TJs between the cells. *Blue – cellular nucleus, green – ZO-1*

The measurement of the TEER of the HIBCPP cell layer on cell culture inserts was used both daily to determine the confluency and readiness of the cells for the experiments and during the experiments, with higher TEER value indicating stronger barrier integrity. It was performed with a STX 01 chopstick voltohmmeter electrode connected to a Millicell®-ERS voltohmmeter. Before each batch of

measurements, the electrode was left for 10 minutes in 80% ethanol. Following sterilization, it was immersed in the same medium the cells were currently grown in (either 10% HIBCPP or 1% HIBCPP medium) to calibrate and wash the remaining ethanol away. During the measurement, the electrode was oriented in such a way that the shorter arm of the electrode was almost touching the bottom of the filter compartment while the longer arm was almost touching the inside of the well compartment. After waiting for a few seconds for the measured value to stabilize, it was recorded, and then the process was continued for all filters on the cell culture plate – if the medium for any of the filters was of a different coloration or murky, it was skipped and measured last to avoid potential contamination. Since the aim of the measurement was to check the resistance, the selected output value of the voltohmmeter was in Ohms (Ω). To calculate the TEER on the entire surface of the cell culture insert filter, the obtained value was multiplied with the effective surface area of the filter listed by the manufacturer (0.336 cm^2 for the inserts for 24-well plates and 1.131 cm^2 for the inserts for 12-well plates) and resulted in the value expressed as $\Omega \times \text{cm}^2$.

The measurement of the permeability of the cellular layer for complex sugars (whose transport through the cellular barrier should be very low if the barrier is functional) was performed during the infection experiments to evaluate the status of the cellular barriers of cells on individual cell culture insert filters. The sugar used for the measurement of the permeability of the cellular layer for complex sugars was FITC-labeled inulin. Before the infection of the cells at the start of the experiment, $50 \mu\text{l}$ of the $500 \mu\text{g/ml}$ FITC-inulin solution (pre-heated, vortexed and cooled to room temperature) was added inside the filter compartment of every insert for a final concentration of $50 \mu\text{g/ml}$ – since the cells were grown in an inverted model, this would expose their basolateral side to inulin. At the end of the experiment (or at designated intervals), $200 \mu\text{l}$ of medium from the well compartment of each insert was pipetted into black MicroWell™ 96-well plates in duplicates and measured with an Infinite M200 multiwell plate reader. The excitation wavelength for FITC-inulin was 490 nm and the fluorescing wavelength was 520 nm. A FITC-inulin sample designed to simulate the maximal concentration of FITC-inulin in the well compartment in case of the absence of barrier function was incubated in parallel to the experimental samples ($50 \mu\text{l}$ of the $500 \mu\text{g/ml}$ in $950 \mu\text{l}$ of 1% HIBCPP medium resulting in a final concentration of $25 \mu\text{g/ml}$), and serial dilutions of this sample were used to create a standard curve which was utilized to calculate the percentage of FITC-inulin that passed from the filter compartments into the well compartments during the course of the experiment.

2.2.2.3. Cellular infection experiment setup

2.2.2.3.1. Setup in cell culture plates and culture slides

Infection experiments with cells were performed only with confluent cells. In case of HBMEC, bEnd.3 and HeLa cells grown in cell culture inserts and culture slides, the confluency was confirmed by light microscopy. Since there is ample evidence that the serum present in the blood contains factors that inhibit the formation of the cellular barrier, the medium in which the cells were grown had to be removed one day prior to the experiment to enable the cellular barrier to form properly (Chang, Wang, and Caldwell 1997; Chang et al. 1997; Gath et al. 1997; Haselbach et al. 2001). The 10% HBMEC medium was removed and the cells were washed twice with SFM, followed by addition of fresh, pre-warmed 1% HBMEC medium.

After the confirmation of confluency by light microscopy on the day the experiment was to be performed, the old medium was removed and fresh, pre-warmed 1% HBMEC medium was added to them, and they were left to recover in the incubator (1 h, 5% CO₂, 37 °C). It was critical to ensure the correct volumes in either the wells of cell culture plates or the chambers of culture slides to allow a correct measurement of the bacterial concentration during the experiments. The total volume in the wells of cell culture plates was either 1000 µl (for 12-well plates) or 2000 µl (for 6-well plates), while the total volume in the chambers of culture slides was 300 µl – the difference between these volumes and volumes of all the other liquids added for the experiment (bacterial inoculum, etc.) was filled with 1% HBMEC medium before the placing of the cells in the incubator for recovery. Unless it was otherwise specifically required, all the other liquid components were added to the wells/chamber immediately before the infection. The bacterial inoculum was prepared (as described in 2.2.1.1.) during the recovery of the cells. To initiate the experiment, bacteria were added in a multiplicity of infection (MOI) of 10 (for the number of HBMEC, bEnd.3 and HeLa cells during confluency, refer to Table 5.). Bacterial growth controls were set up in parallel, with same volumes of bacterial inoculum being added to microcentrifuge tubes containing 1% HBMEC medium, which were diluted and plated on Columbia sheep agar blood plates and quantified on the following day. At the end of the experiment, the medium was removed from the cells, followed by washing with either PBS or SFM, depending on whether the samples were intended for analysis by PCR, Western blotting or IF microscopy.

2.2.2.3.2. Setup in culture inserts

In case of HIBCPP cells grown on culture inserts, confirmation of barrier function was obtained by TEER measurement. Under normal circumstances, daily measurement of the cellular TEER would show a gradual increase in the values measured. After reaching a measured value of 100 Ω x cm², the 10% HIBCPP medium was removed and the inserts with cells were washed twice with SFM before being

placed in fresh, pre-warmed 1% HIBCPP medium in new 24-well culture plates. This medium exchange sped up the increase of the TEER value of the cells that normally resulted in a TEER peak value after 1-2 days, followed by a rapid decrease within the next 1-2 days. It was established in the group of Prof. Horst Schrotten that the state of the cells (including confluency) is ideal for the experiments when the measured TEER values are in the range of 270-800 $\Omega \times \text{cm}^2$, and the experiment could commence on any day on which a required number of filters was found to be within these values (data not shown).

After the confirmation of barrier function by TEER measurement, the cells were placed in fresh, pre-warmed 1% medium in new 24-well culture plates and left to recover in the incubator (1 h, 5% CO₂, 37 °C). Precise volumes were used for each of the compartments for purposes of later bacterial quantification. The total volume in the well compartment was 1000 μl , while the total volume in the filter compartment was 500 μl – the difference between these volumes and volumes of all the other liquids added for the experiment (bacterial inoculum, FITC-inulin solution, etc.) was filled with 1% HIBCPP medium before placing the cells in the incubator for recovery. All the other liquid components were added either to the filter compartment, well compartment or both immediately before the infection, unless there was a specific need to add something in advance. While the cells were recovering, the bacterial inoculum was prepared (as described in 2.2.1.1.) as well as the FITC-inulin solution (as described in 2.2.2.2.). To initiate the experiment, bacteria were added so that the MOI was 10 – since the number of HIBCPP cells on each of the culture insert filters when they are confluent was taken to be 4×10^5 cells, the number of bacteria added to each filter compartment was 4×10^6 (40 μl of a 1×10^8 CFU/ml inoculum). To enable later quantification, bacterial growth control samples were run together with the main samples, with the same volumes of bacterial inoculum being added to microcentrifuge tubes containing 1% HIBCPP medium. At the last time-point of the experiment, the medium was removed from all compartments, and the cells were washed with either PBS or SFM, depending on whether the samples were intended for analysis by PCR, Western blotting or IF microscopy.

2.2.2.4. Cell viability assessment

LIVE/DEAD Viability/Cytotoxicity Kit for mammalian cells was used in experiments in which it was important to track the survival of cells throughout their course. Immediately after the intended time-point (usually the end of the experiment), the control samples intended for viability assessment were washed once with SFM. A mixture of two fluorescent dyes – ethidium homodimer (stock 2 mM) and calceine green (stock 4 mM) – was prepared by diluting them (1:500 for ethidium homodimer and 1:8000 for calceine green) in SFM and applied to the cells, after which they were placed in the incubator (15 min, 5% CO₂, 37 °C). At the end of the incubation period, the cells were washed three

times with SFM and left in the final volume of SFM for IF microscopy assessment. An Observer Z1 microscope (10x magnification) was used to observe the cells and ZEN Imaging Software was utilized to take the pictures. The living cells could be observed as emitting green light due to being stained with calcein green (excitation and emission wavelengths of 495 and 515 nm, respectively), whose non-fluorescing form is converted into a green-fluorescing form by intracellular esterases. The dead cells, on the other hand, could be observed as emitting red light due to being stained with ethidium homodimer (excitation and emission wavelengths of 535 and 617 nm, respectively), which fluoresces strongly only if bound to the DNA but is unable to penetrate the membrane of living cells. Examples for visual representation of these stainings are shown in Figure 7.

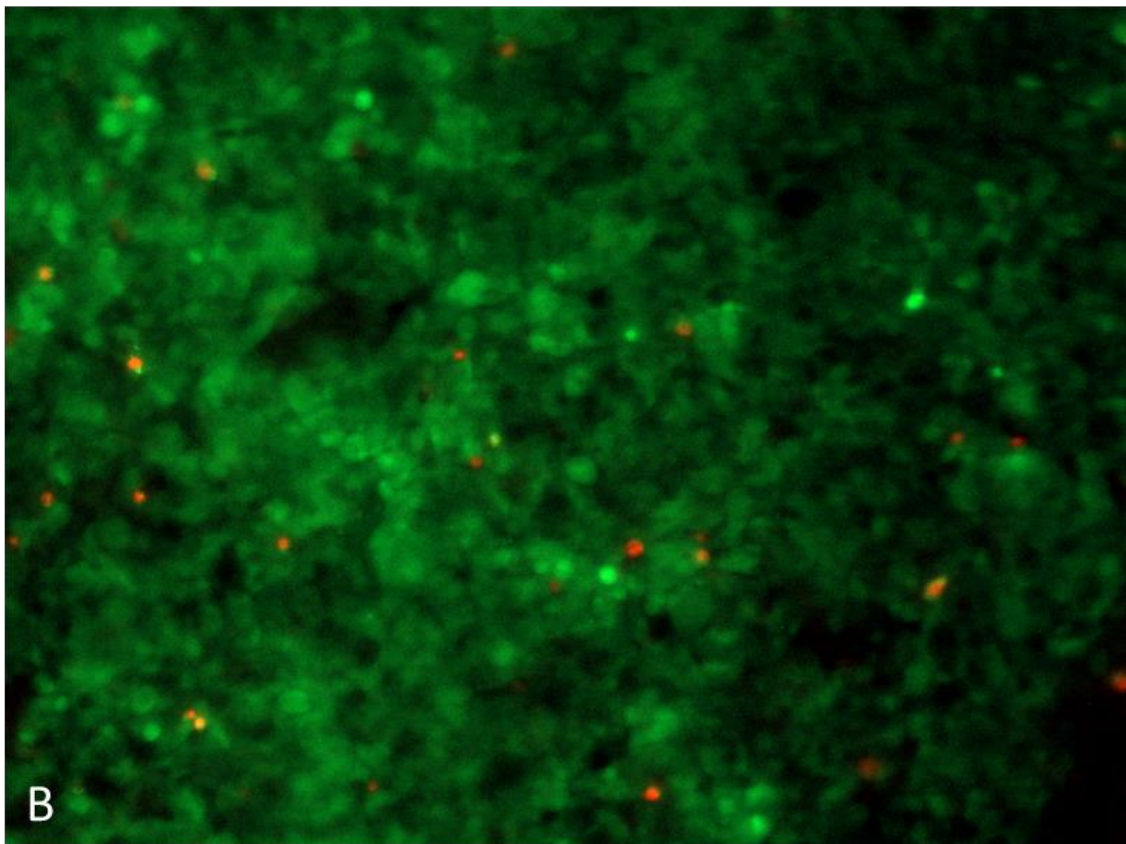
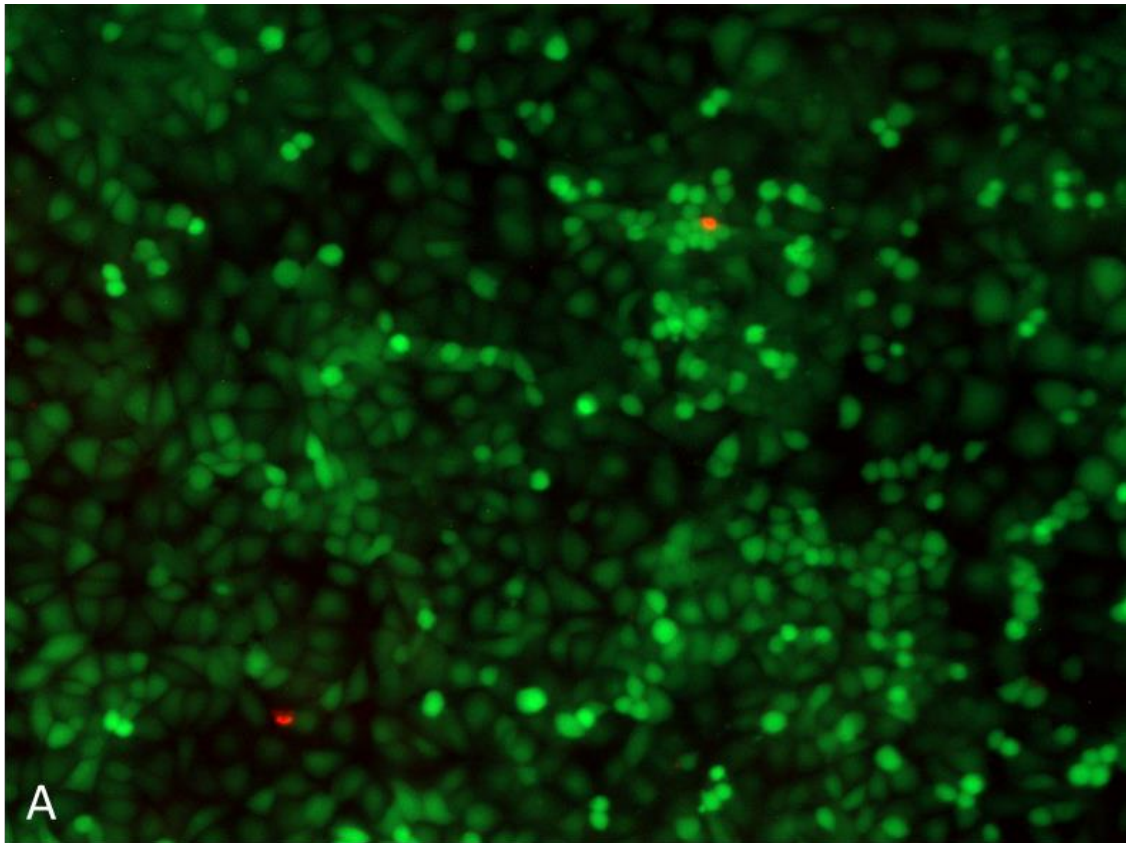


Figure 7. The result of viability assessment staining in HBMEC (A) and HIBCPC cells (B). Green-colored cells are living while the red-colored cells are dead.

2.2.3. In vivo experiments

The protocols for various methods used in mouse experiments were based primarily on those described by Bou Ghanem and colleagues (Bou Ghanem, Myers-Morales, and D'Orazio 2013). All the work with mice was performed in a BSL2 cabinet to prevent both the exposure of mice to outside contaminants and the contamination of the outside space by infected mice.

2.2.3.1. Animal ethics statement

In vivo mouse infection experiments, sacrificing of mice and subsequent organ extraction, handling and analysis of extracted organs were carried out by the author of this thesis (Franjo Banovic), Prof. Dr. rer. nat. Christian Schwerk and technicians of the Animal Core Facility of the Medical Faculty Mannheim, within the said facility. All work was done in compliance with the principles outlined in the European Convention for the Protection of Vertebrate Animals Used for Experimental and Other Scientific Purposes, as well as the German Animal Protection Law (Tierschutzgesetz). The animal experiments were approved by Regierungspräsidium Karlsruhe (Abteilung 3 – Landwirtschaft, ländlicher Raum, Veterinär- und Lebensmittelwesen) under the permit number 35-9185.81/G-275/16.

2.2.3.2. Preparation of contaminated bread

The method used for bread contamination utilized the mixture of PBS and melted butter to suspend the bacteria in for better consistency of results (Bou Ghanem, Myers-Morales, and D'Orazio 2013). A bacterial aliquot prepared for *in vivo* experiments (as described in 2.2.1.1.) was thawed on ice, mixed with either 10 ml of BHI medium in a 15 ml centrifuge tube or 50 ml of BHI medium in a 50 ml centrifuge tube and incubated in the water bath (6 h, 37 °C). During the incubation of the bacterial culture, white bread and salted butter – both previously cut into small, cube-shaped pieces or chunks which were stored in individual microcentrifuge tubes – were taken out of the fridge. The bread pieces were left to warm at room temperature, while the butter chunks were melted at 55 °C together with a small volume of PBS for bacterial resuspension. Following the end of the incubation, the concentration of bacteria was determined by OD₆₀₀ measurement and extrapolation from the calibration growth curve (refer to 2.2.1.3.), and the total number of bacteria could be obtained by multiplication with the volume of the bacterial culture. Since the goal was to concentrate the bacteria so that approximately 1×10^9 bacteria can be added to every bread piece, the bacteria were pelleted by centrifugation (14000 x g, 10 min). After the removal of the supernatant, they were resuspended in a calculated volume of pre-warmed PBS (enough to have the required number of bacteria in 6 µl per bread piece) and mixed well with a calculated volume of pre-vortexed melted butter (enough to have 9 µl per bread piece). Working fast and in small batches (enough mixture for no more than 10 bread pieces at a time) due to quick solidifying of butter, 15 µl of the suspension was pipetted onto each bread piece within a

microcentrifuge tube, while care was taken that the volume was fully absorbed by the bread piece without smearing over the inside of the microcentrifuge tubes. The number of infected bread pieces prepared was always such that there was at least one piece per mouse and several extra pieces left for determining the titer of the actual inoculum. This was done by adding 1 ml of sterile PBS to one of the microcentrifuge tubes containing a contaminated bread piece, 1 min of vortexing, preparation of serial dilutions and plating on Columbia sheep blood agar plates.

2.2.3.3. Infection of mice

Mice were fasted 12 h before the infection to ensure the willingness to consume contaminated bread – the same was done with non-infected control mice to maintain the same conditions for all. They were placed in new IVCs with raised wire flooring units (to prevent coprophagy), minimal bedding and no food, but with unrestricted access to water.

To infect the mice on the following morning, each of the mice designated for infection was placed in an empty plastic box, and one contaminated bread piece was given to it using sterile forceps. The mice usually consumed the bread piece within 5 minutes – in the case that they needed a longer period of time for eating, they were set aside and not disturbed until the bread piece was eaten. In rare instances, the mice had to be force fed the bread pieces using sterile forceps, but only if they refused to eat for longer than 60 minutes. Although Bou Ghanem and colleagues reported a preference for feeding during the dark cycle for Balb/c/By/J mice in contrast to C57BL/6 who were receptive to feeding at all times, no such difference was observed in this study (data not shown) (Bou Ghanem, Myers-Morales, and D'Orazio 2013). Following the consumption of contaminated bread pieces, mice were returned to their original IVCs (raised wired flooring, minimal bedding) but were given food again. Mice were kept in these cages for the rest of the experiment.

2.2.3.4. Administration of immunosuppressants and CD44v6-blocking peptides

Immunosuppressants – cyclosporine A and hydrocortisone sodium succinate – were prepared as stock solutions (refer to 2.1.7.) and frozen so that their stability can be ensured. Before the beginning of each batch of mouse experiments, working aliquots of each were prepared and stored in the freezer alongside the stock solutions. Mice in the groups designated for immunosuppression were given the immunosuppressants daily for the duration of the experiment (or until the death of the animal). The amount used was 2 mg of hydrocortisone sodium succinate (200 µl of 10 mg/ml solution in 0.9% NaCl) and 2 mg of cyclosporine A (400 µl of 5 mg/ml water emulsion) per mouse, administered by intraperitoneal injection using a 30 G needle. Since cyclosporine A was prepared as an emulsion,

needles with a broader opening had to be used when administering it to avoid clogging of the needle (25 G rather than 30 G needle).

Stock solutions of CD44v6-blocking peptides (refer to 2.1.4.) were kept in the freezer once prepared. Smaller working aliquots were prepared before the initiation of an experiment with each batch of mice and kept at 4 °C for the duration of that experiment. Either PBS control, mouse-specific (QP14) or human-specific peptide (KR14) were administered to designated mice groups on the day of infection (before the infection itself) and every second day afterwards for the duration of the experiment (or until the death of the animal). Since the aim was to use 1 mg of peptide per kg of mouse body weight for either of the peptides (e.g. 20 µg for a mouse with a weight of 20 g), the amount given was 100 µl of 1 mg/kg of body weight solution (the weight taken was the average of each group). Both the peptides and the PBS control were administered by intraperitoneal injection.

2.2.3.5. Sacrificing of mice and organ extraction

The method used to sacrifice the mice was an intracardiac injection of a xylazine/ketamine mixture. Before the sacrifice itself, the mice were anesthetized by exposure to isoflurane inside a plastic holding box for a few minutes. They were then taken out of the box and had 200 µl of freshly prepared xylazine/ketamine (1:8) mixture injected intracardially using a 23 G needle, which resulted in an almost instantaneous, painless death for the animal. Without removing the needle from the heart, the syringe was exchanged for an empty one containing heparin, and as much blood as possible was drawn from the heart of the animal and stored on ice. The mouse was placed on an overturned plastic box and thoroughly sprayed over the abdomen and the neck area with 70% ethanol to disinfect and wet the fur. Its head was removed with sterile scissors and processed to harvest the brain. To open the torso, skin on the lower abdomen was grabbed with a pair of forceps, pulled and a horizontal cut on it was made from hip to hip of the hind mouse legs. This was followed by a vertical cut from the middle of lower abdomen to sternum. Both of these cuts went through both skin and the peritoneal wall, but care was taken that the internal organs (especially the intestines) were not nicked by the scissors during the cutting. The mass of intestinal organs was removed from the abdominal cavity by careful cutting of connective tissue and blood vessels ending with a cutting of esophagus on one side and the rectum on the other. The microcentrifuge tubes for all of the organ samples were pre-weighed, and were placed on ice immediately after the extraction of organs to be transferred from the animal facility to the laboratory inside a sealed sample box.

To harvest the brain, sterile surgical scissors were used to cut the skin of the head from the neck to the nose along the top of the head, and the resulting two flaps of skin were pulled towards the ears to expose the skull and facial bones. After fixating the head on the plastic box lid placed on the surface of

the BSL2 cabinet, the snout was cut off and an incision in the middle of the front end of the skull was made with the blunt end of the surgical scissors. The scissors were then used like a lever to slowly split the skull open along the central suture, while taking care not to damage the brain. The two halves of the skull were then separated, and the brain was extracted by cutting of all the nerves connecting it to the head by sterile microsurgical scissors and letting it slide into a microcentrifuge tube containing 1.5 ml of sterile dH₂O.

To harvest the liver, blood vessels connecting it to the surrounding tissue and organs were cut aseptically and it was transferred into a microcentrifuge tube containing 2.5 ml of sterile dH₂O.

To harvest the spleen, it was grasped by sterile forceps and liberated by cutting aseptically the blood vessels on both of its ends, and subsequently transferred into a microcentrifuge tube containing 2.5 ml of sterile dH₂O.

To harvest the mesenteric lymph nodes (MLN), they were first carefully cut off from the intestine and placed into a sterile 60 mm dish on ice, after which all of the fat was removed from them by rolling them over the surface of the dish using sterile forceps. The number of lymph nodes obtained varied between individual mice, but it was usually between 3-5 nodes per mouse. After the removal of fat, the MLN were transferred into a microcentrifuge tube containing 0.75 ml of sterile dH₂O.

2.2.3.6. Homogenization and plating of organs

To assess the number of bacteria in the organs, they had to be homogenized, serially diluted and plated on agar plates for quantification after overnight incubation. Oxford (*Listeria*-selective formulation) agar plates were used to inhibit the growth of non-*Listeria* bacterial species that might have possibly contaminated the organs. All organs were prepared using a tissue homogenizer – with the exception of the MLN, which were processed by application of cell strainers. The blood samples were serially diluted and plated without additional treatment.

To homogenize the MLN, a sterile cell strainer was placed in a sterile 50 ml centrifuge tube for each mouse sample, and the MLN were transferred to the top of the strainer screen. A plunger from a sterile 3 ml syringe was used to mash the nodes into the cell strainer screen, which was then covered in 0.75 ml of sterile dH₂O. The centrifuge tube was then centrifuged (5 min, 300 x g), following which the cell strainer was removed and the centrifuge tube closed.

The three remaining tissues were prepared using a tissue homogenizer at 60% power. Before each homogenization, the homogenizer probe was placed in a 50 ml centrifuge tube containing approximately 25 ml of 70% ethanol (disinfection tube) and run for 15 seconds to disinfect it. After the

disinfection, it was placed in another 50 ml tube containing about 25 ml of sterile dH₂O (dilution tube) and run for another 15 seconds to dilute the ethanol. Each organ sample was homogenized for 30 seconds at 60% power. The probe was cleaned after each sample by being run for 15 seconds in a different 50 ml tube containing approximately 25 ml of sterile dH₂O (cleaning tube), followed by running in the disinfection tube and the dilution tube before the processing of next organ sample. A fresh cleaning tube was prepared for each animal group and organ type.

The homogenates of all five organ sample types – blood, brain, liver, MLN and spleen – had a known approximate volume across different mice and different experiments (Table 6.), and these were used to calculate the total number of bacteria for the entire organ. The only exception was blood, in case of which the number of bacteria was expressed as CFU/ml due to impossibility of obtaining the exactly same volumes of blood from each animal. The samples were serially diluted (10-fold steps) six times, and 10 µl of each dilution step were plated on Oxford (*Listeria*-selective formulation) agar plates. The plates were placed in the incubator overnight (5% CO₂, 37 °C) so that the bacteria could be quantified on the following day.

Table 6. Volumes of organ sample types after the homogenization

| Organ | Total volume (ml) |
|--------------|--------------------------|
| Blood | 0.3-1 |
| Brain | 3 |
| Liver | 3.5 |
| Spleen | 3 |
| MLN | 1.5 |

2.2.4. Molecular techniques

2.2.4.1. IF microscopy

2.2.4.1.1. Sample preparation and staining

IF microscopy was the preferred choice for the observation of molecules or structures of interest on the cellular surface, and the double IF (DIF) method in particular was used to quantify cell-adhered and/or invaded bacteria from the samples obtained in *in vitro* infection experiments (refer to 2.2.2.3.) (Schwerk et al. 2012; Gründler et al. 2013; Dinner et al. 2017). All the antibodies used for IF stainings can be found in 2.1.5.

To use the DIF method for quantification of adhered and/or invaded bacteria, they first had to be stained. After the removal of the bacteria-containing medium, the cells were washed three times with

SFM/1% BSA and left in the third wash for 20 minutes to block the sample before incubation with the primary antibody and to remove remaining unattached and uninvaded bacteria. The DIF staining consists of two steps, both of which contain primary and secondary antibody incubations: the first step was used to stain the extracellular bacteria, and the second step to stain both the extracellular and intracellular bacteria. To begin the first step, cells were – following the blocking with SFM/1% BSA – incubated with the primary antibody (Rabbit anti-*Lm*, diluted 1:500 in SFM/1% BSA) for 20 minutes, which enabled it to bind to extracellular bacteria. This incubation period was followed by two washes with SFM/1% BSA and a third one with SFM to remove the excess primary antibody. Subsequently, cells were incubated with 3.7% formaldehyde solution for 10-15 minutes for fixing and washed two times with PBS to dilute the formaldehyde. When this point was reached, the samples were usually placed at 4 °C overnight. Subsequently, PBS was removed from the cells and they were washed three times with PBS/1% BSA – in case of cells grown on cell culture inserts, the filters with the cells were cut out of the inserts and placed in the wells of a cell culture plate right before this washing step to ease the handling. They were then incubated with the first secondary antibody (Chicken anti-rabbit Alexa Fluor® 594, diluted 1:250 in PBS/1% BSA) for 15 minutes in darkness to make the cell-adhered bacteria fluoresce red when subjected to IF microscopy. The excess antibody was washed away by three more washes with PBS/1% BSA and the cells were permeabilized by a 10-minute incubation with 1% BSA/0.5% Triton/PBS to expose the bacteria inside the cells to antibodies. Permeabilization was stopped by three more washes with PBS/1% BSA and the cells were left in the third wash for 30 minutes for sample blocking. The second step of DIF staining began with the second incubation with the primary antibody, this time for 30 minutes and in darkness, so that it could bind to both the intracellular and extracellular bacteria. Subsequently, the cells were washed again washed for three times with PBS/1% BSA to remove the unbound antibody. The last part of the DIF staining consisted of incubation of the cells with the mixture of second secondary antibody (Donkey anti-rabbit Alexa Fluor® 488, diluted 1:500 in PBS/1% BSA), phalloidin (Alexa Fluor™ 660 Phalloidin, diluted 1:250 in PBS/1% BSA) and DAPI (diluted 1:50000 in PBS/1% BSA) for 60 minutes in darkness, with the aim of fluorescently labeling all the bacteria (labeled by antibody – green fluorescence), cellular nuclei (labeled DAPI – blue fluorescence) and actin cytoskeleton (labeled by phalloidin – infrared fluorescence) present in the sample when subjected to IF microscopy. After the end of this incubation, the cells were washed three times with PBS/1% BSA to remove all the components of the mixture from them. The last step of the sample preparation process was mounting of samples on microscope slides. In case of cells grown in culture slides, all liquid was removed from the chambers and the plastic casing forming the chambers of the slide was slowly and carefully removed from the slide, after which the space with cells was covered with ProLong™ Gold Antifade mounting reagent. In case of the cells grown on cell culture

inserts, the cut-out filters were taken out of the wells by forceps and excess liquid was removed by gently tapping them on the side against dry paper tissues, after which they were placed on microscope slides in such a manner that the cell-covered side of the filter membrane was turned upwards and covered with ProLong™ Gold Antifade mounting reagent. In both cases, the cells were then covered with cover slips, and the microscope slides placed diagonally on the side on top of dry tissue paper for several days to ensure that excess ProLong™ Gold Antifade would be drained by the paper. All slides prepared in this manner were clearly and precisely marked before the beginning of sample preparation.

Cellular samples where the goal was to observe surface or intracellular molecules or structures were stained by standard, single-step IF staining rather than double-step DIF staining, with different primary antibodies.

2.2.4.1.2. IF microscopy and image generation

All samples prepared as described in 2.2.4.1.1. were analyzed by IF microscopy on Observer Z1 light microscope (63x magnification – with immersion). Immersion oil was applied to the sample slides before the microscopy and they were then placed on the objective of the microscope. Samples could be observed on four different channels – blue, green, infrared and red. The blue channel was used to show the cellular nuclei stained by DAPI, while the infrared channel was used to outline the phalloidin-stained actin cytoskeleton of the cells. The other two channels were applied to observe the molecules or structures of interest as well as stained bacteria. Since the infrared channel was invisible by eye on the microscope and there was often a need to have the entire picture of stained targets visible, ZEN Imaging Software was utilized to both observe the sample and generate pictures of it. In cases where a 3D image of the sample was required, Apotome® was used in conjunction with ZEN Imaging Software to create z-stacks – sets of multiple images taken at different focus distances resulting in a 3D representation of the observed part of the sample.

2.2.4.1.3. Bacterial quantification

The number of bacteria present in the sample could be quantified by IF microscopy. For each sample, 20 fields of view were randomly selected and the mean value of bacteria counted in them was calculated. With the assumption of equal distribution of bacteria throughout the sample, this number could be extrapolated to the number of bacteria present in the entire sample, since both the area of a single field of view and the area of the entire sample were known. Finally, the infection rate of the bacteria could be obtained by dividing the calculated number of bacteria present in the sample with

the number of bacteria grown in the growth control for the same time point and multiplying this number with 100 to express it as a percentage.

2.2.4.2. PCR

2.2.4.2.1. RNA isolation

To detect the presence of specific mRNA or any changes in their levels over time and/or in various conditions in the samples obtained from either the uninfected cells or those used in the *in vitro* infection experiments (refer to 2.2.2.3.), RNA of these cells first had to be extracted and purified. After the initial wash with PBS, all the remaining liquid was removed from the cells by careful pipetting. They were then covered in a known volume of RLT buffer: in case of cells in cell culture plates, the buffer was simply added directly to the well, while in the case of cells on culture inserts it was added to the outer side of the filter membrane of upturned inserts placed in empty wells of 12-well cell culture plates. In both cases, cells were lysed by the buffer and simultaneous careful pipetting and scratching of the cell-covered surface with the pipette tip to ensure the highest possible yield of cellular material. The lysates obtained from the duplicates/triplicates of the same condition in the same experiment were pooled, transferred to microcentrifuge tubes and flash-frozen in liquid N₂, and could be either stored at -80 °C or thawed on ice to continue with the isolation and purification. Either RNeasy Micro or RNeasy Mini Kits (depending on the available starting material across experiments) were used for this purpose in accordance with the manufacturer's instructions. Following the purification, the concentration and quality of purified RNA were determined with NanoDrop® ND1000 spectrophotometer and its accompanying software, and the purified RNA was flash-frozen in liquid N₂ and stored at -80 °C.

2.2.4.2.2. cDNA synthesis

cDNA had to be synthesized from the RNA samples (refer to 2.2.4.2.1.) to be used as a template for semi-quantitative PCR. AffinityScript QPCR cDNA Synthesis Kit was used in preparation of cDNA reaction mixtures in accordance with the manufacturer's instructions. The cDNA synthesis reaction was performed using a Thermocycler 2720. Reaction mixtures for cDNA synthesis as well as the PCR program used are shown in Tables 7 and 8, respectively.

Table 7. cDNA synthesis reaction mixture (for a single sample)

| Component | Volume (μl) |
|---|-----------------------------------|
| First Strand Master Mix | 10 |
| Random Primers | 3 |
| AffinityScript Reverse Transcriptase/RNase Block Enzyme Mixture | 0.8 |
| RNA sample (0.5 μ g) | * |
| RNA-free dH ₂ O | * |
| Total | 20 |

*Depends on the concentration of the RNA sample

Table 8. PCR program for cDNA synthesis

| Step | Time (min) | Temperature ($^{\circ}$C) |
|------------------|-------------------|---|
| Primer annealing | 5 | 25 |
| cDNA synthesis | 15 | 42 |
| End of reaction | 5 | 95 |
| Rest | ∞ | 4 |

2.2.4.2.3. Semi-quantitative PCR

The cDNA obtained in the previous step (refer to 2.2.4.2.2.) could be used as a template for semi-quantitative PCR. To enable relative assessment of the initial quantity of the gene material in the sample, several PCR mixtures of each sample were prepared and subjected to PCR reaction, which was paused after 26 cycles (to avoid complete saturation of the bands observed after gel electrophoresis) when some of them were removed, and continued till the end (30 cycles) with the remaining reaction mixtures. The PCR reaction was performed using Thermocycler 2720 and Taq DNA Polymerase Kit (1000U) was used in preparation of the reaction mixtures in accordance with the manufacturer's instructions. Reaction mixtures for PCR as well as the PCR program used are shown in Tables 9 and 10, respectively.

Table 9. PCR reaction mixture for semi-quantitative PCR (for a single sample)

| Component | Volume (μ l) |
|--|-------------------|
| 10x PCR Buffer | 2.5 |
| dNTP mixture (10 mM each) | 1 |
| Fw + rev primer pair mix (1:10 of each primer stock) | 1 |
| Taq polymerase | 0.125 |
| cDNA sample | 0.5 |
| RNA-free dH ₂ O | 19.875 |
| Total | 25 |

Table 10. PCR program for semi-quantitative PCR

| Step | Time (min) | Temperature ($^{\circ}$ C) |
|----------------------|------------|-----------------------------|
| Initial denaturation | 2 | 94 |
| Denaturation | 0.5 | 94 |
| Primer annealing | 0.5 | 58-62* |
| Extension | 1 | 72 |
| Final extension | 7 | 72 |
| Rest | ∞ | 4 |

} 26x - 30x

*Depending on the primer

Primers used for the semi-quantitative PCR are listed under 2.1.7. The PCR reaction samples were subjected to agarose gel electrophoresis (1.5% agarose, +EtBr, 120 V, 50 min) in Sub-Cell GT electrophoresis cells after the PCR was completed. To visualize the results, gels were placed on Biovision-3026WL/26MX, illuminated with UV light and photographed. The size of the products on the resulting pictures was estimated in comparison to the DNA size standard, Gene Ruler 100 bp DNA Ladder.

2.2.4.3. Western blotting

2.2.4.3.1. Protein extract generation and extract concentration measurement

Protein extracts from either the uninfected cells or those used in the *in vitro* infection experiments (refer to 2.2.2.3.) were used to detect the presence of specific proteins – including the presence of phosphorylated forms of those proteins – and changes in their levels over time and/or in various conditions. To obtain protein extracts, cells were washed with PBS twice and covered in a known

volume of RIPA buffer after the removal of all excess PBS: in case of cells in cell culture plates, the buffer was simply added directly to the well, while in the case of cells on culture inserts it was added to the outer side of the filter membrane of upturned inserts placed in empty wells of 12-well cell culture plates. In both cases, cells were lysed by the buffer and simultaneous careful pipetting and scratching of the cell-covered surface with the pipette tip to ensure the highest possible yield of cellular material. The obtained protein extracts from the duplicates/triplicates of the same condition in the same experiment were pooled, transferred to microcentrifuge tubes, flash-frozen in liquid N₂ and stored at -20 °C.

The concentration of the extracts was determined immediately after thawing, to ensure that the precise amount of protein extract could be added during the preparation of the samples for Western blotting. Since the samples were measured by the Lowry method, a standard curve was set up by using six standard samples with concentrations of BSA calibrated to cover the concentration range of 0 – 10 mg/ml which were prepared in advance (Lowry et al. 1951). The DC Protein Assay kit was used to prepare the extract and the standard samples according to the manufacturer's instructions, after which the absorption of the samples was measured on Infinite M200 multiwell plate reader at 660 nm. The concentration of the extracts was calculated by comparison with the standard curve.

2.2.4.3.2. Sample preparation

To be able to detect the different proteins in the protein extract by Western blotting, they first had to be separated by sodium dodecyl sulphate–polyacrylamide gel electrophoresis (SDS-PAGE). Before the preparation of the samples, protein extracts were thawed on ice while NuPAGE™ LDS Sample Buffer was warmed up to 37 °C and mixed with DTT (5 µl Loading Buffer (4X) + 1 µl DTT (1M) per sample). A single sample was prepared by pipetting 6 µl of the Loading Buffer with DTT, calculated volume of the protein extract (corresponding to either 10 or 20 µg of protein) and filling the rest with dH₂O up to 20 µl (or eventually 25 µl). Since the same protein extracts were often used for detection of multiple proteins with similar molecular weights, sample mixes were prepared so that they contained enough volume for the required number of samples of the same extract plus 10% of the total volume of the sample mix. The sample mixes were then briefly vortexed to mix the components, incubated for 10 min at 99 °C and centrifuged (5 min, maximum microcentrifuge speed).

2.2.4.3.3. Gel electrophoresis

Before the initialization of gel electrophoresis, NuPAGE™ Novex™ 4-12 % Bis-Tris gels were placed in XCell SureLock Mini-Cell electrophoresis chambers, which were subsequently filled with running buffer (mixture of 20 ml NuPAGE™ MOPS SDS Running Buffer (20X) + 380 ml dH₂O per chamber) in such a

way that both the upper and lower parts of the gels were immersed in the buffer. After washing the slots of the gels twice with running buffer, Novex Sharp Protein Standard was pipetted in designated slots, while the other slots were filled with previously prepared samples. The current was run through the chamber at constant voltage (200 V) for 35-50 minutes.

2.2.4.3.4. Wet Western blot

For wet Western blotting, a TE22 Mighty Small Transfer Tank was filled with transfer buffer (50 ml NuPAGE™ Transfer Buffer (20X) + 200 ml methanol + 800 ml dH₂O) and set to cool down to 4 °C. As soon as SDS-PAGE was done, the gel holders were opened and the gels were placed within a blotting sandwich – each gel was put atop a piece of sponge and two pieces of chromatography paper, covered by a piece of nitrocellulose membrane and two more pieces of chromatography paper and another piece of sponge, with everything finally being placed in a secured plastic holder. The blotting sandwiches were placed into the transfer tank so that the transfer could be initiated. The current that ran through the transfer tank was set to either constant voltage (20 V) for 16 h or constant amperage (400 mA) for 2.5 h. After the transfer, the membranes were taken out of the sandwich and the marker points on them were marked with a pen for easier orientation during later cutting of the membranes. They were finally washed once in TBS-T.

To block the unspecific binding during antibody incubation, membranes were incubated for 1 h in the blocking solution (5% milk powder solution in dH₂O) and subsequently washed once more in TBS-T. The membranes were then cut into strips based on the molecular weight of the proteins targeted for analysis and placed into designated primary antibody solutions (refer to 2.1.5.1.) for overnight incubation on Duomax 1030 platform shaker (4 °C).

On the following day, the membranes were washed three times with TBS-T and then placed into the solution of designated HRP-coupled secondary antibodies (refer to 2.1.5.2.) for 1 h incubation on Duomax 1030 platform shaker (in darkness). Following the incubation, the membranes were washed three more times with TBS-T.

2.2.4.3.5. Detection and result analysis

To detect and visualize the proteins on the membrane, a 1:1 mixture of substrates from the Immobilon Western Chemiluminescent HRP kit was prepared – the HRP coupled with the secondary antibodies oxidizes the components from the detection kit, which results in a chemiluminescent signal. The membrane pieces were taken out of TBS-T wash and excess buffer was removed from them. They were placed on transparent plastic foil and each membrane piece was covered with the Chemiluminescent mixture (about 100 µl per piece, depending on the piece size). The chemiluminescence was detected

by Chemi Smart 5100 chemiluminescence detector and visualized by Chemi Capt 5000 software. The results from the obtained images could then be quantified by using the ImageJ software, where the software would determine a value in a designated area based on the intensity of the signal.

2.2.4.4. RTK phosphorylation array

2.2.4.4.1. Protein extract generation and extract concentration measurement

To obtain the protein extracts from either the uninfected cells or those used in the *in vitro* infection experiments (refer to 2.2.2.3.) for use with the RTK phosphorylation array, cells were washed twice with PBS and covered in a known volume of the kit-provided lysis buffer after the removal of all excess PBS. In case of cells in cell culture plates, the buffer was added directly to the well, while in the case of cells on culture inserts it was added to the outer side of the filter membrane of upturned inserts placed in empty wells of 12-well cell culture plates. In both cases, cells were lysed by the buffer and simultaneous careful pipetting and scratching of the cell-covered surface with the pipette tip to ensure the highest possible yield of cellular material. The obtained protein extracts from multiple samples of the same condition in the same experiment were pooled, transferred to microcentrifuge tubes, flash-frozen in liquid N₂ and stored at -20 °C. The samples obtained for this part of the project were protein extracts of either uninfected or *Lm*-infected HBMEC and HIBCPP cells.

The concentration of the extracts was determined in the same manner as described in 2.2.4.3.1.

2.2.4.4.2. RTK phosphorylation array protocol and result analysis

Since RTKs were shown to be involved in the cellular entry of multiple different human pathogens (including *Lm*), Human RTK Phosphorylation Array C1 was used to assess the effect that contact with *Lm* has on the activation (through phosphorylation of specific amino-acids) of 71 different human RTKs in HBMEC and HIBCPP cells (Figure 8).

The Human RTK Phosphorylation Array C1 manual was closely followed during the usage of the array. The chemiluminescence on the membranes was detected by Chemi Smart 5100 chemiluminescence detector and visualized by Chemi Capt 5000 software. The results from the obtained images were then quantified by ImageJ software with a Protein Array Analyzer add-on, where the software would determine a value in a designated area based on the intensity of the signal. Positive control values were used for normalization between different membranes, while negative control values were used to measure the background response (Figure 9). RayBio Analysis Tool (provided by the manufacturer) was used to analyze the quantified data obtained by ImageJ.

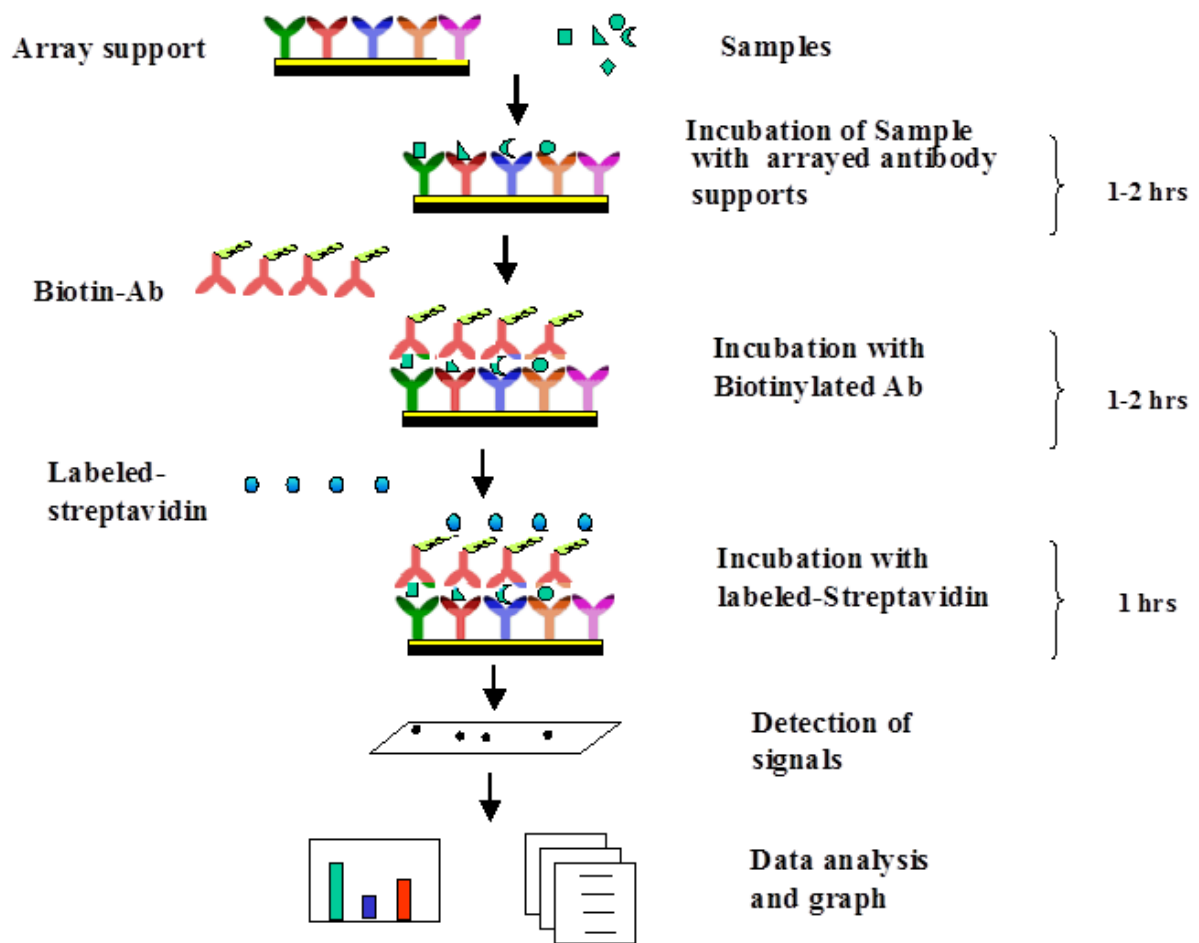


Figure 8. Visual representation of the array's mode of action (figure taken from the Human RTK Phosphorylation Array C1 manual).

| Each antibody is spotted in duplicate horizontally | | | | | | | | | | | | |
|--|----------------------|---|-----------------------|---|-----------------|---|--------|---|-------|---|--------------------------|---|
| | A | B | C | D | E | F | G | H | I | K | K | L |
| 1 | POS1 | | POS2 | | POS3 | | ABL1 | | ACK | | ALK-1 | |
| 2 | NEG | | NEG | | Axl | | Bik | | BMX | | Btk | |
| 3 | Csk | | Dtk | | EGFR | | EphA1 | | EphA2 | | EphA3 | |
| 4 | EphA4 | | EphA5 | | EphA6 | | EphA7 | | EphA8 | | EphB1 | |
| 5 | EphB2 | | EphB3 | | EphB4 | | EphB6 | | ErbB2 | | ErbB3 | |
| 6 | ErbB4 | | FAK | | FER | | FGFR1 | | FGFR2 | | FGFR2 (alpha isoform) | |
| 7 | Fgr | | FRK | | Fyn | | Hck | | HGFR | | IGF-1 R | |
| 8 | Insulin R (CD220) | | Itk | | JAK1 | | JAK2 | | JAK3 | | LCK | |
| 9 | LTK | | Lyn | | M-ATK | | M-CSFR | | MUSK | | NGFR (TNFRSF16) | |
| 10 | PDGFRA | | PDGFRB | | PYK2 | | RET | | ROR1 | | ROR2 | |
| 11 | ROS | | RYK | | SCFR (CD117) | | SRMS | | SYK | | Tec | |
| 12 | Tie-1 | | Tie-2 | | TNK1 | | TRKB | | TXK | | NEG | |
| 13 | Tyk2 | | TYRO 10 (DDR2/TKT) | | VEGFR2 | | VEGFR3 | | ZAP70 | | PO54 | |

Figure 9. Array map (figure taken from the Human RTK Phosphorylation Array C1 manual). POS – positive control (controlled amount of biotinylated antibody printed onto the array), NEG – negative control (buffer printed (no antibodies) used to measure the baseline responses)

2.2.5. Statistics

Statistical analysis of the data presented in this study was performed with SAS System, release 9.4 (SAS Institute Inc., Cary, NC, USA). For results presented in Figures 15B, 16, 18 and 22, a two-sample *t*-test was used to compare mean values of two groups. Analysis of variance (ANOVA) was performed in case of multiple differently treated groups. In case of a significant result, Dunnett's test was used as a multiple comparison procedure. For results presented in Figures 15A, 21, 25 and 26, a two-sample Wilcoxon test was used to compare mean values of two groups. Kruskal-Wallis test was performed in case of multiple differently treated groups.

P-values were considered as being significant (*), very significant (**) or extremely significant (***/****) when <0.05, <0.01 or <0.001/0.0001.

3. RESULTS

3.1. Listerial invasion *in vitro*

3.1.1. HBMEC and HIBCPP cells express proteins relevant for *Lm* invasion

Lm utilizes the proteins of the host cell for its own purposes, many of which are crucial for its successful colonization of and survival within the host (Radoshevich and Cossart 2018). Due to the fact that the expression of these proteins is not uniform across all the cells of the body, it is necessary to ensure that the cell lines used as models for bacterial interaction (primarily adherence and invasion) experiments actually express them. Although the number of human and animal proteins that interact in one way or another with *Lm* is rather large, during this study only those known to interact with the VFs of *Lm* relevant to this study – Ecad (with InIA), Met (with InIB) and vimentin (presumably with InIF) – were investigated (refer to 1.4.1).

Analysis by semi-quantitative PCR and Western blotting demonstrated that HIBCPP cells (as an epithelial cell line) express E-cadherin (one of the markers of epithelial cells), but do not express vimentin (a marker of mesenchymal cells). On the other hand, HBMEC (as an endothelial cell line) do not express Ecad, but do express vimentin (due to being cells of mesenchymal origin). Both cell lines express Met (which is normally expressed in both endothelial and epithelial cells) and both of them express ZO-1 (a tight junction marker protein), although the level of transcription and expression of the two is somewhat different between the two cell lines (Figure 10).

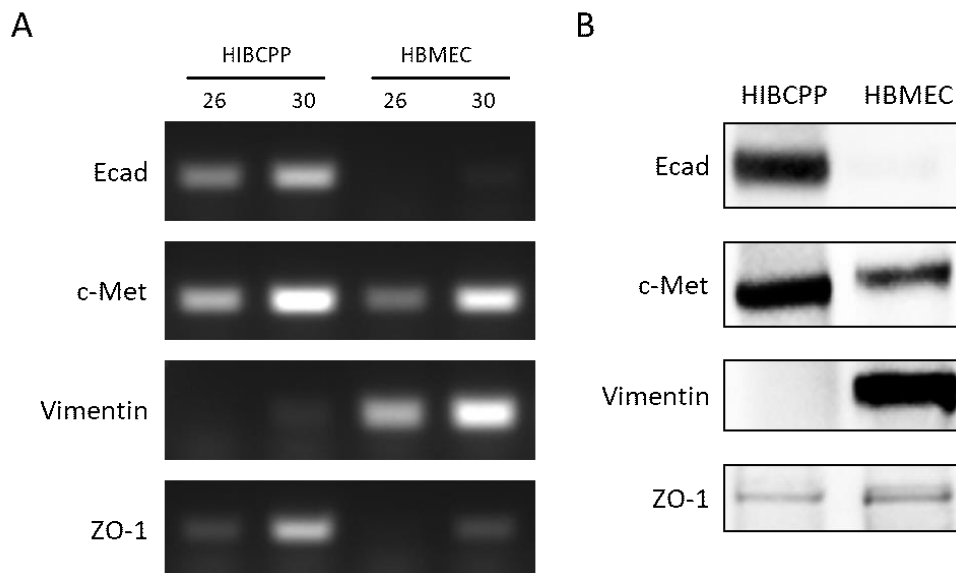


Figure 10. Differences in molecular expression patterns between HIBCPP cells and HBMEC. (A) Overview of the transcription levels of genes of interest in both cell lines, as obtained through semi-quantitative PCR (numbers 26 and 30 denote the number of PCR cycles). (B) Protein expression level of proteins of interest in both cell lines, as obtained through Western blotting. *The presented data were selected as representative of the average outcome of multiple performed experiments. Met is labeled as c-Met in the figure.*

Immunostaining and visualization using IF microscopy was further used to confirm that the molecular profile of the cell lines used in the study is suitable for investigation of listerial invasion dependent on Ecad, Met and vimentin (Figures 11-13). Additionally, cellular localization of these proteins can be visualized by IF staining, ensuring that they are present on the cellular surface and therefore readily available to the bacteria. This is particularly important for vimentin, which is – in cells that express it – always present intracellularly but not always extracellularly (Figure 13).

In HIBCPP cells, Ecad was observed as localized at intercellular junctions, often colocalizing with ZO-1, confirming previous observations found in the literature (refer to 1.2.1.2.), while it was not observed in HBMEC at all (Figure 11). Met was detected on the cellular surface of both cell lines, confirming previous observations found in the literature (refer to 1.5.1.), with it being seemingly more noticeable in HIBCPP cells than in HBMEC (Figure 12). In HBMEC, vimentin was found both intracellularly and on the cellular surface, confirming previous observations reported in the literature (Satelli and Li 2011; Huang et al. 2016), while it was not observed in HIBCPP cells at all (Figure 13).

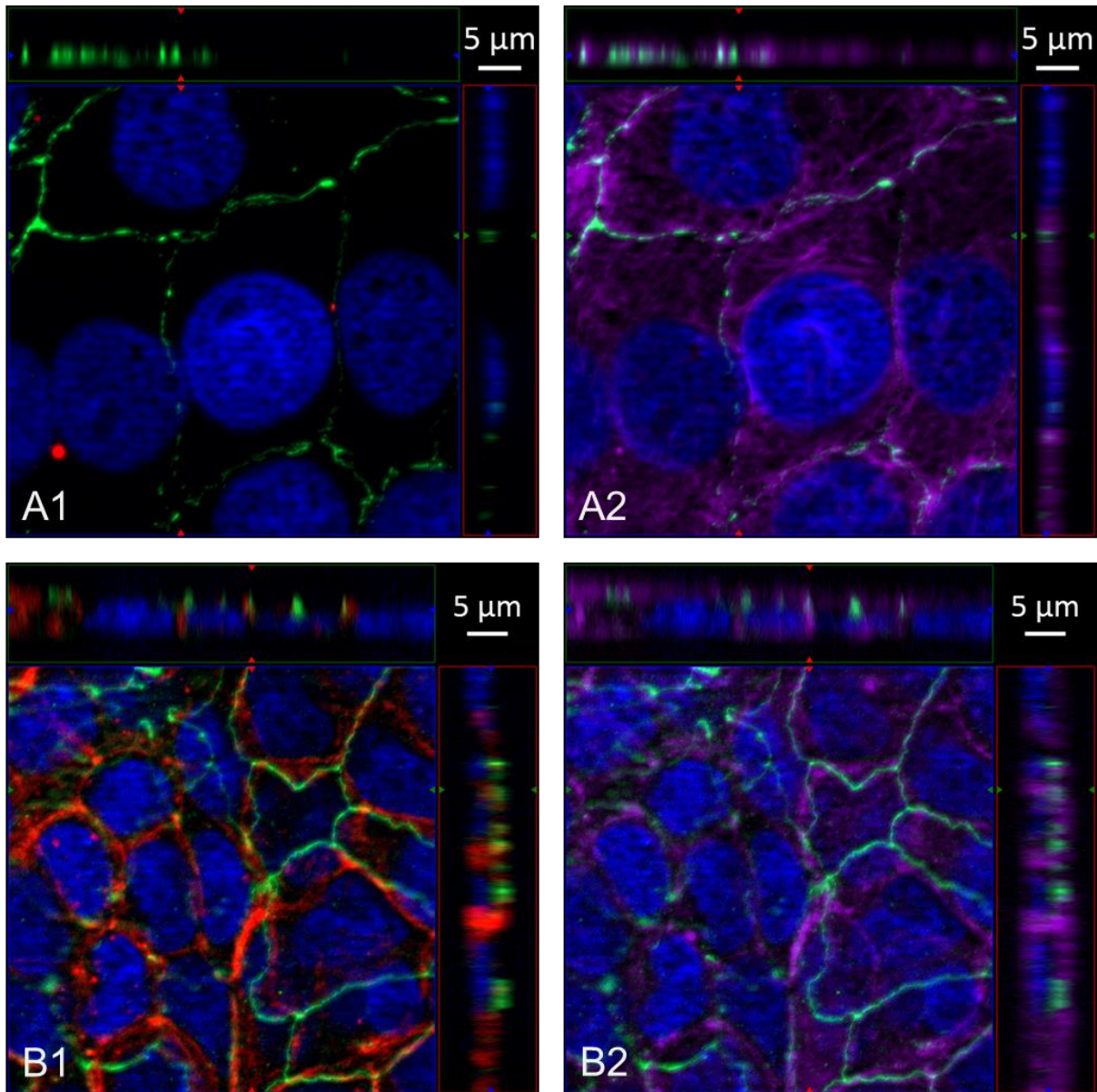


Figure 11. Ecad staining in HBMEC (A) and HIBCPC cells (B) confirms presence of Ecad in HIBCPC cells and its complete absence in HBMEC. Images to the right (marked with 2) are taken from the same field of view as images on the left (marked with 1). The samples were immunostained and visualized using IF microscopy, with panels of the figure representing Apotome images (frontal view in the center and cross-section views above and to the right of the center). For A1 and B1: blue – cellular nucleus, green – ZO-1, red – Ecad. For A2 and B2: blue – cellular nucleus, green – ZO-1, purple – actin. The presented images show fields of view representative for each of the observed samples.

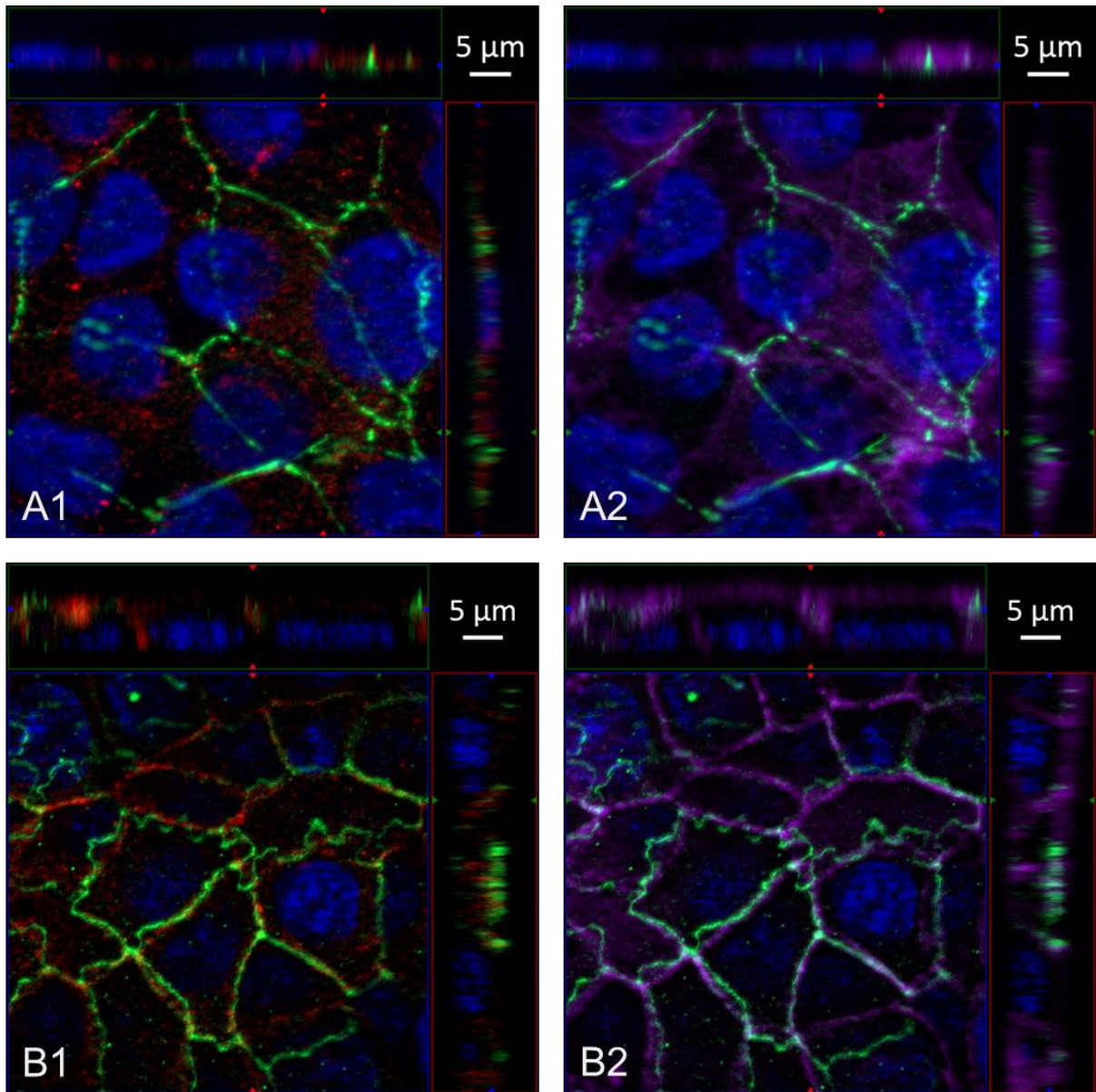


Figure 12. Met staining in HBMEC (A) and HIBCPP cells (B) confirms presence of Met in both cell lines, with apparently stronger presence in HIBCPP (in agreement with the obtained data on protein expression). Images to the right (marked with 2) are taken from the same field of view as images on the left (marked with 1). The samples were immunostained and visualized using IF microscopy, with panels of the figure representing Apotome images (frontal view in the center and cross-section views above and to the right of the center). For A1 and B1: blue – cellular nucleus, green – ZO-1, red – Met. For A2 and B2: blue – cellular nucleus, green – ZO-1, purple – actin. The presented images show fields of view representative for each of the observed samples.

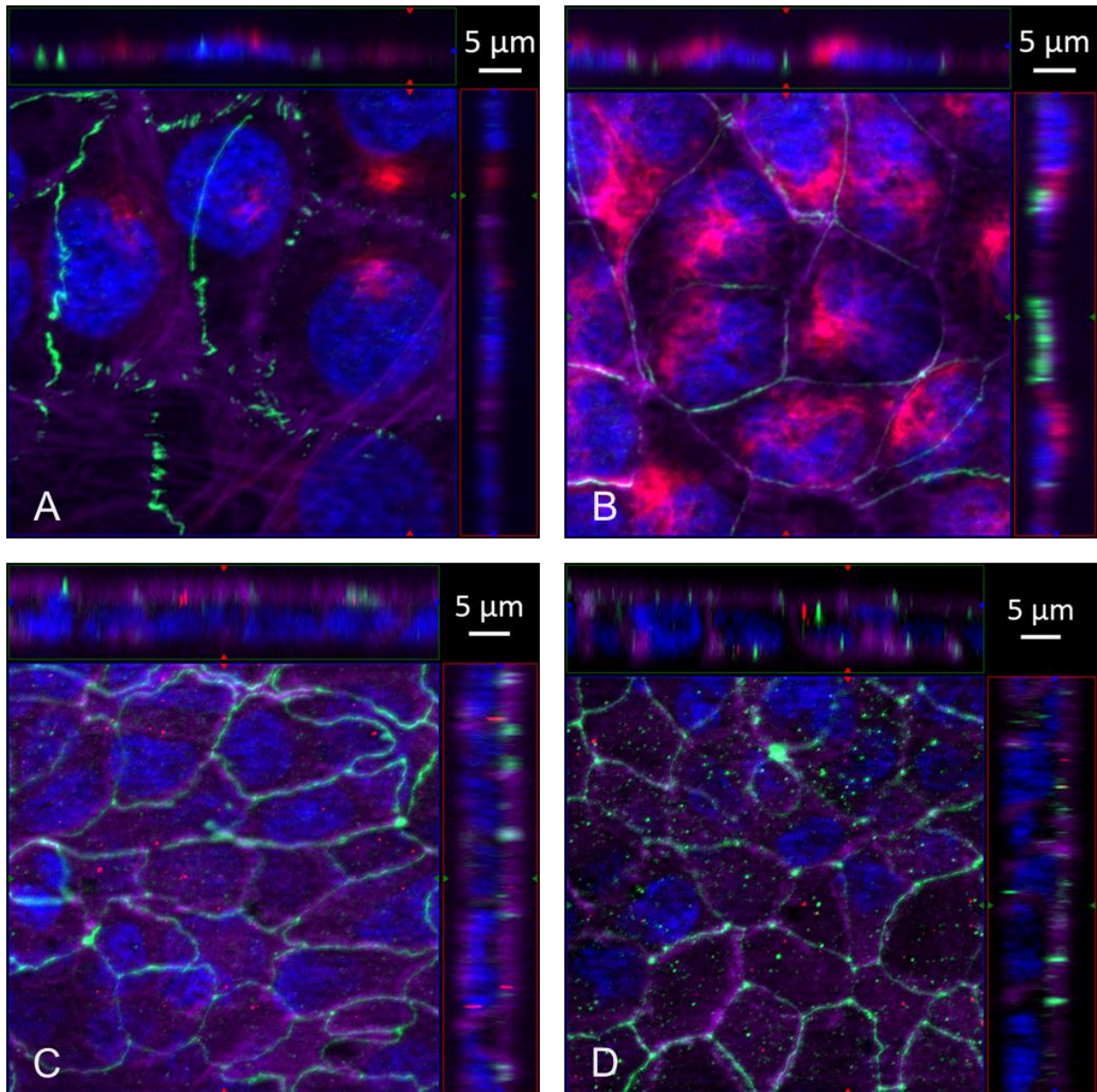


Figure 13. Vimentin staining in HBMEC (A and B) and HIBCPP cells (C and D) confirms presence of vimentin in HBMEC and its complete absence in HIBCPP cells. Images to the right (B and D) were taken from the samples which were permeabilized before the binding of the anti-vimentin antibody and therefore show the total vimentin present in the cells. Images on the left (A and C) were not permeabilized before the binding of the anti-vimentin antibody and therefore show only vimentin present on the surface of the cells. The samples were immunostained and visualized using IF microscopy, with panels of the figure representing Apotome images (frontal view in the center and cross-section views above and to the right of the center). *Blue – cellular nucleus, green – ZO-1, purple – actin, red – vimentin.* The presented images show fields of view representative for each of the observed samples.

3.1.2. Confirmation of differential side-specific invasion of HBMEC and HIBCPP cells by *Lm*

The entry of *Lm* into cell lines that exhibit cellular polarity is usually not equally effective on both sides of the cell – basolateral or apical – due to differential localization of the key proteins *Lm* exploits for entry into the cells. This can be observed in the listerial invasion of the HIBCPP cells, where *Lm* shows preference for invasion from the basolateral side, due to both Ecad and Met – receptors for InIA and InIB – being present on the basolateral side of the cell layer (Gründler et al. 2013).

A test with HBMEC and HIBCPP cells grown in chamber slides was performed to demonstrate the difference in the preference of *Lm* for different sides of the two cell lines. While the bacteria were able to invade the HIBCPP cells only at those points where the cellular layer was damaged or discontinued, there were no such restrictions in regards to the invasion of the HBMEC (Figure 14). This indicates that *Lm* invades into the HBMEC from the apical side, but can efficiently invade HIBCPP cells only from the basolateral side of the cellular layer, and both of these observations conform with what is currently known from the literature (Greiffenberg et al. 2000; Gründler et al. 2013).

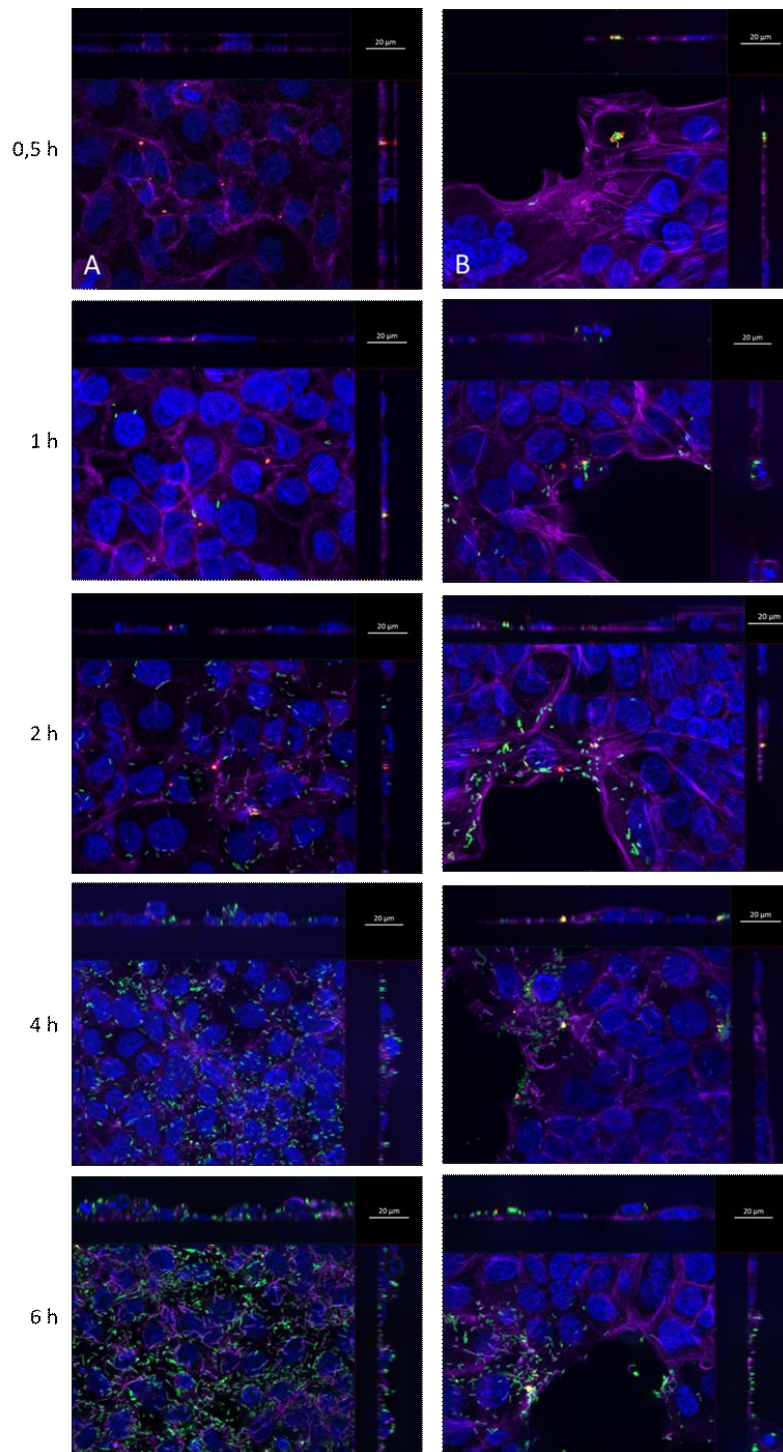


Figure 14. Listerial invasion into the HBMEC (A) and HIBCPP cells (B) over time. Cells were grown on chamber slides (and therefore had the apical side of the layer oriented towards the medium) until confluent and were then infected with wild type *Lm* EGDe (MOI = 10). There are only a few internalized bacteria in both cell lines until the third timepoint (2 h post-infection), and from then onwards, the number of invading bacteria increases rapidly. The samples were immunostained and visualized using IF microscopy, with panels of the figure representing Apotome images (frontal view in the center and cross-section views above and to the right of the center). Blue – cellular nucleus, green – internalized bacteria, orange (overlap of green and red) – surface-attached bacteria, purple – actin. The presented images show fields of view representative for each of the observed samples.

3.1.3. Different internalins are required for invasion of *Lm* into HBMEC and HIBCPP cells

Due to different molecular expression patterns of the HBMEC and the HIBCPP cells, it is reasonable to hypothesize that *Lm* utilizes different VFs for invasion into these cells. To test this assumption, both cell lines were infected with the wild type *Lm* EGDe as well as with deletion mutants for InIs A, B and F (*Lm* EGDe Δ *inIA*, *Lm* EGDe Δ *inIB*, *Lm* EGDe Δ *inIAB* and *Lm* EGDe Δ *inIF*).

It was reported that listerial invasion into HBMEC requires InIB but not InIA, and a previous publication from the group of Prof. Horst Schroten demonstrates that *Lm* uses both InIA and InIB for efficient invasion into the HIBCPP cells (Greiffenberg et al. 1998; Gründler et al. 2013). Invasion experiments conducted within this study mostly confirm these previous findings (Figure 15). The results show that *Lm* depends heavily on InIB for invasion into the HBMEC (which express Met but not Ecad) and confirm the dependence of *Lm* on both InIA and InIB for invasion into the HIBCPP cells (which express both Met and Ecad).

InIF was presented as relevant for listerial invasion into several human and murine cell lines, but only in conditions of ROCK inhibition, and was later more specifically described as interacting with cell surface vimentin (Kirchner and Higgins 2008; Ghosh et al. 2018). Experiments conducted within this study aimed to investigate whether InIF has a role in listerial invasion into HBMEC and HIBCPP cells without ROCK inhibition, and they confirmed the findings reported for other cell lines (Figure 15) (Bastounis, Yeh, and Theriot 2018). Under the standard conditions (i.e. without ROCK inhibition), InIF was seemingly not observed as necessary for entry into either of the cell lines, although HBMEC express vimentin – the reported binding partner of InIF – and HIBCPP cells do not.

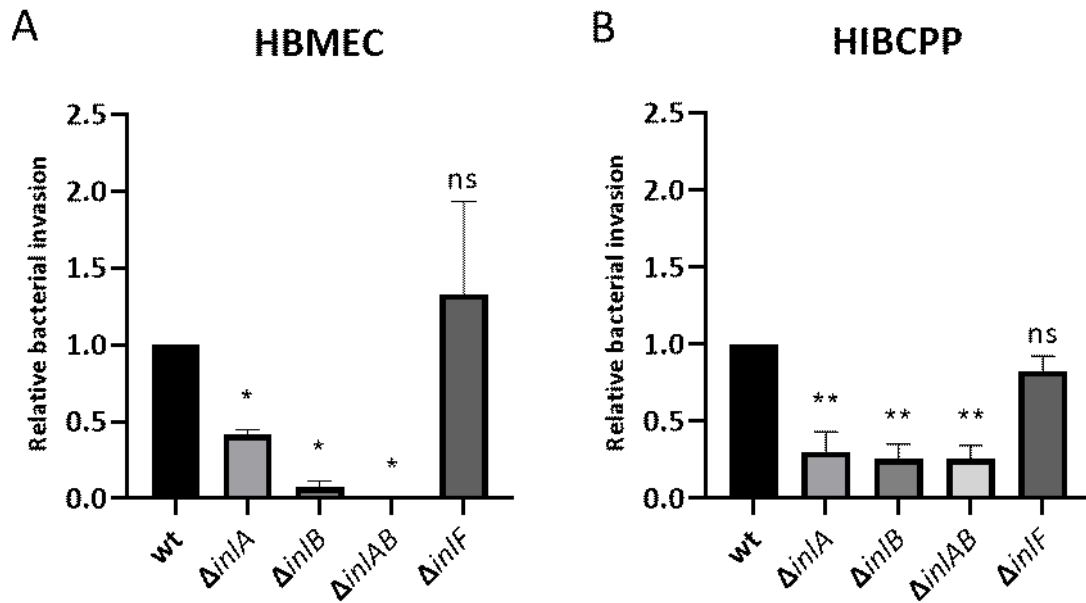


Figure 15. *Lm* utilizes different InIs for entry into HBMEC (A) and HIBCPP cells (B). HBMEC were grown on chamber slides (apical side of the layer oriented upwards) until confluent (as determined by microscopy), while HIBCPP cells were grown in inverted cell culture inserts (basolateral side of the layer oriented upwards) until a functional barrier was established (as determined by measuring the TEER). The cells were then infected with wild type and mutant *Lm* EGDe (MOI = 10) and co-incubated for 4 h before the removal of bacteria and fixation of cells. The samples were immunostained and then visualized and quantified using IF microscopy. (A) * = significant ($p < 0,05$), ns = not significant (significance determined in relation to the invasion of the wild type bacteria). (B) ** = very significant ($p < 0,01$), ns = not significant (significance determined in relation to the invasion of the wild type bacteria).

3.1.4. Modulation of surface vimentin reduces the invasion of *Lm* into HBMEC cells

Vimentin was implicated as an important target for *Lm* (10403S strain) during the invasion of the BBB models *in vitro* (murine bEnd.3 and human hCMEC microvascular endothelial cell lines) and *in vivo* (murine infection model) and is also a known interaction partner for a number of bacterial pathogens (Mak and Brüggemann 2016; Ghosh et al. 2018). To determine its relevance for invasion of *Lm* into HBMEC and HIBCPP cells, the cells were infected with wild type *Lm* EGDe after pre-incubation with increasing concentrations of withaferin A (WitA), a known surface vimentin modulator (Ghosh et al. 2018).

Other researchers report a decrease in invasion rates of *Lm* in their respective *in vitro* models, although they either pre-treated the cells with ROCK inhibitors or infected them with bacterial mutants unable to spread cell-to-cell (*Lm* Δ*actA*) (Bastounis, Yeh, and Theriot 2018; Ghosh et al. 2018). The experimental setup applied in this study – in addition to using different cell lines – also used wild-type bacteria and did not apply ROCK inhibitors (i.e. the cells were pre-treated only with WitA). HIBCPP cells – a cell line shown to not express vimentin – served as an additional control (refer to 3.1.1.). The

outcome of the experiments was mostly in agreement with findings of other groups (Figure 16) (Bastounis, Yeh, and Theriot 2018; Ghosh et al. 2018). The results show a statistically significant, WitA concentration-dependent decrease of invaded *Lm* in HBMEC cells as well as a weaker, statistically non-significant and WitA concentration-dependent decrease of invaded *Lm* in HIBCPP cells, which could be attributed to slightly cytotoxic effects WitA might have on HIBCPP even at low concentrations as well as its off-target effects on the cell (Bastounis, Yeh, and Theriot 2018).

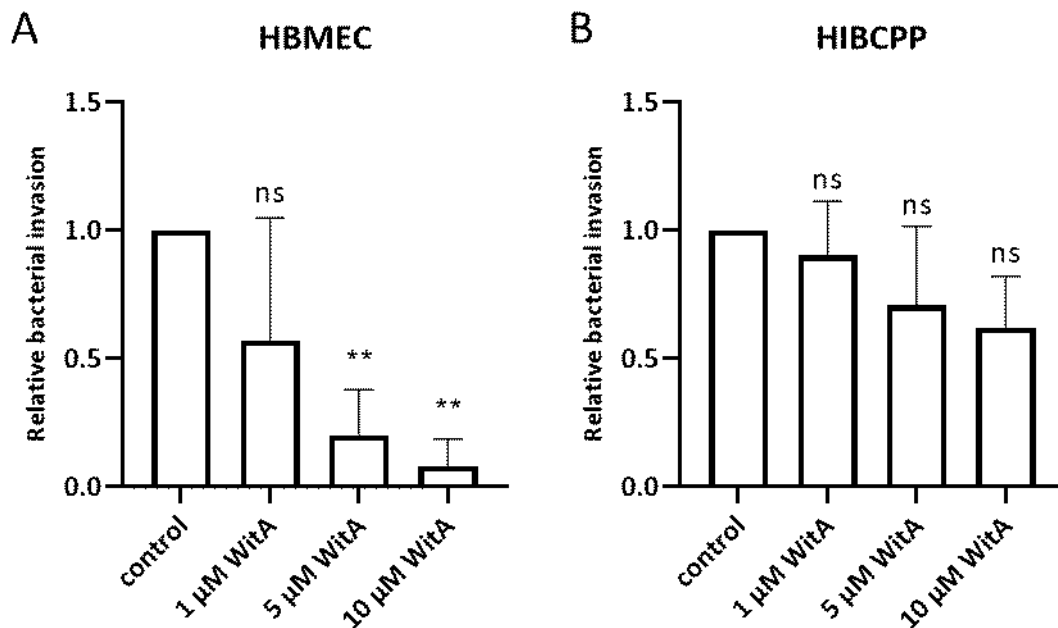


Figure 16. *Lm* requires surface vimentin for entry into HBMEC (A) but not for entry into HIBCPP cells (B). HBMEC were grown on chamber slides (apical side of the layer oriented upwards) until confluent (as determined by microscopy), while HIBCPP cells were grown in inverted cell culture inserts (basolateral side of the layer oriented upwards) until a functional barrier was established (as determined by measuring the TEER). The cells were pre-incubated with WitA (/, 1 μM, 5 μM or 10 μM) for 0.5 h and then infected with wild type *Lm* EGDe (MOI = 10) and co-incubated for 4 h before the removal of bacteria and fixation of cells. The samples were immunostained and then visualized and quantified using IF microscopy. (A) ** = very significant ($p < 0,01$), ns = not significant (significance determined in relation to the invasion of the wild type bacteria). (B) ns = not significant (significance determined in relation to the invasion of the wild type bacteria into the untreated cells).

Although WitA can be safely used for pre-treatment of cells, it was also reported to be cytotoxic in concentrations above 10 μM (Bastounis, Yeh, and Theriot 2018). Therefore, additional control samples were prepared and used during the experiments (and treated with the LIVE/DEAD viability kit after the experiments) to exclude the possibility of observed changes in invasion rates actually being a result of WitA-mediated cell deaths (Figure 17). The results demonstrated that WitA did not have obvious cytotoxic effect on the cells in concentrations used in the experiments.

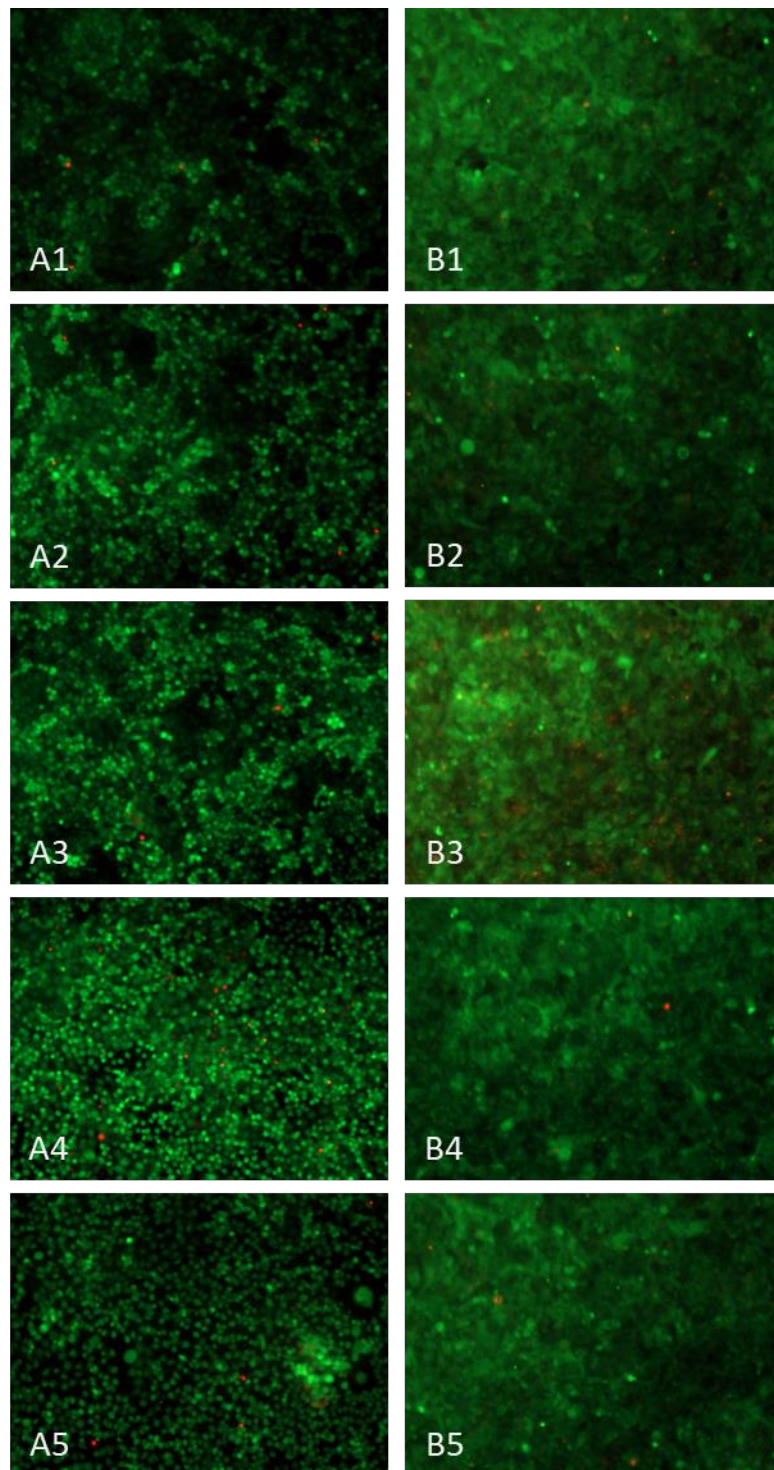


Figure 17. Co-incubation with WitA in presence of *Lm* does not visibly affect survival of either HBMEC (A) or HIBCPP cells (B). The order of the samples is as follows: 1 – control (untreated cells); 2 – infected cells (with *Lm* EGDe wt); 3-5 – WitA-pre-incubated cells cells (3 – 1 μ M WitA; 4 – 5 μ M WitA; 5 – 10 μ M WitA). The cells in 3-5 were pre-incubated with WitA for 0.5 h and then infected with wild type *Lm* EGDe (MOI = 10) and co-incubated for 4 h before the removal of bacteria and treatment with the LIVE/DEAD kit components. Following the staining, they were visualized and assessed using IF microscopy. Green – metabolically active cells, red – dead cells. The presented images show fields of view representative for each of the observed samples across multiple experiments.

3.1.5. Incubation with CD44v6-blocking peptides has no effect on listerial invasion rates

CD44v6-blocking peptides were previously reported to inhibit the entry of *Lm* into HeLa cells, although there was some controversy concerning the importance of CD44v6 for listerial invasion (Jung et al. 2009; Dortet et al. 2010). To assess their effectiveness in inhibition of *Lm* invasion into cells of the BBB and the BCSFB, experiments were performed with multiple cell lines – human HBMEC (microvascular endothelium) and HIBCPP cells (CP epithelium) and murine bEnd.3 cells (microvascular endothelium). To replicate the findings of Jung and colleagues, experiments were also performed with HeLa cells (Jung et al. 2009). Cells were pre-incubated with either KR14, QP14 or were not pre-incubated (control) – in the case of the human cell lines (HBMEC, HeLa and HIBCPP cells), QP14 acted as the control peptide, while in the case of the murine cell line (bEnd.3 cells) this role was filled by KR14. Following the pre-incubation with the peptides, the cells were infected with either the wild type *Lm* EGDe or the InIA-deficient deletion mutant strain of *Lm* EGDe (*Lm* EGDe Δ *inIA*). *Lm* EGDe Δ *inIA* was used to exclude the possibility for the bacteria to utilize the InIA-Ecad route for entry into the cells and enable the focus on the changes in invasion rates related to cell entry mediated by interaction of InIB with Met (and presumably CD44v6) as the only remaining major route of invasion.

The results show no real difference in listerial invasion rates into the cells after the pre-incubation with neither KR14 nor QP14 for neither the wild type bacteria nor the InIA deletion mutant, and the same was observed for all four tested cell lines (Figure 18).

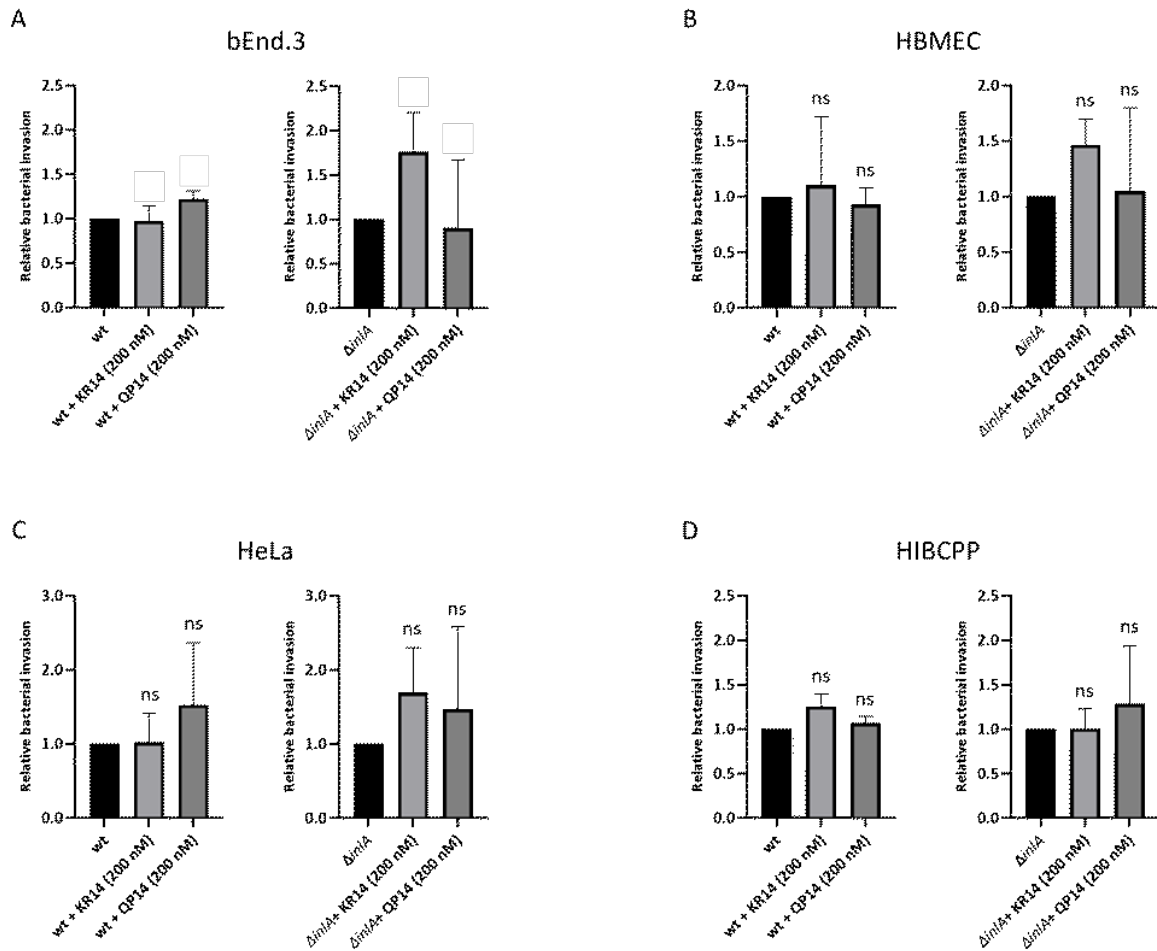


Figure 18. Pre-incubation with CD44v6-blocking antibodies does not affect invasion rates of *Lm* into bEnd.3 (A), HBMEC (B), HeLa (C) and HIBCPP (D) cells. bEnd.3, HBMEC and HeLa cells were grown on chamber slides (side of the layer oriented upwards) until confluent (as determined by microscopy), while HIBCPP cells were grown in inverted cell culture inserts (basolateral side of the layer oriented upwards) until a functional barrier was established (as determined by measuring the TEER). The cells were pre-incubated with KR14 or QP14 (200 nM) for 0.5 h and then infected with either wild type *Lm* EGDe or the InIA deletion mutant strain (MOI = 10) and co-incubated for 4 h before the removal of bacteria and fixation of cells. The samples were immunostained and then visualized and quantified using IF microscopy. (A) *Not enough experiments for statistical analysis.* (B) *ns = not significant (significance determined in relation to the invasion of either the wild type bacteria or the InIA deletion mutant into the untreated cells).* (C) *ns = not significant (significance determined in relation to the invasion of either the wild type bacteria or the InIA deletion mutant into the untreated cells).* (D) *ns = not significant (significance determined in relation to the invasion of either the wild type bacteria or the InIA deletion mutant into the untreated cells).*

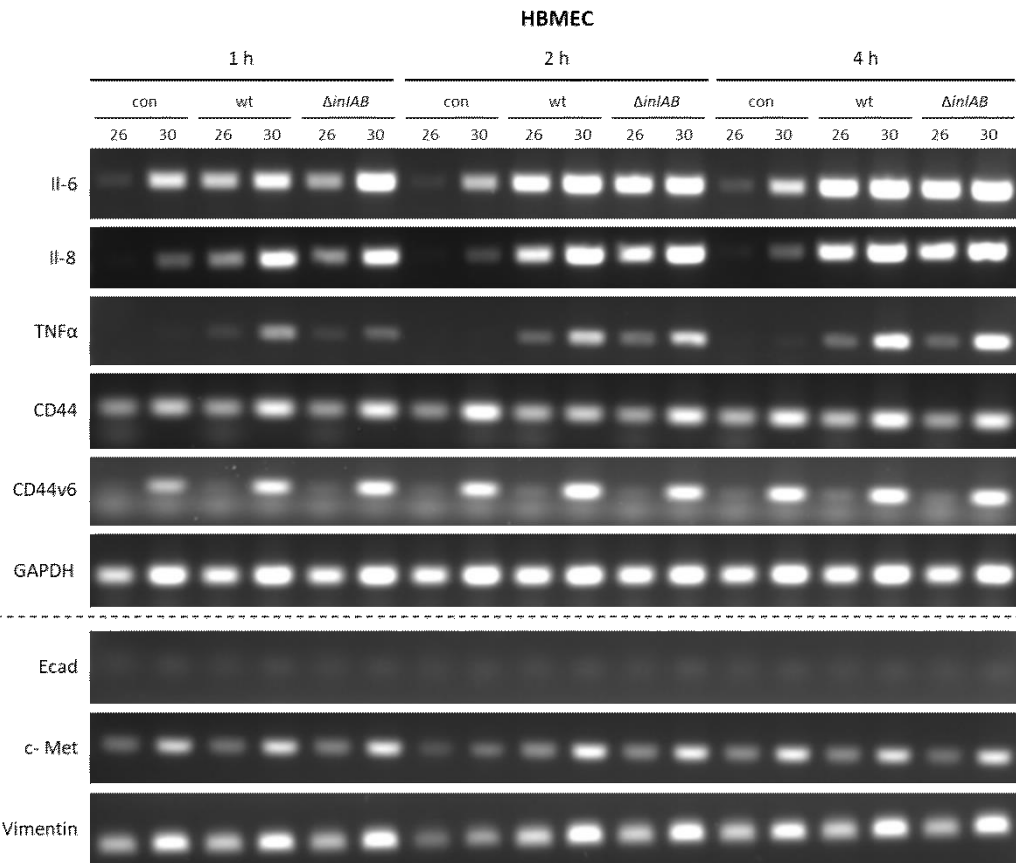
3.2. Downstream cellular signaling affected by listerial invasion

3.2.1. *Lm* invasion upregulates inflammation-related genes but does not affect the transcription of interaction partners of listerial VFs in HBMEC and HIBCPP cells

It was previously demonstrated in the group of Prof. Horst Schrotten that the interaction between *Lm* and HIBCPP cells results in a rapid increase of transcription of inflammation-related genes in HIBCPP cells (Dinner et al. 2017). Building upon these findings, the goal was to determine a) whether the results obtained in HIBCPP cells can be recapitulated in HBMEC, b) whether the *Lm* $\Delta inIAB$ double deletion mutant causes similar effects, c) whether the transcription of the genes of any of the known interaction partners of listerial VFs (CD44v6, Ecad, Met and vimentin) is modified by *Lm* infection and d) how these changes do occur over time. In order to achieve this, time course infection experiments with both cell lines were conducted, where the cells were infected with either the wild type *Lm* EGDe or the double deletion mutant for InIs A and B (*Lm* EGDe $\Delta inIAB$).

The results of the semi-quantitative PCR performed on the samples obtained from the experiments indicate that the co-incubation of both cell lines with *Lm* – regardless of the presence or absence of the products of *inIAB* operon – leads to the upregulation of inflammation-related genes, and also that the transcription of genes of none of the previously mentioned invasion-related surface proteins changes following the infection of the cells (Figure 19). These findings are in line with the information currently present in the literature (Wang et al. 2011; Dinner et al. 2017).

A



B

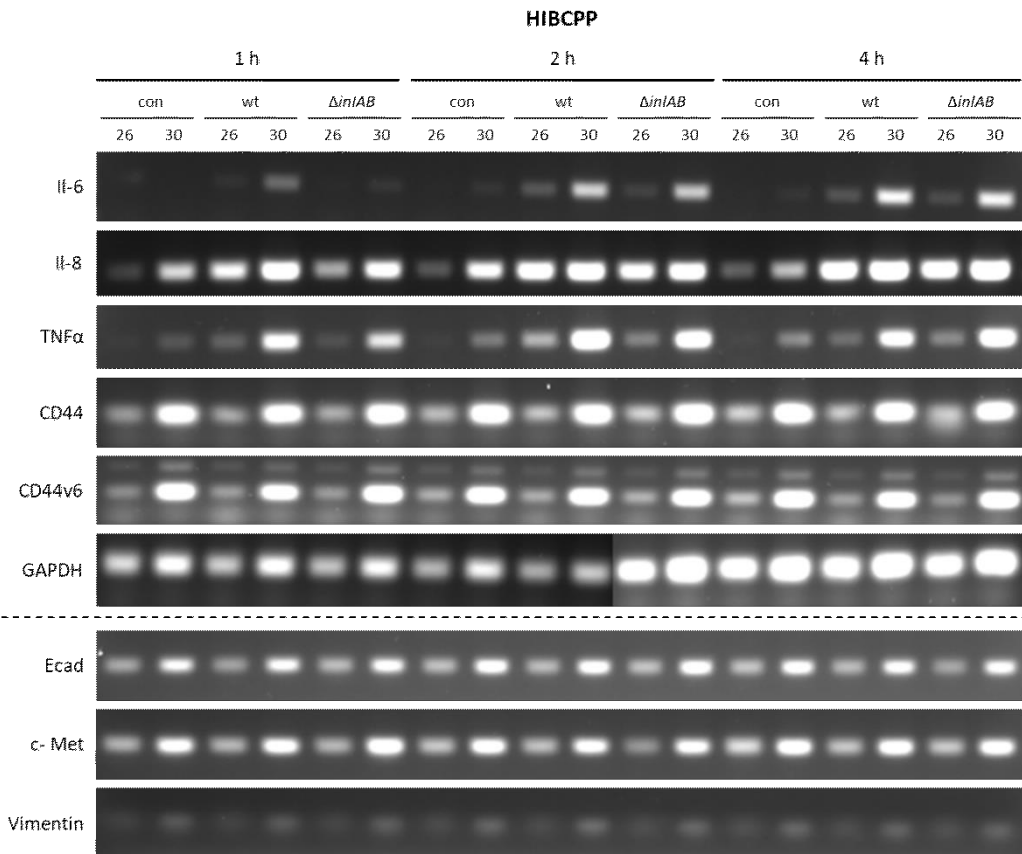


Figure 19. Contact with *Lm* causes a strong upregulation of inflammation-related (IL-6, IL-8 and TNF α) genes in both HBMEC (A) and HIBCPP cells (B), but the transcription of reported interaction partners of listerial VFs (CD44v6, Ecad, Met and vimentin) remains constant. HBMEC were grown on chamber slides (apical side of the layer oriented upwards) until confluent (as determined by microscopy), while HIBCPP cells were grown in inverted cell culture inserts (basolateral side of the layer oriented upwards) until a functional barrier was established (as determined by measuring the TEER). The cells were infected with either wild type *Lm* EGDe or *Lm* EGDe Δ *inlAB* double deletion mutant (MOI = 10) and co-incubated for 1-4 h before the removal of bacteria and lysis of cells. Following the lysis of the cells, samples were subjected to semi-quantitative PCR. *con* = uninfected cells; *wt* = cells infected with wild type *Lm* EGDe; Δ *inlAB* = cells infected with *Lm* EGDe Δ *inlAB*. Numbers 26 and 30 denote the number of PCR cycles.

3.2.2. Infection with *Lm* activates components of the MAPK pathways in HBMEC

Previous work done within the group of Prof. Horst Schroten showed that the invasion of HIBCPP cells by *Lm* triggers downstream signaling via MAPK pathway (Dinner et al. 2017). Since Dinner and colleagues did not investigate MAPK activation in HBMEC, experiments were conducted to investigate this issue. Both HBMEC and HIBCPP cells (serving as an additional control) were incubated either with or without wild type *Lm* EGDe. Following the incubation period, bacteria were removed and cells were lysed to generate protein samples, which were subjected to Western blot analysis.

The obtained results repeated the observed findings for HIBCPP cells and the activation of p38 in HBMEC, confirming previous findings (Opitz et al. 2006; Dinner et al. 2017) (Figure 20). However, ERK1/2 showed same (heightened, in comparison to HIBCPP) levels of phosphorylation in both infected and uninfected samples (Figure 20).

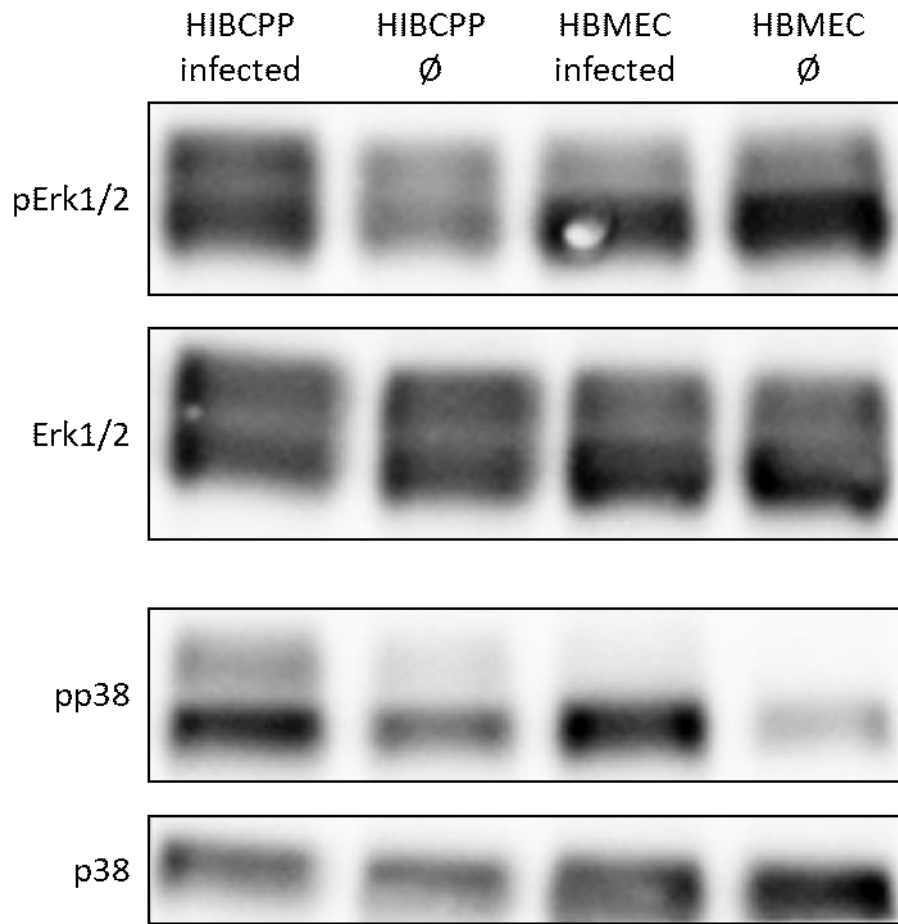


Figure 20. *Lm* infection triggers the activation of MAPK pathways in both HBMEC and HIBCPP cells. HBMEC were grown on chamber slides (apical side of the layer oriented upwards) until confluent (as determined by microscopy), while HIBCPP cells were grown in inverted cell culture inserts (basolateral side of the layer oriented upwards) until a functional barrier was established (as determined by measuring the TEER). The cells were either uninfected or infected with wild type *Lm* EGDe (MOI = 10) and co-incubated for 4 h before the removal of bacteria and lysis of cells. Following the lysis of the cells, the concentration of the samples was measured and they were subjected to Western blotting. *infected* = cells infected with wild type *Lm* EGDe; \emptyset = uninfected cells. The presented data were selected as representative of the average outcome of multiple performed experiments.

3.2.3. Inhibition of MAPK signaling reduces listerial invasion into HBMEC

It was previously demonstrated that the inhibition of MAPK signaling decreases the rates of listerial invasion into HIBCPP cells (Dinner et al. 2017). In order to assess whether these effects on listerial invasion into epithelial cells also apply to listerial invasion into endothelial cells, HBMEC were infected with wild type *Lm* EGDe after pre-incubation with inhibitors of MAPK pathway components ERK1/2 (U0126) and/or p38 (SB203580). The experimental setup used for the invasion into the HIBCPP (including the concentrations of the inhibitory compounds) by Dinner and colleagues was used as a template for these experiments (Dinner et al. 2017).

Experimental results have shown that the inhibition of both ERK1/2 and p38 as well as p38 alone causes a statistically significant decrease in rates of *Lm* entry into the HBMEC (Figure 21). The inhibition of ERK1/2 alone, on the other hand, led to no constant discernible difference in the invasion rates across experiments in comparison to the untreated cells.

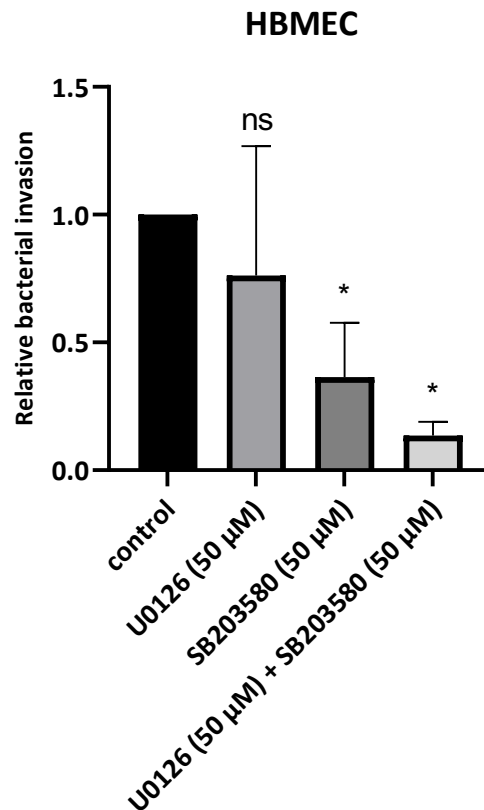


Figure 21. Pre-incubation with p38-inhibiting compound SB203580 causes a statistically significant drop in invasion of *Lm* into HBMEC, but pre-incubation with ERK1/2-inhibiting compound U0126 does not. HBMEC were grown on chamber slides (apical side of the layer oriented upwards) until confluent (as determined by microscopy) and were then pre-incubated with either U0126 (50 μM), SB203580 (50 μM) or both for 1 h, after which they were infected with wild type *Lm* EGDe (MOI = 10) and co-incubated for 4 h before the removal of bacteria and fixation of cells. The samples were immunostained and then visualized and quantified using IF microscopy. * = significant ($p < 0,05$), ns = not significant (significance determined in relation to the invasion of the wild type bacteria into the untreated cells).

3.2.4. Inhibition of the dynamin assembly machinery reduces listerial invasion into HBMEC

Literature on *Lm* invasion of non-phagocytic cells outlines the vital importance of the dynamin assembly machinery for successful bacterial internalization (Pizarro-Cerdá, Kühbacher, and Cossart 2012; Dinner et al. 2017). In order to confirm this observation in endothelial cells, HBMEC were infected with wild type *Lm* EGDe after pre-incubation with increasing concentrations of Dynasore, a known inhibitor of dynamin. The experimental setup used by Dinner and colleagues in HIBCPP cells was used as a template for these experiments (Dinner et al. 2017).

The results of invasion experiments performed with HBMEC whose dynamin assembly was inhibited showed a very high, concentration-dependent and statistically significant decrease in listerial invasion in comparison to the untreated cells (Figure 22). These observations are concurrent with the current understanding of the endocytosis-based mode of cellular entry utilized by *Lm* and data on listerial invasion into HIBCPP cells in conditions of dynamin assembly inhibition (Veiga and Cossart 2005; Dinner et al. 2017).

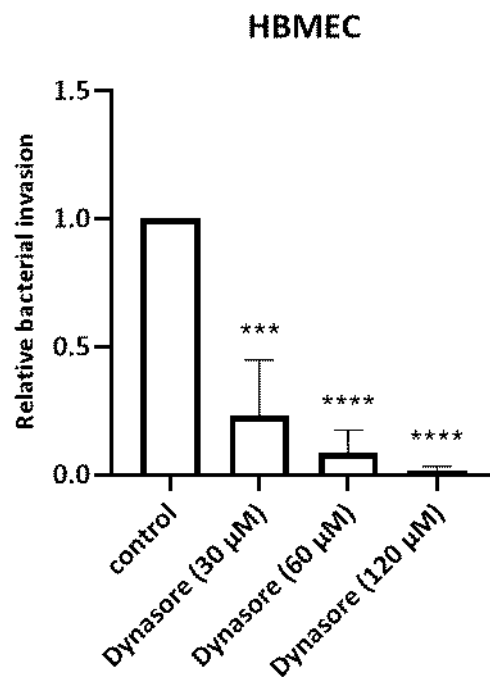


Figure 22. Pre-incubation with dynamin assembly inhibitor Dynasore causes a strong and statistically significant decrease in invasion rates of *Lm* into HBMEC, which is dependent on the concentration of Dynasore. HBMEC were grown on chamber slides (apical side of the layer oriented upwards) until confluent (as determined by microscopy) and were then pre-incubated with Dynasore (30 μM, 60 μM or 120 μM) for 0.5 h, after which they were infected with wild type *Lm* EGDe (MOI = 10) and co-incubated for 4 h before the removal of bacteria and fixation of cells. The samples were immunostained and then visualized and quantified using IF microscopy. *** = extremely significant ($p < 0.001$), **** = extremely significant ($p < 0.0001$) (significance determined in relation to the invasion of the wild type bacteria into the untreated cells).

3.2.5. *Lm* invasion activates multiple RTKs in both HBMEC and HIBCPP cells

RTKs are known to be important cellular entry points for a number of different bacteria and viruses, including *Lm* (which utilizes the RTK Met) (refer to 1.5.1) (Haqshenas and Doerig 2019). In order to investigate potential effects of listerial interaction with the cell on other RTKs and possible differences in post-infection RTK phosphorylation patterns between endothelial and epithelial cells, HBMEC and HIBCPP cells were infected with the wild type *Lm* EGDe, following which the cells were lysed and analyzed using the Human RTK Phosphorylation Array C1.

The results of the infection experiments in both cell lines indicate that a number of RTKs show different levels of phosphorylation following the co-incubation with *Lm* in comparison to the uninfected cells (Figure 23). As expected, Met (labeled as HGFR in the assay) was strongly activated in both cell lines, which also served as an additional control for the efficacy of cell infection. Although the majority of RTKs whose level of phosphorylation changed following the infection were affected in only one of the two cell lines, there were some overlaps – BMX, EphA4, FGFR1, IGF-I R, Insulin R, JAK3, LCK, LTK, Met, Tec and ZAP70 were affected in both cell lines. Interestingly, a few targets (BMX, Insulin R, LTK, Tec and ZAP70) behaved differently between the two cell lines, showing increased level of phosphorylation in HBMEC cells and a decreased level of phosphorylation in HIBCPP.

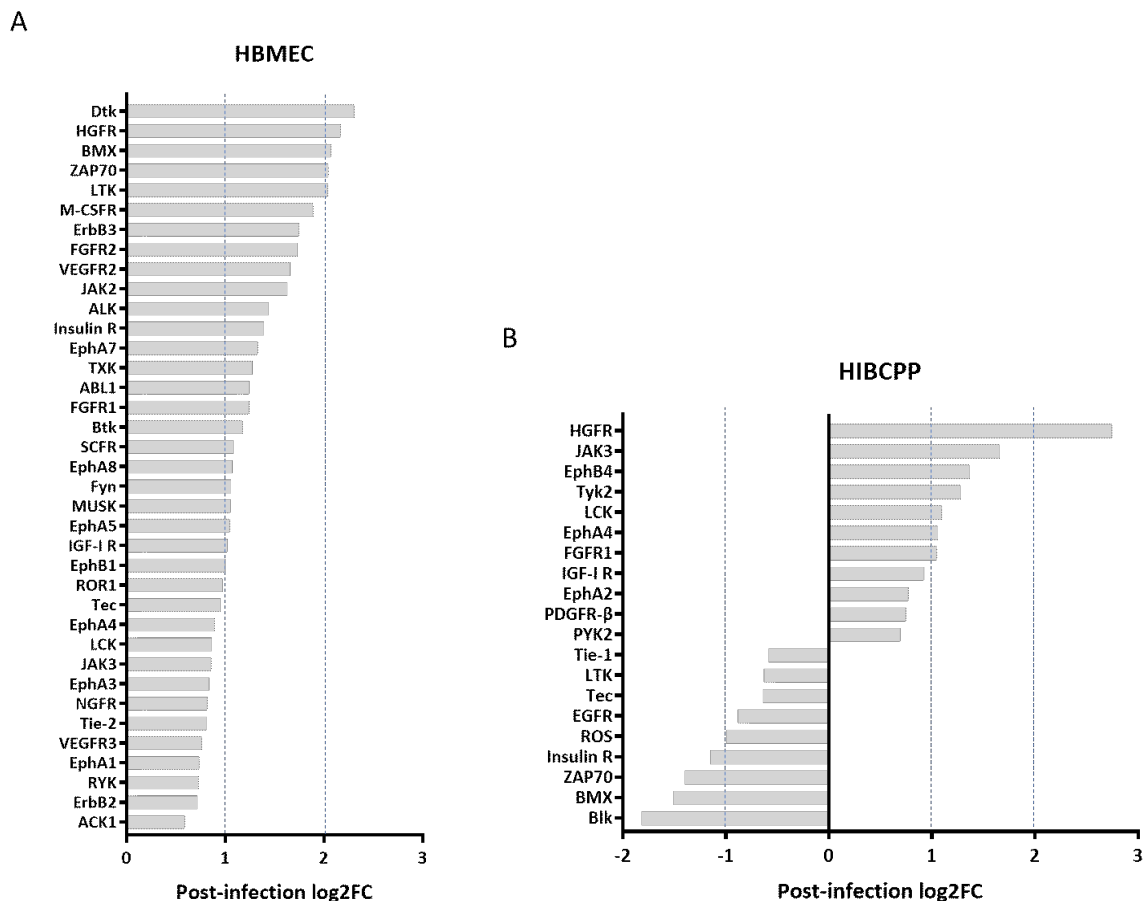


Figure 23. Co-incubation with *Lm* affects the activation state (observed as a change in phosphorylation levels) of multiple RTKs in both HBMEC and HIBCPP cells. HBMEC were grown on chamber slides (apical side of the layer oriented upwards) until confluent (as determined by microscopy), while HIBCPP cells were grown in inverted cell culture inserts (basolateral side of the layer oriented upwards) until a functional barrier was established (as determined by measuring the TEER). The cells were then infected with wild type *Lm* EGDe (MOI = 10) and co-incubated for 4 h before the removal of bacteria and lysis of cells. The samples were treated with the components of Human RTK Phosphorylation Array C1, following which the chemiluminescence was detected by Chemi Smart 5100 chemiluminescence detector and visualized by Chemi Capt 5000 software. The obtained visual data was then quantified by ImageJ software with a Protein Array Analyzer add-on and entered into the analysis software tool provided by the manufacturer to obtain final results. *The results are expressed as log₂FC – logarithms of ratios of the chemiluminescence intensity of uninfected and infected cell samples (samples were previously standardized using the instructions from the kit), and are usually referred to in the literature simply as “fold changes”. Met is labeled as HGFR in the figure.*

In order to check whether these findings could be observed using other, more conventional methods, infection experiments with the same setup were performed, and the samples obtained in them were subjected to Western blot analysis using antibodies against several select targets of interest. Correspondence with the group of Prof. Veronique Orian-Rousseau (KIT, Karlsruhe) has revealed that Met becomes subject to the activity of cellular phosphatases within minutes of its phosphorylation (internal communication). To compensate for this, due to both Western blotting being comparatively less sensitive than the antibody array and the possibility of other tyrosine kinases also being dephosphorylated relatively fast in standard experimental conditions (with no experiment having a shorter co-incubation time than 1 h), an additional set of samples was included in the experiments. The cells in this set were co-incubated with Na_3VO_4 , a commonly used inhibitor of phosphatases, at 1 mM, a concentration known to be non-cytotoxic to cells – also confirmed for HBMEC and HIBCPP cells (data not shown) – while still causing an almost complete cessation of phosphatase activity (Kaeffer et al. 1997).

The results of the experiments in HIBCPP cells show that both the samples incubated with pan-antibodies and the samples incubated with phospho-antibodies either had no difference in intensity related to whether they were or were not infected, or were not detectable at all (Figure 24B). Although the same was observed in several samples obtained from the HBMEC cells for either pan-antibodies, phospho-antibodies or both, there was a visible increase of phosphorylation level in BMX, Dtk, JAK3, LTK, Met and possibly ZAP70 (Figure 24A). Notably, these changes could be seen only in samples co-incubated with Na_3VO_4 .

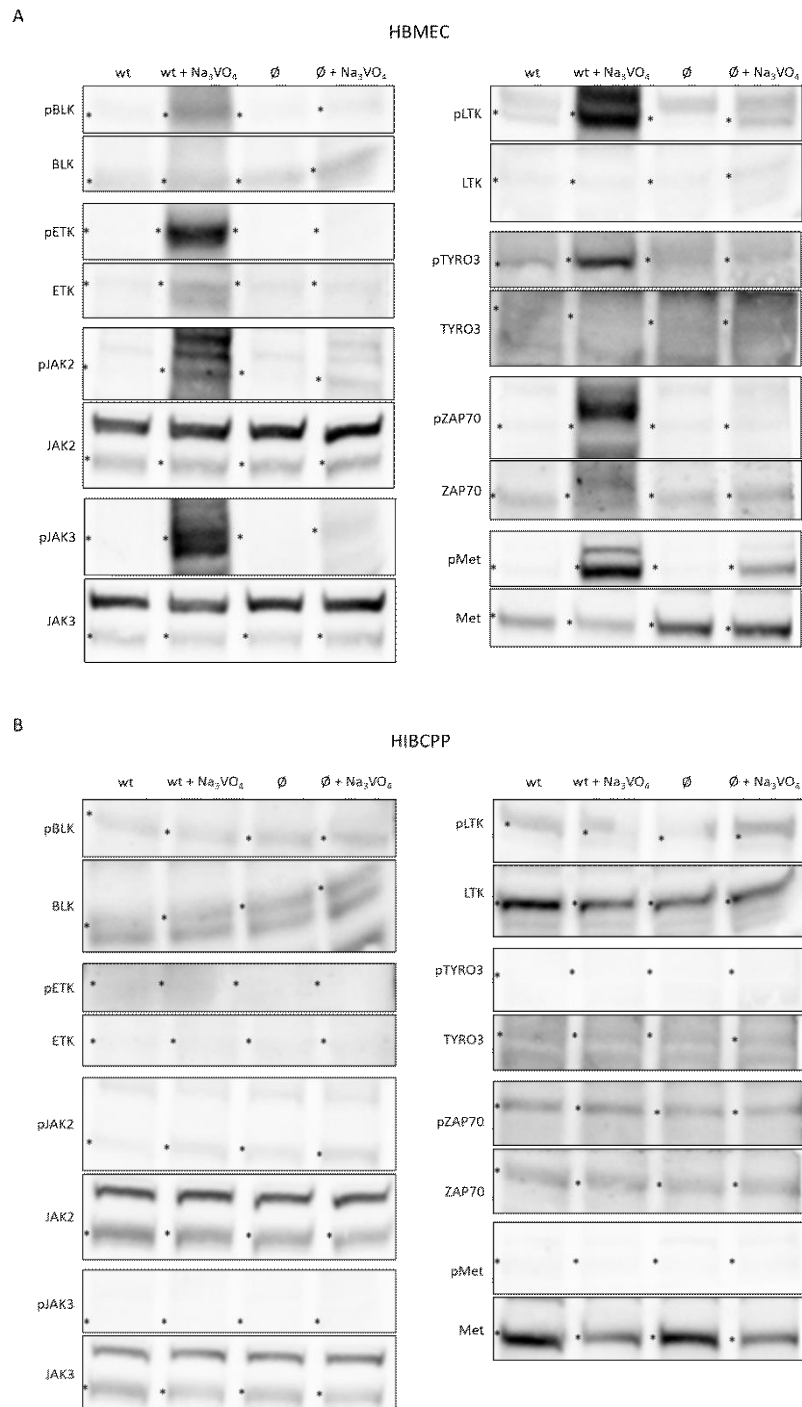


Figure 24. Effects of *Lm* infection on levels of phosphorylated forms of select tyrosine kinases in HBMEC (A) and HIBCPP (B) cells. HBMEC were grown on chamber slides (apical side of the layer oriented upwards) until confluent (as determined by microscopy), while HIBCPP cells were grown in inverted cell culture inserts (basolateral side of the layer oriented upwards) until a functional barrier was established (as determined by measuring the TEER). The cells were either uninfected or infected with wild type *Lm* EGDe (MOI = 10) and co-cubated for 4 h before the removal of bacteria and lysis of cells. Following the lysis of the cells, the concentration of the samples was measured and they were subjected to Western blotting. *wt* = cells infected with wild type *Lm* EGDe; *wt + Na₃VO₄* = as *wt* but with 1 mM *Na₃VO₄*; \emptyset = uninfected cells; $\emptyset + Na_3VO_4$ = as \emptyset but with 1 mM *Na₃VO₄*. The presented data were selected as representative of the average outcome of multiple performed experiments.

3.3. Listerial invasion *in vivo*

The infection experiments were modeled on the method described by Bou Ghanem and colleagues, with the main difference being the introduction of immunosuppressants to cause immunodeficiency, often noted as a prerequisite for systemic spread of orally acquired *Lm* (Bou Ghanem, Myers-Morales, and D'Orazio 2013; Radoshevich and Cossart 2018; Banović, Schrotten, and Schwerk 2020).

The main goal of the mouse experiments envisioned within the scope of this project was to assess the importance of functional *Lm*-CD44v6 interactions for listerial entry into various mouse organs, especially the brain. An additional goal was to evaluate the importance of immunosuppression for the onset of systemic listeriosis in mice orally infected with contaminated food. Collaboration partners from the group of Prof. Veronique Orian-Rousseau (Institute of Biological and Chemical Systems – Functional Molecular Systems, Karlsruhe Institute of Technology, Karlsruhe, Germany) work on generation of transgenic mice with inducible KO of CD44/CD44v6 in the microvascular endothelium and CP epithelium.

3.3.1. *Lm* is able to infect mice of both tested strains (BALB/cByJRj and C57BL/6JRj) and spreads systemically to various organs of immunosuppressed mice

Before the initiation of mouse experiments with CD44v6-blocking peptides, it was necessary to establish what would be the most efficient setup for efficient infection of mice (i.e. which conditions lead to highest bacterial loads in observed organs), so that it could be used as a control group in further experiments. Two mouse strains (BALB/cByJRj and C57BL/6JRj) were used in the test, as well as two different conditions (immunosuppression or no immunosuppression), making up for a total of four different groups. The mice of the BALB/cByJRj strain are known to be especially susceptible to oral *Lm* infection, while the C57BL/6JRj strain provides a genetic background similar to the one which will be presented by the transgenic mice with an inducible KO of CD44/CD44v6 in future experiments (Bou Ghanem et al. 2012; Bergmann et al. 2013).

The results of the experiments reveal a statistically significant increase in bacterial loads in livers, MLNs and spleens – as well as a statistically non-significant but observable increase in bacterial loads in brains – of the immunosuppressed mice when compared to the non-immunosuppressed mice of the same strain, and this increase was present in mice of both tested strains. The only statistically significant difference in organ bacterial loads between the strains was observed for the livers of non-immunosuppressed mice (Figure 25).

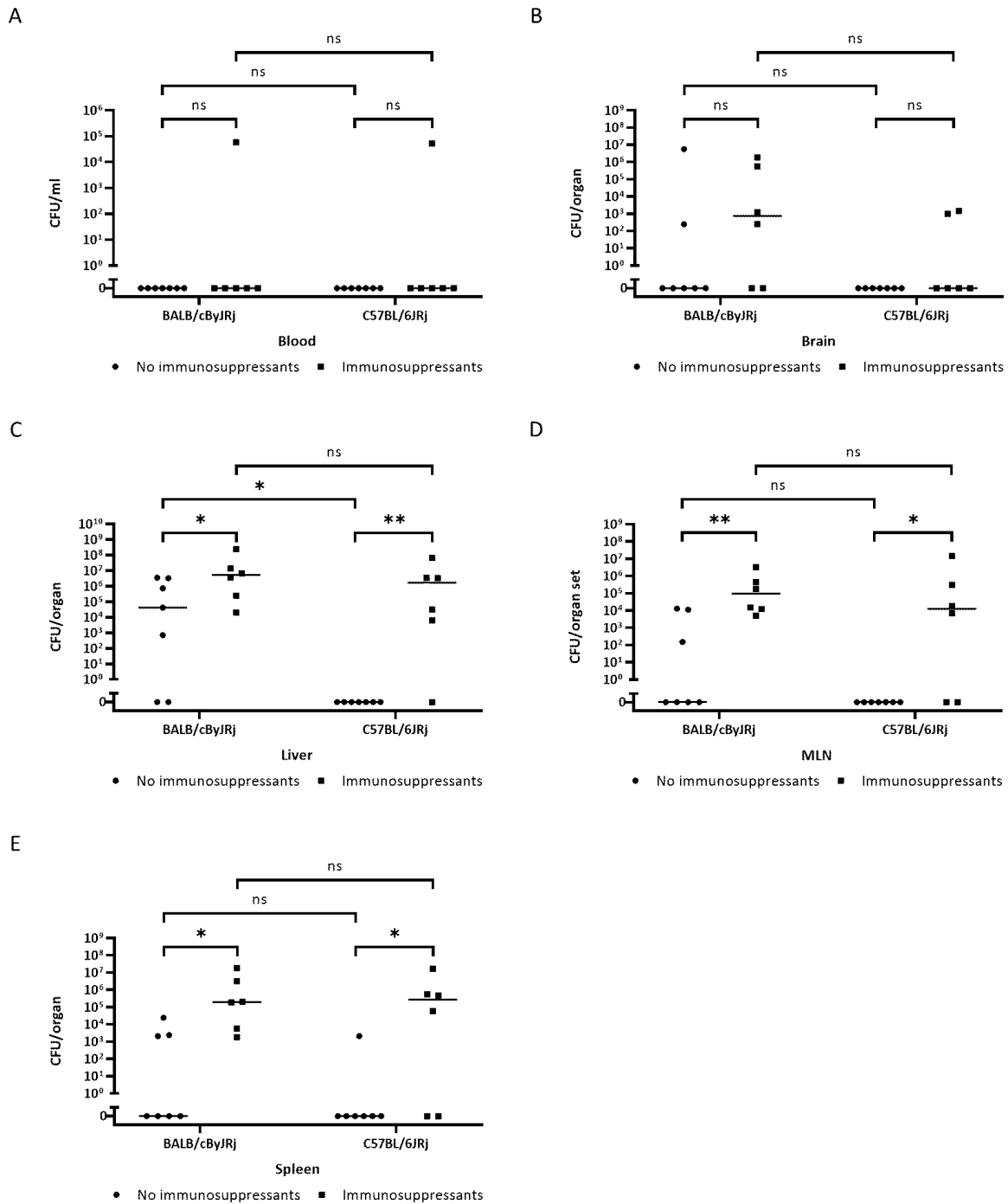


Figure 25. Immunosuppression leads to increased bacterial loads in brains (B), livers (C), MLNs (D) and spleens (E) of the infected mice of both strains. Experiments were conducted according to the previously described methods (refer to 2.2.3.). BALB/cByJRj = mice of the BALB/cByJRj strain infected with wild type Lm EGDe; C57BL/6JRj = mice of the C57BL/6JRj strain infected with wild type Lm EGDe. # of mice/group = 7 (for non-immunosuppressed mice) and 6 (for immunosuppressed mice – 1 BALB/cByJRj mouse had to be sacrificed before infection due to meeting criteria for sacrifice; 1 C57BL/6JRj mouse was found dead in the cage during the experiment with time of death between observation intervals); * = significant ($p < 0,05$), ** = very significant ($p < 0,01$), ns = not significant (significance determined between each group).

3.3.2. Treatment with CD44v6-blocking peptides results in no observable difference in the bacterial load in organs of immunosuppressed C57BL/6JRj mice

Contact between Met, CD44v6 and HGF – the standard ligand of Met – is required for the initiation of signaling downstream of Met (Orian-Rousseau et al. 2002). Although it was investigated whether the same is true for contact between Met, CD44v6 and InIB – listerial VF that binds to Met – no real conclusion has been reached as of yet, since published results did not present a uniform answer (Jung et al. 2009; Dortet et al. 2010). In order to assess the importance of this interaction for systemic spread of *Lm* in mice, CD44v6-blocking peptides were used to disrupt the contact between CD44v6 and its other two interaction partners, Met and InIB (Matzke et al. 2005; Jung et al. 2009; Matzke-Ogi et al. 2016). Since immunosuppression was shown to be the only relevant condition in the selection experiments conducted previously, it was decided that the immunosuppressed C57BL/6JRj mice will be used for the experiments with CD44v6-blocking peptides (refer to 3.3.1.). There were three different conditions – untreated, treated with KR14 and treated with QP14 – which made up for a total of three different groups (refer to 2.2.3.4.). Untreated mice served as the control group, and mice treated with KR14 served as a peptide control group.

Experimental results show no statistically significant difference in organ bacterial loads between the groups for any of the tested organs (Figure 25).

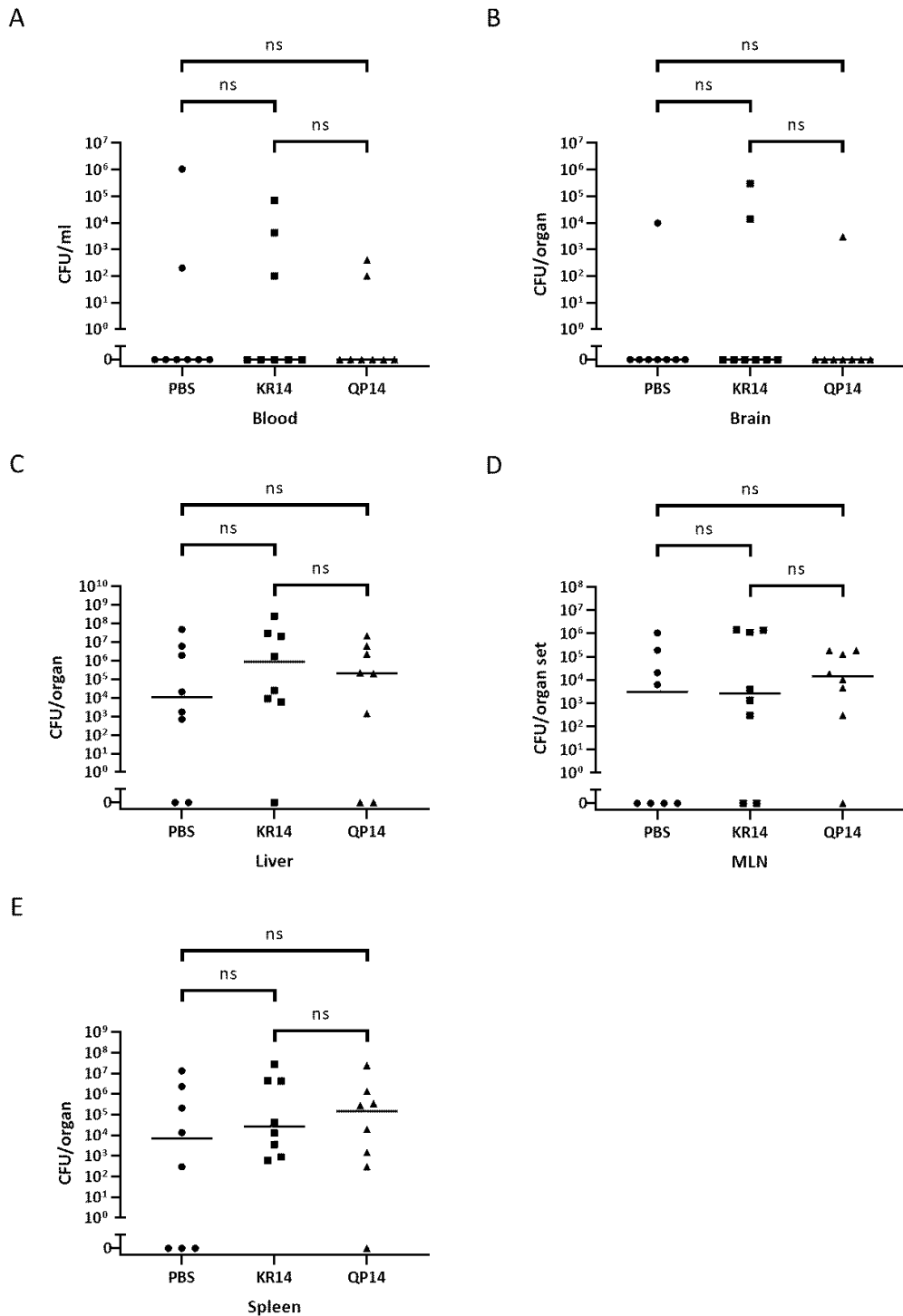


Figure 27. Treatment with CD44v6-blocking peptides does not affect bacterial loads in organs of immunosuppressed C57BL/6JRj mice. Experiments were conducted according to the previously described methods (refer to 2.2.3.). *PBS* = immunosuppressed mice of the C57BL/6JRj strain infected with wild type Lm EGDe injected with 100 μ l of PBS every second day; *KR14* = immunosuppressed mice of the C57BL/6JRj strain infected with wild type Lm EGDe injected with 100 μ l of 1 mg/kg of body weight solution of KR14 every second day; *QP14* = immunosuppressed mice of the C57BL/6JRj strain infected with wild type Lm EGDe injected with 100 μ l of 1 mg/kg of body weight solution of QP14 every second day. # of mice/group = 8; ns = not significant (significance determined between each group).

4. DISCUSSION

4.1. Listerial infection in *in vitro* BBB/BCSFB cellular models

Cellular *in vitro* models are a common choice for research of intracellular pathogens, especially in regard to entry into complex-to-simulate environments like the CNS and its surrounding barriers (since they are relatively cheaper, simpler to use and more readily available than the alternative 3D models), and research of *Lm* is no exception (Redzic 2013; Ruck, Bittner, and Meuth 2015; Radoshevich and Cossart 2018; Banović, Schrotten, and Schwerk 2020). Most of the investigatory efforts have been aimed at the penetration of the BBB, but there are also examples of usage of BCSFB invasion models (Greiffenberg et al. 1998; Bergmann et al. 2002; Dortet et al. 2010; Gründler et al. 2013; Ghosh et al. 2018; Radoshevich and Cossart 2018; Banović, Schrotten, and Schwerk 2020).

The cell lines utilized in this study were HBMEC (used as a model of the BBB) and HIBCPP (used as a model of the BCSFB). Although *Lm* possesses a large number of VFs, of which many have as of yet unknown interaction partners, the duo of InIs encoded by the *inlAB* operon – regarded as the most important of listerial VFs – have known binding partners on the cellular surface, as well as InIF, another listerial VF investigated in this study (refer to 1.4.) (Radoshevich and Cossart 2018; Banović, Schrotten, and Schwerk 2020). To ensure and confirm the suitability of these cell lines for the experiments, it was necessary to verify whether they express receptors for at least some of the above listed InIs, as well as whether they express proteins required for barrier function of the cell layer (such as ZO-1, a component of the TJs).

Obtained results indicate that both cell lines express ZO-1 and Met (Figure 10), as well as that they are localized at the boundaries of cells within the cell layer (Figures 11-13), which is in agreement with previous findings (Eigenmann et al. 2013; Gründler et al. 2013; Puthiyakunnon et al. 2017; Dahm et al. 2018). Ecad was detected (Figure 10) and localized (Figure 11) in HIBCPP cells but not in the HBMEC, which was in line with both the current knowledge and the expectations (due to Ecad being an epithelial cell marker) (Takeichi 1988; Gründler et al. 2013). Finally, vimentin was expressed in HBMEC but not in HIBCPP (Figure 10), and also localized both as a part of the cytoskeleton and on the surface of the cells in HBMEC (Figure 13), which was expected due to vimentin being an endothelial cell marker (Boraas and Ahsan 2016). Expression of vimentin was already described for primary brain microvascular endothelial cells and HBMEC cell line, but its presence on the cellular surface of these cells was not directly shown in publications (Chi et al. 2010; Huang et al. 2016). Literature on the presence of vimentin in CP epithelium is not unanimous, since it was detected by some authors but remained unobserved by others (Kasper, Karsten, and Stosiek 1986; Miettinen, Clark, and Virtanen 1986; Shimomoto et al. 2004; Lazarevic and Engelhardt 2016). It should be noted, however, that

vimentin is one of the most recognized markers of epithelial-mesenchymal transition (EMT), a process which occurs in embryogenesis as well as in carcinogenesis and leads to loss of epithelial cell traits (Satelli and Li 2011). This raises a question of whether the reports of vimentin in CP epithelium were actually reports of cancerous tissue of epithelial origin that has undergone EMT and lost the epithelial tissue traits (including the ability to form barriers) rather than of native CP epithelial cells, as the publications where presence of vimentin was reported were done in either transformed epithelial cell lines or samples taken from CP tumors (Kasper, Karsten, and Stosiek 1986; Miettinen, Clark, and Virtanen 1986; Shimomoto et al. 2004; Lazarevic and Engelhardt 2016). Still, the epithelial CP cell line used in this study – HIBCPP – shares the lack of vimentin expression and an ability to form functional barriers with primary CP epithelial cells, confirming its suitability as a CP epithelial model (Figures 10 and 13) (Lazarevic and Engelhardt 2016).

4.1.1. Role of Ecad and Met in cellular attachment and invasion by *Lm*

InIA and InIB and the interactions they establish with their cellular receptors – Ecad and Met, respectively – are among the most thoroughly investigated facets of listerial pathology (Gaillard et al. 1991; Dramsi et al. 1995; Radoshevich and Cossart 2018; Banović, Schroten, and Schwerk 2020). While the interaction between InIB and Met appears more important for invasion and spreading within the host due to the wider distribution of Met in tissues and cells of the body, the canonical route of listerial penetration into the body – via the gastrointestinal system – seems to be dependent mostly on the interaction between InIA and Ecad (Lingnau et al. 1995; Jonquières, Pizarro-Cerdá, and Cossart 2001; Lecuit et al. 2001; Jacquet et al. 2004; Pentecost et al. 2006; Pizarro-Cerdá, Kühbacher, and Cossart 2012).

Interaction of bacterial pathogens with these receptors is not limited to *Lm*, however. Notable bacterial pathogens such as *Clostridium botulinum* (via HA complex), *Fusobacterium nucleatum* (via FadA), *Staphylococcus aureus* (via Alpha toxin) and *Streptococcus pneumoniae* (via PsaA) can all interact with Ecad, while *Helicobacter pylori* (via CagA) interacts with both Ecad and Met (Churin et al. 2003; Anderton et al. 2007; Murata-Kamiya et al. 2007; Kwak et al. 2012; Rubinstein et al. 2013; Lee et al. 2014; Dash, Duraivelan, and Samanta 2021). *Lm* remains the only bacterial pathogen known to utilize Ecad and Met for invasion into cells, however.

Considering the fact that both cell lines utilized in this study express Met but only the HIBCPP cells express Ecad (Figure 10), it is to be expected that the deletion of InIA and/or InIB would not affect the invasion rates of *Lm* into HBMEC and HIBCPP cells in the same way. The deletion of InIA, InIB or both causes a similar decrease in bacterial invasion (down to 25-30% or wild-type invasion rate) into the HIBCPP cells (Figure 15), implying an interdependent mode of action for the two InIs, confirming the

findings reported by Gründler and colleagues (Gründler et al. 2013). The remaining capacity of *Lm* for invasion into HIBCPP cells even if both InIA and InIB are deleted is likely conferred by other listerial VF, such as other InIs (InIC, InIGHE or others) or LLO (Bergmann et al. 2002; Phelps et al. 2018). The deletion of InIB causes a drastic drop in bacterial invasion (down to 7% of wild-type invasion rate) into the HBMEC (Figure 15), confirming previous findings (Greiffenberg et al. 1998; Parida et al. 1998). Surprisingly, the invasion rate of Δ InIA mutant was also decreased (down to 40% of wild-type invasion rate), and the deletion of both InIs blocked the invasion almost completely (down to <1% of wild-type invasion rate) (Figure 15), which contradicts the data presented by Greiffenberg and colleagues (Greiffenberg et al. 1998). Still, these results mirror the findings reported by Parida and colleagues, and could imply differences in the *Lm* strains and/or mutants as well as cell lines utilized in the research by the two groups: while the former used strain *Lm* EGD and HUVECs, the latter used strain *Lm* EGDe and HBMECs (also used in this study) (Parida et al. 1998; Greiffenberg et al. 1998).

In endothelial and epithelial cells, cell polarization results in different membrane composition of apical and basolateral sides of the cell. The results shown earlier in this study (Figures 11-12) confirm previously reported localization of Ecad and Met on the basolateral side of HIBCPP cells (Gründler et al. 2013). It is difficult to determine the exact localization of Met on HBMEC cells due to their extreme flatness (Figure 12). However, the ability of *Lm* to uniformly invade HBMEC monolayers from the apical side suggests that Met is located on the apical side of HBMEC cells (Figure 14).

IF microscopic images of the invasion process, which demonstrated that the *Lm* approaching the HIBCPP cell layer from the apical side could infect only the cells located at the holes in the cellular layer, or the cells adjacent to them (to which the bacteria spread utilizing actin comet tails) (Figure 14) are in accord with the previously reported preference of *Lm* for basolateral invasion of the HIBCPP cells due to basolateral localization of Ecad and Met (Gründler et al. 2013). On the other hand, IF image analysis of HBMEC infection highlighted the ability of *Lm* to invade HBMEC apically (Figure 14).

The preference for either the apical or the basolateral side of polarized cells is not unusual in bacteria capable of traversing the human body, such as *Campylobacter jejuni*, *Neisseria meningitidis*, *Shigella flexneri* and *Streptococcus suis* (Mounier et al. 1992; Tenenbaum et al. 2009; Schwerk et al. 2012; Hatayama et al. 2018). When the physiological orientation and function of the polar cells that can be invaded is considered, it becomes apparent that a pathogen (such as *Lm*) often favors the entry from the side of the cellular layer that can bring it deeper into the host's body (i.e. entry from the apical side when crossing the endothelial cells of the BBB to move from the lumen of the microvascular blood vessel into the brain parenchyma) (Radoshevich and Cossart 2018).

4.1.1.1. Role of CD44 in cellular attachment and invasion by *Lm*

Observed interactions between CD44 and several species of pathogenic bacteria (*Lm*, *Mycobacterium tuberculosis*, *Shigella* spp., *S. aureus* and *Streptococcus pyogenes*) – where CD44 usually plays a role as either a receptor or a co-receptor for bacterial adhesion and/or invasion – are of particular interest for investigation and understanding of bacterial internalization mechanics (Moffat et al. 1996; Schragar et al. 1998; Cywes, Stamenkovic, and Wessels 2000; Skoudy et al. 2000; Eriksson et al. 2003; Leemans et al. 2003; Montanari et al. 2018). When using a CD44-mediated entry route for cellular invasion, bacterial pathogens mainly target cells belonging to epithelial (e.g. keratinocytes), ECM-related (e.g. fibroblasts) and leukocyte (e.g. macrophages) cellular populations, all of which demonstrate both a high expression of CD44 and a high rate of GAG uptake (Montanari et al. 2018). While some of the bacteria utilize GAG-binding properties of CD44 to interact with it via their GAGs (such as *S. pyogenes*, which binds it using hyaluronan present in its capsule), others bind to it via specific ligands expressed on the bacterial surface (such as members of genus *Shigella*, which bind to CD44 via IpaB) (Schragar et al. 1998; Cywes, Stamenkovic, and Wessels 2000; Skoudy et al. 2000; Montanari et al. 2018). Another curious example of bacterial exploitation of CD44 can be seen in *Lm*, which was shown to utilize CD44-mediated signaling to enhance its survival in the cytoplasm of infected fibroblasts and macrophages in mouse models (Eriksson et al. 2003).

Due to their role in Met signaling, CD44v6 isoforms of CD44 were investigated in regard to their relevance for InlB-Met-mediated listerial invasion. Since the formation of the same ligand-receptors-cytoskeletal components complex observed after the binding of HGF to Met could be detected by immunoprecipitation following the induction of the cells with InlB – although HGF and InlB share no homology and bind to different spots on Met – it could be reasonably assumed that interrupting this association could hamper the InlB-Met-dependent listerial invasion (Niemann et al. 2007; Orian-Rousseau et al. 2007; Jung et al. 2009). A study performed on HeLa cells (which do not express Ecad) reported the dependence of the bacteria on CD44v6 for successful invasion – both the uptake of the InlB-coated beads and the entry of *Lm* itself were significantly decreased when contact between Met and CD44v6 was disrupted by blocking antibodies, peptides or CD44v6-targeting siRNA (Jung et al. 2009). These findings are still controversial, however, since another study performed in several cell lines including HeLa found no difference in levels of bacterial invasion following transfection with either CD44v6-targeting or total CD44-targeting siRNA, and the authors also observed transcription but not expression of CD44v6 in HeLa cells (Dortet et al. 2010). The attempt to replicate the results of Jung and colleagues using CD44v6-blocking peptides, wild type *Lm* EGDe and *Lm* EGDe Δ *inlA* and four cell lines susceptible to InlB-Met mediated invasion – bEnd.3, HBMEC, HeLa and HIBCPP – did not lead to the same outcome, since there was no statistically significant difference in bacterial invasion rates

between the control and peptide-treated samples in any of the tested cell lines (Figure 18) (Jung et al. 2009). Possible reasons for this discrepancy could be a) the usage of a different bacterial quantification method and/or b) differences in purity of peptide batches used in two studies (Prof. Veronique Orian-Rousseau, internal communication), although the question still remains open.

4.1.2. Role of vimentin in cellular attachment and invasion by *Lm*

Vimentin is an intermediate filament protein found primarily in mesenchymal (e.g. endothelial) cells, and can be detected both intracellularly and extracellularly (Figure 13) (Danielsson et al. 2018; Patteson et al. 2020). It serves multiple roles inside the cell, including (but not limited to) the provision of flexibility to the cytoskeleton, assistance in anchoring of cellular organelles and lipid droplet formation (Danielsson et al. 2018; Patteson et al. 2020). Extracellular vimentin is more relevant for this study, since it was described as an interaction partner (mostly in the context of CNS invasion) for several intracellular pathogens – Dengue virus (via NS4a), *E. coli* K1 (via IbeA), Group B *Streptococcus* (via BspC) and *Lm* (via InIF or independently of InIF) (Chi et al. 2010; Teo and Chu 2014; Bastounis, Yeh, and Theriot 2018; Ghosh et al. 2018; Deng et al. 2019).

The observation of a strong decrease in listerial invasion into vimentin-expressing HBMEC exposed to the vimentin modulator WitA (Figure 16) confirms the findings in HMEC-1 described by Bastounis and colleagues (Bastounis, Yeh, and Theriot 2018). On the other hand, the work of Ghosh and colleagues implicated InIF as a key listerial factor for interaction with vimentin during invasion into hCMEC/D3, and only under the conditions of ROCK inhibition (Kirchner and Higgins 2008; Ghosh et al. 2018). While the results presented in this study did confirm that the removal of InIF does not have any visible effect on listerial invasion if ROCK inhibitors are not used (Figure 15), the previously mentioned WitA-induced decrease in listerial invasion into HBMEC was also observed without usage of ROCK inhibitors (Figure 16). The answer to this seeming contradiction was addressed by Bastounis and colleagues, who noted that the possible significant (but as-of-yet unidentified) differences between various human microvascular endothelial cell lines could affect which listerial VFs would be important for the invasion into them (Bastounis, Yeh, and Theriot 2018).

4.2. Cellular signaling in the CNS during listerial invasion

4.2.1. Effects of cellular attachment and invasion by *Lm* on gene transcription levels

It is well established that the invasion of cells by intracellular pathogens (e.g. enteroviruses, *Lm*, *N. meningitidis*, *S. pneumoniae* and *S. suis*) in BBB and BCSFB *in vitro* models triggers the transcriptional changes (mostly in the form of upregulation) of a number of inflammation-related genes, including cytokines such as interleukins and TNF α (Vadeboncoeur et al. 2003; Liang et al. 2004; Banerjee et al. 2010; Schwerk et al. 2011; Schneider et al. 2012; Steinmann et al. 2013; Borkowski et al. 2014;

Koopmans et al. 2014; Dick et al. 2017; Klein, Garber, and Howard 2017). Experiments conducted within the scope of this study confirmed these findings, since contact with *Lm* EGDe – even the deletion mutant lacking both InIA and InIB – caused a quick and strong upregulation of IL-6, IL-8 and TNF α in both HBMEC and HIBCPP cells (Figure 19).

Since the changes in transcription levels of some of the transmembrane proteins reported as participating in listerial invasion – Ecad and vimentin in particular – could affect intercellular communication and stability of the blood-brain barriers as well as effectiveness of bacterial invasion, it was investigated whether they are affected by cellular contact and/or infection with *Lm*. However, the experimental data presented in this study does not show any post-infection changes in transcription levels of CD44 (and CD44v6), Ecad, Met and vimentin in either of the two tested cell lines, showing that *Lm* does not rely on the dysregulation of their transcription during invasion into these cells (Figure 19).

4.2.2. Effects of cellular attachment and invasion by *Lm* on MAPK signaling pathways

MAPKs are central constituents of MAPK signaling pathway. They are involved in cellular response to a variety of different (potentially harmful) triggers, from oxidative stress to infection, and affect the transcription levels of a plethora of different genes including (but not limited to) those related to apoptosis, migration and proliferation of cells (Pearson et al. 2001; Raman, Chen, and Cobb 2007). There are many examples of bacterial pathogens exploiting cellular signaling pathways, including MAPK signaling pathway, and a few among them are: *Bacillus anthracis* (inactivates all MKKs except MKK5 via LF subunit of anthrax toxin); enteropathogenic *E. coli* (inactivates JNK and p38 via NleD); *Salmonella enterica* ser. Typhimurium (inactivates MKK4 and MKK7 via AvrA); *S. flexneri* (inactivates ERK1/2 and p38 via OspF) and *Vibrio parahaemolyticus* (inactivates MKK 1 and MKK6 via VopA) (Duesbery et al. 1998; Li et al. 2007; Trosky et al. 2007; Jones et al. 2008; Baruch et al. 2011; Krachler, Woolery, and Orth 2011; Gur-Arie and Rosenshine 2015).

Although most examples of bacterial interaction with the MAPK signaling pathways revolve around inhibition or disruption of signal transduction, *Lm* was shown to activate rather than inactivate ERK1/2, p38 or both in most of the tested cell lines (with trophoblast giant cells used by Hashino and colleagues being a notable exception) (Tang, Rosenshine, and Finlay 1994; Tang et al. 1996; Weiglein et al. 1997; Opitz et al. 2006; Hashino et al. 2015; Dinner et al. 2017). The results regarding the post-attachment/invasion activation of ERK1/2 and p38 in HIBCPP cells presented in this study recapitulate the findings presented by Dinner and colleagues (Figure 20) (Dinner et al. 2017). While the post-attachment/invasion activation of both ERK1/2 and p38 MAPK pathways could be expected for HBMEC based on the findings of other groups, the results obtained in this study present a different picture:

p38 was activated during infection by *Lm*, but ERK1/2 was in an activated state both in the control group cells and the *Lm*-infected cells (Figure 20).

Interestingly, functional MAPK signaling seems to be vital for the efficient listerial invasion into both the cell lines where it is activated as well as those where it is inactivated by *Lm*, since the usage of specific inhibitors for the members of the MAPK pathway decreases the bacterial entry rates into the cells, with simultaneous usage of several inhibitors leading to a stronger effect (Opitz et al. 2006; Hashino et al. 2015; Dinner et al. 2017). The results of experiments performed in HBMEC demonstrate the same for p38 inhibition, but show no statistically significant difference for inhibition of ERK1/2 (Figure 21). Although it could – when combined with previously shown data on protein phosphorylation (Figure 20) – theoretically indicate a permanently active state of ERK1/2 in HBMEC, it is hard to make such a claim without more evidence, since it contradicts the current knowledge on the topic (Rush et al. 2007). Other possible explanations for these findings could lie in different growth conditions, protocols and sources of HBMEC used by different groups.

4.2.3. Role of dynamin in cellular attachment and invasion by *Lm*

A multitude of intracellular pathogens rely on exploitation of the host cell's endocytotic machinery in general to gain entrance into the host cell, and dynamin in particular has been marked as a required component for these events – several examples of dynamin-exploiting pathogens are *Lm*, *Porphyromonas gingivalis*, *S. aureus* and *Yersinia pseudotuberculosis* (Agerer et al. 2005; Veiga and Cossart 2005; Amano 2007; Veiga et al. 2007; Dinner et al. 2017).

Both of the two currently most described routes for listerial entry into non-phagocytic cells – InIA-Ecad route and InIB-Met route – rely heavily on interaction with dynamin (Veiga and Cossart 2005; Veiga et al. 2007; Pentecost et al. 2010; Ireton, Rigano, and Dowd 2014; Dinner et al. 2017). One of the methods utilized to investigate the relevance of dynamin for listerial invasion was pre-treatment of cells with Dynasore – a dynamin-specific inhibitor – before infection with *Lm*, through which this concept was demonstrated in multiple cell lines (Veiga et al. 2007; Pentecost et al. 2010; Dinner et al. 2017). Results from experiments performed on HBMEC presented in this study (Figure 22) confirm the relevance of dynamin for listerial invasion reported in literature, with Dynasore causing a strong, concentration-dependent drop in listerial invasion rates into the cells.

4.2.4. RTKs in cellular attachment and invasion by *Lm*

Many intracellular pathogens – mostly viruses, but also bacteria, protists and a few fungi – are able to use various RTKs for different purposes, especially hijacking their endocytotic machinery to gain access into the cell and/or pass through the barriers of the body (Haqshenas and Doerig 2019). RTKs which

are known to be involved with bacterial pathogen invasion include EGFR/ErbB1/Her1 (*C. jejuni* – unknown mechanism, likely indirectly through integrin clustering and subsequent activation in lipid rafts; *Chlamydia pneumoniae* – directly via Pmp21; *Neisseria gonorrhoeae* – unknown mechanism, possibly via pilus interaction; *S. enterica* ser. Typhimurium – directly via Rck; *S. aureus* – directly via SpA), EphA2 (*Chlamydia trachomatis* – directly via an unknown binding partner), ErbB2/Her2/Neu (*Mycobacterium leprae* – directly via an unknown binding partner, without usual heterodimerization of ErbB2 with one of the other ErbB proteins; *N. gonorrhoeae* – unknown mechanism; *N. meningitidis* – unknown mechanism, likely via pilus interaction), one or more FGFRs (*C. trachomatis* – indirectly using FGF2 as a bridge between the elementary bodies of *C. trachomatis* and the receptor) and PDGFR (*C. jejuni* – unknown mechanism; *C. trachomatis* – directly via an unknown binding partner) (Table 11) (Hoffmann et al. 2001; Tapinos, Ohnishi, and Rambukkana 2006; Elwell et al. 2008; Kim et al. 2011; Krause-Gruszczynska et al. 2011; Soong et al. 2011; Swanson et al. 2011; Edwards et al. 2013; Mölleken, Becker, and Hegemann 2013; Subbarayal et al. 2015; Elwell, Mirrashidi, and Engel 2016; Wiedemann et al. 2016; Ho et al. 2017). Lastly, as mentioned previously, Met is the only RTK confirmed as utilized for intracellular invasion by *Lm* (Shen et al. 2000).

Table 11. Overview of RTKs known to interact with intracellular pathogens during invasion.

| | EGFR | EphA2 | ErbB2 | FGFR | Met | PDGFR |
|---|------|-------|-------|------|-----|-------|
| <i>Campylobacter jejuni</i> | + | | | | | + |
| <i>Chlamydia pneumoniae</i> | + | | | | | |
| <i>Chlamydia trachomatis</i> | | + | | + | | + |
| <i>Listeria monocytogenes</i> | | | | | + | |
| <i>Mycobacterium leprae</i> | | | + | | | |
| <i>Neisseria gonorrhoeae</i> | + | | + | | | |
| <i>Neisseria meningitidis</i> | | | + | | | |
| <i>Salmonella enterica</i> ser. Typhimurium | + | | | | | |
| <i>Staphylococcus aureus</i> | + | | | | | |

The results of sample analysis using Human RTK Phosphorylation Array C1 have identified many RTKs in HBMEC and HIBCPP cell lines as having a different post-infection activation level (PIAL) when compared to non-infected cells (Figure 23). Due to the large number of RTKs involved, the focus was on those which have shown at least a 3-fold PIAL change (i.e. $\log_2FC \geq 1,584962501$ for an increase in activation level and $\log_2FC \leq -1,584962501$ for a decrease in activation level). In HBMEC, there were only targets with an increase in PIAL, and they were (from the one with the highest change to the one with the lowest): Dtk, Met, BMX, ZAP70, LTK, M-CSFR, ErbB3, FGFR2, VEGFR2 and JAK2. In HIBCPP cells, there were only 3 targets which have shown at least a 3-fold PIAL change: Met and JAK3 had an increase in PIAL while BLK had a decrease in PIAL. Interestingly, all RTKs listed as being involved with other pathogens have shown at least a 1.5-fold PIAL change in at least one of the two tested cell lines (Tables 11-12) – EGFR, EphA2 and PDGFR in the HIBCPP cells and ErbB2 in HBMEC. Interestingly, FGFRs (linked to *C. trachomatis* invasion) – FGFR1 and FGFR2 – have shown the strongest PIAL change in comparison to other pathogen-related RTKs – it was at least a 2-fold change for FGFR1 in both cell lines and at least a 3-fold change for FGFR2 in HBMEC. None of the RTKs mentioned except Met have so far been linked to *Lm* invasion, hinting at the existence of a whole new as-of-yet unexplored range of *Lm*-host cell interactions and marking the potential targets for future investigation.

Table 12. Overview of post-infection RTK activation level changes in HBMEC and HIBCPP cells.

↑/↓ - at least 1.5-fold change; ↑↑/↓↓ - at least 2-fold change; ↑↑↑/↓↓↓ - at least 3-fold change

| | HBMEC | HIBCPP |
|-----------|-------|--------|
| ABL1 | ↑↑ | |
| ACK1 | ↑ | |
| ALK | ↑↑ | |
| Blk | | ↓↓↓ |
| BMX | ↑↑↑ | ↓↓ |
| Btk | ↑↑ | |
| Dtk | ↑↑↑ | |
| EGFR | | ↓ |
| EphA1 | ↑ | |
| EphA2 | | ↑ |
| EphA3 | ↑ | |
| EphA4 | ↑ | ↑↑ |
| EphA5 | ↑↑ | |
| EphA7 | ↑↑ | |
| EphA8 | ↑↑ | |
| EphB1 | ↑ | |
| EphB4 | | ↑↑ |
| ErbB2 | ↑ | |
| ErbB3 | ↑↑↑ | |
| FGFR1 | ↑↑ | ↑↑ |
| FGFR2 | ↑↑↑ | |
| Fyn | ↑↑ | |
| HGFR | ↑↑↑ | ↑↑↑ |
| IGF-I R | ↑↑ | ↑ |
| Insulin R | ↑↑ | ↓↓ |
| JAK2 | ↑↑↑ | |
| JAK3 | ↑ | ↑↑↑ |
| LCK | ↑ | ↑↑ |
| LTK | ↑↑↑ | ↓ |
| M-CSFR | ↑↑↑ | |
| MUSK | ↑↑ | |
| NGFR | ↑ | |
| PDGFR-β | | ↑ |
| PYK2 | | ↑ |
| ROR1 | ↑ | |
| ROS | | ↓ |
| RYK | ↑ | |
| SCFR | ↑↑ | |
| Tec | ↑ | ↓ |
| Tie-1 | | ↓ |
| Tie-2 | ↑ | |
| TXK | ↑↑ | |
| Tyk2 | | ↑↑ |
| VEGFR2 | ↑↑↑ | |
| VEGFR3 | ↑ | |
| ZAP70 | ↑↑↑ | ↓↓ |

Since the fact that Met becomes rapidly dephosphorylated post-activation (and so do possibly other RTKs) (refer to 3.2.5.) became known to the author of this study only after the experiment with Human RTK Phosphorylation Array C1 was already performed, it was necessary to evaluate the observed findings using an additional set of samples co-incubated with Na_3VO_4 to prevent RTK dephosphorylation (refer to 3.2.5.). For this purpose, 7 targets were chosen for Western blotting analysis on basis of relatively high PIAL change – BLK, BMX (also known as ETK; labeled so on Figure 24), Dtk (also known as TYRO3; labeled so on Figure 24), JAK2, JAK3, LTK and ZAP70, with Met added as a control. The majority of the targets – with the exception of JAK3 and Met (whose PIAL was increased in both cell lines) and JAK2 (whose PIAL was increased only in HBMEC) – were selected specifically because they were affected differently by the listerial infection, i.e. had an increased PIAL in HBMEC, but a decreased one in HIBCPP cells (Table 12).

Since most of the selected targets had a supposedly decreased PIAL in HIBCPP cells, the fact that their phosphorylation could not be detected via Western blotting – a less sensitive method than the Human RTK Phosphorylation Array C1 – is not very surprising (Figure 24B). However, lack of any signal for phosphorylated forms of JAK3 and Met (which had a supposedly strongly increased PIAL) was unexpected, as were very weak signals for half of the total protein targets. Possible explanations for this issue are a) problems with antibody binding, b) problems with preparation of protein samples, c) Western blotting not being sensitive enough for detection of the targets at their native intracellular levels or d) a combination of listed causes. In case of the HBMEC, a strong signal was detected for phosphorylated forms of 4 targets, which paralleled the results of the Human RTK Phosphorylation Array C1 – BMX, Dtk, LTK and Met (Figures 23-24A, Table 12). A strong observed signal for the phosphorylated form of JAK3 is surprising, since the PIAL change of JAK3 in the antibody array was relatively low in HBMEC (Figures 23-24A, Table 12). Very weak signals for some of the total protein targets were puzzling, especially in cases of BMX and LTK – who displayed a very strong signal for the phosphorylated form of the protein – indicating antibody-binding problems for the antibodies in question. It is notable, however, that signals for the phosphorylated forms of the proteins could be observed only in the samples treated with Na_3VO_4 . This confirms the assumption that most of the tested samples were subject to rapid dephosphorylation following the initial phosphorylation, implying that the actual PIAL changes of RTKs tested with the Human RTK Phosphorylation Array C1 would likely be higher if Na_3VO_4 was added to the cells, and possibly include some targets which were below the detection limit in the performed assay. Further investigation is required before any definitive claims can be made about the involvement of specific signaling pathways and the identity of involved interaction partners.

4.3. Listerial infection in *in vivo* mouse models

The most readily available and utilized animal experimental model, the mouse, is considered to be difficult to use for investigation of gastrointestinal listerial infection due to relatively poor penetration of bacteria through the gut barrier, which is likely a consequence of the fact that the mouse variant of Ecad (which is the primary receptor for listerial cell invasion in the gut) is bound by InlA inefficiently (refer to 1.4.1.1.) (Lecuit et al. 1999). Most of the attempts to overcome the issue of poor Ecad-InlA binding in mice can be broadly divided into administering changes to either the mice (i.e. generation of transgenic mice expressing both human and murine Ecad) or the bacteria (i.e. generation of *Lm* with InlA adapted to mouse Ecad) (Wollert et al. 2007; Disson et al. 2008).

However, Bou Ghanem and colleagues argued that the results of these studies implied importance of InlA only in later stages of infection rather than the initial ones. They instead pointed at the standard method of inoculation in mice – oral gavage – as the potential source of the problem (Bou Ghanem et al. 2012). Significant variability in bacterial loads observed in infected animals as well as sometimes drastically different course of disease even within the same test groups (regardless of animal or bacterial strains or other experimental conditions) were highlighted as an indication of possible esophageal/gastric injuries occurring during oral gavage procedure. In essence, oral gavage would result in intravenous rather than oral infection of every mouse injured during its application, and is therefore highly dependent on individual skill, experience and concentration of the experimenter (Bou Ghanem et al. 2012). Feeding with contaminated food has been suggested as an alternative which does not resort to usage of genetically manipulated mice, puts less stress on mice during the infection event, is truer to the natural circumstances of infection and is more reproducible (Bou Ghanem et al. 2012; Bou Ghanem, Myers-Morales, and D'Orazio 2013). The feeding method used in this study led to establishment of infection in mice confirmed by plating of feces samples (data not shown) as well as animal organ samples post-mortem (refer to 3.3.).

4.3.1. Effect of immunosuppression on efficiency of oral infection by *Lm* in mice

Immunodeficiency is a known contributor – if not a condition – for emergence of more severe forms of orally acquired listeriosis, most often manifesting as a systemic spread of *Lm* to various organs of the body, including liver, spleen and brain (Radoshevich and Cossart 2018; Banović, Schrotten, and Schwerk 2020). A common approach in overcoming mouse resistance to oral listerial infection applied by many researchers in the past was to use a very high bacterial load in the inoculum, with mixed results (Bou Ghanem, Myers-Morales, and D'Orazio 2013). The blocking of cell-mediated immune response in mice by hydrocortisone and cyclosporine A presented itself as an elegant way to both a) simulate the circumstances in which systemic listeriosis most often manifests clinically in humans and

b) compensate for the mouse Ecad-InIA binding-induced handicap in bacterial invasion through the gut (North 1971; Strauss, Heymer, and Hof 1985; Drevets and Bronze 2008; Radaelli et al. 2018).

Results presented in this study (Figure 25) show statistically significant higher bacterial loads in livers, MLNs and spleens of immunosuppressed infected mice, but not in their blood or brains. It could be argued that – due to the necessity of an established bacteremia for CNS invasion – a longer incubation period could have resulted in a higher bacterial load in the brains of immunosuppressed mice since there is an observable increasing trend in bacterial loads, but it cannot be categorically stated based on the presented data (Figure 25) (Berche 1995). BALB/cByJRj mice have known defects in immune response and were reported to be more susceptible to listerial invasion, and the results for non-immunocompromised mice show a trend (with statistical significance in case of livers) of higher bacterial loads in the organs of BALB/cByJRj mice than in the same organs of C57BL/6JRj mice (Figure 25) (Bou Ghanem et al. 2012; Bergmann et al. 2013; Radaelli et al. 2018). Interestingly, there was no real difference in bacterial loads in organs between the mouse strains in immunosuppressed groups, showcasing the importance of cell-mediated immune response to clearance of listerial infection in mice (Figure 25) (North 1971; Strauss, Heymer, and Hof 1985; Bou Ghanem et al. 2012; Bergmann et al. 2013; Radaelli et al. 2018). More importantly, the results indicate that a functional cell-mediated immune response could be a more important factor in systemic spread and persistence of *Lm* post-oral infection than the existence of a functional InIA-Ecad interaction, although more research – preferably with mice expressing human Ecad as well as *Lm* expressing mouse-adapted InIA – is required to advance this theory.

4.3.2. Effect of CD44v6-blocking peptides on efficiency of oral infection by *Lm* in mice

Interaction between CD44v6, Met and HGF is necessary for phosphorylation of Met, the first step in Met-mediated downstream signal transmission, and CD44v6-blocking peptides have been described as a method for disruption of this interaction in *in vitro* and *in vivo* models (Matzke et al. 2005; Orian-Rousseau et al. 2002; Hasenauer et al. 2013; Matzke-Ogi et al. 2016; Hartmans et al. 2017; Li et al. 2017). Although most of the work utilizing CD44v6-blocking peptides has been done in cancer research, they were also used in investigation of listerial invasion *in vitro* to block the triggering of Met by InIB (Jung et al. 2009). Findings presented in this study show no statistically significant effects of CD44v6-blocking peptides on the numbers of bacteria found in the organs of infected mice (Figure 26), which is in line with data from *in vitro* experiments (Figure 18) (refer to 4.1.1.1.). Although this could be taken as an argument for the claim against the involvement and importance of CD44v6 in InIB-Met interaction (as argued by Dortet and colleagues), other explanations should be considered as well, such as a) potential unidentified problems during preparation and/or administration of peptide solutions/suspensions and b) possible variations in quality between different peptide batches (Prof. Veronique Orian-Rousseau, internal communication) (Dortet et al. 2010).

5. CONCLUSION AND OUTLOOK

Although *Lm* is relatively rare as a causative agent of food poisoning, it remains noteworthy due to the seriousness of the clinical picture of systemic listeriosis, particularly *Lm*-induced meningitis, which has mortality rates of up to 40% in immunocompromised individuals. Therefore, understanding of the mechanisms it uses to invade the CNS could lead to the development of treatment options causing significant drops in morbidity and mortality associated with listeriosis.

Multiple experiments conducted within this study outline both the similarities and the differences of the entry of *Lm* into HBMEC and HIBCPP cells, reflecting the molecular expression patterns of the two cell lines and potential differences in entry routes employed by *Lm* to penetrate the BBB and the BCSFB. As expected, InIB was shown to be the VF of highest importance for invasion into HBMEC (Ecad-negative, Met-positive), while InIA and InIB jointly contributed to the invasion into the HIBCPP cells (Ecad-positive, Met-positive). Further analysis confirmed that MAPKs and dynamin play as important a role for HBMEC as they do for HIBCPP cells, although the role of Erk1/2 seems to be negligible in HBMEC. Experiments focused on the intermediate filament protein vimentin hint at its importance for invasion into HBMEC, but not necessarily through interaction with InIF. Further studies are required to decipher a possible involvement of InIF, including an analysis of the role of ROCKs.

The results of the RTK phosphorylation array revealed several new possible targets for further investigation, some of which were previously connected to other bacterial pathogens. Interestingly, the RTK activation pattern was quite different between the HBMEC and the HIBCPP cells, hinting at potentially more complex differences in the mechanics of listerial internalization between the two cell lines than what was originally assumed. Due to a lack of literature on listerial interaction with RTKs other than Met and their known role in interaction with pathogens, a possibility for new investigative tracks into *Lm*-related cell signaling presents itself from this direction.

Initial experiments with mice have shown that immunosuppression renders mice much more susceptible to *Lm* regardless of the supposed resistance of mice to listerial infection, indicating that there might be more to it than just the inability of InIA to effectively bind to mouse Ecad. The experiments focused on blocking of InIB-Met-CD44v6 interactions using CD44v6-blocking peptides failed to produce the expected outcome in both the tested cell lines and mice, possibly due to problems associated with peptide generation and/or preparation. Mice with inducible KO for CD44/CD44v6 as well as CD44v6-KO HBMEC and HIBCPP cells have been generated by the group's collaboration partners, which will enable further investigation of the role of CD44/CD44v6 during CNS invasion by *Lm* in future infection experiments.

REFERENCE LIST

- Abbott, N. J., L. Rönnbäck, and E. Hansson. 2006. 'Astrocyte-endothelial interactions at the blood-brain barrier', *Nat Rev Neurosci*, 7: 41-53.
- Agerer, F., S. Lux, A. Michel, M. Rohde, K. Ohlsen, and C. R. Hauck. 2005. 'Cellular invasion by *Staphylococcus aureus* reveals a functional link between focal adhesion kinase and cortactin in integrin-mediated internalisation', *J Cell Sci*, 118: 2189-200.
- Amano, A. 2007. 'Disruption of epithelial barrier and impairment of cellular function by *Porphyromonas gingivalis*', *Front Biosci*, 12: 3965-74.
- Amasheh, S., N. Meiri, A. H. Gitter, T. Schöneberg, J. Mankertz, J. D. Schulzke, and M. Fromm. 2002. 'Claudin-2 expression induces cation-selective channels in tight junctions of epithelial cells', *J Cell Sci*, 115: 4969-76.
- Anderson, J. M., and C. M. Van Itallie. 2009. 'Physiology and function of the tight junction', *Cold Spring Harb Perspect Biol*, 1: a002584.
- Anderton, J. M., G. Rajam, S. Romero-Steiner, S. Summer, A. P. Kowalczyk, G. M. Carlone, J. S. Sampson, and E. W. Ades. 2007. 'E-cadherin is a receptor for the common protein pneumococcal surface adhesin A (PsaA) of *Streptococcus pneumoniae*', *Microb Pathog*, 42: 225-36.
- Andreone, B. J., B. W. Chow, A. Tata, B. Lacoste, A. Ben-Zvi, K. Bullock, A. A. Deik, D. D. Ginty, C. B. Clish, and C. Gu. 2017. 'Blood-Brain Barrier Permeability Is Regulated by Lipid Transport-Dependent Suppression of Caveolae-Mediated Transcytosis', *Neuron*, 94: 581-94.e5.
- Antal, E. A., E. M. Løberg, P. Bracht, K. K. Melby, and J. Maehlen. 2001. 'Evidence for intraaxonal spread of *Listeria monocytogenes* from the periphery to the central nervous system', *Brain Pathol*, 11: 432-8.
- Appelt-Menzel, A., A. Cubukova, K. Günther, F. Edenhofer, J. Piontek, G. Krause, T. Stüber, H. Walles, W. Neuhaus, and M. Metzger. 2017. 'Establishment of a Human Blood-Brain Barrier Co-culture Model Mimicking the Neurovascular Unit Using Induced Pluri- and Multipotent Stem Cells', *Stem Cell Reports*, 8: 894-906.
- Autret, Nicolas, Iharilalao Dubail, Patrick Trieu-Cuot, Patrick Berche, and Alain Charbit. 2001. 'Identification of New Genes Involved in the Virulence of *Listeria monocytogenes* by Signature-Tagged Transposon Mutagenesis', *Infection and Immunity*, 69: 2054-65.
- Baehr, C., V. Reichel, and G. Fricker. 2006. 'Choroid plexus epithelial monolayers--a cell culture model from porcine brain', *Cerebrospinal Fluid Res*, 3: 13.
- Balandyté, L., I. Brodard, J. Frey, A. Oevermann, and C. Abril. 2011. 'Ruminant rhombencephalitis-associated *Listeria monocytogenes* alleles linked to a multilocus variable-number tandem-repeat analysis complex', *Appl Environ Microbiol*, 77: 8325-35.

- Banerjee, A., N. M. Van Sorge, T. R. Sheen, S. Uchiyama, T. J. Mitchell, and K. S. Doran. 2010. 'Activation of brain endothelium by pneumococcal neuraminidase NanA promotes bacterial internalization', *Cell Microbiol*, 12: 1576-88.
- Banizs, B., M. M. Pike, C. L. Millican, W. B. Ferguson, P. Komlosi, J. Sheetz, P. D. Bell, E. M. Schwiebert, and B. K. Yoder. 2005. 'Dysfunctional cilia lead to altered ependyma and choroid plexus function, and result in the formation of hydrocephalus', *Development*, 132: 5329-39.
- Banović, F., H. Schroten, and C. Schwerk. 2020. 'Potential Roles and Functions of Listerial Virulence Factors during Brain Entry', *Toxins (Basel)*, 12.
- Baruch, K., L. Gur-Arie, C. Nadler, S. Koby, G. Yerushalmi, Y. Ben-Neriah, O. Yogev, E. Shaulian, C. Guttman, R. Zarivach, and I. Rosenshine. 2011. 'Metalloprotease type III effectors that specifically cleave JNK and NF- κ B', *Embo j*, 30: 221-31.
- Bastounis, E. E., Y. T. Yeh, and J. A. Theriot. 2018. 'Matrix stiffness modulates infection of endothelial cells by *Listeria monocytogenes* via expression of cell surface vimentin', *Mol Biol Cell*, 29: 1571-89.
- Bauer, H. C., I. A. Krizbai, H. Bauer, and A. Traweger. 2014. "'You Shall Not Pass"-tight junctions of the blood brain barrier', *Front Neurosci*, 8: 392.
- Ben-Zvi, A., B. Lacoste, E. Kur, B. J. Andreone, Y. Mayshar, H. Yan, and C. Gu. 2014. 'Mfsd2a is critical for the formation and function of the blood-brain barrier', *Nature*, 509: 507-11.
- Berche, P. 1995. 'Bacteremia is required for invasion of the murine central nervous system by *Listeria monocytogenes*', *Microb Pathog*, 18: 323-36.
- Bergmann, B., D. Raffelsbauer, M. Kuhn, M. Goetz, S. Hom, and W. Goebel. 2002. 'InIA- but not InIB-mediated internalization of *Listeria monocytogenes* by non-phagocytic mammalian cells needs the support of other internalins', *Mol Microbiol*, 43: 557-70.
- Bergmann, S., P. M. Beard, B. Pasche, S. Lienenklaus, S. Weiss, C. G. Gahan, K. Schughart, and A. Lengeling. 2013. 'Influence of internalin A murinisation on host resistance to orally acquired listeriosis in mice', *BMC Microbiol*, 13: 90.
- Berndt, P., L. Winkler, J. Cording, O. Breitzkreuz-Korff, A. Rex, S. Dithmer, V. Rausch, R. Blasig, M. Richter, A. Sporbert, H. Wolburg, I. E. Blasig, and R. F. Haseloff. 2019. 'Tight junction proteins at the blood-brain barrier: far more than claudin-5', *Cell Mol Life Sci*, 76: 1987-2002.
- Bierne, H., E. Gouin, P. Roux, P. Caroni, H. L. Yin, and P. Cossart. 2001. 'A role for cofilin and LIM kinase in *Listeria*-induced phagocytosis', *J Cell Biol*, 155: 101-12.
- Bierne, H., H. Miki, M. Innocenti, G. Scita, F. B. Gertler, T. Takenawa, and P. Cossart. 2005. 'WASP-related proteins, Abi1 and Ena/VASP are required for *Listeria* invasion induced by the Met receptor', *J Cell Sci*, 118: 1537-47.
- Bierne, H., E. Milohanic, and M. Kortebi. 2018. 'To Be Cytosolic or Vacuolar: The Double Life of *Listeria monocytogenes*', *Front Cell Infect Microbiol*, 8: 136.

Bierne, H., C. Sabet, N. Personnic, and P. Cossart. 2007. 'Internalins: a complex family of leucine-rich repeat-containing proteins in *Listeria monocytogenes*', *Microbes Infect*, 9: 1156-66.

Bittner, S., T. Ruck, M. K. Schuhmann, A. M. Herrmann, H. Moha ou Maati, N. Bobak, K. Göbel, F. Langhauser, D. Stegner, P. Ehling, M. Borsotto, H. C. Pape, B. Nieswandt, C. Kleinschnitz, C. Heurteaux, H. J. Galla, T. Budde, H. Wiendl, and S. G. Meuth. 2013. 'Endothelial TWIK-related potassium channel-1 (TREK1) regulates immune-cell trafficking into the CNS', *Nat Med*, 19: 1161-5.

Bonazzi, M., M. Lecuit, and P. Cossart. 2009. '*Listeria monocytogenes* internalin and E-cadherin: from structure to pathogenesis', *Cell Microbiol*, 11: 693-702.

Bonazzi, M., L. Vasudevan, A. Mallet, M. Sachse, A. Sartori, M. C. Prevost, A. Roberts, S. B. Taner, J. D. Wilbur, F. M. Brodsky, and P. Cossart. 2011. 'Clathrin phosphorylation is required for actin recruitment at sites of bacterial adhesion and internalization', *J Cell Biol*, 195: 525-36.

Bonazzi, M., E. Veiga, J. Pizarro-Cerdá, and P. Cossart. 2008. 'Successive post-translational modifications of E-cadherin are required for InlA-mediated internalization of *Listeria monocytogenes*', *Cell Microbiol*, 10: 2208-22.

Boraas, L. C., and T. Ahsan. 2016. 'Lack of vimentin impairs endothelial differentiation of embryonic stem cells', *Sci Rep*, 6: 30814.

Borges, N., F. Shi, I. Azevedo, and K. L. Audus. 1994. 'Changes in brain microvessel endothelial cell monolayer permeability induced by adrenergic drugs', *Eur J Pharmacol*, 269: 243-8.

Borkowski, J., L. Li, U. Steinmann, N. Quednau, C. Stump-Guthier, C. Weiss, P. Findeisen, N. Gretz, H. Ishikawa, T. Tenenbaum, H. Schrotten, and C. Schwerk. 2014. '*Neisseria meningitidis* elicits a pro-inflammatory response involving I κ B ζ in a human blood-cerebrospinal fluid barrier model', *J Neuroinflammation*, 11: 163.

Bosse, T., J. Ehinger, A. Czuchra, S. Benesch, A. Steffen, X. Wu, K. Schloen, H. H. Niemann, G. Scita, T. E. Stradal, C. Brakebusch, and K. Rottner. 2007. 'Cdc42 and phosphoinositide 3-kinase drive Rac-mediated actin polymerization downstream of c-Met in distinct and common pathways', *Mol Cell Biol*, 27: 6615-28.

Bou Ghanem, E. N., G. S. Jones, T. Myers-Morales, P. D. Patil, A. N. Hidayatullah, and S. E. D'Orazio. 2012. 'InlA promotes dissemination of *Listeria monocytogenes* to the mesenteric lymph nodes during food borne infection of mice', *PLoS Pathog*, 8: e1003015.

Bou Ghanem, E. N., T. Myers-Morales, and S. E. F. D'Orazio. 2013. 'A mouse model of foodborne *Listeria monocytogenes* infection', *Curr Protoc Microbiol*, 31: 9b.3.1-9b.3.16.

Braun, L., B. Ghebrehiwet, and P. Cossart. 2000. 'gC1q-R/p32, a C1q-binding protein, is a receptor for the InlB invasion protein of *Listeria monocytogenes*', *Embo j*, 19: 1458-66.

Braun, L., F. Nato, B. Payrastre, J. C. Mazié, and P. Cossart. 1999. 'The 213-amino-acid leucine-rich repeat region of the *Listeria monocytogenes* InlB protein is sufficient for entry into mammalian cells, stimulation of PI 3-kinase and membrane ruffling', *Mol Microbiol*, 34: 10-23.

Braun, L., H. Ohayon, and P. Cossart. 1998. 'The InlB protein of *Listeria monocytogenes* is sufficient to promote entry into mammalian cells', *Mol Microbiol*, 27: 1077-87.

Bublitz, M., L. Polle, C. Holland, D. W. Heinz, M. Nimtz, and W. D. Schubert. 2009. 'Structural basis for autoinhibition and activation of Auto, a virulence-associated peptidoglycan hydrolase of *Listeria monocytogenes*', *Mol Microbiol*, 71: 1509-22.

Bublitz, Maike, Christin Holland, Christophe Sabet, Joachim Reichelt, Pascale Cossart, Dirk W. Heinz, Helene Bierne, and Wolf-Dieter Schubert. 2008. 'Crystal Structure and Standardized Geometric Analysis of InlJ, a Listerial Virulence Factor and Leucine-Rich Repeat Protein with a Novel Cysteine Ladder', *Journal of Molecular Biology*, 378: 87-96.

Cabanes, D., O. Dussurget, P. Dehoux, and P. Cossart. 2004. 'Auto, a surface associated autolysin of *Listeria monocytogenes* required for entry into eukaryotic cells and virulence', *Mol Microbiol*, 51: 1601-14.

Camejo, A., F. Carvalho, O. Reis, E. Leitão, S. Sousa, and D. Cabanes. 2011. 'The arsenal of virulence factors deployed by *Listeria monocytogenes* to promote its cell infection cycle', *Virulence*, 2: 379-94.

Campisi, M., S. H. Lim, V. Chiono, and R. D. Kamm. 2021. '3D Self-Organized Human Blood-Brain Barrier in a Microfluidic Chip', *Methods Mol Biol*, 2258: 205-19.

Carmeliet, P., M. G. Lampugnani, L. Moons, F. Breviario, V. Compernelle, F. Bono, G. Balconi, R. Spagnuolo, B. Oosthuyse, M. Dewerchin, A. Zanetti, A. Angellilo, V. Mattot, D. Nuyens, E. Lutgens, F. Clotman, M. C. de Ruiter, A. Gittenberger-de Groot, R. Poelmann, F. Lupu, J. M. Herbert, D. Collen, and E. Dejana. 1999. 'Targeted deficiency or cytosolic truncation of the VE-cadherin gene in mice impairs VEGF-mediated endothelial survival and angiogenesis', *Cell*, 98: 147-57.

Castro Dias, M., C. Coisne, P. Baden, G. Enzmann, L. Garrett, L. Becker, S. M. Höltner, M. Hrabě de Angelis, U. Deutsch, and B. Engelhardt. 2019. 'Claudin-12 is not required for blood-brain barrier tight junction function', *Fluids Barriers CNS*, 16: 30.

Castro Dias, M., C. Coisne, I. Lazarevic, P. Baden, M. Hata, N. Iwamoto, D. M. F. Francisco, M. Vanlandewijck, L. He, F. A. Baier, D. Stroka, R. Bruggmann, R. Lyck, G. Enzmann, U. Deutsch, C. Betsholtz, M. Furuse, S. Tsukita, and B. Engelhardt. 2019. 'Claudin-3-deficient C57BL/6J mice display intact brain barriers', *Sci Rep*, 9: 203.

Castro Dias, M., J. A. Mapunda, M. Vladymyrov, and B. Engelhardt. 2019. 'Structure and Junctional Complexes of Endothelial, Epithelial and Glial Brain Barriers', *Int J Mol Sci*, 20.

Chang, C. W., L. Ye, D. M. Defoe, and R. B. Caldwell. 1997. 'Serum inhibits tight junction formation in cultured pigment epithelial cells', *Invest Ophthalmol Vis Sci*, 38: 1082-93.

Chang, C., X. Wang, and R. B. Caldwell. 1997. 'Serum opens tight junctions and reduces ZO-1 protein in retinal epithelial cells', *J Neurochem*, 69: 859-67.

Chen, C., B. N. Nguyen, G. Mitchell, S. R. Margolis, D. Ma, and D. A. Portnoy. 2018. 'The Listeriolysin O PEST-like Sequence Co-opts AP-2-Mediated Endocytosis to Prevent Plasma Membrane Damage during Listeria Infection', *Cell Host Microbe*, 23: 786-95.e5.

Chi, F., T. D. Jong, L. Wang, Y. Ouyang, C. Wu, W. Li, and S. H. Huang. 2010. 'Vimentin-mediated signalling is required for IbeA+ E. coli K1 invasion of human brain microvascular endothelial cells', *Biochem J*, 427: 79-90.

Cho, C. F., J. M. Wolfe, C. M. Fadzen, D. Calligaris, K. Hornburg, E. A. Chiocca, N. Y. R. Agar, B. L. Pentelute, and S. E. Lawler. 2017. 'Blood-brain-barrier spheroids as an in vitro screening platform for brain-penetrating agents', *Nat Commun*, 8: 15623.

Christie, M. P., B. A. Johnstone, R. K. Tweten, M. W. Parker, and C. J. Morton. 2018. 'Cholesterol-dependent cytolysins: from water-soluble state to membrane pore', *Biophys Rev*, 10: 1337-48.

Churin, Y., L. Al-Ghoul, O. Kepp, T. F. Meyer, W. Birchmeier, and M. Naumann. 2003. 'Helicobacter pylori CagA protein targets the c-Met receptor and enhances the motogenic response', *J Cell Biol*, 161: 249-55.

Cornford, E. M., S. Hyman, and B. E. Swartz. 1994. 'The human brain GLUT1 glucose transporter: ultrastructural localization to the blood-brain barrier endothelia', *J Cereb Blood Flow Metab*, 14: 106-12.

Cossart, P., M. F. Vicente, J. Mengaud, F. Baquero, J. C. Perez-Diaz, and P. Berche. 1989. 'Listeriolysin O is essential for virulence of Listeria monocytogenes: direct evidence obtained by gene complementation', *Infect Immun*, 57: 3629-36.

Cywes, C., I. Stamenkovic, and M. R. Wessels. 2000. 'CD44 as a receptor for colonization of the pharynx by group A Streptococcus', *J Clin Invest*, 106: 995-1002.

Dahm, T., O. Adams, S. Boettcher, S. Diedrich, V. Morozov, G. Hansman, P. Fallier-Becker, S. Schädler, C. J. Burkhardt, C. Weiss, C. Stump-Guthier, H. Ishikawa, H. Schrotten, C. Schwerk, T. Tenenbaum, and H. Rudolph. 2018. 'Strain-dependent effects of clinical echovirus 30 outbreak isolates at the blood-CSF barrier', *J Neuroinflammation*, 15: 50.

Damkier, H. H., P. D. Brown, and J. Praetorius. 2013. 'Cerebrospinal fluid secretion by the choroid plexus', *Physiol Rev*, 93: 1847-92.

Dando, S. J., A. Mackay-Sim, R. Norton, B. J. Currie, J. A. St John, J. A. Ekberg, M. Batzloff, G. C. Ulett, and I. R. Beacham. 2014. 'Pathogens penetrating the central nervous system: infection pathways and the cellular and molecular mechanisms of invasion', *Clin Microbiol Rev*, 27: 691-726.

Daneman, R. 2012. 'The blood-brain barrier in health and disease', *Ann Neurol*, 72: 648-72.

Daneman, R., L. Zhou, D. Agalliu, J. D. Cahoy, A. Kaushal, and B. A. Barres. 2010. 'The mouse blood-brain barrier transcriptome: a new resource for understanding the development and function of brain endothelial cells', *PLoS One*, 5: e13741.

Danielsson, F., M. K. Peterson, H. Caldeira Araújo, F. Lautenschläger, and A. K. B. Gad. 2018. 'Vimentin Diversity in Health and Disease', *Cells*, 7.

Dash, S., K. Duraivelan, and D. Samanta. 2021. 'Cadherin-mediated host-pathogen interactions', *Cell Microbiol.*

Davis, G. E., W. Koh, and A. N. Stratman. 2007. 'Mechanisms controlling human endothelial lumen formation and tube assembly in three-dimensional extracellular matrices', *Birth Defects Res C Embryo Today*, 81: 270-85.

Deng, L., B. L. Spencer, J. A. Holmes, R. Mu, S. Rego, T. A. Weston, Y. Hu, G. F. Sanches, S. Yoon, N. Park, P. E. Nagao, H. F. Jenkinson, J. A. Thornton, K. S. Seo, A. H. Nobbs, and K. S. Doran. 2019. 'The Group B Streptococcal surface antigen I/II protein, BspC, interacts with host vimentin to promote adherence to brain endothelium and inflammation during the pathogenesis of meningitis', *PLoS Pathog*, 15: e1007848.

Dick, J., S. Hebling, J. Becam, M. K. Taha, and A. Schubert-Unkmeir. 2017. 'Comparison of the inflammatory response of brain microvascular and peripheral endothelial cells following infection with *Neisseria meningitidis*', *Pathog Dis*, 75.

Dinner, S., J. Kaltschmidt, C. Stump-Guthier, S. Hetjens, H. Ishikawa, T. Tenenbaum, H. Schroten, and C. Schwerk. 2017. 'Mitogen-activated protein kinases are required for effective infection of human choroid plexus epithelial cells by *Listeria monocytogenes*', *Microbes Infect*, 19: 18-33.

Disson, O., S. Grayo, E. Huillet, G. Nikitas, F. Langa-Vives, O. Dussurget, M. Ragon, A. Le Monnier, C. Babinet, P. Cossart, and M. Lecuit. 2008. 'Conjugated action of two species-specific invasion proteins for fetoplacental listeriosis', *Nature*, 455: 1114-8.

Disson, O., and M. Lecuit. 2012. 'Targeting of the central nervous system by *Listeria monocytogenes*', *Virulence*, 3: 213-21.

Dons, L., K. Weclawicz, Y. Jin, E. Bindseil, J. E. Olsen, and K. Kristensson. 1999. 'Rat dorsal root ganglia neurons as a model for *Listeria monocytogenes* infections in culture', *Med Microbiol Immunol*, 188: 15-21.

Dortet, L., E. Veiga, M. Bonazzi, and P. Cossart. 2010. 'CD44-independent activation of the Met signaling pathway by HGF and InlB', *Microbes Infect*, 12: 919-27.

Dortet, Laurent, Serge Mostowy, Ascel Samba Louaka, Edith Gouin, Marie-Anne Nahori, Erik A. C. Wiemer, Olivier Dussurget, and Pascale Cossart. 2011. 'Recruitment of the Major Vault Protein by InlK: A *Listeria monocytogenes* Strategy to Avoid Autophagy', *PLOS Pathogens*, 7: e1002168.

- Doumith, M., C. Buchrieser, P. Glaser, C. Jacquet, and P. Martin. 2004. 'Differentiation of the major *Listeria monocytogenes* serovars by multiplex PCR', *J Clin Microbiol*, 42: 3819-22.
- Dramsi, S., I. Biswas, E. Maguin, L. Braun, P. Mastroeni, and P. Cossart. 1995. 'Entry of *Listeria monocytogenes* into hepatocytes requires expression of InlB, a surface protein of the internalin multigene family', *Mol Microbiol*, 16: 251-61.
- Dramsi, S., P. Dehoux, M. Lebrun, P. L. Goossens, and P. Cossart. 1997. 'Identification of four new members of the internalin multigene family of *Listeria monocytogenes* EGD', *Infect Immun*, 65: 1615-25.
- Dramsi, S., C. Kocks, C. Forestier, and P. Cossart. 1993. 'Internalin-mediated invasion of epithelial cells by *Listeria monocytogenes* is regulated by the bacterial growth state, temperature and the pleiotropic activator *prfA*', *Mol Microbiol*, 9: 931-41.
- Drevets, D. A. 1998. '*Listeria monocytogenes* virulence factors that stimulate endothelial cells', *Infect Immun*, 66: 232-8.
- . 1999. 'Dissemination of *Listeria monocytogenes* by infected phagocytes', *Infect Immun*, 67: 3512-7.
- Drevets, D. A., and M. S. Bronze. 2008. '*Listeria monocytogenes*: epidemiology, human disease, and mechanisms of brain invasion', *FEMS Immunol Med Microbiol*, 53: 151-65.
- Drevets, D. A., T. A. Jelinek, and N. E. Freitag. 2001. '*Listeria monocytogenes*-infected phagocytes can initiate central nervous system infection in mice', *Infect Immun*, 69: 1344-50.
- Drevets, D. A., P. J. Leenen, and R. A. Greenfield. 2004. 'Invasion of the central nervous system by intracellular bacteria', *Clin Microbiol Rev*, 17: 323-47.
- Drevets, D. A., R. T. Sawyer, T. A. Potter, and P. A. Campbell. 1995. '*Listeria monocytogenes* infects human endothelial cells by two distinct mechanisms', *Infect Immun*, 63: 4268-76.
- Duesbery, N. S., C. P. Webb, S. H. Leppla, V. M. Gordon, K. R. Klimpel, T. D. Copeland, N. G. Ahn, M. K. Oskarsson, K. Fukasawa, K. D. Paull, and G. F. Vande Woude. 1998. 'Proteolytic inactivation of MAP-kinase-kinase by anthrax lethal factor', *Science*, 280: 734-7.
- Ebnet, K., A. Suzuki, Y. Horikoshi, T. Hirose, M. K. Meyer Zu Brickwedde, S. Ohno, and D. Vestweber. 2001. 'The cell polarity protein ASIP/PAR-3 directly associates with junctional adhesion molecule (JAM)', *Embo j*, 20: 3738-48.
- Edwards, V. L., L. C. Wang, V. Dawson, D. C. Stein, and W. Song. 2013. '*Neisseria gonorrhoeae* breaches the apical junction of polarized epithelial cells for transmigration by activating EGFR', *Cell Microbiol*, 15: 1042-57.
- Eigenmann, D. E., G. Xue, K. S. Kim, A. V. Moses, M. Hamburger, and M. Oufir. 2013. 'Comparative study of four immortalized human brain capillary endothelial cell lines, hCMEC/D3, hBMEC, TY10, and BB19, and optimization of culture conditions, for an in vitro blood-brain barrier model for drug permeability studies', *Fluids Barriers CNS*, 10: 33.

- Eisenreich, W., T. Dandekar, J. Heesemann, and W. Goebel. 2010. 'Carbon metabolism of intracellular bacterial pathogens and possible links to virulence', *Nat Rev Microbiol*, 8: 401-12.
- Elwell, C. A., A. Ceesay, J. H. Kim, D. Kalman, and J. N. Engel. 2008. 'RNA interference screen identifies Abl kinase and PDGFR signaling in Chlamydia trachomatis entry', *PLoS Pathog*, 4: e1000021.
- Elwell, C., K. Mirrashidi, and J. Engel. 2016. 'Chlamydia cell biology and pathogenesis', *Nat Rev Microbiol*, 14: 385-400.
- Engelhardt, B., P. Vajkoczy, and R. O. Weller. 2017. 'The movers and shapers in immune privilege of the CNS', *Nat Immunol*, 18: 123-31.
- Eriksson, E., L. Dons, A. G. Rothfuchs, P. Heldin, H. Wigzell, and M. E. Rottenberg. 2003. 'CD44-regulated intracellular proliferation of Listeria monocytogenes', *Infect Immun*, 71: 4102-11.
- Faralla, C., E. E. Bastounis, F. E. Ortega, S. H. Light, G. Rizzuto, L. Gao, D. K. Marciano, S. Nocadello, W. F. Anderson, J. R. Robbins, J. A. Theriot, and A. I. Bakardjiev. 2018. 'Listeria monocytogenes InIP interacts with afadin and facilitates basement membrane crossing', *PLoS Pathog*, 14: e1007094.
- Faralla, C., G. A. Rizzuto, D. E. Lowe, B. Kim, C. Cooke, L. R. Shiow, and A. I. Bakardjiev. 2016. 'InIP, a New Virulence Factor with Strong Placental Tropism', *Infect Immun*, 84: 3584-96.
- Ferraris, D. M., E. Gherardi, Y. Di, D. W. Heinz, and H. H. Niemann. 2010. 'Ligand-mediated dimerization of the Met receptor tyrosine kinase by the bacterial invasion protein InIB', *J Mol Biol*, 395: 522-32.
- Furuse, M., M. Hata, K. Furuse, Y. Yoshida, A. Haratake, Y. Sugitani, T. Noda, A. Kubo, and S. Tsukita. 2002. 'Claudin-based tight junctions are crucial for the mammalian epidermal barrier: a lesson from claudin-1-deficient mice', *J Cell Biol*, 156: 1099-111.
- Furuse, M., T. Hirase, M. Itoh, A. Nagafuchi, S. Yonemura, S. Tsukita, and S. Tsukita. 1993. 'Occludin: a novel integral membrane protein localizing at tight junctions', *J Cell Biol*, 123: 1777-88.
- Gaillard, J. L., P. Berche, C. Frehel, E. Gouin, and P. Cossart. 1991. 'Entry of L. monocytogenes into cells is mediated by internalin, a repeat protein reminiscent of surface antigens from gram-positive cocci', *Cell*, 65: 1127-41.
- Gaillard, J. L., P. Berche, and P. Sansonetti. 1986. 'Transposon mutagenesis as a tool to study the role of hemolysin in the virulence of Listeria monocytogenes', *Infect Immun*, 52: 50-5.
- Gaillard, P. J., L. H. Voorwinden, J. L. Nielsen, A. Ivanov, R. Atsumi, H. Engman, C. Ringbom, A. G. de Boer, and D. D. Breimer. 2001. 'Establishment and functional characterization of an in vitro model of the blood-brain barrier, comprising a co-culture of brain capillary endothelial cells and astrocytes', *Eur J Pharm Sci*, 12: 215-22.

Garrido-Urbani, S., P. F. Bradfield, and B. A. Imhof. 2014. 'Tight junction dynamics: the role of junctional adhesion molecules (JAMs)', *Cell Tissue Res*, 355: 701-15.

Gath, U., A. Hakvoort, J. Wegener, S. Decker, and H. J. Galla. 1997. 'Porcine choroid plexus cells in culture: expression of polarized phenotype, maintenance of barrier properties and apical secretion of CSF-components', *Eur J Cell Biol*, 74: 68-78.

Ge, S., L. Song, and J. S. Pachter. 2005. 'Where is the blood-brain barrier ... really?', *J Neurosci Res*, 79: 421-7.

Gekara, N. O., K. Westphal, B. Ma, M. Rohde, L. Groebe, and S. Weiss. 2007. 'The multiple mechanisms of Ca²⁺ signalling by listeriolysin O, the cholesterol-dependent cytolysin of *Listeria monocytogenes*', *Cell Microbiol*, 9: 2008-21.

Geraghty, R. J., C. Krummenacher, G. H. Cohen, R. J. Eisenberg, and P. G. Spear. 1998. 'Entry of alphaherpesviruses mediated by poliovirus receptor-related protein 1 and poliovirus receptor', *Science*, 280: 1618-20.

Ghosh, P., E. M. Halvorsen, D. A. Ammendolia, N. Mor-Vaknin, M. X. D. O'Riordan, J. H. Brumell, D. M. Markovitz, and D. E. Higgins. 2018. 'Invasion of the Brain by *Listeria monocytogenes* Is Mediated by InlF and Host Cell Vimentin', *mBio*, 9.

Gow, A., C. M. Southwood, J. S. Li, M. Pariali, G. P. Riordan, S. E. Brodie, J. Danias, J. M. Bronstein, B. Kachar, and R. A. Lazzarini. 1999. 'CNS myelin and sertoli cell tight junction strands are absent in Osp/claudin-11 null mice', *Cell*, 99: 649-59.

Greiffenberg, L., W. Goebel, K. S. Kim, J. Daniels, and M. Kuhn. 2000. 'Interaction of *Listeria monocytogenes* with human brain microvascular endothelial cells: an electron microscopic study', *Infect Immun*, 68: 3275-9.

Greiffenberg, L., W. Goebel, K. S. Kim, I. Weiglein, A. Bubert, F. Engelbrecht, M. Stins, and M. Kuhn. 1998. 'Interaction of *Listeria monocytogenes* with human brain microvascular endothelial cells: InlB-dependent invasion, long-term intracellular growth, and spread from macrophages to endothelial cells', *Infect Immun*, 66: 5260-7.

Gründler, T. 2014. 'Die Rolle von InlA und InlB bei der Invasion von *Listeria monocytogenes* in einem humanen Modell der Blut-Liquor-Schranke', Heidelberg University.

Gründler, T., N. Quednau, C. Stump, V. Orian-Rousseau, H. Ishikawa, H. Wolburg, H. Schroten, T. Tenenbaum, and C. Schwerk. 2013. 'The surface proteins InlA and InlB are interdependently required for polar basolateral invasion by *Listeria monocytogenes* in a human model of the blood-cerebrospinal fluid barrier', *Microbes Infect*, 15: 291-301.

Guldimann, C., B. Lejeune, S. Hofer, S. L. Leib, J. Frey, A. Zurbriggen, T. Seuberlich, and A. Oevermann. 2012. 'Ruminant organotypic brain-slice cultures as a model for the investigation of CNS listeriosis', *Int J Exp Pathol*, 93: 259-68.

- Gumbiner, B. M., and P. D. McCrea. 1993. 'Catenins as mediators of the cytoplasmic functions of cadherins', *J Cell Sci Suppl*, 17: 155-8.
- Günzel, D., and A. S. Yu. 2013. 'Claudins and the modulation of tight junction permeability', *Physiol Rev*, 93: 525-69.
- Gur-Arie, Lihi, and Ilan Rosenshine. 2015. 'Subversion of MAPK signaling by pathogenic bacteria', *MAP Kinase*, 4.
- Hamon, M. A., D. Ribet, F. Stavru, and P. Cossart. 2012. 'Listeriolysin O: the Swiss army knife of Listeria', *Trends Microbiol*, 20: 360-8.
- Haqshenas, G., and C. Doerig. 2019. 'Targeting of host cell receptor tyrosine kinases by intracellular pathogens', *Sci Signal*, 12.
- Harter, E., C. Lassnig, E. M. Wagner, A. Zaiser, M. Wagner, and K. Rychli. 2019. 'The Novel Internalins InIP1 and InIP4 and the Internalin-Like Protein InIP3 Enhance the Pathogenicity of Listeria monocytogenes', *Front Microbiol*, 10: 1644.
- Hartmans, E., V. Orian-Rousseau, A. Matzke-Ogi, A. Karrenbeld, D. J. de Groot, S. de Jong, G. M. van Dam, R. S. Fehrmann, and W. B. Nagengast. 2017. 'Functional Genomic mRNA Profiling of Colorectal Adenomas: Identification and in vivo Validation of CD44 and Splice Variant CD44v6 as Molecular Imaging Targets', *Theranostics*, 7: 482-92.
- Hartz, A. M., D. S. Miller, and B. Bauer. 2010. 'Restoring blood-brain barrier P-glycoprotein reduces brain amyloid-beta in a mouse model of Alzheimer's disease', *Mol Pharmacol*, 77: 715-23.
- Haselbach, M., J. Wegener, S. Decker, C. Engelbertz, and H. J. Galla. 2001. 'Porcine Choroid plexus epithelial cells in culture: regulation of barrier properties and transport processes', *Microsc Res Tech*, 52: 137-52.
- Hasenauer, S., D. Malingier, D. Koschut, G. Pace, A. Matzke, A. von Au, and V. Orian-Rousseau. 2013. 'Internalization of Met requires the co-receptor CD44v6 and its link to ERM proteins', *PLoS One*, 8: e62357.
- Hashino, M., M. Tachibana, T. Nishida, H. Hara, K. Tsuchiya, M. Mitsuyama, K. Watanabe, T. Shimizu, and M. Watarai. 2015. 'Inactivation of the MAPK signaling pathway by Listeria monocytogenes infection promotes trophoblast giant cell death', *Front Microbiol*, 6: 1145.
- Hatayama, S., T. Shimohata, S. Amano, J. Kido, A. Q. Nguyen, Y. Sato, Y. Kanda, A. Tentaku, S. Fukushima, M. Nakahashi, T. Uebanso, K. Mawatari, and A. Takahashi. 2018. 'Cellular Tight Junctions Prevent Effective Campylobacter jejuni Invasion and Inflammatory Barrier Disruption Promoting Bacterial Invasion from Lateral Membrane in Polarized Intestinal Epithelial Cells', *Front Cell Infect Microbiol*, 8: 15.
- Herold, R., H. Schrotten, and C. Schwerk. 2019. 'Virulence Factors of Meningitis-Causing Bacteria: Enabling Brain Entry across the Blood-Brain Barrier', *Int J Mol Sci*, 20.

- Hertzig, T., M. Weber, L. Greiffenberg, B. S. Holthausen, W. Goebel, K. S. Kim, and M. Kuhn. 2003. 'Antibodies present in normal human serum inhibit invasion of human brain microvascular endothelial cells by *Listeria monocytogenes*', *Infect Immun*, 71: 95-100.
- Hirase, T., J. M. Staddon, M. Saitou, Y. Ando-Akatsuka, M. Itoh, M. Furuse, K. Fujimoto, S. Tsukita, and L. L. Rubin. 1997. 'Occludin as a possible determinant of tight junction permeability in endothelial cells', *J Cell Sci*, 110 (Pt 14): 1603-13.
- Ho, J., D. L. Moyes, M. Tavassoli, and J. R. Naglik. 2017. 'The Role of ErbB Receptors in Infection', *Trends Microbiol*, 25: 942-52.
- Hoffmann, I., E. Eugène, X. Nassif, P. O. Couraud, and S. Bourdoulous. 2001. 'Activation of ErbB2 receptor tyrosine kinase supports invasion of endothelial cells by *Neisseria meningitidis*', *J Cell Biol*, 155: 133-43.
- Huang, S. H., F. Chi, L. Peng, T. Bo, B. Zhang, L. Q. Liu, X. Wu, N. Mor-Vaknin, D. M. Markovitz, H. Cao, and Y. H. Zhou. 2016. 'Vimentin, a Novel NF- κ B Regulator, Is Required for Meningitic *Escherichia coli* K1-Induced Pathogen Invasion and PMN Transmigration across the Blood-Brain Barrier', *PLoS One*, 11: e0162641.
- Huber, J. D., R. D. Egleton, and T. P. Davis. 2001. 'Molecular physiology and pathophysiology of tight junctions in the blood-brain barrier', *Trends Neurosci*, 24: 719-25.
- Ikeda, W., S. Kakunaga, S. Itoh, T. Shingai, K. Takekuni, K. Satoh, Y. Inoue, A. Hamaguchi, K. Morimoto, M. Takeuchi, T. Imai, and Y. Takai. 2003. 'Tage4/Nectin-like molecule-5 heterophilically trans-interacts with cell adhesion molecule Nectin-3 and enhances cell migration', *J Biol Chem*, 278: 28167-72.
- Ikenouchi, J., M. Furuse, K. Furuse, H. Sasaki, S. Tsukita, and S. Tsukita. 2005. 'Tricellulin constitutes a novel barrier at tricellular contacts of epithelial cells', *J Cell Biol*, 171: 939-45.
- Indra, I., S. Hong, R. Troyanovsky, B. Kormos, and S. Troyanovsky. 2013. 'The adherens junction: a mosaic of cadherin and nectin clusters bundled by actin filaments', *J Invest Dermatol*, 133: 2546-54.
- Inoue, T., K. Narita, Y. Nonami, H. Nakamura, and S. Takeda. 2015. 'Observation of the Ciliary Movement of Choroid Plexus Epithelial Cells Ex Vivo', *J Vis Exp*: e52991.
- Ireton, K., B. Payrastre, H. Chap, W. Ogawa, H. Sakaue, M. Kasuga, and P. Cossart. 1996. 'A role for phosphoinositide 3-kinase in bacterial invasion', *Science*, 274: 780-2.
- Ireton, K., L. A. Rigano, and G. C. Dowd. 2014. 'Role of host GTPases in infection by *Listeria monocytogenes*', *Cell Microbiol*, 16: 1311-20.
- Ishiwata, I., C. Ishiwata, E. Ishiwata, Y. Sato, K. Kiguchi, T. Tachibana, H. Hashimoto, and H. Ishikawa. 2005. 'Establishment and characterization of a human malignant choroids plexus papilloma cell line (HIBCPP)', *Hum Cell*, 18: 67-72.

- Iwamoto, N., T. Higashi, and M. Furuse. 2014. 'Localization of angulin-1/LSR and tricellulin at tricellular contacts of brain and retinal endothelial cells in vivo', *Cell Struct Funct*, 39: 1-8.
- Jacquet, C., M. Doumith, J. I. Gordon, P. M. Martin, P. Cossart, and M. Lecuit. 2004. 'A molecular marker for evaluating the pathogenic potential of foodborne *Listeria monocytogenes*', *J Infect Dis*, 189: 2094-100.
- Jin, Y., L. Dons, K. Kristensson, and M. E. Rottenberg. 2001. 'Neural route of cerebral *Listeria monocytogenes* murine infection: role of immune response mechanisms in controlling bacterial neuroinvasion', *Infect Immun*, 69: 1093-100.
- Jiwani, S., Y. Wang, G. C. Dowd, A. Gianfelice, P. Pichestapong, B. Gavicherla, N. Vanbennekorn, and K. Ireton. 2012. 'Identification of components of the host type IA phosphoinositide 3-kinase pathway that promote internalization of *Listeria monocytogenes*', *Infect Immun*, 80: 1252-66.
- Jones, R. M., H. Wu, C. Wentworth, L. Luo, L. Collier-Hyams, and A. S. Neish. 2008. 'Salmonella AvrA Coordinates Suppression of Host Immune and Apoptotic Defenses via JNK Pathway Blockade', *Cell Host Microbe*, 3: 233-44.
- Jonquière, R., H. Bierne, F. Fiedler, P. Gounon, and P. Cossart. 1999. 'Interaction between the protein InlB of *Listeria monocytogenes* and lipoteichoic acid: a novel mechanism of protein association at the surface of gram-positive bacteria', *Mol Microbiol*, 34: 902-14.
- Jonquière, R., J. Pizarro-Cerdá, and P. Cossart. 2001. 'Synergy between the N- and C-terminal domains of InlB for efficient invasion of non-phagocytic cells by *Listeria monocytogenes*', *Mol Microbiol*, 42: 955-65.
- Joó, F. 1985. 'The blood-brain barrier in vitro: Ten years of research on microvessels isolated from the brain', *Neurochem Int*, 7: 1-25.
- Jung, C., A. Matzke, H. H. Niemann, C. Schwerk, T. Tenenbaum, and V. Orian-Rousseau. 2009. 'Involvement of CD44v6 in InlB-dependent *Listeria* invasion', *Mol Microbiol*, 72: 1196-207.
- Kaeffer, B., C. Bénard, H. M. Blottière, and C. Cherbut. 1997. 'Treatment of rat proximal and distal colonic cells with sodium orthovanadate enhances their adhesion and survival in primary culture', *Cell Biol Int*, 21: 303-14.
- Karlsson, W. K., Z. B. Harboe, C. Roed, J. B. Monrad, M. Lindelof, V. A. Larsen, and D. Kondziella. 2017. 'Early trigeminal nerve involvement in *Listeria monocytogenes* rhombencephalitis: case series and systematic review', *J Neurol*, 264: 1875-84.
- Kasper, M., U. Karsten, and P. Stosiek. 1986. 'Detection of cytokeratin(s) in epithelium of human plexus choroideus by monoclonal antibodies', *Acta Histochem*, 78: 101-3.
- Kelley, M. W. 2006. 'Regulation of cell fate in the sensory epithelia of the inner ear', *Nat Rev Neurosci*, 7: 837-49.

- Khelef, N., M. Lecuit, H. Bierne, and P. Cossart. 2006. 'Species specificity of the *Listeria monocytogenes* InlB protein', *Cell Microbiol*, 8: 457-70.
- Kim, J. H., S. Jiang, C. A. Elwell, and J. N. Engel. 2011. 'Chlamydia trachomatis co-opts the FGF2 signaling pathway to enhance infection', *PLoS Pathog*, 7: e1002285.
- Kim, K. S. 2008. 'Mechanisms of microbial traversal of the blood-brain barrier', *Nat Rev Microbiol*, 6: 625-34.
- Kim, M., C. Fevre, M. Lavina, O. Disson, and M. Lecuit. 2021. 'Live Imaging Reveals *Listeria* Hijacking of E-Cadherin Recycling as It Crosses the Intestinal Barrier', *Curr Biol*, 31: 1037-47.e4.
- Kirchner, M., and D. E. Higgins. 2008. 'Inhibition of ROCK activity allows InlF-mediated invasion and increased virulence of *Listeria monocytogenes*', *Mol Microbiol*, 68: 749-67.
- Klein, R. S., C. Garber, and N. Howard. 2017. 'Infectious immunity in the central nervous system and brain function', *Nat Immunol*, 18: 132-41.
- Kobe, B., and A. V. Kajava. 2001. 'The leucine-rich repeat as a protein recognition motif', *Curr Opin Struct Biol*, 11: 725-32.
- Koch, A. W., S. Pokutta, A. Lustig, and J. Engel. 1997. 'Calcium binding and homoassociation of E-cadherin domains', *Biochemistry*, 36: 7697-705.
- Kooij, G., K. Kopplin, R. Blasig, M. Stuiver, N. Koning, G. Govers, S. M. van der Pol, B. van Het Hof, M. Gollasch, J. A. Drexhage, A. Reijkerkerk, I. C. Meij, R. Mebius, T. E. Willnow, D. Müller, I. E. Blasig, and H. E. de Vries. 2014. 'Disturbed function of the blood-cerebrospinal fluid barrier aggravates neuro-inflammation', *Acta Neuropathol*, 128: 267-77.
- Koopmans, M. M., M. C. Brouwer, M. Geldhoff, M. V. Seron, J. Houben, A. van der Ende, and D. van de Beek. 2014. 'Cerebrospinal fluid inflammatory markers in patients with *Listeria monocytogenes* meningitis', *BBA Clin*, 1: 44-51.
- Krachler, A. M., A. R. Woolery, and K. Orth. 2011. 'Manipulation of kinase signaling by bacterial pathogens', *J Cell Biol*, 195: 1083-92.
- Kratzer, I., A. Vasiljevic, C. Rey, M. Fevre-Montange, N. Saunders, N. Strazielle, and J. F. Gherzi-Egea. 2012. 'Complexity and developmental changes in the expression pattern of claudins at the blood-CSF barrier', *Histochem Cell Biol*, 138: 861-79.
- Krause-Gruszczynska, M., M. Boehm, M. Rohde, N. Tegtmeyer, S. Takahashi, L. Buday, O. A. Oyarzabal, and S. Backert. 2011. 'The signaling pathway of *Campylobacter jejuni*-induced Cdc42 activation: Role of fibronectin, integrin beta1, tyrosine kinases and guanine exchange factor Vav2', *Cell Commun Signal*, 9: 32.
- Krause, G., L. Winkler, C. Piehl, I. Blasig, J. Piontek, and S. L. Müller. 2009. 'Structure and function of extracellular claudin domains', *Ann N Y Acad Sci*, 1165: 34-43.

- Kutuzov, N., H. Flyvbjerg, and M. Lauritzen. 2018. 'Contributions of the glycocalyx, endothelium, and extravascular compartment to the blood-brain barrier', *Proc Natl Acad Sci U S A*, 115: E9429-e38.
- Kuwabara, H., Y. Kokai, T. Kojima, R. Takakuwa, M. Mori, and N. Sawada. 2001. 'Occludin regulates actin cytoskeleton in endothelial cells', *Cell Struct Funct*, 26: 109-16.
- Kwak, Y. K., E. Vikström, K. E. Magnusson, B. Vécsey-Semjén, P. Colque-Navarro, and R. Möllby. 2012. 'The Staphylococcus aureus alpha-toxin perturbs the barrier function in Caco-2 epithelial cell monolayers by altering junctional integrity', *Infect Immun*, 80: 1670-80.
- Lam, J. G. T., S. Vadia, S. Pathak-Sharma, E. McLaughlin, X. Zhang, J. Swanson, and S. Seveau. 2018. 'Host cell perforation by listeriolysin O (LLO) activates a Ca²⁺-dependent cPKC/Rac1/Arp2/3 signaling pathway that promotes Listeria monocytogenes internalization independently of membrane resealing', *Mol Biol Cell*, 29: 270-84.
- Lancaster, M. A., and J. A. Knoblich. 2014. 'Generation of cerebral organoids from human pluripotent stem cells', *Nat Protoc*, 9: 2329-40.
- Lauer, A. N., M. März, S. Meyer, M. Meurer, N. de Buhr, J. Borkowski, C. Weiß, H. Schroten, and C. Schwerk. 2019. 'Optimized cultivation of porcine choroid plexus epithelial cells, a blood-cerebrospinal fluid barrier model, for studying granulocyte transmigration', *Lab Invest*, 99: 1245-55.
- Lazarevic, I., and B. Engelhardt. 2016. 'Modeling immune functions of the mouse blood-cerebrospinal fluid barrier in vitro: primary rather than immortalized mouse choroid plexus epithelial cells are suited to study immune cell migration across this brain barrier', *Fluids Barriers CNS*, 13: 2.
- Lecuit, M., S. Dramsi, C. Gottardi, M. Fedor-Chaiken, B. Gumbiner, and P. Cossart. 1999. 'A single amino acid in E-cadherin responsible for host specificity towards the human pathogen Listeria monocytogenes', *Embo j*, 18: 3956-63.
- Lecuit, M., R. Hurme, J. Pizarro-Cerda, H. Ohayon, B. Geiger, and P. Cossart. 2000. 'A role for alpha-and beta-catenins in bacterial uptake', *Proc Natl Acad Sci U S A*, 97: 10008-13.
- Lecuit, M., D. M. Nelson, S. D. Smith, H. Khun, M. Huerre, M. C. Vacher-Lavenu, J. I. Gordon, and P. Cossart. 2004. 'Targeting and crossing of the human maternofetal barrier by Listeria monocytogenes: role of internalin interaction with trophoblast E-cadherin', *Proc Natl Acad Sci U S A*, 101: 6152-7.
- Lecuit, M., S. Vandormael-Pournin, J. Lefort, M. Huerre, P. Gounon, C. Dupuy, C. Babinet, and P. Cossart. 2001. 'A transgenic model for listeriosis: role of internalin in crossing the intestinal barrier', *Science*, 292: 1722-5.
- Lee, K., X. Zhong, S. Gu, A. M. Krueel, M. B. Dorner, K. Perry, A. Rummel, M. Dong, and R. Jin. 2014. 'Molecular basis for disruption of E-cadherin adhesion by botulinum neurotoxin A complex', *Science*, 344: 1405-10.

- Leemans, J. C., S. Florquin, M. Heikens, S. T. Pals, R. van der Neut, and T. Van Der Poll. 2003. 'CD44 is a macrophage binding site for Mycobacterium tuberculosis that mediates macrophage recruitment and protective immunity against tuberculosis', *J Clin Invest*, 111: 681-9.
- Lehtinen, M. K., C. S. Bjornsson, S. M. Dymecki, R. J. Gilbertson, D. M. Holtzman, and E. S. Monuki. 2013. 'The choroid plexus and cerebrospinal fluid: emerging roles in development, disease, and therapy', *J Neurosci*, 33: 17553-9.
- Lemmon, M. A., and J. Schlessinger. 2010. 'Cell signaling by receptor tyrosine kinases', *Cell*, 141: 1117-34.
- Lenz, L. L., S. Mohammadi, A. Geissler, and D. A. Portnoy. 2003. 'SecA2-dependent secretion of autolytic enzymes promotes Listeria monocytogenes pathogenesis', *Proc Natl Acad Sci U S A*, 100: 12432-7.
- Li, H., H. Xu, Y. Zhou, J. Zhang, C. Long, S. Li, S. Chen, J. M. Zhou, and F. Shao. 2007. 'The phosphothreonine lyase activity of a bacterial type III effector family', *Science*, 315: 1000-3.
- Li, L., M. Schmitt, A. Matzke-Ogi, P. Wadhvani, V. Orian-Rousseau, and P. A. Levkin. 2017. 'CD44v6-Peptide Functionalized Nanoparticles Selectively Bind to Metastatic Cancer Cells', *Adv Sci (Weinh)*, 4: 1600202.
- Liang, C. C., M. J. Sun, H. Y. Lei, S. H. Chen, C. K. Yu, C. C. Liu, J. R. Wang, and T. M. Yeh. 2004. 'Human endothelial cell activation and apoptosis induced by enterovirus 71 infection', *J Med Virol*, 74: 597-603.
- Liddel, S. A., S. Temple, K. Møllgård, R. Gehwolf, A. Wagner, H. Bauer, H. C. Bauer, T. N. Phoenix, K. M. Dziegielewska, and N. R. Saunders. 2012. 'Molecular characterisation of transport mechanisms at the developing mouse blood-CSF interface: a transcriptome approach', *PLoS One*, 7: e33554.
- Lindén, S. K., H. Bierne, C. Sabet, C. W. Png, T. H. Florin, M. A. McGuckin, and P. Cossart. 2008. 'Listeria monocytogenes internalins bind to the human intestinal mucin MUC2', *Arch Microbiol*, 190: 101-4.
- Lingnau, A., E. Domann, M. Hudel, M. Bock, T. Nichterlein, J. Wehland, and T. Chakraborty. 1995. 'Expression of the Listeria monocytogenes EGD inA and inB genes, whose products mediate bacterial entry into tissue culture cell lines, by PrfA-dependent and -independent mechanisms', *Infect Immun*, 63: 3896-903.
- Lippmann, E. S., A. Al-Ahmad, S. M. Azarin, S. P. Palecek, and E. V. Shusta. 2014. 'A retinoic acid-enhanced, multicellular human blood-brain barrier model derived from stem cell sources', *Sci Rep*, 4: 4160.
- Lowry, O. H., N. J. Rosebrough, A. L. Farr, and R. J. Randall. 1951. 'Protein measurement with the Folin phenol reagent', *J Biol Chem*, 193: 265-75.

- Lun, M. P., E. S. Monuki, and M. K. Lehtinen. 2015. 'Development and functions of the choroid plexus-cerebrospinal fluid system', *Nat Rev Neurosci*, 16: 445-57.
- Lyck, R., N. Ruderisch, A. G. Moll, O. Steiner, C. D. Cohen, B. Engelhardt, V. Makrides, and F. Verrey. 2009. 'Culture-induced changes in blood-brain barrier transcriptome: implications for amino-acid transporters in vivo', *J Cereb Blood Flow Metab*, 29: 1491-502.
- Maiden, M. C., J. A. Bygraves, E. Feil, G. Morelli, J. E. Russell, R. Urwin, Q. Zhang, J. Zhou, K. Zurth, D. A. Caugant, I. M. Feavers, M. Achtman, and B. G. Spratt. 1998. 'Multilocus sequence typing: a portable approach to the identification of clones within populations of pathogenic microorganisms', *Proc Natl Acad Sci U S A*, 95: 3140-5.
- Mak, T. N., and H. Brüggenmann. 2016. 'Vimentin in Bacterial Infections', *Cells*, 5.
- Marino, M., M. Banerjee, R. Jonquière, P. Cossart, and P. Ghosh. 2002. 'GW domains of the *Listeria monocytogenes* invasion protein InlB are SH3-like and mediate binding to host ligands', *Embo j*, 21: 5623-34.
- Marino, M., L. Braun, P. Cossart, and P. Ghosh. 1999. 'Structure of the InlB leucine-rich repeats, a domain that triggers host cell invasion by the bacterial pathogen *L. monocytogenes*', *Mol Cell*, 4: 1063-72.
- Martìn-Padura, I., S. Lostaglio, M. Schneemann, L. Williams, M. Romano, P. Fruscella, C. Panzeri, A. Stoppacciaro, L. Ruco, A. Villa, D. Simmons, and E. Dejana. 1998. 'Junctional adhesion molecule, a novel member of the immunoglobulin superfamily that distributes at intercellular junctions and modulates monocyte transmigration', *J Cell Biol*, 142: 117-27.
- Matzke-Ogi, A., K. Jannasch, M. Shatirishvili, B. Fuchs, S. Chiblak, J. Morton, B. Tawk, T. Lindner, O. Sansom, F. Alves, A. Warth, C. Schwager, W. Mier, J. Kleeff, H. Ponta, A. Abdollahi, and V. Orian-Rousseau. 2016. 'Inhibition of Tumor Growth and Metastasis in Pancreatic Cancer Models by Interference With CD44v6 Signaling', *Gastroenterology*, 150: 513-25.e10.
- Matzke, A., P. Herrlich, H. Ponta, and V. Orian-Rousseau. 2005. 'A five-amino-acid peptide blocks Met- and Ron-dependent cell migration', *Cancer Res*, 65: 6105-10.
- Maury, M. M., Y. H. Tsai, C. Charlier, M. Touchon, V. Chenal-Francois, A. Leclercq, A. Criscuolo, C. Gaultier, S. Roussel, A. Brisabois, O. Disson, E. P. C. Rocha, S. Brisse, and M. Lecuit. 2016. 'Uncovering *Listeria monocytogenes* hypervirulence by harnessing its biodiversity', *Nat Genet*, 48: 308-13.
- Mellman, I., and W. J. Nelson. 2008. 'Coordinated protein sorting, targeting and distribution in polarized cells', *Nat Rev Mol Cell Biol*, 9: 833-45.
- Meng, W., and M. Takeichi. 2009. 'Adherens junction: molecular architecture and regulation', *Cold Spring Harb Perspect Biol*, 1: a002899.

Mengaud, J., H. Ohayon, P. Gounon, R. M. Mege, and P. Cossart. 1996. 'E-cadherin is the receptor for internalin, a surface protein required for entry of *L. monocytogenes* into epithelial cells', *Cell*, 84: 923-32.

Miaczynska, M. 2013. 'Effects of membrane trafficking on signaling by receptor tyrosine kinases', *Cold Spring Harb Perspect Biol*, 5: a009035.

Miettinen, M., R. Clark, and I. Virtanen. 1986. 'Intermediate filament proteins in choroid plexus and ependyma and their tumors', *Am J Pathol*, 123: 231-40.

Milohanic, E., R. Jonquière, P. Cossart, P. Berche, and J. L. Gaillard. 2001. 'The autolysin Ami contributes to the adhesion of *Listeria monocytogenes* to eukaryotic cells via its cell wall anchor', *Mol Microbiol*, 39: 1212-24.

Mineta, K., Y. Yamamoto, Y. Yamazaki, H. Tanaka, Y. Tada, K. Saito, A. Tamura, M. Igarashi, T. Endo, K. Takeuchi, and S. Tsukita. 2011. 'Predicted expansion of the claudin multigene family', *FEBS Lett*, 585: 606-12.

Moffat, F. L., Jr., T. Han, Z. M. Li, M. D. Peck, R. E. Falk, P. B. Spalding, W. Jy, Y. S. Ahn, A. J. Chu, and L. Y. Bourguignon. 1996. 'Involvement of CD44 and the cytoskeletal linker protein ankyrin in human neutrophil bacterial phagocytosis', *J Cell Physiol*, 168: 638-47.

Möller, K., E. Becker, and J. H. Hegemann. 2013. 'The *Chlamydia pneumoniae* invasin protein Pmp21 recruits the EGF receptor for host cell entry', *PLoS Pathog*, 9: e1003325.

Monnot, A. D., and W. Zheng. 2013. 'Culture of choroid plexus epithelial cells and in vitro model of blood-CSF barrier', *Methods Mol Biol*, 945: 13-29.

Montanari, E., C. Di Meo, A. Oates, T. Coviello, and P. Matricardi. 2018. 'Pursuing Intracellular Pathogens with Hyaluronan. From a 'Pro-Infection' Polymer to a Biomaterial for 'Trojan Horse' Systems', *Molecules*, 23.

Montesano, R., M. S. Pepper, U. Möhle-Steinlein, W. Risau, E. F. Wagner, and L. Orci. 1990. 'Increased proteolytic activity is responsible for the aberrant morphogenetic behavior of endothelial cells expressing the middle T oncogene', *Cell*, 62: 435-45.

Mounier, J., T. Vasselon, R. Hellio, M. Lesourd, and P. J. Sansonetti. 1992. '*Shigella flexneri* enters human colonic Caco-2 epithelial cells through the basolateral pole', *Infect Immun*, 60: 237-48.

Mühlebach, M. D., M. Mateo, P. L. Sinn, S. Prüfer, K. M. Uhlig, V. H. Leonard, C. K. Navaratnarajah, M. Frenzke, X. X. Wong, B. Sawatsky, S. Ramachandran, P. B. McCray, Jr., K. Cichutek, V. von Messling, M. Lopez, and R. Cattaneo. 2011. 'Adherens junction protein nectin-4 is the epithelial receptor for measles virus', *Nature*, 480: 530-3.

Muoio, V., P. B. Persson, and M. M. Sendeski. 2014. 'The neurovascular unit - concept review', *Acta Physiol (Oxf)*, 210: 790-8.

- Murakami, T., E. A. Felinski, and D. A. Antonetti. 2009. 'Occludin phosphorylation and ubiquitination regulate tight junction trafficking and vascular endothelial growth factor-induced permeability', *J Biol Chem*, 284: 21036-46.
- Murata-Kamiya, N., Y. Kurashima, Y. Teishikata, Y. Yamahashi, Y. Saito, H. Higashi, H. Aburatani, T. Akiyama, R. M. Peek, Jr., T. Azuma, and M. Hatakeyama. 2007. 'Helicobacter pylori CagA interacts with E-cadherin and deregulates the beta-catenin signal that promotes intestinal transdifferentiation in gastric epithelial cells', *Oncogene*, 26: 4617-26.
- Muto, S., M. Hata, J. Taniguchi, S. Tsuruoka, K. Moriwaki, M. Saitou, K. Furuse, H. Sasaki, A. Fujimura, M. Imai, E. Kusano, S. Tsukita, and M. Furuse. 2010. 'Claudin-2-deficient mice are defective in the leaky and cation-selective paracellular permeability properties of renal proximal tubules', *Proc Natl Acad Sci U S A*, 107: 8011-6.
- Naik, P., and L. Cucullo. 2012. 'In vitro blood-brain barrier models: current and perspective technologies', *J Pharm Sci*, 101: 1337-54.
- Nakagawa, S., M. A. Deli, H. Kawaguchi, T. Shimizudani, T. Shimonono, A. Kittel, K. Tanaka, and M. Niwa. 2009. 'A new blood-brain barrier model using primary rat brain endothelial cells, pericytes and astrocytes', *Neurochem Int*, 54: 253-63.
- Naor, D., S. Nedvetzki, I. Golan, L. Melnik, and Y. Faitelson. 2002. 'CD44 in cancer', *Crit Rev Clin Lab Sci*, 39: 527-79.
- Narita, K., T. Kawate, N. Kakinuma, and S. Takeda. 2010. 'Multiple primary cilia modulate the fluid transcytosis in choroid plexus epithelium', *Traffic*, 11: 287-301.
- Niemann, H. H., V. Jäger, P. J. Butler, J. van den Heuvel, S. Schmidt, D. Ferraris, E. Gherardi, and D. W. Heinz. 2007. 'Structure of the human receptor tyrosine kinase met in complex with the Listeria invasion protein InlB', *Cell*, 130: 235-46.
- Nieuwdorp, M., M. C. Meuwese, H. Vink, J. B. Hoekstra, J. J. Kastelein, and E. S. Stroes. 2005. 'The endothelial glycocalyx: a potential barrier between health and vascular disease', *Curr Opin Lipidol*, 16: 507-11.
- Nitta, T., M. Hata, S. Gotoh, Y. Seo, H. Sasaki, N. Hashimoto, M. Furuse, and S. Tsukita. 2003. 'Size-selective loosening of the blood-brain barrier in claudin-5-deficient mice', *J Cell Biol*, 161: 653-60.
- Noma, K., N. Oyama, and J. K. Liao. 2006. 'Physiological role of ROCKs in the cardiovascular system', *Am J Physiol Cell Physiol*, 290: C661-8.
- North, R. J. 1971. 'The action of cortisone acetate on cell-mediated immunity to infection. Suppression of host cell proliferation and alteration of cellular composition of infective foci', *J Exp Med*, 134: 1485-500.
- Nzou, G., R. T. Wicks, E. E. Wicks, S. A. Seale, C. H. Sane, A. Chen, S. V. Murphy, J. D. Jackson, and A. J. Atala. 2018. 'Human Cortex Spheroid with a Functional Blood Brain Barrier for High-Throughput Neurotoxicity Screening and Disease Modeling', *Sci Rep*, 8: 7413.

- Oddo, A., B. Peng, Z. Tong, Y. Wei, W. Y. Tong, H. Thissen, and N. H. Voelcker. 2019. 'Advances in Microfluidic Blood-Brain Barrier (BBB) Models', *Trends Biotechnol*, 37: 1295-314.
- Oevermann, A., A. Zurbriggen, and M. Vandeveld. 2010. 'Rhombencephalitis Caused by *Listeria monocytogenes* in Humans and Ruminants: A Zoonosis on the Rise?', *Interdiscip Perspect Infect Dis*, 2010: 632513.
- Omidi, Y., L. Campbell, J. Barar, D. Connell, S. Akhtar, and M. Gumbleton. 2003. 'Evaluation of the immortalised mouse brain capillary endothelial cell line, b.End3, as an in vitro blood-brain barrier model for drug uptake and transport studies', *Brain Res*, 990: 95-112.
- Opitz, B., A. Püschel, W. Beermann, A. C. Hocke, S. Förster, B. Schmeck, V. van Laak, T. Chakraborty, N. Suttorp, and S. Hippenstiel. 2006. '*Listeria monocytogenes* activated p38 MAPK and induced IL-8 secretion in a nucleotide-binding oligomerization domain 1-dependent manner in endothelial cells', *J Immunol*, 176: 484-90.
- Orian-Rousseau, V., L. Chen, J. P. Sleeman, P. Herrlich, and H. Ponta. 2002. 'CD44 is required for two consecutive steps in HGF/c-Met signaling', *Genes Dev*, 16: 3074-86.
- Orian-Rousseau, V., H. Morrison, A. Matzke, T. Kastilan, G. Pace, P. Herrlich, and H. Ponta. 2007. 'Hepatocyte growth factor-induced Ras activation requires ERM proteins linked to both CD44v6 and F-actin', *Mol Biol Cell*, 18: 76-83.
- Orsi, R. H., H. C. den Bakker, and M. Wiedmann. 2011. '*Listeria monocytogenes* lineages: Genomics, evolution, ecology, and phenotypic characteristics', *Int J Med Microbiol*, 301: 79-96.
- Osborne, S. E., and J. H. Brumell. 2017. 'Listeriolysin O: from bazooka to Swiss army knife', *Philos Trans R Soc Lond B Biol Sci*, 372.
- Overduin, M., T. S. Harvey, S. Bagby, K. I. Tong, P. Yau, M. Takeichi, and M. Ikura. 1995. 'Solution structure of the epithelial cadherin domain responsible for selective cell adhesion', *Science*, 267: 386-9.
- Ozaki-Kuroda, K., H. Nakanishi, H. Ohta, H. Tanaka, H. Kurihara, S. Mueller, K. Irie, W. Ikeda, T. Sakai, E. Wimmer, Y. Nishimune, and Y. Takai. 2002. 'Nectin couples cell-cell adhesion and the actin scaffold at heterotypic testicular junctions', *Curr Biol*, 12: 1145-50.
- Padden, M., S. Leech, B. Craig, J. Kirk, B. Brankin, and S. McQuaid. 2007. 'Differences in expression of junctional adhesion molecule-A and beta-catenin in multiple sclerosis brain tissue: increasing evidence for the role of tight junction pathology', *Acta Neuropathol*, 113: 177-86.
- Pägelow, D., C. Chhatbar, A. Beineke, X. Liu, A. Nerlich, K. van Vorst, M. Rohde, U. Kalinke, R. Förster, S. Halle, P. Valentin-Weigand, M. W. Hornef, and M. Fulde. 2018. 'The olfactory epithelium as a port of entry in neonatal neurolisteriosis', *Nat Commun*, 9: 4269.

- Parida, S. K., E. Domann, M. Rohde, S. Müller, A. Darji, T. Hain, J. Wehland, and T. Chakraborty. 1998. 'Internalin B is essential for adhesion and mediates the invasion of *Listeria monocytogenes* into human endothelial cells', *Mol Microbiol*, 28: 81-93.
- Parra, M. C., F. Baquero, and J. C. Perez-Diaz. 2007. 'The role of apoptosis in *Listeria monocytogenes* neural infection: listeriolysin O interaction with neuroblastoma Neuro-2a cells', *Infect Genet Evol*, 8: 59-67.
- Pasche, B., S. Kalaydjiev, T. J. Franz, E. Kremmer, V. Gailus-Durner, H. Fuchs, M. Hrabé de Angelis, A. Lengeling, and D. H. Busch. 2005. 'Sex-dependent susceptibility to *Listeria monocytogenes* infection is mediated by differential interleukin-10 production', *Infect Immun*, 73: 5952-60.
- Patteson, A. E., A. Vahabikashi, R. D. Goldman, and P. A. Janmey. 2020. 'Mechanical and Non-Mechanical Functions of Filamentous and Non-Filamentous Vimentin', *Bioessays*, 42: e2000078.
- Pearson, G., F. Robinson, T. Beers Gibson, B. E. Xu, M. Karandikar, K. Berman, and M. H. Cobb. 2001. 'Mitogen-activated protein (MAP) kinase pathways: regulation and physiological functions', *Endocr Rev*, 22: 153-83.
- Pentecost, M., J. Kumaran, P. Ghosh, and M. R. Amieva. 2010. '*Listeria monocytogenes* internalin B activates junctional endocytosis to accelerate intestinal invasion', *PLoS Pathog*, 6: e1000900.
- Pentecost, M., G. Otto, J. A. Theriot, and M. R. Amieva. 2006. '*Listeria monocytogenes* invades the epithelial junctions at sites of cell extrusion', *PLoS Pathog*, 2: e3.
- Petersen, N., L. Torz, K. H. R. Jensen, G. M. Hjortø, K. Spiess, and M. M. Rosenkilde. 2020. 'Three-Dimensional Explant Platform for Studies on Choroid Plexus Epithelium', *Front Cell Neurosci*, 14: 108.
- Phelps, C. C., S. Vadia, E. Arnett, Y. Tan, X. Zhang, S. Pathak-Sharma, M. A. Gavrillin, and S. Seveau. 2018. 'Relative Roles of Listeriolysin O, InlA, and InlB in *Listeria monocytogenes* Uptake by Host Cells', *Infect Immun*, 86.
- Piffaretti, J. C., H. Kressebuch, M. Aeschbacher, J. Bille, E. Bannerman, J. M. Musser, R. K. Selander, and J. Rocourt. 1989. 'Genetic characterization of clones of the bacterium *Listeria monocytogenes* causing epidemic disease', *Proc Natl Acad Sci U S A*, 86: 3818-22.
- Pilgrim, S., A. Kolb-Mäurer, I. Gentschev, W. Goebel, and M. Kuhn. 2003. 'Deletion of the gene encoding p60 in *Listeria monocytogenes* leads to abnormal cell division and loss of actin-based motility', *Infect Immun*, 71: 3473-84.
- Pizarro-Cerdá, J., A. Kühbacher, and P. Cossart. 2012. 'Entry of *Listeria monocytogenes* in mammalian epithelial cells: an updated view', *Cold Spring Harb Perspect Med*, 2.

- Pokutta, S., K. Herrenknecht, R. Kemler, and J. Engel. 1994. 'Conformational changes of the recombinant extracellular domain of E-cadherin upon calcium binding', *Eur J Biochem*, 223: 1019-26.
- Ponta, H., L. Sherman, and P. A. Herrlich. 2003. 'CD44: from adhesion molecules to signalling regulators', *Nat Rev Mol Cell Biol*, 4: 33-45.
- Popowska, M. 2004. 'Analysis of the peptidoglycan hydrolases of *Listeria monocytogenes*: multiple enzymes with multiple functions', *Pol J Microbiol*, 53 Suppl: 29-34.
- Popowska, Magdalena, Agata Krawczyk-Balska, Rafał Ostrowski, and Mickaël Desvaux. 2017. 'InlL from *Listeria monocytogenes* Is Involved in Biofilm Formation and Adhesion to Mucin', *Frontiers in Microbiology*, 8.
- Pratakpiriya, W., A. P. Ping Teh, A. Radtanakantikanon, N. Pirarat, N. Thi Lan, M. Takeda, S. Techangamsuwan, and R. Yamaguchi. 2017. 'Expression of canine distemper virus receptor nectin-4 in the central nervous system of dogs', *Sci Rep*, 7: 349.
- Prats, N., V. Briones, M. M. Blanco, J. Altimira, J. A. Ramos, L. Domínguez, and A. Marco. 1992. 'Choroiditis and meningitis in experimental murine infection with *Listeria monocytogenes*', *Eur J Clin Microbiol Infect Dis*, 11: 744-7.
- Precht, C., P. Vermathen, D. Henke, A. Staudacher, J. Lauper, T. Seuberlich, A. Oevermann, and D. Schweizer-Gorgas. 2020. 'Correlative Magnetic Resonance Imaging and Histopathology in Small Ruminant *Listeria* Rhombencephalitis', *Front Neurol*, 11: 518697.
- Puthiyakunnon, S., X. He, S. Boddu, S. H. Huang, and H. Cao. 2017. 'C-Met Inhibitors are Potential Novel Therapeutic Agents Against *Listeria monocytogenes* Infection Through Blocking the Bacteria Entry into Nonphagocytic Cells', *Curr Top Med Chem*, 17: 278-89.
- Radaelli, E., S. F. Santagostino, R. S. Sellers, and C. F. Brayton. 2018. 'Immune Relevant and Immune Deficient Mice: Options and Opportunities in Translational Research', *Ilar j*, 59: 211-46.
- Radoshevich, L., and P. Cossart. 2018. '*Listeria monocytogenes*: towards a complete picture of its physiology and pathogenesis', *Nat Rev Microbiol*, 16: 32-46.
- Ragon, M., T. Wirth, F. Hollandt, R. Lavenir, M. Lecuit, A. Le Monnier, and S. Brisse. 2008. 'A new perspective on *Listeria monocytogenes* evolution', *PLoS Pathog*, 4: e1000146.
- Rajabian, T., B. Gavicherla, M. Heisig, S. Müller-Altrock, W. Goebel, S. D. Gray-Owen, and K. Ireton. 2009. 'The bacterial virulence factor InlC perturbs apical cell junctions and promotes cell-to-cell spread of *Listeria*', *Nat Cell Biol*, 11: 1212-8.
- Raleigh, D. R., A. M. Marchiando, Y. Zhang, L. Shen, H. Sasaki, Y. Wang, M. Long, and J. R. Turner. 2010. 'Tight junction-associated MARVEL proteins marveld3, tricellulin, and occludin have distinct but overlapping functions', *Mol Biol Cell*, 21: 1200-13.

- Raman, M., W. Chen, and M. H. Cobb. 2007. 'Differential regulation and properties of MAPKs', *Oncogene*, 26: 3100-12.
- Redzic, Z. B. 2013. 'Studies on the human choroid plexus in vitro', *Fluids Barriers CNS*, 10: 10.
- Redzic, Z. B., A. J. Isakovic, S. T. Misirlic Dencic, D. Popadic, and M. B. Segal. 2006. 'Uneven distribution of nucleoside transporters and intracellular enzymatic degradation prevent transport of intact [14C] adenosine across the sheep choroid plexus epithelium as a monolayer in primary culture', *Cerebrospinal Fluid Res*, 3: 4.
- Riento, K., and A. J. Ridley. 2003. 'ROCKs: multifunctional kinases in cell behaviour', *Nat Rev Mol Cell Biol*, 4: 446-56.
- Rikitake, Y., K. Mandai, and Y. Takai. 2012. 'The role of nectins in different types of cell-cell adhesion', *J Cell Sci*, 125: 3713-22.
- Ronholm, J., L. Wang, I. Hayashi, M. Sugai, Z. Zhang, X. Cao, and M. Lin. 2012. 'The *Listeria monocytogenes* serotype 4b autolysin IspC has N-acetylglucosaminidase activity', *Glycobiology*, 22: 1311-20.
- Rubinstein, M. R., X. Wang, W. Liu, Y. Hao, G. Cai, and Y. W. Han. 2013. '*Fusobacterium nucleatum* promotes colorectal carcinogenesis by modulating E-cadherin/ β -catenin signaling via its FadA adhesin', *Cell Host Microbe*, 14: 195-206.
- Ruck, T., S. Bittner, and S. G. Meuth. 2015. 'Blood-brain barrier modeling: challenges and perspectives', *Neural Regen Res*, 10: 889-91.
- Rupp, S., M. Bärtschi, J. Frey, and A. Oevermann. 2017. 'Hyperinvasiveness and increased intercellular spread of *Listeria monocytogenes* sequence type 1 are independent of listeriolysin S, internalin F and internalin J1', *J Med Microbiol*, 66: 1053-62.
- Rush, S., G. Khan, A. Bamisaiye, P. Bidwell, H. A. Leaver, and M. T. Rizzo. 2007. 'c-jun amino-terminal kinase and mitogen activated protein kinase 1/2 mediate hepatocyte growth factor-induced migration of brain endothelial cells', *Exp Cell Res*, 313: 121-32.
- Sabet, C., M. Lecuit, D. Cabanes, P. Cossart, and H. Bierne. 2005. 'LPXTG protein InlJ, a newly identified internalin involved in *Listeria monocytogenes* virulence', *Infect Immun*, 73: 6912-22.
- Sabet, C., A. Toledo-Arana, N. Personnic, M. Lecuit, S. Dubrac, O. Poupel, E. Gouin, M. A. Nahori, P. Cossart, and H. Bierne. 2008. 'The *Listeria monocytogenes* virulence factor InlJ is specifically expressed in vivo and behaves as an adhesin', *Infect Immun*, 76: 1368-78.
- Saitou, M., K. Fujimoto, Y. Doi, M. Itoh, T. Fujimoto, M. Furuse, H. Takano, T. Noda, and S. Tsukita. 1998. 'Occludin-deficient embryonic stem cells can differentiate into polarized epithelial cells bearing tight junctions', *J Cell Biol*, 141: 397-408.

- Saitou, M., M. Furuse, H. Sasaki, J. D. Schulzke, M. Fromm, H. Takano, T. Noda, and S. Tsukita. 2000. 'Complex phenotype of mice lacking occludin, a component of tight junction strands', *Mol Biol Cell*, 11: 4131-42.
- Satelli, A., and S. Li. 2011. 'Vimentin in cancer and its potential as a molecular target for cancer therapy', *Cell Mol Life Sci*, 68: 3033-46.
- Schlech, W. F. 2019. 'Epidemiology and Clinical Manifestations of *Listeria monocytogenes* Infection', *Microbiol Spectr*, 7.
- Schlech, W. F., 3rd, P. M. Lavigne, R. A. Bortolussi, A. C. Allen, E. V. Haldane, A. J. Wort, A. W. Hightower, S. E. Johnson, S. H. King, E. S. Nicholls, and C. V. Broome. 1983. 'Epidemic listeriosis--evidence for transmission by food', *N Engl J Med*, 308: 203-6.
- Schneider, H., C. E. Weber, J. Schoeller, U. Steinmann, J. Borkowski, H. Ishikawa, P. Findeisen, O. Adams, R. Doerries, C. Schwerk, H. Schroten, and T. Tenenbaum. 2012. 'Chemotaxis of T-cells after infection of human choroid plexus papilloma cells with Echovirus 30 in an in vitro model of the blood-cerebrospinal fluid barrier', *Virus Res*, 170: 66-74.
- Schrager, H. M., S. Albertí, C. Cywes, G. J. Dougherty, and M. R. Wessels. 1998. 'Hyaluronic acid capsule modulates M protein-mediated adherence and acts as a ligand for attachment of group A *Streptococcus* to CD44 on human keratinocytes', *J Clin Invest*, 101: 1708-16.
- Schuerch, D. W., E. M. Wilson-Kubalek, and R. K. Tweten. 2005. 'Molecular basis of listeriolysin O pH dependence', *Proc Natl Acad Sci U S A*, 102: 12537-42.
- Schwerk, C., R. Adam, J. Borkowski, H. Schneider, M. Klenk, S. Zink, N. Quednau, N. Schmidt, C. Stump, A. Sagar, B. Spellerberg, T. Tenenbaum, D. Koczan, L. Klein-Hitpass, and H. Schroten. 2011. 'In vitro transcriptome analysis of porcine choroid plexus epithelial cells in response to *Streptococcus suis*: release of pro-inflammatory cytokines and chemokines', *Microbes Infect*, 13: 953-62.
- Schwerk, C., T. Papandreou, D. Schuhmann, L. Nickol, J. Borkowski, U. Steinmann, N. Quednau, C. Stump, C. Weiss, J. Berger, H. Wolburg, H. Claus, U. Vogel, H. Ishikawa, T. Tenenbaum, and H. Schroten. 2012. 'Polar invasion and translocation of *Neisseria meningitidis* and *Streptococcus suis* in a novel human model of the blood-cerebrospinal fluid barrier', *PLoS One*, 7: e30069.
- Schwerk, C., T. Tenenbaum, K. S. Kim, and H. Schroten. 2015. 'The choroid plexus-a multi-role player during infectious diseases of the CNS', *Front Cell Neurosci*, 9: 80.
- Screaton, G. R., M. V. Bell, D. G. Jackson, F. B. Cornelis, U. Gerth, and J. I. Bell. 1992. 'Genomic structure of DNA encoding the lymphocyte homing receptor CD44 reveals at least 12 alternatively spliced exons', *Proc Natl Acad Sci U S A*, 89: 12160-4.
- Seveau, S., H. Bierne, S. Giroux, M. C. Prévost, and P. Cossart. 2004. 'Role of lipid rafts in E-cadherin-- and HGF-R/Met--mediated entry of *Listeria monocytogenes* into host cells', *J Cell Biol*, 166: 743-53.

- Shen, Y., M. Naujokas, M. Park, and K. Ireton. 2000. 'InIB-dependent internalization of *Listeria* is mediated by the Met receptor tyrosine kinase', *Cell*, 103: 501-10.
- Shimomoto, T., M. Yoshida, M. Takahashi, F. Uematsu, A. Maekawa, and D. Nakae. 2004. 'A case report of a choroid plexus carcinoma spontaneously occurring in the right lateral ventricle of a 14-week-old, female Donryu rat', *Toxicol Pathol*, 32: 264-8.
- Shockman, G. D., and J. V. Höltje. 1994. 'Chapter 7 Microbial peptidoglycan (murein) hydrolases.' in J. M. Ghuysen and R. Hakenbeck (eds.), *New Comprehensive Biochemistry* (Elsevier).
- Shukla, D., P. M. Scanlan, V. Tiwari, V. Sheth, C. Clement, G. Guzman-Hartman, T. S. Dermody, and T. Valyi-Nagy. 2006. 'Expression of nectin-1 in normal and herpes simplex virus type 1-infected murine brain', *Appl Immunohistochem Mol Morphol*, 14: 341-7.
- Skoudy, A., J. Mounier, A. Aruffo, H. Ohayon, P. Gounon, P. Sansonetti, and G. Tran Van Nhieu. 2000. 'CD44 binds to the *Shigella* IpaB protein and participates in bacterial invasion of epithelial cells', *Cell Microbiol*, 2: 19-33.
- Sladojevic, N., S. M. Stamatovic, A. M. Johnson, J. Choi, A. Hu, S. Dithmer, I. E. Blasig, R. F. Keep, and A. V. Andjelkovic. 2019. 'Claudin-1-Dependent Destabilization of the Blood-Brain Barrier in Chronic Stroke', *J Neurosci*, 39: 743-57.
- Sokolova, O., N. Heppel, R. Jägerhuber, K. S. Kim, M. Frosch, M. Eigenthaler, and A. Schubert-Unkmeir. 2004. 'Interaction of *Neisseria meningitidis* with human brain microvascular endothelial cells: role of MAP- and tyrosine kinases in invasion and inflammatory cytokine release', *Cell Microbiol*, 6: 1153-66.
- Soong, G., F. J. Martin, J. Chun, T. S. Cohen, D. S. Ahn, and A. Prince. 2011. 'Staphylococcus aureus protein A mediates invasion across airway epithelial cells through activation of RhoA GTPase signaling and proteolytic activity', *J Biol Chem*, 286: 35891-98.
- Sousa, S., D. Cabanes, L. Bougnères, M. Lecuit, P. Sansonetti, G. Tran-Van-Nhieu, and P. Cossart. 2007. 'Src, cortactin and Arp2/3 complex are required for E-cadherin-mediated internalization of *Listeria* into cells', *Cell Microbiol*, 9: 2629-43.
- Srinivasan, B., A. R. Kolli, M. B. Esch, H. E. Abaci, M. L. Shuler, and J. J. Hickman. 2015. 'TEER measurement techniques for in vitro barrier model systems', *J Lab Autom*, 20: 107-26.
- Stavru, F., F. Bouillaud, A. Sartori, D. Ricquier, and P. Cossart. 2011. '*Listeria monocytogenes* transiently alters mitochondrial dynamics during infection', *Proc Natl Acad Sci U S A*, 108: 3612-7.
- Steed, E., N. T. Rodrigues, M. S. Balda, and K. Matter. 2009. 'Identification of MarvelD3 as a tight junction-associated transmembrane protein of the occludin family', *BMC Cell Biol*, 10: 95.
- Steinemann, A., I. Galm, S. Chip, C. Nitsch, and I. P. Maly. 2016. 'Claudin-1, -2 and -3 Are Selectively Expressed in the Epithelia of the Choroid Plexus of the Mouse from Early

Development and into Adulthood While Claudin-5 is Restricted to Endothelial Cells', *Front Neuroanat*, 10: 16.

Steinmann, U., J. Borkowski, H. Wolburg, B. Schröppel, P. Findeisen, C. Weiss, H. Ishikawa, C. Schwerk, H. Schrotten, and T. Tenenbaum. 2013. 'Transmigration of polymorphnuclear neutrophils and monocytes through the human blood-cerebrospinal fluid barrier after bacterial infection in vitro', *J Neuroinflammation*, 10: 31.

Stiffler, M. A., J. R. Chen, V. P. Grantcharova, Y. Lei, D. Fuchs, J. E. Allen, L. A. Zaslavskaja, and G. MacBeath. 2007. 'PDZ domain binding selectivity is optimized across the mouse proteome', *Science*, 317: 364-9.

Stins, M. F., J. Badger, and K. S. Kim. 2001. 'Bacterial invasion and transcytosis in transfected human brain microvascular endothelial cells', *Microb Pathog*, 30: 19-28.

Stone, N. L., T. J. England, and S. E. O'Sullivan. 2019. 'A Novel Transwell Blood Brain Barrier Model Using Primary Human Cells', *Front Cell Neurosci*, 13: 230.

Strauss, R., B. Heymer, and H. Hof. 1985. 'Effects of cyclosporin A on experimental infection with *Listeria monocytogenes*', *Clin Exp Immunol*, 62: 491-8.

Subbarayal, P., K. Karunakaran, A. C. Winkler, M. Rother, E. Gonzalez, T. F. Meyer, and T. Rudel. 2015. 'EphrinA2 receptor (EphA2) is an invasion and intracellular signaling receptor for *Chlamydia trachomatis*', *PLoS Pathog*, 11: e1004846.

Swanson, K. V., J. M. Griffiss, V. L. Edwards, D. C. Stein, and W. Song. 2011. '*Neisseria gonorrhoeae*-induced transactivation of EGFR enhances gonococcal invasion', *Cell Microbiol*, 13: 1078-90.

Tachibana, K., H. Nakanishi, K. Mandai, K. Ozaki, W. Ikeda, Y. Yamamoto, A. Nagafuchi, S. Tsukita, and Y. Takai. 2000. 'Two cell adhesion molecules, nectin and cadherin, interact through their cytoplasmic domain-associated proteins', *J Cell Biol*, 150: 1161-76.

Taddei, A., C. Giampietro, A. Conti, F. Orsenigo, F. Breviario, V. Pirazzoli, M. Potente, C. Daly, S. Dimmeler, and E. Dejana. 2008. 'Endothelial adherens junctions control tight junctions by VE-cadherin-mediated upregulation of claudin-5', *Nat Cell Biol*, 10: 923-34.

Takai, Y., W. Ikeda, H. Ogita, and Y. Rikitake. 2008. 'The immunoglobulin-like cell adhesion molecule nectin and its associated protein afadin', *Annu Rev Cell Dev Biol*, 24: 309-42.

Takai, Y., K. Irie, K. Shimizu, T. Sakisaka, and W. Ikeda. 2003. 'Nectins and nectin-like molecules: roles in cell adhesion, migration, and polarization', *Cancer Sci*, 94: 655-67.

Takeichi, M. 1988. 'The cadherins: cell-cell adhesion molecules controlling animal morphogenesis', *Development*, 102: 639-55.

Tang, P., I. Rosenshine, P. Cossart, and B. B. Finlay. 1996. '*Listeriolysin O* activates mitogen-activated protein kinase in eucaryotic cells', *Infect Immun*, 64: 2359-61.

Tang, P., I. Rosenshine, and B. B. Finlay. 1994. 'Listeria monocytogenes, an invasive bacterium, stimulates MAP kinase upon attachment to epithelial cells', *Mol Biol Cell*, 5: 455-64.

Tapinos, N., M. Ohnishi, and A. Rambukkana. 2006. 'ErbB2 receptor tyrosine kinase signaling mediates early demyelination induced by leprosy bacilli', *Nat Med*, 12: 961-6.

Tenenbaum, T., T. Papandreou, D. Gellrich, U. Friedrichs, A. Seibt, R. Adam, C. Wewer, H. J. Galla, C. Schwerk, and H. Schroten. 2009. 'Polar bacterial invasion and translocation of Streptococcus suis across the blood-cerebrospinal fluid barrier in vitro', *Cell Microbiol*, 11: 323-36.

Tenenbaum, T., B. Spellerberg, R. Adam, M. Vogel, K. S. Kim, and H. Schroten. 2007. 'Streptococcus agalactiae invasion of human brain microvascular endothelial cells is promoted by the laminin-binding protein Lmb', *Microbes Infect*, 9: 714-20.

Teo, C. S., and J. J. Chu. 2014. 'Cellular vimentin regulates construction of dengue virus replication complexes through interaction with NS4A protein', *J Virol*, 88: 1897-913.

Thomsen, L. B., A. Burkhart, and T. Moos. 2015. 'A Triple Culture Model of the Blood-Brain Barrier Using Porcine Brain Endothelial cells, Astrocytes and Pericytes', *PLoS One*, 10: e0134765.

Tietz, S., and B. Engelhardt. 2015. 'Brain barriers: Crosstalk between complex tight junctions and adherens junctions', *J Cell Biol*, 209: 493-506.

Tietz, S., T. Périnat, G. Greene, G. Enzmann, U. Deutsch, R. Adams, B. Imhof, M. Aurrand-Lions, and B. Engelhardt. 2018. 'Lack of junctional adhesion molecule (JAM)-B ameliorates experimental autoimmune encephalomyelitis', *Brain Behav Immun*, 73: 3-20.

Toh, Y. C., C. Zhang, J. Zhang, Y. M. Khong, S. Chang, V. D. Samper, D. van Noort, D. W. Hutmacher, and H. Yu. 2007. 'A novel 3D mammalian cell perfusion-culture system in microfluidic channels', *Lab Chip*, 7: 302-9.

Trosky, J. E., Y. Li, S. Mukherjee, G. Keitany, H. Ball, and K. Orth. 2007. 'VopA inhibits ATP binding by acetylating the catalytic loop of MAPK kinases', *J Biol Chem*, 282: 34299-305.

Tsai, Y. H., R. H. Orsi, K. K. Nightingale, and M. Wiedmann. 2006. 'Listeria monocytogenes internalins are highly diverse and evolved by recombination and positive selection', *Infect Genet Evol*, 6: 378-89.

Uchida, Y., T. Sumiya, M. Tachikawa, T. Yamakawa, S. Murata, Y. Yagi, K. Sato, A. Stephan, K. Ito, S. Ohtsuki, P. O. Couraud, T. Suzuki, and T. Terasaki. 2019. 'Involvement of Claudin-11 in Disruption of Blood-Brain, -Spinal Cord, and -Arachnoid Barriers in Multiple Sclerosis', *Mol Neurobiol*, 56: 2039-56.

Urich, E., S. E. Lazic, J. Molnos, I. Wells, and P. O. Freskgård. 2012. 'Transcriptional profiling of human brain endothelial cells reveals key properties crucial for predictive in vitro blood-brain barrier models', *PLoS One*, 7: e38149.

- Urich, E., C. Patsch, S. Aigner, M. Graf, R. Iacone, and P. O. Freskgård. 2013. 'Multicellular self-assembled spheroidal model of the blood brain barrier', *Sci Rep*, 3: 1500.
- Vadeboncoeur, N., M. Segura, D. Al-Numani, G. Vanier, and M. Gottschalk. 2003. 'Pro-inflammatory cytokine and chemokine release by human brain microvascular endothelial cells stimulated by *Streptococcus suis* serotype 2', *FEMS Immunol Med Microbiol*, 35: 49-58.
- Vadia, S., E. Arnett, A. C. Haghighat, E. M. Wilson-Kubalek, R. K. Tweten, and S. Seveau. 2011. 'The pore-forming toxin listeriolysin O mediates a novel entry pathway of *L. monocytogenes* into human hepatocytes', *PLoS Pathog*, 7: e1002356.
- Vadia, S., and S. Seveau. 2014. 'Fluxes of Ca²⁺ and K⁺ are required for the listeriolysin O-dependent internalization pathway of *Listeria monocytogenes*', *Infect Immun*, 82: 1084-91.
- van der Helm, M. W., A. D. van der Meer, J. C. Eijkel, A. van den Berg, and L. I. Segerink. 2016. 'Microfluidic organ-on-chip technology for blood-brain barrier research', *Tissue Barriers*, 4: e1142493.
- van Meer, G., B. Gumbiner, and K. Simons. 1986. 'The tight junction does not allow lipid molecules to diffuse from one epithelial cell to the next', *Nature*, 322: 639-41.
- Vanlandewijck, M., L. He, M. A. Mäe, J. Andrae, K. Ando, F. Del Gaudio, K. Nahar, T. Lebouvier, B. Laviña, L. Gouveia, Y. Sun, E. Raschperger, M. Räsänen, Y. Zarb, N. Mochizuki, A. Keller, U. Lendahl, and C. Betsholtz. 2018. 'A molecular atlas of cell types and zonation in the brain vasculature', *Nature*, 554: 475-80.
- Veiga, E., and P. Cossart. 2005. '*Listeria* hijacks the clathrin-dependent endocytic machinery to invade mammalian cells', *Nat Cell Biol*, 7: 894-900.
- Veiga, E., J. A. Guttman, M. Bonazzi, E. Boucrot, A. Toledo-Arana, A. E. Lin, J. Enninga, J. Pizarro-Cerdá, B. B. Finlay, T. Kirchhausen, and P. Cossart. 2007. 'Invasive and adherent bacterial pathogens co-opt host clathrin for infection', *Cell Host Microbe*, 2: 340-51.
- Vestweber, D. 2015. 'Cadherins in tissue architecture and disease', *J Mol Med (Berl)*, 93: 5-11.
- Vollmer, W., B. Joris, P. Charlier, and S. Foster. 2008. 'Bacterial peptidoglycan (murein) hydrolases', *FEMS Microbiol Rev*, 32: 259-86.
- Wang, C., C. H. Chou, C. Tseng, X. Ge, and L. M. Pinchuk. 2011. 'Early gene response of human brain microvascular endothelial cells to *Listeria monocytogenes* infection', *Can J Microbiol*, 57: 441-6.
- Wang, L., and M. Lin. 2007. 'Identification of IspC, an 86-kilodalton protein target of humoral immune response to infection with *Listeria monocytogenes* serotype 4b, as a novel surface autolysin', *J Bacteriol*, 189: 2046-54.

———. 2008. 'A novel cell wall-anchored peptidoglycan hydrolase (autolysin), IspC, essential for *Listeria monocytogenes* virulence: genetic and proteomic analysis', *Microbiology (Reading)*, 154: 1900-13.

Wang, Y. I., H. E. Abaci, and M. L. Shuler. 2017. 'Microfluidic blood-brain barrier model provides in vivo-like barrier properties for drug permeability screening', *Biotechnol Bioeng*, 114: 184-94.

Wang, Y., N. Wang, B. Cai, G. Y. Wang, J. Li, and X. X. Piao. 2015. 'In vitro model of the blood-brain barrier established by co-culture of primary cerebral microvascular endothelial and astrocyte cells', *Neural Regen Res*, 10: 2011-7.

Warren, M. S., N. Zerangue, K. Woodford, L. M. Roberts, E. H. Tate, B. Feng, C. Li, T. J. Feuerstein, J. Gibbs, B. Smith, S. M. de Morais, W. J. Dower, and K. J. Koller. 2009. 'Comparative gene expression profiles of ABC transporters in brain microvessel endothelial cells and brain in five species including human', *Pharmacol Res*, 59: 404-13.

Watanabe, M., J. E. Buth, N. Vishlaghi, L. de la Torre-Ubieta, J. Taxidis, B. S. Khakh, G. Coppola, C. A. Pearson, K. Yamauchi, D. Gong, X. Dai, R. Damoiseaux, R. Aliyari, S. Liebscher, K. Schenke-Layland, C. Caneda, E. J. Huang, Y. Zhang, G. Cheng, D. H. Geschwind, P. Golshani, R. Sun, and B. G. Novitsch. 2017. 'Self-Organized Cerebral Organoids with Human-Specific Features Predict Effective Drugs to Combat Zika Virus Infection', *Cell Rep*, 21: 517-32.

Wei, P., R. Bao, and Y. Fan. 2020. 'Brainstem Encephalitis Caused by *Listeria monocytogenes*', *Pathogens*, 9.

Weiglein, I., W. Goebel, J. Troppmair, U. R. Rapp, A. Demuth, and M. Kuhn. 1997. '*Listeria monocytogenes* infection of HeLa cells results in listeriolysin O-mediated transient activation of the Raf-MEK-MAP kinase pathway', *FEMS Microbiol Lett*, 148: 189-95.

Wiedemann, A., L. Mijouin, M. A. Ayoub, E. Barilleau, S. Canepa, A. P. Teixeira-Gomes, Y. Le Vern, M. Rosselin, E. Reiter, and P. Velge. 2016. 'Identification of the epidermal growth factor receptor as the receptor for *Salmonella* Rck-dependent invasion', *Faseb j*, 30: 4180-91.

Wiedmann, M., J. L. Bruce, C. Keating, A. E. Johnson, P. L. McDonough, and C. A. Batt. 1997. 'Ribotypes and virulence gene polymorphisms suggest three distinct *Listeria monocytogenes* lineages with differences in pathogenic potential', *Infect Immun*, 65: 2707-16.

Wolburg, H., and W. Paulus. 2010. 'Choroid plexus: biology and pathology', *Acta Neuropathol*, 119: 75-88.

Wolburg, H., K. Wolburg-Buchholz, J. Kraus, G. Rascher-Eggstein, S. Liebner, S. Hamm, F. Duffner, E. H. Grote, W. Risau, and B. Engelhardt. 2003. 'Localization of claudin-3 in tight junctions of the blood-brain barrier is selectively lost during experimental autoimmune encephalomyelitis and human glioblastoma multiforme', *Acta Neuropathol*, 105: 586-92.

Wolburg, H., K. Wolburg-Buchholz, S. Liebner, and B. Engelhardt. 2001. 'Claudin-1, claudin-2 and claudin-11 are present in tight junctions of choroid plexus epithelium of the mouse', *Neurosci Lett*, 307: 77-80.

Wollert, T., B. Pasche, M. Rochon, S. Deppenmeier, J. van den Heuvel, A. D. Gruber, D. W. Heinz, A. Lengeling, and W. D. Schubert. 2007. 'Extending the host range of *Listeria monocytogenes* by rational protein design', *Cell*, 129: 891-902.

Wyss, L., J. Schäfer, S. Liebner, M. Mittelbronn, U. Deutsch, G. Enzmann, R. H. Adams, M. Aurrand-Lions, K. H. Plate, B. A. Imhof, and B. Engelhardt. 2012. 'Junctional adhesion molecule (JAM)-C deficient C57BL/6 mice develop a severe hydrocephalus', *PLoS One*, 7: e45619.

Yasumi, M., K. Shimizu, T. Honda, M. Takeuchi, and Y. Takai. 2003. 'Role of each immunoglobulin-like loop of nectin for its cell-cell adhesion activity', *Biochem Biophys Res Commun*, 302: 61-6.

Zhang, T., D. Bae, and C. Wang. 2015. 'Listeriolysin O mediates cytotoxicity against human brain microvascular endothelial cells', *FEMS Microbiol Lett*, 362: fnv084.

Zhang, Y., K. Chen, S. A. Sloan, M. L. Bennett, A. R. Scholze, S. O'Keeffe, H. P. Phatnani, P. Guarnieri, C. Caneda, N. Ruderisch, S. Deng, S. A. Liddelow, C. Zhang, R. Daneman, T. Maniatis, B. A. Barres, and J. Q. Wu. 2014. 'An RNA-sequencing transcriptome and splicing database of glia, neurons, and vascular cells of the cerebral cortex', *J Neurosci*, 34: 11929-47.

Zhang, Y., S. A. Sloan, L. E. Clarke, C. Caneda, C. A. Plaza, P. D. Blumenthal, H. Vogel, G. K. Steinberg, M. S. Edwards, G. Li, J. A. Duncan, 3rd, S. H. Cheshier, L. M. Shuer, E. F. Chang, G. A. Grant, M. G. Gephart, and B. A. Barres. 2016. 'Purification and Characterization of Progenitor and Mature Human Astrocytes Reveals Transcriptional and Functional Differences with Mouse', *Neuron*, 89: 37-53.

ABBREVIATIONS

| | |
|--------|--|
| AJ | Adherens junction |
| BBB | Blood-brain barrier |
| BCSFB | Blood-cerebrospinal fluid barrier |
| BHI | Brain heart infusion |
| BSA | Bovine serum albumin |
| CAM | Cell adhesion molecule |
| CC | Clonal complex |
| CDC | Cholesterol-dependent cytolysin |
| CFU | Colony-forming unit |
| CNS | Central nervous system |
| CP | Choroid plexus |
| CSF | Cerebrospinal fluid |
| DAPI | 4',6-diamidino-2-phenylindole |
| DIF | double immunofluorescence |
| DMSO | Dimethyl sulfoxide |
| DTT | Dithiothreitol |
| Ecad | E-cadherin |
| ECM | Extracellular matrix |
| EDTA | Ethylenediaminetetraacetic acid |
| EMT | Epithelial-mesenchymal transition |
| ER | Endoplasmic reticulum |
| ERK1/2 | Extracellular signal-regulated kinases 1 and 2 |
| FCS | Fetal calf serum |
| FITC | Fluorescein isothiocyanate |
| GAG | Glycosaminoglycan |
| HBMEC | Human brain microvascular endothelial cells |
| HGF | Hepatocyte growth factor |
| HIBCPP | Human choroid plexus papilloma |
| IF | Immunofluorescence |
| InI | Internalin (any member of the internalin protein family) |
| InIA | Internalin (specifically InIA, since it was the first discovered internalin) |
| IVC | Individually ventilated cage |
| JAM | Junctional adhesion molecule |

| | |
|-------------------|--|
| KR14 | Human-specific CD44v6-blocking peptide |
| LLO | Listeriolysin O |
| <i>Lm</i> | <i>Listeria monocytogenes</i> |
| <i>Lm</i> EGDe | <i>Listeria monocytogenes</i> EGDe strain |
| LRR | Leucine-rich repeat |
| LTA | Lipoteichoic acid |
| MAGUK | Membrane-associated guanylate kinase |
| MAPK | Mitogen-activated protein kinase |
| MLN | Mesenteric lymph node |
| MLST | Multilocus sequence typing |
| MOI | Multiplicity of infection |
| MucBP | Mucin-binding protein |
| NVU | Neurovascular unit |
| OD ₆₀₀ | optical density of a sample measured at a wavelength of 600 nm |
| PBS | Phosphate buffered saline |
| PI3K | Phosphoinositide 3-kinase |
| PIAL | Post-infection activation level |
| PKB (also Akt) | Protein kinase B |
| PSC | Pluripotent stem cell |
| PTS | Phosphotransferase system |
| QP14 | Mouse-specific CD44v6-blocking peptide |
| ROCK | Rho-associated protein kinase |
| RTK | Receptor tyrosine kinase |
| SDS-PAGE | Sodium dodecyl sulphate–polyacrylamide gel electrophoresis |
| TAMP | Tight junction-associated MARVEL protein |
| TEER | Transepithelial electric resistance |
| TJ | Tight junction |
| VF | Virulence factor |
| ZO | Zona occludens |

LIST OF FIGURES

| | |
|---|----|
| Figure 1. The architecture of vascular barriers of the brain – the BBB and the BCSFB | 11 |
| Figure 2. Overview of the types of models of the BBB (and partially the BCSFB) | 20 |
| Figure 3. Different possible entry points for listerial CNS invasion | 24 |
| Figure 4. A graphical representation of interactions between <i>Lm</i> (in blue) and the CNS-localized, non-phagocytic host cell (in pink), mediated by listerial VF..... | 26 |
| Figure 5. Calibration curve for <i>Lm</i> EGDe wt used for calculation of bacterial concentration of inoculums used for <i>in vivo</i> experiments | 56 |
| Figure 6. ZO-1 staining in HBMEC (A) and HIBCPP cells (B) outlines the presence of TJs between the cells | 61 |
| Figure 7. The result of viability assessment staining in HBMEC (A) and HIBCPP cells (B)..... | 66 |
| Figure 8. Visual representation of the array's mode of action..... | 80 |
| Figure 9. Array map | 81 |
| Figure 10. Differences in molecular expression patterns between HIBCPP cells and HBMEC..... | 82 |
| Figure 11. Ecad staining in HBMEC (A) and HIBCPP cells (B) confirms presence of Ecad in HIBCPP cells and its complete absence in HBMEC | 84 |
| Figure 12. Met staining in HBMEC (A) and HIBCPP cells (B) confirms presence of Met in both cell lines, with apparently stronger presence in HIBCPP | 85 |
| Figure 13. Vimentin staining in HBMEC (A and B) and HIBCPP cells (C and D) confirms presence of vimentin in HBMEC and its complete absence in HIBCPP cells | 86 |
| Figure 14. Listerial invasion into the HBMEC (A) and HIBCPP cells (B) over time | 88 |
| Figure 15. <i>Lm</i> utilizes different InIs for entry into HBMEC (A) and HIBCPP cells (B)..... | 90 |
| Figure 16. <i>Lm</i> requires surface vimentin for entry into HBMEC (A) but not for entry into HIBCPP cells (B)..... | 91 |
| Figure 17. Co-incubation with WitA in presence of <i>Lm</i> does not visibly affect survival of either HBMEC (A) or HIBCPP cells (B) | 92 |
| Figure 18. Pre-incubation with CD44v6-blocking antibodies does not affect invasion rates of <i>Lm</i> into bEnd.3 (A), HBMEC (B), HeLa (C) and HIBCPP (D) cells | 94 |

Figure 19. Contact with *Lm* causes a strong upregulation of inflammation-related (Il-6, Il-8 and TNF α) genes in both HBMEC (A) and HIBCPP cells (B), but the transcription of reported interaction partners of listerial VFs (CD44v6, Ecad, Met and vimentin) remains constant.....97

Figure 20. *Lm* infection triggers the activation of MAPK pathways in both HBMEC and HIBCPP cells..98

Figure 21. Pre-incubation with p38-inhibiting compound SB203580 causes a statistically significant drop in invasion of *Lm* into HBMEC, but pre-incubation with ERK1/2-inhibiting compound U0126 does not.....99

Figure 22. Pre-incubation with dynamin assembly inhibitor Dynasore causes a strong and statistically significant decrease in invasion rates of *Lm* into HBMEC, which is dependent on the concentration of Dynasore100

Figure 23. Co-incubation with *Lm* affects the activation state (observed as a change in phosphorylation levels) of multiple RTKs in both HBMEC and HIBCPP cells.....102

Figure 24. Effects of *Lm* infection on levels of phosphorylated forms of select tyrosine kinases in HBMEC (A) and HIBCPP (B) cells104

Figure 25. Immunosuppression leads to increased bacterial loads in brains (B), livers (C), MLNs (D) and spleens (E) of the infected mice of both strains106

Figure 27. Treatment with CD44v6-blocking peptides does not affect bacterial loads in organs of immunosuppressed C57BL/6JRj mice108

LIST OF TABLES

| | |
|---|-----|
| Table 1. OD ₆₀₀ readings corresponding with the concentration of 1 x 10 ⁸ CFU/ml used for preparation of inoculum for <i>in vitro</i> experiments | 55 |
| Table 2. PCR reaction mixture for <i>Lm</i> strain verification (for a single sample) | 57 |
| Table 3. PCR program for <i>Lm</i> strain verification..... | 57 |
| Table 4. Combinations of primers used for <i>Lm</i> strain verification PCR and the expected product size for each of the combinations by strain | 58 |
| Table 5. Expected number of cells per compartment for all of the used cell lines (when confluent)... | 60 |
| Table 6. Volumes of organ sample types after the homogenization..... | 71 |
| Table 7. cDNA synthesis reaction mixture (for a single sample) | 75 |
| Table 8. PCR program for cDNA synthesis..... | 75 |
| Table 9. PCR reaction mixture for semi-quantitative PCR (for a single sample) | 76 |
| Table 10. PCR program for semi-quantitative PCR | 76 |
| Table 11. Overview of RTKs known to interact with intracellular pathogens during invasion. | 116 |
| Table 12. Overview of post-infection RTK activation level changes in HBMEC and HIBCPP cells. | 118 |

ACKNOWLEDGEMENTS

This work was supported by the Deutsche Forschungsgemeinschaft (SCHW 703/3-1).

There were many people whose contributions – no matter whether great or small – were invaluable for the creation of this work. Although I will try not to miss anyone, hold it not against me if I do, and know that it was by omission rather than by intent.

First of all, I would like to thank Prof. Horst Schrotten, the head of the Children's Clinic at UMM, for everything I was provided with during my time in the group.

I would also like to thank Prof. Michael Lanzer, Prof. Jacomine Krijnse-Locker, Dr. Alessia Ruggieri and Dr. Silvia Portugal for either advice and suggestions given during my TAC meetings, constructive discussion and willingness to be the members of my thesis defense committee, or both.

I am grateful to my supervisor, Prof. Christian Schwerk, for his help and assistance during the course of this project as well as during the writing of the thesis.

Among everyone from the Schrotten group, I want to give praise to Selina, Svenja and Walter. You provided help above and beyond call of duty, and I will not forget that. Special thanks also go to my medical buddies – Cihan, Christian, Gina and Lukas. Was great with you around, folks!

I also want to thank all the other members of the group, both current and former, for their support and help during our time together. Alexa, Alina, Carolin, Fatemeh, Julia, Lea, Marie, Rosanna, Sandrin, Ulli, Vasily, Wiltrud and anyone else I might have missed: I don't know half of you half as well as I should like, and I like less than half of you half as well as you deserve. You made my time in the lab memorable!

I was blessed with a number of amazing friends over the years, and I would like to thank all of them for being in my life, making it worthwhile and – quite often – patiently suffering one of my long-winded trains of thought. You are amazing – yes, all of you (and I won't list you since you all know I am talking about you 😊)!

I wish to thank my family – Mom, Dad and Ana. Although our apartment was often way too small to contain all of us within, we somehow managed to survive, thrive and get along. Turned out quite nice!

Last but definitely not the least... I want to thank Ani: my friend, my companion, my wife. Thank you for giving me focus and direction. And thanks to not-so-little Lydia, too – you are a piece of work, but you are OUR piece of work!